

VOLUME 76

AUGUST 17, 1972

NUMBER 17

JPCHAX

THE JOURNAL OF

PHYSICAL
CHEMISTRY

PUBLISHED BIWEEKLY BY THE AMERICAN CHEMICAL SOCIETY

THE JOURNAL OF PHYSICAL CHEMISTRY

BRYCE CRAWFORD, Jr., *Editor*

STEPHEN PRAGER, *Associate Editor*

ROBERT W. CARR, Jr., FREDERIC A. VAN-CATLEDGE, *Assistant Editors*

EDITORIAL BOARD: A. O. ALLEN (1970-1974), J. R. BOLTON (1971-1975),
F. S. DANTON (1972-1976), M. FIXMAN (1970-1974),
H. S. FRANK (1970-1974), R. R. HENTZ (1972-1976), J. R. HUIZENGA (1969-1973),
W. J. KAUFMANN (1969-1973), R. L. KAY (1972-1976), W. R. KRIGBAUM (1969-1973),
R. A. MARCUS (1968-1972), W. J. MOORE (1969-1973), J. A. POPLE (1971-1975),
B. S. RABINOVITCH (1971-1975), H. REISS (1970-1974), S. A. RICE (1969-1975),
F. S. ROWLAND (1968-1972), R. L. SCOTT (1968-1972),
R. SEIFERT (1968-1972), W. A. ZISMAN (1972-1976)

CHARLES R. BERTSCH, *Manager, Editorial Production*

AMERICAN CHEMICAL SOCIETY, 1155 Sixteenth St., N.W., Washington, D. C. 20036

Books and Journals Division

JOHN K. CRUM, *Director*

JOSEPH H. KUNEY, *Head, Business Operations Department*

RUTH REYNARD, *Assistant to the Director*

©Copyright, 1972, by the American Chemical Society. Published biweekly by the American Chemical Society at 20th and Northampton Sts., Easton, Pa. 18042. Second-class postage paid at Washington, D. C., and at additional mailing offices.

All manuscripts should be sent to *The Journal of Physical Chemistry*, Department of Chemistry, University of Minnesota, Minneapolis, Minn. 55455.

Additions and Corrections are published once yearly in the final issue. See Volume 75, Number 26 for the proper form.

Extensive or unusual alterations in an article after it has been set in type are made at the author's expense, and it is understood that by requesting such alterations the author agrees to defray the cost thereof.

The American Chemical Society and the Editor of *The Journal of Physical Chemistry* assume no responsibility for the statements and opinions advanced by contributors.

Correspondence regarding accepted copy, proofs, and reprints should be directed to Editorial Production Office, American Chemical Society, 20th and Northampton Sts., Easton, Pa. 18042. Manager: CHARLES R. BERTSCH. Assistant Editor: EDWARD A. BORGER. Editorial Assistant: JOSEPH E. YURVAT.

Advertising Office: Centcom, Ltd. (formerly Century Communications Corporation), 142 East Avenue, Norwalk, Conn. 06851.

Business and Subscription Information

Remittances and orders for subscriptions and for single copies,

notices of changes of address and new professional connections, and claims for missing numbers should be sent to the Subscription Service Department, American Chemical Society, 1155 Sixteenth St., N.W., Washington, D. C. 20036. Allow 4 weeks for changes of address. Please include an old address label with the notification.

Claims for missing numbers will not be allowed (1) if received more than sixty days from date of issue, (2) if loss was due to failure of notice of change of address to be received before the date specified in the preceding paragraph, or (3) if the reason for the claim is "missing from files."

Subscription rates (1972): members of the American Chemical Society, \$20.00 for 1 year; to nonmembers, \$60.00 for 1 year. Those interested in becoming members should write to the Admissions Department, American Chemical Society, 1155 Sixteenth St., N.W., Washington, D. C. 20036. Postage to Canada and countries in the Pan-American Union, \$5.00; all other countries, \$6.00. Single copies for current year: \$3.00. Rates for back issues from Volume 56 to date are available from the Special Issues Sales Department, 1155 Sixteenth St., N.W., Washington, D. C. 20036.

This publication and the other ACS periodical publications are now available on microfilm. For information write to: MICROFILM, Special Issues Sales Department, 1155 Sixteenth St., N.W., Washington, D. C. 20036.

THE JOURNAL OF PHYSICAL CHEMISTRY

Volume 76, Number 17 August 17, 1972

JPCHAx 76(17) 2343-2484 (1972)

- A Kinetic Study of the Monomer-Dimer Equilibrium in Aqueous Vanadium(IV) Tetrasulfophthalocyanine Solutions **Robert D. Farina,* D. J. Halko, and J. H. Swinehart** 2343
- The Kinetics of Adsorption of Carbon Monoxide on Alumina **A. Stanislaus, M. J. B. Evans,* and R. F. Mann** 2349
- Reactions Involving Electron Transfer at Semiconductor Surfaces. III. Dissociation of Methyl Iodide over Zinc Oxide **Joseph Cunningham* and A. L. Penny** 2353
- Reactions Involving Electron Transfer at Semiconductor Surfaces. IV. Zinc Oxide Promoted Photoreductions in Aqueous Solutions at Neutral pH **Joseph Cunningham* and Hanaa Zainal** 2362
- Radiolysis of Liquid 2,2,4-Trimethylpentane. Kinetics of Scavenging Processes **Stefan J. Rzad* and Krishan M. Bansal** 2374
- Radiolysis of Liquid 2,2,4-Trimethylpentane. Effect of Charge Scavengers on Product Formation **Krishan M. Bansal and Stefan J. Rzad*** 2381
- The Production of Halide Ion in the Radiolysis of Aqueous Solutions of the 5-Halouracils **Krishan M. Bansal, Larry K. Patterson, and Robert H. Schuler*** 2386
- Pulse Radiolysis Studies of 5-Halouracils in Aqueous Solutions **L. K. Patterson* and K. M. Bansal** 2392
- Electron Spin Resonance Study of Radicals Produced in Irradiated Aqueous Solutions of 5-Halouracils **P. Neta** 2399
- Nitrogen-14 Nuclear Magnetic Resonance Study of 1,5-Disubstituted Tetrazoles **Edward B. Baker and Alexander I. Popov*** 2403
- Intermolecular Charge-Transfer Studies. Thioamide-Iodine System **R. Abu-Eittah* and A. El-Kourashy** 2405
- An Ultrasonic Shear Wave Study of the Mechanical Properties of a Nematic Liquid Crystal **Y. S. Lee, Sherman L. Golub, and Glenn H. Brown*** 2409
- Some Comparisons of the RRK and RRKM Theories of Thermal Unimolecular Reaction. Energy Distributions and the s Parameter **Gordon B. Skinner and B. S. Rabinovitch*** 2418
- CNDO-CI Studies of the Effects of Multiple Substitution on the Electronic Spectrum of *p*-Benzoquinone **Philip E. Stevenson** 2424
- Studies of the Ester Group. I. *Ab Initio* Calculations on Methyl Formate **Håkan Wennerström,* Sture Forsén, and Björn Roos** 2430
- Determination of the Partial Specific Volume of Macromolecular Solutes from Light Scattering **Wilfried Heller** 2437
- Nuances of the $\bar{E}CE$ Mechanism. IV. Theory of Cyclic Voltammetry and Chronoamperometry and the Electrochemical Reduction of Hexacyanochromate(III) **Stephen W. Feldberg* and Ljubomir Jeftic** 2439
- Effective Fixed Charge Density Governing Membrane Phenomena. IV. Further Study of Activity Coefficients and Mobilities of Small Ions in Charged Membranes **Tetuo Ueda,* Naoki Kamo, Naobumi Ishida, and Yonosuke Kobatake** 2447
- Conductance of an Intermolecular Charge-Transfer Complex within an Ion Pair. **Hans Güsten* and Leo Klasinc** 2452
- Hydration of Perchlorate, Tetraphenylboride, and Nitrate Ions in Some Organic Solvents **T. Kenjo and R. M. Diamond*** 2454
- Selectivity in Heterovalent Anion Exchange. Ion Pairing *vs.* Ion Hydration **J. Bucher, R. M. Diamond,* and B. Chu** 2459

Diffusion of Acetic Acid Dimers and Their Homomorphs	F. A. L. Dullien* and G. H. Shroff*	2463
Ion-Molecule Reactions of Diborane and Oxygen-Containing Compounds	Robert C. Dunbar	2467
Diffusion in Mixed Solvents. III. Iodine in Nonpolar Solutions. Evidence for Charge-Transfer Interaction	Koichiro Nakanishi* and Sonoko Kitajima	2470
Solvent Effects in Organic Chemistry. XIV. Solvation of Sodium Salts in Glycerol Acetate Binaries by ²³ Na Nuclear Magnetic Resonance Spectroscopy and Thermodynamics	Edward M. Arnett,* H. C. Ko, and R. J. Minasz	2474
Electron Spin Resonance Spectra of Zwitterion Radicals and Isoelectronic Anion Radicals	Ronald P. Mason* and John E. Harriman	2479

COMMUNICATIONS TO THE EDITOR

Raman Scattering in Sodium-Liquid Ammonia Solutions	Billie L. Smith and W. H. Koehler*	2481
On a Comparison of Isotope Shifts in the Vibrational Spectrum of Gas-Phase and Matrix-Isolated Hydrogen Cyanide	S. D. Gabelnick	2483

AUTHOR INDEX

Abu-Eittah, R., 2405	Dullien, F. A. L., 2463	Harriman, J. E., 2479	Mann, R. F., 2349	Rzad, S. J., 2374, 2381
Arnett, E. M., 2474	Dunbar, R. C., 2467	Heller, W., 2437	Mason, R. P., 2479	Schuler, R. H., 2386
Baker, E. B., 2403	El-Kourashy, A., 2405	Ishida, N., 2447	Minasz, R. J., 2474	Shroff, G. H., 2463
Bansal, K. M., 2374, 2381, 2386, 2392	Evans, M. J. B., 2349	Jeftic, L., 2439	Nakanishi, K., 2470	Skinner, G. B., 2418
Brown, G. H., 2409	Farina, R. D., 2343	Kamo, N., 2447	Neta, P., 2399	Smith, B. L., 2481
Bucher, J., 2459	Feldberg, S. W., 2439	Kenjo, T., 2454	Patterson, L. K., 2386, 2392	Stanislaus, A., 2349
Chu, B., 2459	Forsén, S., 2430	Kitajima, S., 2470	Penny, A. L., 2353	Stevenson, P. E., 2424
Cunningham, J., 2353, 2362	Gabelnick, S. D., 2483	Klasinc, L., 2452	Popov, A. I., 2403	Swinehart, J. H., 2343
Diamond, R. M., 2454, 2459	Golub, S. L., 2409	Ko, H. C., 2474		Ueda, T., 2447
	Güsten, H., 2452	Kobatake, Y., 2447		Wennerström, H., 2430
	Halko, D. J., 2343	Koehler, W. H., 2481	Rabinovitch, B. S., 2418	Zainal, H., 2362
		Lee, Y. S., 2409	Roos, B., 2430	

In papers with more than one author the name of the author to whom inquiries about the paper should be addressed is marked with an asterisk in the by-line.

ANNOUNCEMENT

Conference on Critical Evaluation of Chemical and Physical Structural Information

A conference will be held June 24-29, 1973 at Dartmouth College, Hanover, N. H., to discuss problems in the critical evaluation of structural information derived by diverse experimental and theoretical methods. The objective is to enable scientists utilizing structural information derived from fields outside their own specializations (theoretical calculations, crystallographic diffraction, optical spectroscopy, microwave spectroscopy, nmr and esr spectroscopy, Mössbauer spectroscopy, electron diffraction, electric polarizability, etc.) to evaluate such information critically. Sessions will be devoted to statistical analysis of experimental data, methods of determining molecular symmetry, structural parameters describing molecular geometry, vibrational force fields and parameters, large-amplitude motions (such as internal rotations, inversions, and ring puckering), structural parameters related to electronic charge distribution, and correlation of experimental with theoretical methods of determining structural information.

The conference is sponsored by the Committee on Chemical Crystallography of the National Academy of Sciences—National Research Council, with support from the National Science Foundation. Cochairmen of the organizing committee are Carroll K. Johnson and David R. Lide, Jr. Attendance will be limited to 100-150 participants, by invitation, and proceedings will be published. To receive further information and application forms, available by October 1, 1972, please write to M. A. Paul, Executive Secretary, NRC Division of Chemistry and Chemical Technology, National Academy of Sciences, 2101 Constitution Avenue N.W., Washington, D. C. 20418.

THE JOURNAL OF PHYSICAL CHEMISTRY

Registered in U. S. Patent Office © Copyright, 1972, by the American Chemical Society

VOLUME 76, NUMBER 17 AUGUST 17, 1972

A Kinetic Study of the Monomer-Dimer Equilibrium in Aqueous Vanadium(IV) Tetrasulfophthalocyanine Solutions

by Robert D. Farina,*

Department of Chemistry, Western Kentucky University, Bowling Green, Kentucky 42101

D. J. Halko, and J. H. Swinehart

Department of Chemistry, University of California, Davis, California 95616 (Received April 29, 1971)

Publication costs borne completely by The Journal of Physical Chemistry

Spectroscopic and kinetic studies made on aqueous vanadium(IV) tetrasulfophthalocyanine solutions (V^{IV} -TSPC) over a concentration range of 5×10^{-7} to 5×10^{-5} M give results consistent with a monomer-dimer equilibrium of the type $(VOTSPC)_2^{2i} \xrightleftharpoons[k_b]{k_f} 2VOTSPC^{i-}$ where i could assume one of several possible charges.

The values of k_f and k_b measured at $\mu = 0.006$ ($NaClO_4$) and 50° are $4.5 \pm 0.2 \text{ sec}^{-1}$ and $8.4 \pm 0.8 \times 10^6 \text{ M}^{-1} \text{ sec}^{-1}$, respectively. The activation parameters ΔH^\ddagger and ΔS^\ddagger are $13.6 \pm 1.5 \text{ kcal/mol}$ and $-14 \pm 5 \text{ eu}$ for k_f and $4.9 \pm 1.5 \text{ kcal/mol}$ and $-12 \pm 5 \text{ eu}$ for k_b . The ratio of rate constants at different temperatures gives concentration quotients which are not in good agreement with the spectral values. Reasons for the nonagreement between the spectral and kinetic results are presented. Some possible reaction mechanisms for the dimerization process are discussed. Preliminary results on the rates of reduction of the vanadium complex are also included.

Introduction

Although there have been a number of reviews on the chemistry of phthalocyanines,¹ much less work has been done on the aqueous chemistry of their tetrasulfonated derivatives. The preparation for a number of transition metal complexes of 4,4',4'',4'''-tetrasulfophthalocyanine (TSPC) is described in the literature.² Magnetic studies have been made on several transition metal complexes of TSPC,³ but only the kinetics on the cobalt(II)⁴ and manganese(III)⁵ systems have been reported.

This paper describes a kinetic and spectroscopic study of the monomer-dimer equilibrium of V^{IV} -TSPC in aqueous solution. Some of the factors influencing this equilibrium are also examined. Dithionite and vanadium(II) were added to determine which of the species, monomer or dimer, is more easily reduced.

Experimental Section

Materials. The monosodium salt of 4-sulfophthalic acid used in the preparation of the tetrasodium salt of vanadium(IV)-4,4',4'',4'''-tetrasulfophthalocyanine was prepared from technical grade 4-sulfophthalic acid (Eastman Organic Chemicals). The salt was obtained by adding an appropriate amount of sodium hydroxide to the acid and purifying the resulting precipitate by re-

(1) A. B. P. Lever, "Advances in Inorganic Chemistry and Radiochemistry," Vol. 7, H. J. Emeleus and A. G. Sharpe, Ed., Academic Press, New York, N. Y., 1965, p 27, and references therein.

(2) K. Bernauer and S. Fallab, *Helv. Chim. Acta*, **44**, 1287 (1961).

(3) J. H. Weber and D. H. Busch, *Inorg. Chem.*, **4**, 472 (1965), and references therein.

(4) Z. A. Schelly, R. D. Farina, and E. M. Eyring, *J. Phys. Chem.*, **74**, 617 (1970).

(5) K. Fenkart and C. H. Brubaker, Jr., *J. Inorg. Nucl. Chem.*, **30**, 3245 (1968).

peated recrystallizations from water and acetone. All other chemicals were reagent grade except urea which was used without further purification.

Preparation of Na_4VOTSPC . The compound Na_4VOTSPC was prepared by a procedure identical with that used by Weber and Busch³ on the analogous cobalt(II) complex. Since vanadyl sulfate was the source of vanadium(IV), the procedure of Weber and Busch was modified in that the excess metal ion was removed from the product with 1 *N* sulfuric acid saturated with sodium sulfate instead of the 1 *N* hydrochloric acid saturated with sodium chloride. The final product is a dark blue solid.

Anal. Calcd for $\text{C}_{32}\text{H}_{12}\text{N}_8\text{O}_{13}\text{S}_4\text{Na}_4\text{V} \cdot 3.5\text{H}_2\text{O}$: C, 36.6; H, 1.8; N, 10.7; S, 12.2; Na, 8.7; V, 4.8. Found: C, 35.0; H, 1.8; N, 10.6; S, 12.0; Na, 8.0; V, 4.8.

The amount of vanadium(IV) present in the compound was determined spectrophotometrically by complexation with xylenol orange.⁶ The procedure requires that all of the vanadium(IV) be uncomplexed. This was accomplished by oxidizing the sulfonated phthalocyanine ring with concentrated nitric acid and subsequently heating the solution as described by Linstead.⁷

Spectral Experiments. Figure 1 shows the spectral characteristics of aqueous solutions of V^{IV} -TSPC in the 540- to 780-nm region by use of the Cary 14 recording spectrophotometer. There are two primary bands, one at 660 nm and the other at 692 nm, while a secondary band occurs at 625 nm. When the solutions are diluted, the absorbance at 660 nm decreases more than expected, while the absorbance at 692 nm decreases less than expected. Addition of salts, acid, or base decrease the 692-nm band but increase the 660-nm band. The converse is true when a small amount of pyridine or methanol is added. All of these observations are consistent with the fact that the band at 692 nm is the absorption maximum of the monomer, while the 660-nm band is the absorption maximum of the dimer.

Kinetic Experiments. The temperature-jump apparatus was manufactured by the Messanlagen Studiengesellschaft, GmbH, Goettingen, Germany, and has been described elsewhere.⁸ The solution temperature was increased by discharging a condenser charged to 40 kV through a cell containing the V^{IV} -TSPC solutions 0.006 *M* in sodium perchlorate. The concentration change resulting from the temperature perturbation can be followed spectrophotometrically at a number of wavelengths with the 692-nm band exhibiting the largest spectral change. Therefore, the 692-nm band was selected for all kinetic measurements. For changes in concentration near equilibrium

$$\frac{d\Delta C}{dt} = -\frac{1}{\tau} \Delta C$$

where ΔC is the difference in concentration between a

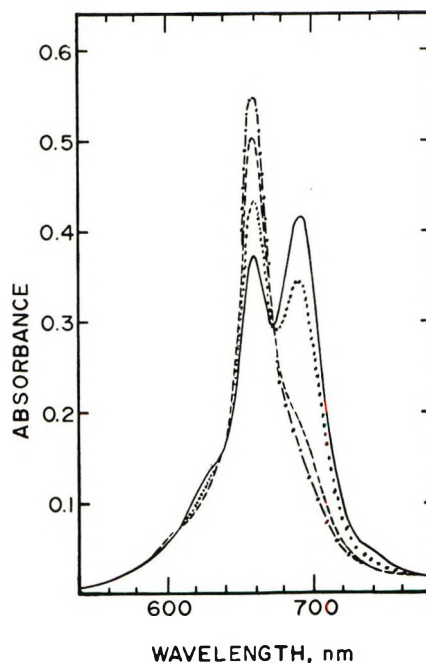


Figure 1. Spectra of solutions: $[\text{Na}_4\text{VOTSPC}]$, temp; 5.0×10^{-7} *M*, 50°, —; 5.0×10^{-7} *M*, 38°,; 5.0×10^{-5} *M*, 50°, ---; and 5.0×10^{-5} *M*, 38°, -·-·-; $\mu = 0.006$ (NaClO_4). Spectral measurements on the 5×10^{-5} and 5×10^{-7} *M* solutions were taken in 1.0- and 10.0-cm cells, respectively.

given time and infinite time (*i.e.*, concentration at the perturbed temperature) and τ is defined as the relaxation time. The traces of light transmission *vs.* time displayed on the oscilloscope were used to obtain the reciprocal relaxation times (τ^{-1}), which are the slopes of the resulting linear plots of $\log \Delta(\text{light transmission})$ *vs.* time. All solutions were allowed to equilibrate at least 20 min prior to the applied temperature perturbation.

Kinetic measurements were made over a total V^{IV} -TSPC concentration range of 5.0×10^{-7} to 5.0×10^{-5} *M* at temperatures of 28.0 ± 0.5 , 38.0 ± 0.5 , and $50.0 \pm 1.0^\circ$. Sodium perchlorate was used to maintain a constant ionic strength of 0.006.

Results and Discussion

Equilibrium Measurements. Fallab and Bernauer² have presented evidence to show that a number of tetrasulfophthalocyanine metal complexes polymerize in solution. Therefore, the immediate problem was to determine the number and kinds of species present in vanadium(IV)-TSPC solutions. Assuming an equilibrium exists between monomer (*M*) and aggregate (M_n) with only one kind of association the following equations are applicable

$$M_n = nM, \text{ where } Q = M^n/M_n \quad (1)$$

$$C = M + nM_n \quad (2)$$

(6) M. Otomo, *Bull. Chem. Soc. Jap.*, **36**, 137 (1963).

(7) R. P. Linstead, *J. Chem. Soc.*, 1016 (1934).

(8) M. Eigen and L. DeMaeyer in "Techniques of Organic Chemistry," Vol. VIII, Part II, A. Weissberger, Ed., Interscience, New York, N. Y., 1963, Chapter XVIII.

$$C\epsilon = M\epsilon_M + M_n\epsilon_n, \epsilon = A/Cd \quad (3)$$

where C is the total concentration of V^{IV} -TSPC; n is the degree of aggregation; A is the absorbance of the solutions at a given wavelength; d is the path length of the cell; Q is the concentration quotient; ϵ , ϵ_M , and ϵ_n are the molar absorptivity of the mixture, monomer, and aggregate, respectively, at that wavelength. By using the method of Kuhn and coworkers⁹ eq 1-3 are combined to give eq 4

$$y = 1/nx + a \quad (4)$$

where

$$y = \log [C(\epsilon - \epsilon_n/n)]$$

$$x = \log [C(\epsilon_M - \epsilon)]$$

and

$$a = (1 - 1/n) \log [\epsilon_M - \epsilon_n/n] + 1/n \log (Q/n)$$

Measurement of the absorbance at different total vanadium(IV)-TSPC concentrations allows x and y to be calculated providing ϵ_M and ϵ_n are known. The molar absorptivity of the monomer, ϵ_M , was obtained by heating a $5.0 \times 10^{-7} M$ V^{IV} -TSPC solution with no added salts until there was no further increase in the absorbance at 692 nm, the absorption maximum of the monomer. This occurred at a temperature of about 75°. It has previously been demonstrated that organic solvents favor the monomer in equilibrium involving tetrasulfonated metallophthalocyanine systems.¹⁰ The addition of either pyridine or methanol in this system favors the formation of the monomer and at a concentration of 5% by weight of the former solvent, the equilibrium shifts completely in favor of the monomer at 28°. The optical absorptivity of the monomer (692 nm) obtained by heating (75°) was in excellent agreement with the value obtained at 28° in the presence of pyridine after a correction is made for solvent expansion. This indicates that the change in optical absorptivity with temperature over a range of 28 to 75° is small and within experimental error.⁴ Low concentrations enhance the formation of monomer as is evidenced by the absorption maximum of the monomer (692 nm) which decreases less than expected when the solutions are diluted while the absorption maximum of the dimer (660 nm) decreases more than expected. The molar absorptivities of the monomer at 692 and 660 nm are 1.6×10^5 and $4.4 \times 10^4 M^{-1} \text{ cm}^{-1}$, respectively, at 28°.

Added salts convert the monomeric species into the dimeric form as proposed by Bernauer and Fallab.² The conversion appears complete at 0.009 M NaClO_4 and 10° for a solution $5.0 \times 10^{-5} M$ in vanadium(IV)-TSPC. Molar absorptivities of the dimer at 660 and 692 nm are 2.4×10^5 and $4.8 \times 10^4 M^{-1} \text{ cm}^{-1}$, respectively, at 28°. Under the above conditions, the absorbance at 660 nm due to the dimer is at a maximum.

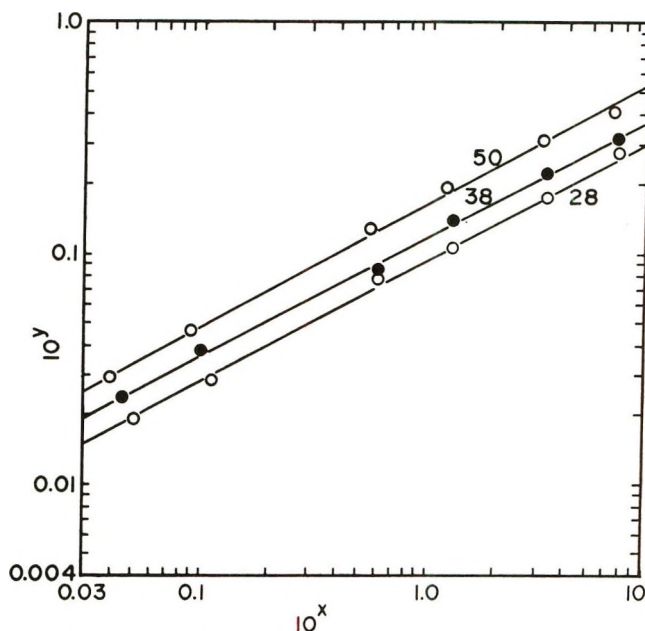


Figure 2. Plot of 10^y vs. 10^x (see eq 4), at 28, 38, and 50° with $\mu = 0.006$ (NaClO_4) and λ 692 nm.

At this point it should be mentioned that when the concentration of NaClO_4 exceeds 0.009 M , there is a slight absorbance decrease at both 692 and 660 nm. This suggests higher polymers form at greater salt concentrations or that association of the constituents of the salt with the monomer or dimer alters their spectral characteristics.

Figure 2 shows plots of 10^y vs. 10^x taken over a total vanadium(IV)-TSPC concentration range of 5.0×10^{-7} to $5.0 \times 10^{-5} M$ at 692 nm. The plots are linear at different temperatures with a slope of $1/n$ (from eq 4). Substitution of the $1/n$ value back into eq 4 allows the concentration quotient, Q , to be calculated. The following results obtained for n at $\mu = 0.006$ (NaClO_4) and different temperatures are 1.94 (28°), 1.95 (38°), and 1.97 (50°). These results indicate that the primary equilibrium is that between monomer and dimer. Spectrophotometric measurements made on 5.0×10^{-7} and $5.0 \times 10^{-5} M$ vanadium(IV)-TSPC solutions, the extremes of the concentration range examined, yield a single isosbestic point (see Figure 1) which is also consistent with a monomer-dimer equilibrium. Table I shows typical values of the monomer-dimer concentration quotients, Q , calculated from the absorbance of different V^{IV} concentrations at 50° and $\mu = 0.006$ (NaClO_4).

Spectral measurements on the dilute solutions were made with a spectral cell of 10-cm path length, while

(9) H. Kuhn, E. Schnabel, and H. Nother in "Recent Progress in the Chemistry of Natural and Synthetic Coloring Matter and Related Fields," T. S. Gore, Ed., Academic Press, New York, N. Y., 1962, pp 561-572.

(10) H. Sigel, P. Waldmeir, and B. Prijs, *Inorg. Nucl. Chem. Lett.*, 1, 161 (1971).

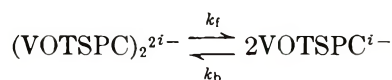
Table I: Spectral Concentration Quotients

Absorbance ^a	[VOTSPC] _T , ^b <i>M</i>	10 ⁷ <i>Q</i> , <i>M</i> ^c
0.041	5.0 × 10 ⁻⁷	3.0
0.068	1.0 × 10 ⁻⁶	2.9
0.230	5.0 × 10 ⁻⁶	3.0
0.395	1.0 × 10 ⁻⁵	2.8
0.855	2.5 × 10 ⁻⁵	3.0
1.570	5.0 × 10 ⁻⁵	3.0

^a Measured at 692 nm. ^b Represents the total concentration, *C*, of V^{IV}-TSPC. ^c The monomer and dimer concentrations were calculated from the equation $A = (\epsilon_M - \epsilon_D/2)M + (\epsilon_D/2)C$.

measurements on the more concentrated solutions were done with a cell of 1-mm path length. The concentration quotients determined spectrally at the different temperatures are $1.1 \pm 0.1 \times 10^{-7} M$ (28°), $1.9 \pm 0.2 \times 10^{-7} M$ (38°), $2.9 \pm 0.1 \times 10^{-7} M$ (50°), respectively, at $\mu = 0.006$ (NaClO₄).

Kinetic Results. Kinetic data obtained at total vanadium(IV)-TSPC concentrations $5 \times 10^{-6} M$ or less give linear plots for the logarithm of the light transmission *vs.* time indicating a single relaxation process. The results are consistent with a dimer-monomer equilibrium



with the reciprocal relaxation time being

$$\tau^{-1} = 4k_b[\text{VOTSPC}^{i-}] + k_f$$

where [VOTSPC^{*i*-}] is the equilibrium monomer concentration having charge *i*. Spectral measurements of the monomer-dimer equilibrium made under the same experimental conditions allows the concentration of the monomer to be calculated from the total vanadium(IV)-TSPC used. Figure 3 is a plot of τ^{-1} *vs.* monomer concentration at different temperatures from which the rate constants were obtained. The values of *k_f* and *k_b* at different temperatures are $0.9 \pm 0.1 \text{ sec}^{-1}$, $4.5 \pm 0.3 \times 10^6 M^{-1} \text{ sec}^{-1}$ (28°); $2.0 \pm 0.2 \text{ sec}^{-1}$, $5.5 \pm 0.5 \times 10^6 M^{-1} \text{ sec}^{-1}$ (38°); and $4.5 \pm 0.2 \text{ sec}^{-1}$, $8.4 \pm 0.8 \times 10^6 M^{-1} \text{ sec}^{-1}$ (50°), respectively, at $\mu = 0.006$ (NaClO₄). The ratio of the rate constants gives the following concentration quotients at various temperatures: $2.0 \pm 0.7 \times 10^{-7} M$ (28°); $3.6 \pm 0.5 \times 10^{-7} M$ (38°); $5.4 \pm 0.7 \times 10^{-7} M$ (50°), respectively, at $\mu = 0.006$ (NaClO₄).

From plots of $\ln(k/T)$ *vs.* $1/T$ the activation parameters ΔH^\ddagger and ΔS^\ddagger are $13.6 \pm 1.5 \text{ kcal/mol}$ and $-14 \pm 5 \text{ eu}$ for *k_f* and $4.9 \pm 1.5 \text{ kcal/mol}$ and $-12 \pm 5 \text{ eu}$ for *k_b*. The difference in the enthalpies of activation for the rate constants *k_f* and *k_b* yields a ΔH° of $8.7 \pm 3.0 \text{ kcal/mol}$.

A comparison of the concentration quotients deter-

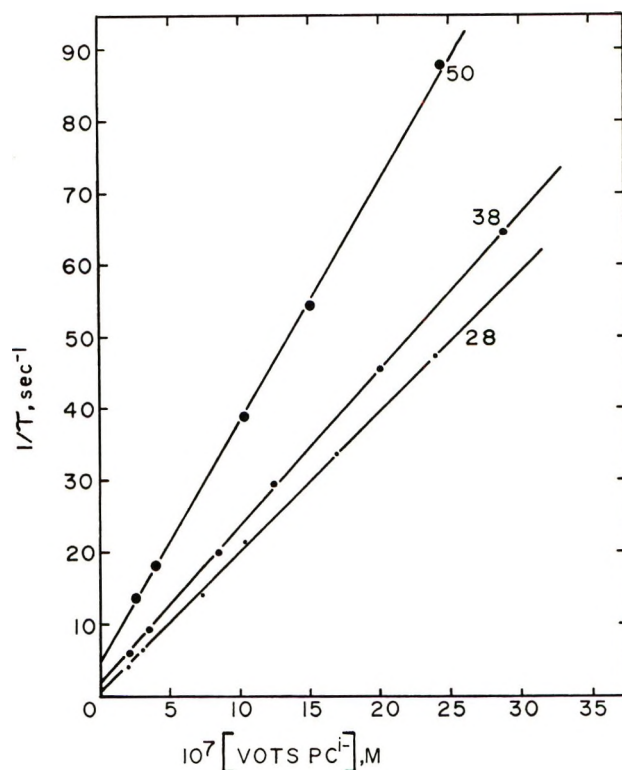
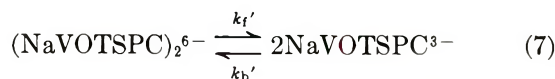
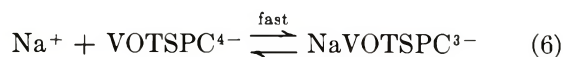
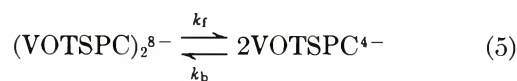


Figure 3. $1/\tau$ *vs.* [VOTSPC^{*i*-}] at 28, 38, and 50° at $\mu = 0.006$ (NaClO₄).

mined from rate data with the values obtained from spectral measurements shows a discrepancy which is outside the limit of experimental error. If the sodium salt of Na₄VOTSPC is completely dissociated in aqueous solution, then the monomeric species would assume a charge of -4 and the dimer -8, respectively. These charges are very high indeed, and it seems rather unlikely that no cation association occurs especially since 0.006 *M* sodium perchlorate is added. Therefore, it is quite possible that one or more species of the type NaVOTSPC³⁻, Na₂VOTSPC²⁻, etc., can form having essentially the same intrinsic optical absorptivities. If it is assumed that a relatively simple condition exists where the following equilibria are proposed



and the equilibrium of (6) occurs rapidly compared to (5) and (7) with (6) being coupled to (7), then the inverse of one relaxation time becomes

$$\frac{1}{\tau} = 4k_b'[\text{NaVOTSPC}^{3-}] \times \frac{K([\text{Na}^+] + [\text{VOTSPC}^{4-}])}{1 + K([\text{Na}^+] + [\text{VOTSPC}^{4-}])} + k_f'$$

which may be simplified to

$$\frac{1}{\tau} \simeq 4k_b'[\text{NaVOTSPC}^{3-}] \frac{K[\text{Na}^+]}{1 + K[\text{Na}^+]} + k_f'$$

where

$$K \equiv \frac{[\text{NaVOTSPC}^{3-}]}{[\text{Na}^+][\text{VOTSPC}^{4-}]}$$

The equilibration of (5) is assumed to be sufficiently slow so that it will not contribute to the relaxation expression shown above. Slower rates would be expected for the higher charged species based on electrostatic arguments.⁴ The concentration quotient obtained from spectral measurements need not be a ratio of a single monomeric and dimeric species but a ratio of their concentration sums

$$Q_{\text{spectral}} = \frac{[\text{monomer, total}]^2}{[\text{dimer, total}]} = \frac{([\text{VOTSPC}^{4-}] + [\text{NaVOTSPC}^{3-}])^2}{[(\text{VOTSPC})_2^{8-}] + [(\text{NaVOTSPC})_2^{6-}]}$$

Substitution of VOTSPC^{4-} in terms of its equilibrium constant, K yields the alternate expression for Q_{spectral}

$$Q_{\text{spectral}} = \frac{[\text{NaVOTSPC}^{3-}]^2 \left[\frac{K[\text{Na}^+] + 1}{K[\text{Na}^+]} \right]^2}{[(\text{VOTSPC})_2^{8-}] + [(\text{NaVOTSPC})_2^{6-}]}$$

By using Q_{spectral} , the quantity

$$[\text{NaVOTSPC}^{3-}] \frac{K[\text{Na}^+] + 1}{K[\text{Na}^+]}$$

can be calculated which is not the expression to be plotted to obtain k_b' and k_f' . Under the proposed conditions the ratio k_f'/k_b' will not be in agreement with the Q_{spectral} value. In an analogous manner it can be shown that there will also be nonagreement between the ratio k_f'/k_b' and the Q_{spectral} value.

A second plausible explanation for the discrepancy between the kinetic and spectral concentration quotients may be due to the formation of small amounts of higher polymers which cannot be detected by spectroscopic methods. Support for both these arguments is presented below from the kinetic studies.

When the total vanadium(IV)-TSPC concentration exceeds $5 \times 10^{-6} M$, plots of the logarithm of the light transmission *vs.* time are slightly curved. If two relaxations are assumed, this is sufficient to represent the data quantitatively. The two relaxation times can be obtained by first determining the longer relaxation time from the linear portion of the curve at long times. The linear portion of the curve is then extended to shorter times and subtracted from the experimental curve. The shorter relaxation time can then be determined from the resultant straight line. Owing to the small absorbance change, the shorter re-

laxation time could not be obtained. However, there were several interesting characteristics associated with the shorter relaxation process. First, two relaxations are detected at the monomer band (692 nm), while only the one slow relaxation is observed at the 660-nm band (dimer maximum). Second, the shorter relaxation process is observed only at concentrations in excess of $5 \times 10^{-6} M$ where both monomer and dimer are present in appreciable amounts. The change in light transmittance associated with the shorter relaxation time increases slightly as the total concentration of V^{IV}-TSPC is increased. The two relaxations are consistent with the proposed cation association in that the faster relaxation time would be associated with the coupled equilibria between (6) and (7), while the slower relaxation would be attributed to equilibrium 5. When the total concentration of V^{IV}-TSPC is increased, larger amounts of $(\text{NaVOTSPC})_2^{6-}$ could be generated, and this would explain the increase in light transmittance observed. Equations 5, 6, and 7 are not the only set of equilibria possible since another set of equilibria could be postulated involving cation associated species such as $\text{Na}_2\text{VOTSPC}^{2-}$, $(\text{Na}_2\text{VOTSPC})_2^{4-}$, etc. The kinetic measurements made at 660 nm either are of insufficient sensitivity to detect two relaxations or there is no measurable difference in the optical absorptivity of the dimeric species.

Two relaxations could also be attributed to higher polymer formation at concentrations exceeding $5 \times 10^{-6} M$, where the polymer is formed from monomer(s) and/or dimer(s) with no cation associated species present. However, in the higher polymer, the dimer either maintains its spectral integrity or measurements carried out at 660 nm are not of sufficient sensitivity to detect the more rapid relaxation process. Kuhn and coworkers^{9,11} have shown from spectral studies of metal-free phthalocyanine sulfonate and copper(II)-TSPC solutions with no added salts, that about 4% of a $10^{-4} M$ total dye concentration is present as a tetramer. Addition of salts increases the tetramer concentration.¹⁰ Therefore, it seems quite plausible that a small amount of complexes having a higher degree of association (*i.e.*, greater than the dimer) can form at the more concentrated vanadium(IV)-TSPC solutions. However, the primary equilibrium at vanadium(IV)-TSPC concentrations of 5.0×10^{-7} to $5.0 \times 10^{-5} M$ is that between monomer and dimer.

A study of the pH dependence was made to determine whether the dimerization process involves hydrolysis. The pH of the V^{IV}-TSPC solutions in the concentration range of 10^{-7} to $5 \times 10^{-5} M$ varies slightly assuming a value of 5.8 ± 0.1 . Introduction of either acid or base has the same effect as salt in that

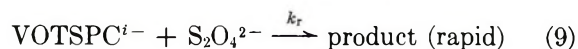
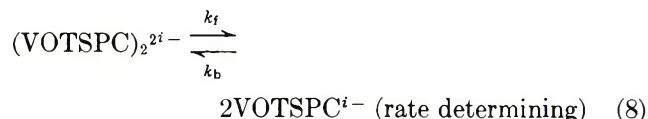
(11) U. Ahrens and H. Kuhn, *Z. Phys. Chem. (Frankfurt am Main)*, **37**, 1 (1963).

the equilibrium is shifted in favor of the dimer. This is presumably due to the increase in the ionic strength of the solution. Kinetics studies made at pH values of 9.1 and 3.0, a range where the monomer-dimer equilibrium is still maintained, give relaxation times which are slower than the values obtained at a pH of 5.8. This observation is consistent with the decrease in the monomer concentration as indicated by spectral measurements. A comparison of these relaxation times at the proposed lower monomer concentration with the values extrapolated from the τ^{-1} vs. monomer concentration plot show good agreement and are well within the discrepancy between the spectral and kinetic results. This same effect has also been observed in the Cu^{II} -TSPC system¹² so hydrolysis can be excluded from the reaction mechanism.

Any further discussion regarding the mechanism by which the dimer is formed should preferably require some knowledge of the dimer structure in solution which is unknown. It has been proposed in the Co^{II} -TSPC system¹³ that the dimer is formed by the overlapping of the extended π -electron clouds of the highly conjugated TSPC molecules of two parallel monomeric species (staggered, stacking), and this structure would certainly be applicable to the V^{IV} -TSPC dimer. Magnetic studies¹⁴ on the oxyvanadium(IV) phthalocyanine complex suggest a five-coordinate structure which is presumably square pyramidal. If this structure represents the monomeric species of V^{IV} -TSPC in solution, then the structure of the dimer could be as described above with the vanadyl oxygen groups probably occupying the two axial trans positions. However, an alternate mechanism involving the formation of a VOV bridged structure cannot be ruled out. Such structures have been proposed in the Mn^{III} -TSPC⁵ and aluminum phthalocyanine systems.¹

Some experiments were conducted with the (Durrum-Gibson) stopped flow apparatus to examine the effect of different reducing agents on the monomer-dimer equilibrium. Preliminary studies using sodium di-

thionite indicate the rate of reduction is independent of dithionite concentration. The results are consistent with the following reaction scheme



Assuming steady-state conditions for the monomeric species the observed rate constant is equal to k_f . The value of the observed rate constant is 0.5 sec^{-1} at about 22° and $\mu = 0.006 M$ which is within experimental error of an extrapolated value of 0.45 sec^{-1} obtained for k_f under the same conditions. This suggests that the monomer is preferentially reduced by dithionite.

A few stopped-flow experiments were also carried out using aqueous vanadium(II) as the reducing agent. The rate of reduction of vanadium(IV)-TSPC was followed spectrophotometrically at 425 nm. When aqueous vanadium(II) and vanadium(IV)-TSPC are mixed, a large absorbance increase occurs at 425 nm which decreases over several minutes. A similar absorbance change is observed for the V^{2+} - $\text{VO}_{\text{aq}}^{2+}$ reaction where an intermediate VOV^{4+} is observed.¹⁵ This suggests reduction occurs by attack of the aqueous vanadium(II) at the vanadium(IV) oxygen in VOTSPC^{i-} . More work will be done in this area to clarify this point.

Acknowledgment. The authors wish to acknowledge support of this work by the National Institutes of Health through Grant GM 11767.

(12) R. Farina, presented at the 23rd Southeastern Regional Meeting of the American Chemical Society, Nashville, Tenn.

(13) Z. A. Schelly, D. J. Harward, P. Hemmes, and E. M. Eyring, *J. Phys. Chem.*, **74**, 3040 (1970).

(14) A. B. P. Lever, *J. Chem. Soc.*, 1821 (1965).

(15) F. B. Baker and T. W. Newton, *Inorg. Chem.*, **3**, 569 (1964).

The Kinetics of Adsorption of Carbon Monoxide on Alumina

by A. Stanislaus, M. J. B. Evans,* and R. F. Mann

Department of Chemistry and Chemical Engineering, Royal Military College of Canada, Kingston, Ontario, Canada (Received February 7, 1972)

Publication costs assisted by the Defence Research Board of Canada

The rate of adsorption of carbon monoxide by alumina has been measured in the temperature range 151–295° by measuring the decrease in pressure in a closed system as a function of time. Analysis of the results using the Elovich equation leads to the conclusion that two distinct adsorption processes occur. The effects of preadsorbed ammonia and water vapor and of reducing the surface with hydrogen and carbon monoxide suggest that surface hydroxyl groups and surface oxide ions are the most probable adsorption sites.

Introduction

Alumina has been used widely as a catalyst and catalyst support in many processes of industrial importance such as isomerization, alkylation, dehydration, cracking, polymerization, and re-forming. Recently the surface properties of alumina have received much attention. Various studies have shown that the alumina surface contains centers of different acidities.^{1–3} Infrared studies of alumina^{4,5} and of ammonia,⁶ pyridine,⁷ carbon dioxide,^{8,9} butene,¹⁰ and acetylene¹¹ adsorbed on alumina have provided considerable information about the surface structure of alumina. Although the adsorption of carbon monoxide on alumina has been investigated by several workers by means of infrared spectroscopy,^{12–15} the adsorption kinetics of the process appears to have received little or no attention.

A detailed investigation of the kinetics of carbon monoxide adsorption on alumina and the effects of preadsorbing ammonia and water vapor on the surface are described in this paper. The effect of reducing the surface prior to adsorption was also studied.

Experimental Section

Materials. *Alumina.* Aluminum hydroxide was precipitated from a solution of aluminum nitrate at 90° by the slow addition of ammonium hydroxide. The precipitate was filtered, washed, and dried at 120° for 48 hr. The alumina was found to have a BET surface area of 169 m² g⁻¹ from a low-temperature nitrogen adsorption isotherm.

Carbon Monoxide. Research grade carbon monoxide was used as supplied (minimum purity 99.99%).

Apparatus and Procedure. The adsorption experiments were carried out in a constant-volume apparatus. The gas pressure in the system was monitored using a digital manometer (Dynasciences Corp., Model DM1), the output of which was recorded continuously. Prior to adsorption kinetic experiments the catalyst was heated in air at 450° and then evacuated for 14 hr at 550°.

As gas was adsorbed by the sample during a run, the pressure decrease in the system was measured. From the known volume of the system and the experimental pressure–time curves, the amount of gas adsorbed as a function of time was calculated.

In the series of experiments involving preadsorbed ammonia or water vapor, the alumina sample was equilibrated with the adsorbate vapor after degassing. The amount of material adsorbed was calculated from the pressure decrease in the closed system. In all cases the equilibrium pressure was negligible.

Data Analysis. The experimental adsorption kinetic data were analyzed using the Elovich equation.^{16,17} In its differential form, the Elovich equation

$$dq/dt = a \exp(-bq) \quad (1)$$

describes the rate of adsorption in terms of the amount adsorbed, q , at time t ; a and b are coefficients which depend on temperature and pressure. The integrated form of the equation is

- (1) H. Pines and W. O. Haag, *J. Amer. Chem. Soc.*, **82**, 2471 (1960).
- (2) A. Stanislaus and L. M. Yeddnapalli, *Can. J. Chem.*, in press.
- (3) L. H. Little, "Infrared Spectra of Adsorbed Species," Academic Press, New York, N. Y., 1966, p 180.
- (4) J. B. Peri and R. B. Hannan, *J. Phys. Chem.*, **64**, 1526 (1960).
- (5) J. B. Peri, *ibid.*, **69**, 211 (1965).
- (6) J. B. Peri, *ibid.*, **69**, 231 (1965).
- (7) E. P. Parry, *J. Catal.*, **2**, 371 (1963).
- (8) N. D. Parkyns, "Third Congress on Catalysis," Vol. II. North-Holland Publishing Co., Amsterdam, 1965, p 914.
- (9) N. D. Parkyns, *J. Chem. Soc.*, **A**, 410 (1969).
- (10) J. B. Peri, *Actes Congr. Int. Catalyse*, **2**, Paris, **1**, 1353 (1961).
- (11) D. J. C. Yates and P. J. Lucchesi, *J. Chem. Phys.*, **35**, 243 (1961).
- (12) N. D. Parkyn, *J. Chem. Soc.*, **A**, 1910 (1967).
- (13) L. H. Little and C. H. Amberg, *Can. J. Chem.*, **40**, 1997 (1962).
- (14) J. B. Peri, *J. Phys. Chem.*, **72**, 2917 (1968).
- (15) V. I. Yakerson, L. I. Lafer, V. Ya. Danyushevskii, and A. M. Rubinshtein, *Izv. Akad. Nauk SSSR, Ser. Khim.*, **26** (1969); *Chem. Abstr.*, **70**, 91142g (1969).
- (16) M. J. D. Low, *Chem. Rev.*, **60**, 267 (1960).
- (17) C. Aharoni and F. C. Tompkins, *Advan. Catal. Relat. Subj.*, **21**, 1 (1970).

$$q = \frac{1}{b} \ln(t + t_0) - \frac{1}{b} \ln t_0 \quad (2)$$

where $t_0 = 1/ab$. If a volume of gas q_0 is adsorbed instantaneously and before eq 1 begins to apply, eq 2 has to be modified¹⁶ to

$$q = \frac{1}{b} \ln(t + k) - \frac{1}{b} \ln t_0 \quad (3)$$

where $k = t_0 \exp(bq_0)$. This modified form of the Elovich equation has been used to analyze data obtained in the present study. By suitable choice of the constant k , the initial portion of each kinetic run could be linearized.

Results

Influence of Temperature. Adsorption kinetics of carbon monoxide on alumina was studied at 151, 205, 258, and 295°. The amount of gas adsorbed, q , in moles per second per gram of catalyst, plotted against $\ln(t + k)$ is shown in Figure 1 for each of these temperatures. Values of the Elovich parameters calculated from the Elovich plots are given in Table I. The subscripts 1 and 2 refer to the first and second linear portions of the Elovich plots. The rate of adsorption of carbon monoxide depends primarily on the value of b ; the smaller the value of b , the larger is the rate of adsorption. The preexponential factor a influences the rate only slightly. From Table I and Figure 1 it will be seen, therefore, that adsorption is very much slower at 151° than at the three higher temperatures.

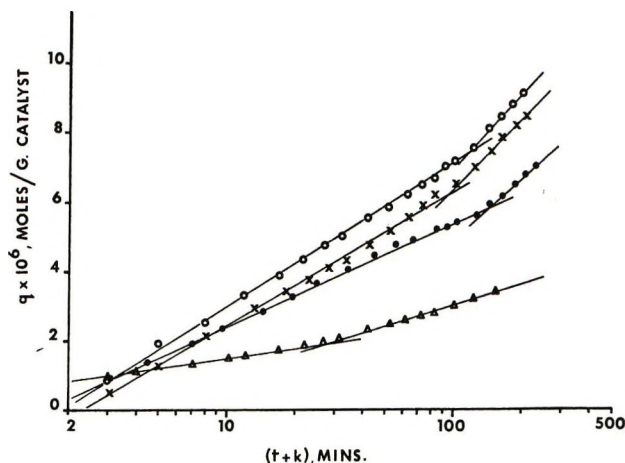


Figure 1. Elovich plots for various temperatures. (Initial CO pressure = 3.66 cm in each case.) Δ , 151°; \bullet , 205°; \times , 258°; \circ , 295°.

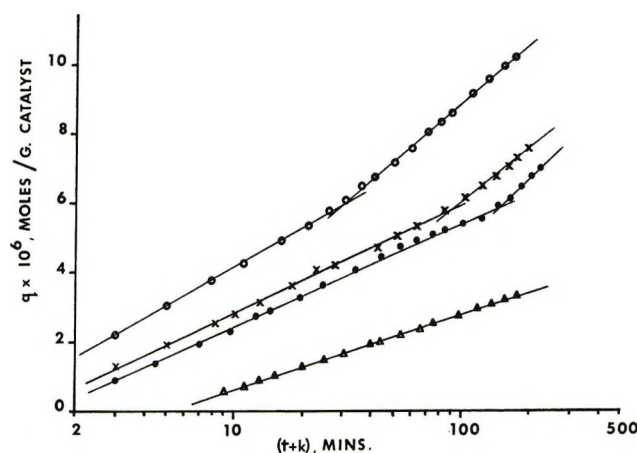


Figure 2. Elovich plots for various initial pressures (temperature 205°): Δ , 1.79 cm; \bullet , 3.66 cm; \times , 8.36 cm; \circ , 16.55 cm.

Table I: Influence of Temperature on Elovich Parameters (Initial CO Pressure = 3.66 cm)

Temp, °C	$b_1 \times 10^{-5}$, (mol/g of cat.) ⁻¹	$b_2 \times 10^{-5}$, (mol/g of cat.) ⁻¹	$a_1 \times 10^7$, (mol/g of cat.) min ⁻¹	$a_2 \times 10^7$, (mol/g of cat.) min ⁻¹	$q_0 \times 10^7$, mol/g of cat.	k , min
151	26.1	12.28	5.26	1.75	7.30	2
205	7.72	4.75	8.23	2.214	5.70	2
258	6.52	3.26	8.60	2.344	...	2
295	5.53	2.94	9.17	2.55	...	2

Table II: Influence of Pressure on Elovich Parameters (Temperature = 205°)^a

Pressure, cm	$b_1 \times 10^{-5}$	$b_2 \times 10^{-5}$	$a_1 \times 10^7$	$a_2 \times 10^7$	$q_0 \times 10^7$	k , min
1.79	10.79	...	1.77	...	2.6	8
3.66	7.72	4.75	8.23	2.214	5.7	2
8.36	7.10	4.52	9.48	3.49	...	2
16.55	6.39	3.93	21.20	8.075	13.0	2

^a Units as in Table I.

Influence of Pressure. Kinetic measurements were made at a variety of initial pressures in order to determine the pressure dependence of the Elovich parameters. The results are summarized in Figure 2. At the lowest initial pressure used, no break was found in the Elovich plot. In all other cases, two linear portions occur, the break being earlier the higher the initial pressure. The Elovich parameters calculated from the graphs in Figure 2 are given in Table II.

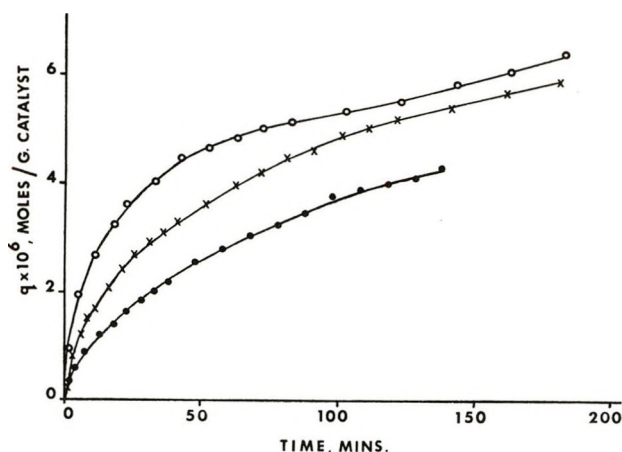
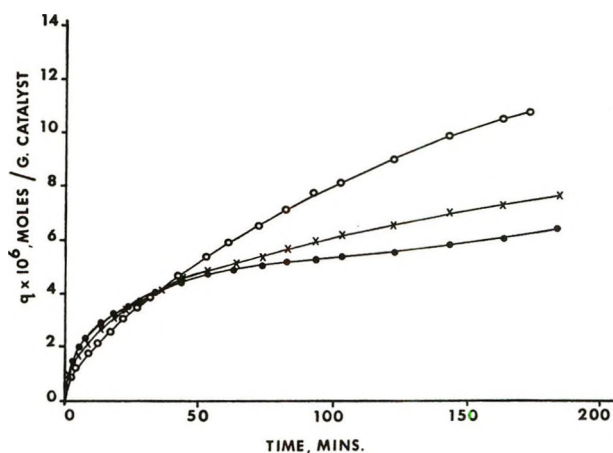
Effect of Preadsorbed Ammonia. Figure 3 shows the q vs. t plots for the adsorption of carbon monoxide on alumina on which ammonia had been preadsorbed com-

pared with adsorption on untreated alumina at the same temperature and initial pressure. It will be seen that both the rate and amount of carbon monoxide adsorbed are decreased by preadsorbed ammonia. Elovich parameters calculated for these runs are given in Table III.

Effect of Preadsorbed Water Vapor. The rate and extent of carbon monoxide adsorption on alumina are

Table III: Influence of Preadsorbed Gases on Elovich Parameters^a

Pre-adsorbed gas	Amount preadsorbed, mol/g of cat.	$b_1 \times 10^{-6}$	$b_2 \times 10^{-6}$	$a_1 \times 10^7$	$a_2 \times 10^7$	$q_0 \times 10^7$	k, min
NH ₃	7.6×10^{-6}	10.44	5.58	4.43	2.55	...	1
NH ₃	13.5×10^{-6}	16.42	6.64	2.76	1.67	...	1
H ₂ O	4.13×10^{-6}	6.05	3.70	4.89	2.45	6.25	5
H ₂ O	10.10×10^{-6}	5.77	2.01	3.94	2.40	4.7	6

^a Units as in Table I. (Initial CO pressure = 3.66 cm.)**Figure 3.** Adsorption of CO as a function of time after preadsorption of ammonia ($T = 205^\circ$; initial CO pressure = 3.66 cm.): O, no NH₃ preadsorbed; X, 7.6×10^{-6} mol of NH₃/g of catalyst preadsorbed; ●, 13.5×10^{-6} mol of NH₃/g of catalyst preadsorbed.**Figure 4.** Adsorption of CO as a function of time after preadsorption of water vapor ($T = 205^\circ$; initial CO pressure = 3.66 cm.): ●, no H₂O preadsorbed; X, 4.13×10^{-6} mol of H₂O/g of catalyst preadsorbed; O, 10.10×10^{-6} mol of H₂O/g of catalyst preadsorbed.

increased by the presence of preadsorbed water vapor as can be seen from Figure 4. Elovich parameters for these runs are included in Table III.

Effect of Reduction of Surface. Two experiments were performed to examine the role of surface oxide and -OH groups in the adsorption of carbon monoxide on alumina. In the first experiment the catalyst was heated in a current of hydrogen at 450° for 3 hr and then evacuated at 550° for 14 hr. The catalyst was cooled to the reaction temperature (205°) and the adsorption kinetics studied. In the other experiment the catalyst was heated in the presence of 7.6 cm pressure of carbon monoxide at 450° for 2 hr. After evacuating at 550° for 14 hr the catalyst was cooled to 205° and the kinetics of carbon monoxide adsorption was mea-

sured. The influence of these reduction treatments on the Elovich parameters can be seen in Table IV.

Discussion

Discontinuities in Elovich plots have been explained in terms of surface heterogeneity, anisotropy, surface contamination, and surface complexes.^{16,17} However, the suggestion by Taylor and Thon¹⁸ that the breaks indicate a change from adsorption on one type of adsorption site to adsorption on another type is considered to be the most likely explanation. Additional evidence for the existence of two types of adsorption site for carbon monoxide on alumina in the temperature range $100\text{--}300^\circ$ has been obtained recently from temperature programmed desorption studies.¹⁹ Both types of site may be present on the outgassed alumina surface or the second type may be induced by adsorption on the first type of site.

The sites involved in the adsorption of carbon monoxide on alumina have been investigated by means of infrared studies.¹²⁻¹⁵ Parkyn¹² and Little and Am-

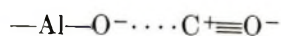
Table IV: Influence of Reduction of Alumina Surface on Elovich Parameters^a

Reducing agent	$b_1 \times 10^{-6}$	$b_2 \times 10^{-6}$	$a_1 \times 10^7$	$a_2 \times 10^7$	$q_0 \times 10^7$	k, min
H ₂	16.80	9.3	6.25	4.115	5.2	2
CO	10.97	4.99	2.97	1.51	1.04	9

^a Units as in Table I. (Initial CO pressure = 3.66 cm.)(18) H. A. Taylor and N. Thon, *J. Amer. Chem. Soc.*, **74**, 4169 (1952).

(19) B. H. Harrison and S. S. Barton, private communication.

berg¹³ have suggested that carbon monoxide is adsorbed on oxide ion sites by a dipole type interaction



Peri¹⁴ suggested that two types of site existed for carbon monoxide on alumina, the oxide ion sites and α -sites ($\text{Al}^+\text{O}^{2-}\text{Al}^+$ groupings). Recently Yakerson and coworkers¹⁵ concluded that $-\text{OH}$ groups participated in the adsorption of CO on alumina.

In the present work the rate and extent of adsorption was reduced by the preadsorption of ammonia. It is known that ammonia is adsorbed on Lewis acid sites (exposed aluminum ions), the surface hydroxyl groups, and surface oxide ions on alumina.³ Since preadsorbed ammonia decreases the rate of carbon monoxide adsorption, it is suggested that these same sites are involved in the adsorption of CO.

Removal of surface oxide and hydroxyl groups by reduction with hydrogen or carbon monoxide also leads to a reduction in the rate of adsorption of carbon monoxide and in the amount adsorbed. This again suggests that surface oxide ions and surface hydroxyl groups are involved in the adsorption of carbon monoxide. Preadsorption of water, presumably creating more $-\text{OH}$ sites, has the opposite effect. The extra $-\text{OH}$ sites are created at the expense of Al^+ sites so that one would expect greater adsorption after preadsorption of water. Thus the evidence suggests that two types of site are involved in the adsorption of carbon monoxide on alumina, these being surface oxide ions and hydroxyl groups. Which of these sites is respon-

sible for the first linear region observed in Elovich plots and which for the second cannot be decided from the results obtained. This interpretation may well be a gross simplification of the actual situation. It is possible that the sites involved in carbon monoxide adsorption are determined to some extent by the nearest neighbor groups on the surface and are not simply all surface hydroxyl or oxide sites. The existence of different types of hydroxyl groups on alumina has been discussed by Peri.²⁰ Thus the two types of site may involve particular arrangements of surface groups rather than just the surface oxide and hydroxyl groups alone.

Conclusions

Analysis of the kinetic data obtained for the adsorption of carbon monoxide on alumina using the Elovich equation shows that two distinct adsorption processes occur, probably involving two types of surface site. Changes observed following preadsorption of ammonia and water vapor and after reduction of the alumina surface by hydrogen and by carbon monoxide suggest that the adsorption of carbon monoxide occurs principally on surface oxide ion and hydroxyl group sites rather than on Al^+ ions.

Acknowledgment. The work described in this paper was supported by the Defence Research Board of Canada, Grant No. 9530-64.

(20) J. B. Peri, *J. Phys. Chem.*, **69**, 220 (1965).

Reactions Involving Electron Transfer at Semiconductor Surfaces. III.

Dissociation of Methyl Iodide over Zinc Oxide¹

by Joseph Cunningham* and A. L. Penny

Department of Chemistry, University College, Cork, Ireland (Received August 9, 1971)

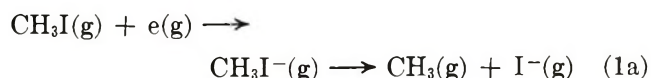
Publication costs borne completely by The Journal of Physical Chemistry

Gaseous methyl iodide has been observed to undergo dissociation when contacted with semiconducting zinc oxide at 20° in the absence of any illumination. Additional dissociation of methyl iodide was observed at the CH₃I-ZnO interface under illumination by ultraviolet light of wavelengths longer than 290 nm. The gas-phase product of the dissociation in the presence and absence of illumination was methane. At room temperature in the dark, adsorption obeyed a Langmuir type isotherm and monolayer coverage was closely approached at all methyl iodide pressures $>5 \times 10^{-2}$ Torr. Conductivity and esr studies of zinc oxide layers showed initial electron localization by adsorbed methyl iodide but also revealed a secondary process which slowly returned electrons to the conduction band. Parallel studies on kinetics of methane formation at CD₃I-ZnO interfaces revealed marked differences between ZnO surfaces preactivated at 350 or 500°. Samples baked *in vacuo* at 350° had lower dark conductivity and CD₃H represented $>50\%$ of methanes produced in the initial 30 min dark reaction, thus implying hydrogen transfer reactions with residual surface hydroxyls. Kinetics of initial methane production, or of decrease in conductivity, were consistent with electron localization being rate determining at these hydroxylated surfaces, followed by fast reaction with surface hydroxyls. Samples baked *in vacuo* to 500° prior to CD₃I adsorption had higher conductivity and CD₄ was the major methane product. Kinetics analysis indicated that electron localization was fast at these dehydroxylated surfaces and that reaction of CD₃I⁻(ads) with CD₃I(ads) was rate determining. The isotopic composition of additional methane produced when CD₃I-ZnO interfaces were illuminated with photons inside the ZnO band edge, resembled the composition of methanes formed in dark reaction at the same surface. The apparent initial quantum efficiency of the photoassisted methane formation was *ca.* 3×10^{-5} , but kinetics of this process, like kinetics of the slow secondary dark reaction, were complex and the mechanisms are not yet fully understood.

Introduction

Investigations carried out by the authors² on the transfer and sharing of electrons between n-type semiconducting oxides and nitrous oxide adsorbed on their surfaces at room temperature revealed dissociation of the nitrous oxide to a very limited extent in the dark and additional dissociation under uv illumination. In explanation of these phenomena it was proposed that nitrous oxide, a well known electron-attaching agent in liquid³ or gaseous systems,^{4,5} decomposed by dissociative electron attachment when contracted with the surfaces of n-type zinc oxide and ferric oxide. This paper presents the results of the continuation of these investigations employing methyl iodide as an adsorbate and zinc oxide as an adsorbent.

Methyl iodide has been widely used as an electron attaching additive in gaseous,^{6,7} liquid,⁸ or heterogeneous systems.^{9,10} It is generally considered that electron attachment in the gas phase is accompanied by dissociation according to



Mass spectrometric studies showed that electrons at thermal energies were sufficient to effect dissociation *via* (1a), but that an electron energy threshold of 2 eV

was required to effect the analogous process with N₂O(g). Since nitrous oxide was already shown to undergo dissociative electron attachment at dark and uv-illuminated zinc oxide surfaces,² the reported lower threshold for dissociative electron attachment to methyl iodide in the gas phase⁷ made it appear probable that methyl iodide would undergo the analogous process (1b) on zinc oxide, *i.e.*



(1) This work is supported in part by the U. S. Air Force Office of Scientific Research through the European Office of Aerospace Research, OAR, United States Air Force, under Contract AF 61(052)-67C-0044.

(2) (a) J. Cunningham, J. J. Kelly, and A. L. Penny, *J. Phys. Chem.*, **74**, 1992 (1970); (b) J. Cunningham, J. J. Kelly, and A. L. Penny, *ibid.*, **75**, 617 (1971).

(3) G. Scholes and M. Simic, *Nature (London)*, **202**, 895 (1964).

(4) A. V. Phelps and R. E. Voshall, *J. Chem. Phys.*, **49**, 3246 (1968).

(5) J. M. Warman, *Nature (London)*, **213**, 381 (1967).

(6) G. Jacobs and A. Henglen, *Z. Naturforsch.*, **19a**, 906 (1964).

(7) V. H. Dibeler and R. M. Reese, *J. Res. Nat. Bur. Stand.*, **54**, 127 (1955).

(8) P. R. Geissler and J. E. Willard, *J. Amer. Chem. Soc.*, **84**, 4627 (1962).

(9) R. F. Claridge and J. E. Willard, *ibid.*, **87**, 4992 (1965).

(10) N. H. Sagert, J. A. Reid, and R. W. Robinson, *Can. J. Chem.*, **48**(1), 17 (1970).

At dark CH_3I -ZnO interfaces, process 1b is only probable when the symbol $e(\text{ZnO})$ in (1b) corresponds to electrons with equilibrium Boltzmann distribution between conduction band and shallow donor levels. The reduced energy of electrons in the valence band or of electrons trapped at deep electron traps (depth $\gg kT$), renders involvement of such electrons in (1b) energetically improbable at the dark interface.

Illuminating a CH_3I -ZnO interface with photons of energies greater than the band gap of ZnO, 3.2 eV (photons of $\lambda < 385$ nm) generates electron-hole pairs which may remain correlated (excitons), or autoionize giving a hole in the valence band plus an electron within the conduction band but initially not in equilibrium with other electrons in that band. Electrons at deep traps may also be promoted into the conduction band by visible and near-infrared illumination. Electron localization as in (1b) might therefore involve electrons from any of these sources at the uv-illuminated CH_3I -ZnO interface. The virtual transparency of methyl iodide at low gas pressures to light of wavelengths >300 nm¹¹ allows these additional photo-induced possibilities for charge transfer to be explored at such wavelengths without significant direct excitation of methyl iodide.

Results reported very recently of infrared studies on high surface area zinc oxides established that extensive hydroxylation of the surface persists after preactivation at 350° but that above this "critical" temperature rapid loss of surface hydroxyls occurs.¹² The possible role of surface hydroxyls in bringing about reaction at dark or illuminated methyl iodide-ZnO interfaces may therefore be examined in the present study by comparison of results obtained over zinc oxide samples preactivated at 350° with results over surfaces preactivated at higher temperatures. Mass spectrometric analysis of product(s) from CD_3I -ZnO interfaces is employed in this study to distinguish clearly between products arising *via* hydrogen-transfer reactions with surface hydroxyls (*e.g.*, CD_3H) and those arising *via* electron attachment (*e.g.*, CD_4 or C_2D_6).

Experimental Section

Materials. Details of the origin, surface area, and electron concentration of the zinc oxide have been given previously, together with a description of the activation treatment of the zinc oxide.² One important practical difference between the N_2O -ZnO and CH_3I -ZnO systems was that exposure of the zinc oxide to methyl iodide poisoned the activity of the oxide, which could not be regenerated by heating under vacuum. Zinc oxide samples were therefore always discarded after conducting a measurement with methyl iodide. Details of the reaction systems used in measurements of gas adsorption, gas decomposition, and oxide conductivity have been given previously^{2a} together with a description of the irradiation system.^{2b} In this present study, however, a 100-W Hanau medium-pressure mercury lamp

was used instead of a 125-W Hanovia. The esr spectra were recorded with a Decca XI spectrometer fitted with a TE_{102} mode rectangular cavity. A simple homodyne detection system was employed and the instrument was operated mainly in a "fixed frequency" mode at 9270.450 MHz and field modulation of 100 kHz. Manganese-doped magnesium oxide was used as a reference for g -value measurements. A finely powdered sample of the doped MgO in a sealed capillary tube was affixed to the outer wall of the esr tube.

Methyl iodide, BDH reagent grade, and methyl- d_3 iodide ($>95\%$ in deuterium), supplied by Prochem Ltd., were degassed under vacuum by the freeze-pump-thaw method and distilled through a 6-in. column of phosphorus pentoxide. Throughout a 6-month storage period the methyl iodide showed no detectable coloration. Methyl chloride, supplied by the Matheson Co., was purified by fractional distillation. Purity of all gases was monitored by mass spectrometric analysis. Mass spectra were recorded on a quadrupole mass spectrometer having an m/e range 4-50. The instrument was unable to resolve below m/e 4.

Experimental Results

A. Dark Reaction. (i) *Adsorption Measurements.* At room temperature the introduction of methyl iodide to a zinc oxide sample previously activated at 500° resulted in a rapid adsorption of methyl iodide. The adsorption isotherm measured at room temperature is shown in Figure 1. The adsorption data fitted a Langmuir isotherm with monolayer coverage corresponding to $V_m = 3.9 \times 10^{-1} \text{ cm}^3$ of methyl iodide. A significant practical consequence of these adsorption measurements was that monolayer coverage appeared to exist for any equilibrium pressure of methyl iodide above 5×10^{-2} Torr.

(ii) *Analysis.* Since mass spectrometric analysis of the product gas showed it to be $>99\%$ methane, which was noncondensable at liquid nitrogen tempera-

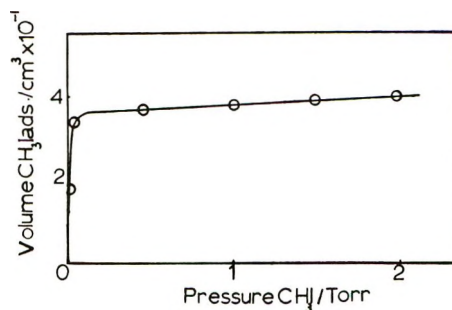


Figure 1. Adsorption of methyl iodide on 0.9-g ZnO sample activated at 500°; adsorption measured at 20°.

(11) J. G. Calvert and J. N. Pitts, "Photochemistry," Wiley, New York, N. Y., 1966.

(12) K. Atherton, G. Newbold, and J. A. Hockey, *Discussions Faraday Soc.*, 52, 33 (1971).

ture, reaction at the CH_3I -ZnO interface could be followed by measuring the pressure of the noncondensable gas with a Pirani gauge after various contact times. No ethane was observed at any stage of reaction. A trace of ethylene was observed but only during the degassing of the zinc oxide at elevated temperatures following a reaction.

In order to determine the source of the fourth hydrogen in the methane product, methyl- d_3 iodide was used in the reaction. Analysis showed the methane to be composed of CD_4 and CD_3H , showing that some hydrogen was supplied by the methyl iodide and some by the zinc oxide (see Table I).

Table I: Effect of Activation Temperature on CD_4 : CD_3H Ratio

Act. temp. °C	CD_4 : CD_3H
350	1:3
430	2:3
450	2:3
480	1:1
490	1:1
430 followed by 5×10^{-3} Torr of D_2 for 5 hr	3:1

(iii) *Influence of Activation Temperature.* The ratio CD_4 : CD_3H in the initial stages of the dark reaction depended on the activation temperature. Table I shows the increase in CD_4 : CD_3H with activation temperature. This suggested that the surface hydrogen content of the zinc oxide decreased with increasing activation. Indirect evidence that this surface hydrogen was probably in the form of OH came from the observation that water was one of the species desorbed during activation procedures. It has been suggested elsewhere¹² that dehydroxylation at high activation temperatures proceeds *via* loss of H_2O from vicinal pairs of surface hydroxyls.

(iv) *Decomposition Kinetics.* Typical results showing the increase in the volume of methane with contact time are shown in Figure 2. Although no outstanding differences are visually apparent in the shapes of the kinetic curves for different activation temperatures, it was found that while kinetic data for lower activation temperatures (350–400°) fitted Elovich kinetic plots, data for higher activation temperatures (480–500°) did not.

(v) *The Effect of Methyl Iodide Pressure.* For zinc oxide activated at 490° the reaction rate after the first 30 min contact was independent of pressure over a range of 4×10^{-2} to 50 Torr. Higher pressures showed a slight increase in the rate of reaction in its initial stages, although no difference was detected between

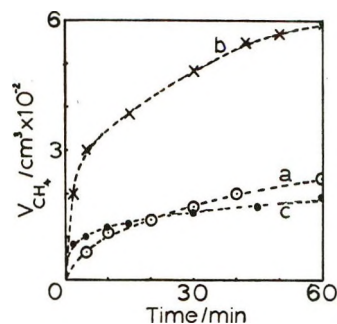


Figure 2. Formation of methane with time over: a, 6 g of ZnO activated at 490°; b, 24 g of ZnO activated at 350°; c, 12 g of ZnO activated at 350°.

these initial rates at 50 and 5 Torr. On the basis of these results it appeared that two processes were contributing to dissociation, an initial fast process with some slight dependence on pressure and a slower secondary process which was essentially pressure independent.

(vi) *Effect of Deuterium.* Zinc oxide, activated at 430°, produced an initial CD_4 : CD_3H ratio of 2:3. When 5×10^{-3} Torr of D_2 was contacted with the zinc oxide at room temperature for 5 hr following activation at 430°, a subsequent reaction of the zinc oxide with methyl iodide in the presence of the D_2 produced a CD_4 : CD_3H ratio of 7:2. This showed participation of *preadsorbed* hydrogen in the formation of product methanes, since D_2 showed no influence when a D_2 - CD_3I mixture was introduced to an activated oxide surface.

(vii) *Competition between Methyl Iodide and Methyl Chloride.* Introduction of a 1:1 mixture of methyl chloride and methyl- d_3 iodide to a zinc oxide sample activated at 490° produced a ratio of methanes resulting from CD_3I (i.e., $\text{CD}_3 + \text{CD}_3\text{H}$) to methanes resulting from CH_3Cl (i.e., $\text{CH}_3\text{D} + \text{CH}_4$) of approximately 4:1. When the CH_3Cl was introduced to the zinc oxide some seconds prior to admitting CD_3I , the above ratio became 2:5, showing that both gases were effective in reacting with surface sites in the fast initial process.

(viii) *Effect of Methyl Iodide on the Nitrous Oxide Decomposition Capacity of Zinc Oxide.* Previous work had shown that 6 g of oxide when activated had a capacity to decompose 9.6×10^{-3} cm³ of nitrous oxide. To a 6-g sample of zinc oxide activated at 490° was introduced 2.3×10^{-2} cm³ of methyl iodide. All was adsorbed. When 1.4×10^{-2} cm³ of nitrous oxide was then introduced, 3.7×10^{-3} cm³ decomposed. This amount of *preadsorbed* methyl iodide thus reduced the nitrous oxide "decomposition capacity" of zinc oxide to 40% of its value after activation at 490°.

(ix) *Esr Measurements.* The esr spectrum of a zinc oxide sample activated at 500° showed an intense singlet at $g = 1.96$ and a weak signal at $g = 2.003$. This was consistent with signals reported by other

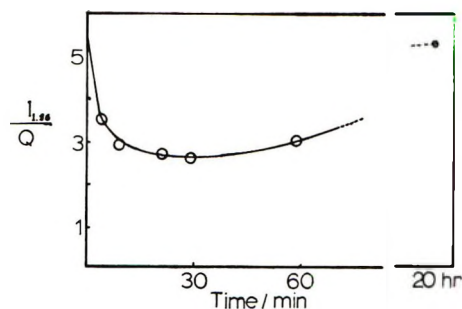


Figure 3. Variation with time of the corrected intensity of $g = 1.96$ ESR signal following introduction of CH_3I .

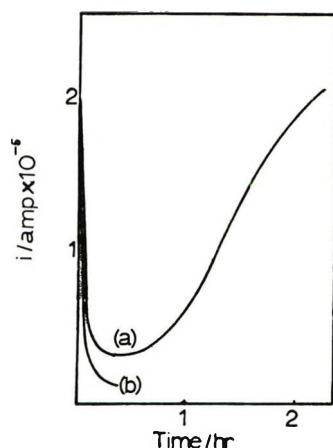


Figure 4. Change in the conductivity of activated ZnO film with time on introduction of (a) 3×10^{-2} Torr of CH_3I and (b) 5×10^{-1} Torr of CH_3I .

workers.^{13,14} The cavity Q , measured under the same conditions as the spectrum, was decreased by a factor of 0.2 relative to the unloaded cavity. Introduction of 5 Torr of methyl iodide caused the apparent intensity of the signal at $g = 1.96$ to decrease significantly but this was accompanied by an increase in the cavity Q . The intensities of the $g = 1.96$ signal ($I_{1.96}$) were normalized with respect to a constant Q . Figure 3 shows the behavior of $I_{1.96}/Q$ with time. The corrected intensity of the $g = 2.003$ signal was not affected by the methyl iodide.

(x) *Conductivity Measurements.* Methyl iodide altered the conductivity of an activated zinc oxide film in the manner shown in Figure 4, where i was the current transported by the film when a 1-V potential difference was applied across it. Note the initial drop and the subsequent rise toward its initial value. When the conductivity had returned to its original activated value, an increase in the methyl iodide pressure had no effect on it but the magnitude of the initial decrease in the current did depend on methyl iodide pressure.

B. Photoreaction. (i) *Analysis.* Because of the relatively large dark reaction occurring initially when methyl iodide was introduced to an activated zinc oxide sample, such dark reaction was allowed to proceed until

its rate had decayed to an approximately constant low value before attempting to measure photoassisted formation of product. Illuminating the dark-equilibrated interface with wavelengths longer than 290 nm caused an increase in the rate of the dissociation of methyl iodide. Use of methyl- d_3 iodide showed that the product gas, which was methane, had a $\text{CD}_4:\text{CD}_3\text{H}$ ratio equal to or greater than that of the preceding dark reaction (see Table II).

Table II: Mass Analyses of Methane Product

Conditions	—Act. temp, 350°—		—Act. temp, 490°—	
	Time, min	$\text{CD}_4/\text{CD}_3\text{H}$	Time, min	$\text{CD}_4/\text{CD}_3\text{H}$
Dark reaction	5	1/3	10	1/1
	15	2/3	20	3/1
	30	2/3	30	3/1
Illumination on	60	2/3	60	4/1
	90	2/3	100	4/1
$\text{CD}_4 : \text{CD}_3\text{H} : \text{CH}_3\text{D} : \text{CH}_4$				
Equimolar mixture CD_3I and CH_3Cl ,				
45 min dark reaction	18	32	3	10
90 min photoreaction	47	33	24	25
CH_3Cl introduced before CD_3I ,				
45 min dark reaction	2	7	4	19
24 hr photoreaction	1	3	6	20
30 min photoreaction	2	7	15	35
120 min photoreaction	3	8	15	35

(ii) *Kinetics.* The appearance of methane from the photoinduced dissociation of methyl iodide is shown in Figure 5. The rapid initial rate decays progressively over a long period. The reaction was not followed for longer than 20 hr at which time the reaction rate was comparable to the dark reaction rate. At methyl iodide pressures of 4×10^{-2} , 5, and 50 Torr the volumes of photoproducted methane product with time appeared identical so that in this pressure range the photoassisted reaction was pressure independent.

(iii) *Quantum Efficiency.* The average quantum efficiency for all wavelengths longer than 290 nm emitted by a 100-W medium-pressure mercury lamp was 3×10^{-5} . This value was based on the volume of methane from the first 60 min of the photoreaction and on the intensity of the radiation at the zinc oxide surface measured by a calibrated uv meter.^{2b}

(iv) *Effect of Methyl Chloride.* An equimolar mixture of CH_3Cl and CD_3I was introduced to an activated

(13) T. Kwan, Symposium on Electronic Phenomena in Chemisorption and Catalysis on Semiconductors, Moscow 1968, Walter De Gruyter & Co., Berlin, 1968, p 184.

(14) (a) P. J. Kokes, *J. Phys. Chem.*, **66**, 99 (1962); (b) M. Setaka, K. M. Sancier, and T. Kwan, *J. Catal.*, **16**, 44 (1970).

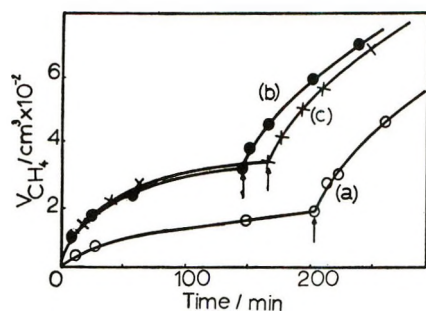


Figure 5. Photoproducted methane at ZnO surface under (a) 4×10^{-2} Torr of CH_3I , (b) 5 Torr CH_3I , and (c) 50 Torr of CH_3I . Arrow indicates start of illumination.

zinc oxide sample. Analyses of the dark reaction and subsequent photoreaction are shown in Table II and show that there is little difference in the ratio of the methanes from CD_3I and CH_3Cl for the dark and photoreactions.

(v) *Conductivity Measurements.* As described in section A(x), the introduction of methyl iodide to an activated zinc oxide film in the dark influenced the current transported by the film (see Figure 4). Illumination of the film when the current was at its minimum resulted in a photocurrent (Figure 6). On removal of the illumination the photocurrent decayed slowly and did not reach its starting value within 60 min. Illumination of the film when the current had returned to its activated value caused a slow, almost linear increase in current (Figure 6) which was greater, however, than the photocurrent at the minimum. Removal of the illumination caused a very slow photocurrent decay. Evidence that methyl iodide was decreasing the photoconductivity came from the observation that an increased photocurrent was always observed when the methyl iodide was condensed at liquid nitrogen temperature.

Discussion

Dark Reaction. Initial Interaction (Contact Times <30 Min). The electrical conductivity of zinc oxide has been attributed to free electrons in the conduction band,^{15,16} and the esr signal at $g = 1.96$ in vacuum-activated zinc oxide samples has been attributed by some workers to conduction band electrons^{13,14} although other workers suggest it may involve donor sites^{17,18} or anion vacancies¹⁹ which are in thermal equilibrium with electrons in the conduction band. The introduction of methyl iodide to an activated zinc oxide sample was here observed to cause both conductivity and esr signal at $g = 1.96$ to decrease during the first 30 min of contact time. These decreases can be attributed to removal of free electrons from the conduction band of zinc oxide due to their localization adjacent to methyl iodide molecules at the surface. Such behavior is consistent with the electronic theories of chemisorption^{20,21} and with the results of many worker demon-

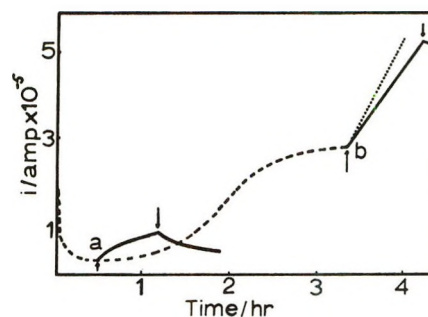


Figure 6. Broken line depicts typical change in conductivity with time in the dark after contacting CH_3I . Solid lines a and b show that, in the presence of CH_3I , illumination beginning at \uparrow achieved greater conductivity which decayed on removal of the light at \downarrow . Dotted line b illustrates greater photoconductivity achieved with equal illumination but with CH_3I condensed.

strating the reactivity of methyl iodide toward electrons.^{7,9} Consideration must therefore be given to the possible chemical consequences of the electron-attachment process shown in (1b).

Mass spectrometric analysis of the product showed methane, but ethane, which would be expected from dimerization of methyl radicals from (1b), did not appear. In reactions involving methyl radicals in other systems the appearance of methane and the absence of ethane has been interpreted on the basis that product arises principally from reactions involving the participation of "hot" methyl radicals. "Hot" methyl radicals possess energy of vibrational or rotational excitation in excess of that possessed by the species in thermal equilibrium. Participation of "hot" methyl radicals is thought to be necessary for methane production because abstraction of a hydrogen atom from a nonradical species requires an activation energy and only "hot" radicals have sufficient energy to meet the activation energy requirements. When experimental conditions are such that "hot" radicals are deactivated without H atom abstraction, they recombine to form ethane. Thus Schultz and Taylor,²² studying the photolysis of methyl iodide with light at 253 nm, found that the presence of a deactivating molecule, *e.g.*, carbon dioxide, reduced the yield of methane and that ethane was formed by combination of the deactivated radicals. Shirom and Willard²³ showed that methyl radicals,

(15) H. Heiland, E. Mollwo, and F. Stockman, *Solid State Phys.*, **8**, 191 (1959).

(16) T. J. Gray, "Experimental Methods in Catalytic Research," R. B. Anderson, Ed., Academic Press, New York, N. Y., 1968.

(17) Y. Fujita and J. Turkevitch, *Discussions Faraday Soc.*, **41**, 407 (1966).

(18) K. A. Muller and J. Schneider, *Phys. Lett.*, **4**, 288 (1965).

(19) P. H. Kasai, *Phys. Rev.*, **130**, 989 (1963).

(20) F. F. Wolkenshtein, "The Electronic Theory of Catalysis on Semiconductors," Pergamon Press, Oxford, 1963.

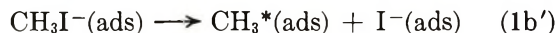
(21) K. Hauße, *Advan. Catal.*, **7**, 213 (1955).

(22) R. D. Schultz and H. A. Taylor, *J. Chem. Phys.*, **18**, 194 (1950).

(23) M. Shirom and J. E. Willard, *J. Phys. Chem.*, **72**, 1702 (1968).

produced by the radiolysis of methyl iodide-3-methylpentane glasses can form methane by hydrogen atom abstraction only when the methyl radicals are created and not later.

Application of these ideas to reaction at the CH_3I -ZnO interface would lead to the suggestion that methane could be formed on zinc oxide by reactions involving "hot" methyl radicals. A variety of reasons could be given for expecting hot methyl radicals to result from dissociative electron attachment to methyl iodide on zinc oxide *via*



First, excess energy released in the reaction cannot be converted to translational energy and so may appear as internal energy of the fragments. Second, the methyl radicals must initially form in a tetrahedral configuration and so may contain as much as 10 kcal/mol of vibrational energy. However, since methane but no ethane was formed, any such "hot" methyl radicals must all undergo fast reactions before they are deactivated. This would correspond to the requirements that the reactions



all be fast, so that kinetics of methane formation should be controlled by the kinetics of methyl radical formation. However, the kinetics of methane formation show differences depending on the amount of OH on the oxide surface (see Figure 7), suggesting that CH_3^* is not an intermediate in the formation of methane. Also, since the times for deactivation of vibrationally excited species in condensed phases are extremely short, *ca.* 10^{-11} sec, the probability of encounters of type 2 or 3 would be very low if similar deactivation times apply on the surfaces of solids. The observation that methyl chloride gave methane product also suggested that a mechanism other than a process of type 1b existed, since methyl radicals from dissociative electron attachment by methyl chloride have an appearance potential of 10 eV,⁷ so that 1b type processes would be unlikely for methyl chloride.

For these three reasons: sensitivity of kinetics to availability of surface OH; observed methane formation from methyl chloride; and the low probability of encounters involving hot radicals on the surface, mechanisms involving hot methyl radicals are not here favored as the explanation for the nonappearance of ethane in the initial reaction on activated zinc oxide surfaces.

A possible alternative mechanism is suggested by the work of Sagert, *et al.*,¹⁰ on the radiolysis of methyl

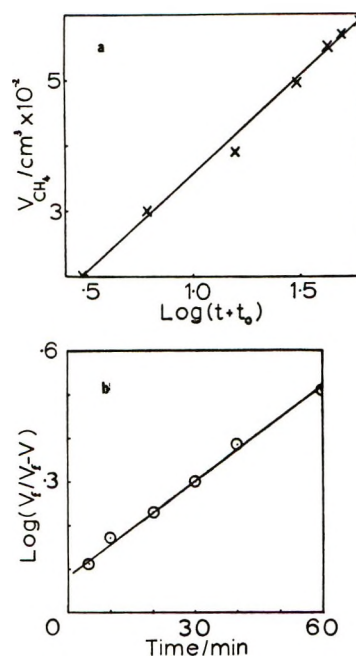
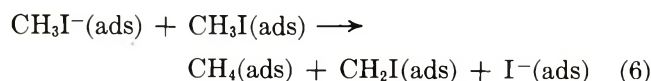
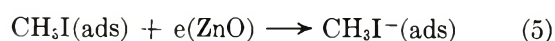
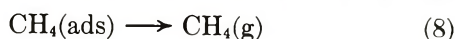
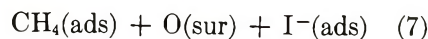
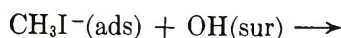


Figure 7. a, Elovich plot for the formation of CH_4 from CH_3I contacted with 24 g of ZnO activated at 350° ; $t_0 = 1$ min. b, First-order plot for the formation of CH_4 from CH_3I contacted with 6 g of ZnO activated at 490° .

iodide absorbed on silica gel. They found that the methyl iodide was an efficient scavenger of electrons produced in the silica gel by γ radiation. The ability of methyl iodide to compete with nitrous oxide for electrons showed that 4.7 electrons were localized (scavenged), by methyl iodide for each 100 eV of energy deposited in the silica gel. However, only 1.2 methyl radicals were produced per 100 eV absorbed by the solid. To explain the observed discrepancy the authors proposed that a methyl iodide anion $\text{CH}_3\text{I}^-(\text{ads})$ was stable in the adsorbed state, having a sufficiently long lifetime to allow it to interact with adsorbed methyl iodide molecules. A similar situation could exist on zinc oxide, particularly since the adsorption isotherm showed that methyl iodide is strongly adsorbed on zinc oxide, and the conductivity studies indicated electron localization by the adsorbed methyl iodide. Figure 5 illustrated that the dark reaction rate was not significantly influenced by methyl iodide pressures at values greater than 10^{-2} Torr. Consequently, it appears to be the adsorbed species, present at saturation coverage above 10^{-2} Torr, which participated in the reaction. The following mechanism is postulated to account for these observations





The following features of experimental results on the dark reaction are consistent with the proposed mechanism.

Adsorption. The Langmuir adsorption isotherm observed experimentally (Figure 1) is fully consistent with existence of the fast reversible equilibrium between gaseous and adsorbed phases represented by (4). Monolayer coverage derived from fit of the data to the Langmuir isotherm corresponded to 0.39 cm³ (STP) of CH₃I adsorbed. An area of 2.8 m²/g of ZnO may be calculated as the surface area involved in the reversible equilibrium of type 4, by taking 24 × 10⁻¹⁸ m² as the area of surface occupied per CH₃I(ads). (This latter value is calculated from liquid density values without corrections for nonideality.) The appreciable difference between a 2.8 m²/g area available to CH₃I and the 4 m²/g available to krypton adsorption at -196° may originate from sintering of the oxide during preactivation at 500° since the krypton adsorption measurements were performed on samples preactivated at 350°.

It might be argued that the transition of an adsorbed methyl iodide to a state of strong chemisorption, as proposed in step 5, and the subsequent reaction with an adsorbed methyl iodide molecule, step 6, should cause a deviation of the data from Langmuir behavior. However, the number of molecules which undergo step 5 is less than 1% of a monolayer (this will be shown later), which is well within the magnitude of experimental error of the adsorption measurements, so that such deviation would not significantly affect the adsorption isotherm.

Conductivity and ESR. In terms of previous interpretations which attribute both conductivity^{15,16} and the esr signal with $g = 1.96$ ^{13,14} to electrons in the conduction band, the initial decrease in the esr signal and in the conductivity are explained by step 5 which proposes that conduction electrons, $e(\text{ZnO})$ are localized at surface adsorbed methyl iodide molecules. This electron localization corresponds, in Wolkenshtein's theory²⁰ to a transition from weak to strong chemisorption or in Hauffe's theory²¹ to the establishment of a boundary layer. Arguments advanced previously by Weisz,²⁴ by Barry and Stone,²⁵ and by the present authors² show that the kinetics of the establishment of such charged boundary layers, and of related processes, should be of the type generally referred to as Elovich kinetics. The form of the Elovich expression appropriate to the reduction in conductivity which should result from process 5 is

$$\frac{i}{i_0} = c \log(t + t_0) + d \dots \quad (9)$$

where i_0 is the equilibrium current in the ZnO film

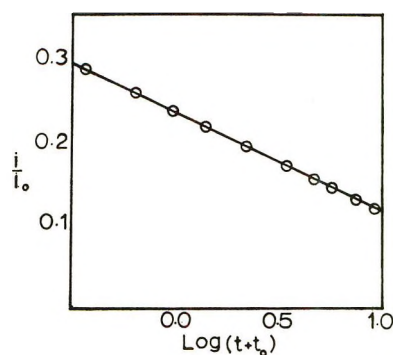


Figure 8. Elovich plot for the decay of ZnO conductivity when contacted with CH₃I in the dark.

prior to admitting CH₃I; i = current at time t subsequent to admission; t_0 is an empirically determined constant. Figure 8 shows that linear plots resulted when the initial decrease in conductivity was plotted according to expression 9. The proximity of the t_0 value to zero suggests, according to Stone's interpretation, that a second process is contributing to the conductivity change. This may be influenced by the secondary process which caused the conductivity increase observed at times >30 min (*cf.* Figure 4), but quantitative description of the reversal in conductivity change has not been achieved. It could be qualitatively understood if I⁻ (or other charged fragments) from steps 6 and 7 slowly reinjected electrons into the conduction band. Our observations that preadsorption of CD₃I onto some surface sites prevented dissociative electron attachment to N₂O, CH₃Cl, or CH₃I subsequently admitted implies that electrons are not rapidly reinjected into the conduction band from CD₃I⁻(ads), *i.e.*, step 5 is not reversible at the sites of initial electron localization.

Due to the nature of the esr measurements it was not possible to make sufficient measurements during the $g = 1.96$ signal decay to achieve a satisfactory kinetic analysis of this process.

Product Composition. The proposed mechanism (4)–(8) accounts for the absence of ethane since no free methyl radicals appear which could combine to give ethane. The appearance of gaseous methane product is satisfactorily explained by steps 6, 7, and 8 of the mechanism. The behavior of the CD₄/CD₃H ratio with temperature of activation and with reaction time can be understood in terms of steps 6 and 7. Since CD₃H from (7) depends on the number of OH groups present on the surface following activation, the amount of CD₃H can be reduced by increasing the temperature of activation and thus reducing the number of surface OH groups. In the course of the initial decomposition on the freshly activated surface, surface OH groups are

(24) P. B. Weisz, *J. Chem. Phys.*, **21**, 1531 (1953).

(25) T. Barry and F. S. Stone, *Proc. Roy. Soc., Ser. A*, **225**, 124 (1960).

depleted whereas the concentration of $\text{CH}_3\text{I}(\text{ads})$ remain constant, because of monolayer coverage and the equilibrium with the gas phase. Therefore, the probability of hydrogen atom abstraction from surface OH groups decreases with reaction time while the probability of hydrogen abstraction from $\text{CH}_3\text{I}(\text{ads})$ remains constant. Since the isotopic composition of additional methane product obtained by uv illumination was always made on surfaces which first had undergone a dark reaction, the mechanism can account for the higher $\text{CD}_4/\text{CD}_3\text{H}$ ratio noted for photoproduct than for product from prior dark reaction (see Table II, $\sim 490^\circ$).

Kinetics of Methane Formation. On the basis of the proposed mechanism, the rate of methane formation is given by the equation

$$\frac{d[\text{CH}_4]}{dt} = k_1[\text{CH}_3\text{I}^-(\text{ads})][\text{OH}(\text{ads})] + k_2[\text{CH}_3\text{I}^-(\text{ads})][\text{CH}_3\text{I}(\text{ads})] \quad (10)$$

For a zinc oxide sample activated at 350° , analysis of the methyl- d_3 iodide reaction products has shown that reaction between $\text{CH}_3\text{I}^-(\text{ads})$ and $\text{OH}(\text{ads})$ predominated, so that the above kinetic expression may be approximated by

$$\frac{d[\text{CH}_4]}{dt} \approx k_1[\text{CH}_3\text{I}^-(\text{ads})][\text{OH}(\text{ads})] \quad (10a)$$

If process 7 is sufficiently fast, the rate of methane formation may be governed by a slow rate of formation of $\text{CH}_3\text{I}^-(\text{ads})$ which in turn should obey the Elovich expression. Consequently, the rate of formation of methane should be given by

$$\frac{d[\text{CH}_4]}{dt} = a \exp(-b[\text{CH}_4]) \quad (11)$$

A plot of V_{CH_4} vs. $\log(t + t_0)$ was linear when t_0 was chosen equal to 1 min (see Figure 7a) for measurements taken on a sample activated at 350° . This showed that the kinetics of methane appearance on such samples were consistent with a surface electron localization process as the rate-determining step.

For zinc oxide samples activated at 500° the surface OH concentration is low and its contribution to methane formation can be neglected. Under these circumstances the rate of methane formation may be approximated by the rate of step 6, i.e.

$$\frac{d[\text{CH}_4]}{dt} \approx k_2[\text{CH}_3\text{I}^-(\text{ads})][\text{CH}_3\text{I}(\text{ads})] \quad (12)$$

Since the total amount of reaction which takes place is less than 1% of a monolayer, $\text{CH}_3\text{I}(\text{ads})$ can be considered constant. The rate expression then becomes

$$\frac{d[\text{CH}_4]}{dt} \approx k_3[\text{CH}_3\text{I}^-(\text{ads})] \quad (13)$$

and an approximation for $\text{CH}_3\text{I}^-(\text{ads})$ becomes necessary to deduce the expected kinetic pattern. Comparing the shapes of the curves representing the formation of methane with time (see Figure 2) and the initial dark conductivity decay with time (see Figure 4), the methane curve shows a slow monotonic decrease in rate while the conductivity shows a rapid decrease to a minimum value. It may therefore be approximated that a boundary layer limited concentration of $\text{CH}_3\text{I}^-(\text{ads})$ is rapidly established, corresponding to the initial sharp drop in conductivity. If this boundary layer limited concentration of $\text{CH}_3\text{I}^-(\text{ads})$ then undergoes reaction to form methane *via* (6), which leaves the surface charged and prevents further chemisorption, the surface concentration of CH_3I^- at any subsequent time when product (V_{CH_4}) has formed may be approximated by

$$[\text{CH}_3\text{I}^-(\text{ads})]_t \approx [\text{CH}_3\text{I}^-(\text{ads})]_0 - (V_{\text{CH}_4})_t \quad (14)$$

Here $[\text{CH}_3\text{I}^-(\text{ads})]_0$ is the initial concentration of $\text{CH}_3\text{I}^-(\text{ads})$ and may be approximated by the volume of methane after 2 hr reaction, $(V_{\text{CH}_4})_t$, which permits integration of eq 13 to the first-order form

$$k_3 t \approx \log \frac{(V_{\text{CH}_4})_t}{(V_{\text{CH}_4})_t - (V_{\text{CH}_4})_0}$$

A plot of $\log(V_{\text{CH}_4})_t / [(V_{\text{CH}_4})_t - (V_{\text{CH}_4})_0]$ vs. t resulted in a straight line (see Figure 7), which showed that in the early stages of the dark reaction, on a zinc oxide surface activated at high temperatures, the methane formation followed pseudo-first-order kinetics in $\text{CH}_3\text{I}^-(\text{ads})$. This is consistent with steps 4, 5, 6, and 8 of the proposed mechanism and with poisoning of electron attachment sites by products of the initial fast reaction.

Secondary Dark Processes at the Methyl Iodide-Zinc Oxide Interface (at Times >30 Min Contact). Figures 3 and 4 illustrate the reversal of the direction of change of the esr signal intensity and of the conductivity in the dark at contact times greater than ca. 30 min between methyl iodide and a zinc oxide activated at 490° . No such reversal was ever noted in previous studies of dissociation *via* electron attachment at N_2O -ZnO interfaces in the dark.² Dark dissociation in N_2O -ZnO systems decreased to very low values at long contact times because electrons remained localized on oxygen fragments and the observed extent of N_2O dissociation corresponded with that calculated from boundary layer theory ($\approx 0.28\%$ of a monolayer). Reversal of conductivity change after 30 min contact time at the CH_3I -ZnO interface suggests that reinjection of electrons occurs from charged product species back into the conduction band. Extent of conversion to methane at this interface at contact times >30 min may not, therefore, be limited by the extent of surface charge but rather by the availability of sites at which electron localization by $\text{CH}_3\text{I}(\text{ads})$ can occur. For N_2O -ZnO systems the boundary layer limited extent of dissocia-

tion ($\approx 0.28\%$ of a monolayer) was closely approached after 2 hr contact time, whereas in CH_3I -ZnO systems similarly preactivated, methane formation after 2 hr contact corresponded to 0.8% of a monolayer, which increase is consistent with the recovery of conductivity at times 0.5–2 hr. The observation that extent of methane formation in the dark attained even after prolonged contact time corresponded only to *ca.* 1% of a monolayer suggests surface heterogeneity; *i.e.*, only this small percentage of all surface sites is capable of adsorbing CH_3I and localizing an electron on it in the dark at room temperature.

Processes at the Uv-Illuminated Methyl Iodide-ZnO Interfaces. The conductivity studies indicated that methyl iodide, like N_2O , reduced the number or mobility of charge carriers when present at the illuminated interface. It was proposed earlier that the additional photoassisted dissociation noted at dark-equilibrated N_2O -ZnO interfaces originated either in additional electron localization by $\text{N}_2\text{O}(\text{ads})$ at the illuminated interface (made possible because localization of holes decreased the magnitude of the negative surface potential set up by prior dark reaction), or because exciton-like states participated in dissociation at the illuminated interface. The major difference between dark-equilibrated N_2O -ZnO and CH_3I -ZnO interfaces was that conductivity and esr indicated the former to retain a negative surface potential indefinitely in the presence

of N_2O whereas CH_3I -ZnO interfaces appeared to lose their surface charge after *ca.* 2 hr contact with CH_3I . A mechanism for photoassisted formation of methane by reduction of a negative surface potential, therefore, seems distinctly improbable for the CH_3I -ZnO system at long contact time. It appears more probable that such methane arises *via* participation of exciton-like states at the illuminated CH_3I -ZnO interface. While present results do not suffice to distinguish definitely between the various mechanisms by which excitons might enhance methane formation, the results in Table II argue against a mechanism in which energy of exciton-like states of ZnO would be converted *via* radiationless processes into dissociation energy of the carbon-halogen bond. The exciton energies 3–3.2 eV are lower than the C-Cl bond energy of 80 kcal/mol and greater than C-I bond energy, but data in Table II show that both CH_3Cl and CD_3I underwent photoassisted conversion to methane at comparable rates.

Acknowledgments. The authors are deeply indebted to Professor Philbin and other colleagues at U.C.D. for encouragement, discussion, and provision of experimental facilities. Support of the work by funds and equipment provided by AFOSR is also gratefully acknowledged, together with provision of zinc oxide samples by D. O. Carpenter of New Jersey Zinc Co. and technical assistance from Mr. Austin of the University of Liverpool.

Reactions Involving Electron Transfer at Semiconductor Surfaces.

IV.^{1a} Zinc Oxide-Promoted Photoreductions in

Aqueous Solutions at Neutral pH

by Joseph Cunningham^{*1b} and Hanaa Zainal

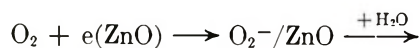
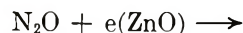
Chemistry Department, University College, Dublin, Ireland (Received November 4, 1971)

Publication costs borne completely by The Journal of Physical Chemistry

Quantum efficiencies of 10^{-3} to 0.29 have been determined for reduction reactions produced by uv illumination of different zinc oxides suspended in aqueous solutions containing NaNO_3 , KMnO_4 , indigo carmine or *p*-nitrosodimethylaniline (PNDA). Consideration is given to factors at the zinc oxide-aqueous solution interface which allowed these quantum efficiencies to exceed by two to three orders of magnitude those previously reported for zinc oxide promoted photoreactions at zinc oxide-gas interfaces. An electron paramagnetic resonance (epr) signal with $g \sim 1.96$ was observed from zinc oxide suspensions in various aqueous solutions, but only when these were illuminated by uv light. This epr signal was used to measure the tendency of various solutes to increase or decrease the number of electrons available at the surface of the illuminated zinc oxide particles while suspended in aqueous solutions. Techniques of competition kinetics were also utilized to check ability of an additive to interact with photoproduct intermediates at these illuminated interfaces. Additives which reduced the epr signal were also shown to be effective in reducing the rate of photobleaching of PNDA and included I^- , CO_3^{2-} , NO_2^- , PO_4^{2-} , and Tl^+ . Additives which increased the epr signal intensity also increased the rate of PNDA photoreduction and included NO_3^- , HCOO^- , and $\text{C}_2\text{H}_5\text{OH}$. Probable reducing and oxidizing processes are discussed for the H_2O -ZnO interface at neutral pH.

Introduction

Literature values²⁻⁸ of the overall quantum efficiency of reactions promoted by uv illumination at the interface between zinc oxides and aqueous solutions containing oxidizable or reducible solutes are orders of magnitude larger than quantum efficiencies recently determined in these laboratories for photoinduced reactions at zinc oxide-gas interfaces.⁹⁻¹¹ The contrast is most evident when quantum efficiency for photo-assisted dissociation of N_2O at ZnO - $\text{N}_2\text{O}(\text{g})$ interfaces ($\phi_{\text{N}_2} \sim 10^{-5}$) is compared with reported quantum efficiencies of 0.1 to 0.35 for photosynthesis of H_2O_2 at ZnO -oxygenated aqueous solution interfaces.²⁻⁶ Electron localization by N_2O in the former and by O_2 in the latter are identified as important steps in the overall mechanisms I and II, respectively. Despite evident



similarities in these mechanisms, no satisfactory explanation of the large difference in apparent overall quantum efficiencies of these processes has been proposed. One objective of the present study was to examine the validity of the striking difference between quantum efficiencies reported for the ZnO -gas and ZnO -aq

solution interfaces. The approach chosen was to determine quantum efficiencies of photoreduction at ZnO -aq solution interfaces with the same zinc oxides and uv lamps as employed here previously in studies of photo-assisted processes at ZnO -gas interfaces. A second objective of the present study was to explore the factors which cause the quantum efficiency of photoreduction to vary widely at various deoxygenated ZnO -aq solution interfaces (from 10^{-5} for H_2 production¹² to 3.0 for photoreduction of methylene blue⁸). Emphasis was placed on the reducing power of the

(1) (a) Work supported in part by the U. S. Air Force Office of Scientific Research through the European Office of Aero-space Research, OAR, U. S. Air Force, under Contract AF 61 (052)-67C-0044. (b) Chemistry Department, University College, Cork, Ireland.

(2) (a) M. C. Markham and K. J. Laidler, *J. Phys. Chem.*, **57**, 363 (1953); (b) G. M. Schwab, *Advan. Catal.*, **9**, 229 (1957).

(3) H. Gerischer, *Surface Sci.*, **97** (1969).

(4) G. Oster and M. Yamamoto, *J. Phys. Chem.*, **70**, 3033 (1966).

(5) J. G. Calvert, K. Theurer, G. T. Rankin, and W. M. MacNevin, *J. Amer. Chem. Soc.*, **76**, 2575 (1954).

(6) L. White, Jr., *ibid.*, **76**, 624 (1954).

(7) J. Kuriacase and C. Markham, *J. Catal.*, **1**, 498 (1962).

(8) T. S. Glikman and E. Podlityaeva, *Ukr. Khim. Zh.*, **22**, 478 (1956).

(9) J. Cunningham, J. J. Kelly, and A. L. Penny, *J. Phys. Chem.*, **74**, 1992 (1970).

(10) J. Cunningham, J. J. Kelly, and A. L. Penny, *ibid.*, **75**, 617 (1971).

(11) J. Cunningham and A. L. Penny, *ibid.*, **76**, 2353 (1972).

(12) A. Bernas, *ibid.*, **68**, 2047 (1964).

illuminated interface by choice of three solutes known, from pulse radiolysis studies,^{13,14} to react rapidly with electrons, *viz.* NO_3^- , MnO_4^- , and *p*-nitrosodimethylaniline (PNDA). This choice may also serve to examine the possible role of charge (by comparison of results from PNDA with those from NO_3^- and MnO_4^-) and of relative positioning of first excited states (since the first excited states of $\text{MnO}_4^-(\text{aq})$ and $\text{PNDA}(\text{aq})$ lie at lower energies than that of $\text{ZnO}(\text{s})$ ¹⁵ but the reverse holds for $\text{NO}_3^-(\text{aq})$ ¹⁶). Indigo carmine was included to test the possibility that OH radicals were active at the illuminated H_2O - ZnO interface, since it, like PNDA, is reported to have high rate constant for reaction with OH radicals.¹⁷

Experimental Section

Materials. The following powdered zinc oxides, provided by courtesy of the New Jersey Zinc Co., were used in this study: SP 500 pure zinc oxide; lithium-doped zinc oxide (Lot No. 631-121-3, containing 463 ppm lithium); and indium-doped zinc oxide (Lot No. 631-121-1, containing 110 ppm indium). Information available from previous work and relevant to the present study is summarized in Table I of ref 10 for the oxides.

Doubly distilled water was used for preparation of all aqueous suspensions of the zinc oxides and also for the preparation of aqueous solutions needed in the study. No acid or base was added to the solutions or suspensions to control or modify their natural pH which remained within ± 0.6 pH unit of 7.4.

Oxygen-free nitrogen gas, supplied by British Oxygen Co., was used to purge all aqueous suspensions of zinc oxide for at least 30 min prior to investigating any photoinduced reaction.

p-Nitrosodimethylaniline supplied by Ralph N. Emanuel Ltd. (Research Chemicals) was used as obtained. 2,7-Dimethyl-3,6-diaza-1,6-cycloheptadiene perchlorate and other chemicals required to prepare optical filter solutions^{18,19} were provided by Koch-Light Laboratories Ltd. The potassium permanganate used in the photolysis reactions was prepared from concentrated solution ampoules supplied by Merck Co. Indigo carmine was AR grade, supplied by Gurr Ltd. (London). Sulfanilamide, ammonium sulfamate, and *N*-(1-naphthyl)ethylenediamine dihydrochloride were supplied by Eastman Kodak Ltd.

Procedure for Studying Photoreductions. The Pyrex equipment illustrated in Figure 1 was assembled and one of the following filter solutions was placed into the annular compartment (d). Different solutes required different filter solutions because the objectives of this study dictated that light be absorbed primarily in the semiconductor to yield electrons, holes, and excitons and *not* by the solute to give its excited states. Filter solutions were therefore selected to remove light which would be absorbed by the solute.

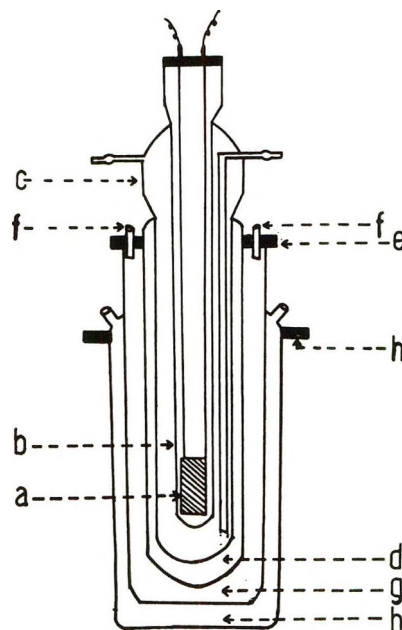


Figure 1. Equipment for studying kinetics and quantum efficiency of photoreductions: a, 75-W medium-pressure Hg-arc lamp held rigidly in quartz jacket; b; c, Pyrex water cooling jacket; d, compartment for filter solutions which surround the lamp; e, Perspex disk excluding air and providing tubes at f for purging system with nitrogen and for removing samples; g, flat-bottomed reaction vessel in which zinc oxide suspensions were prepared and photolyzed; h, flanged outer vessel in which actinometer was placed.

Filter A consisted of a solution of 200 g/l. of $\text{CoCl}_2 \cdot 6\text{H}_2\text{O}$ and 100 g/l. of $\text{NiCl}_2 \cdot 6\text{H}_2\text{O}$ in a mixture of 55% dimethylformamide and 45% water containing 1 mol/l. of HCl, which significantly transmitted only light of wavelengths (290–390 nm) with maximum transmission coinciding with most intense line emission of the lamp at 366 nm.¹⁸

Filter B consisted of a 0.1 g/l. solution of 2,7-dimethyl-3,6-diaza-1,6-cycloheptadiene perchlorate in water which transmitted light of wavelengths longer than 345 nm¹⁹ and which was used for studies on nitrate to avoid absorption by the $n-\pi^*$ transition at 300 nm.¹⁶

Filter C consisted of 200 g/l. of $\text{CuSO}_4 \cdot 5\text{H}_2\text{O}$ and 10 g/l. of $(\text{NH}_4)_2\text{SO}_4 \cdot \text{Fe}_2(\text{SO}_4)_3 \cdot 24\text{H}_2\text{O}$ in 1 l. of water containing 5 ml of concentrated H_2SO_4 which trans-

(13) (a) F. S. Dainton and B. Wisall, *Trans. Faraday Soc.*, **64**, 694 (1968); (b) J. H. Baxendale and A. A. Khan, *Int. J. Radiat. Phys. Chem.*, **1**, 11 (1969).

(14) M. Anbar and P. Neta, *Int. J. Appl. Radiat. Isotop.*, **18**, 493 (1967).

(15) Y. S. Park, C. W. Litton, T. C. Collins, and D. C. Reynolds, *Phys. Rev.*, **143**, 512 (1966).

(16) J. A. Friend and L. E. Lyons, *J. Chem. Soc.*, 1572 (1959).

(17) (a) I. M. Nielsen, Part Vol. II BNWL-715 Pacific Northwest Laboratory Annual Report 1967, D. R. Kalkwar, p 154; (b) I. Kraljic and C. N. Trumbore, *J. Amer. Chem. Soc.*, **87**, 2547 (1965).

(18) W. W. Whadimiroff, *Photochem. Photobiol.*, **5**, 243 (1966).

(19) J. Calvert and J. Pitts, Jr., "Photochemistry," Wiley, New York, N. Y., 1967.

Table I: Properties of Zinc Oxide-Aqueous Solution Suspensions Prior to Photoreduction

Density ^a	Solid	$(\Delta_{ox} - \Delta'_{ox})/\Lambda_{ox}$ ^b	Area ^c	Dark rate ^d	Specific rate ^e	N_e ^f
0.05	ZnO	0.07	0.2			
0.25	ZnO	0.25	0.9			
0.42	ZnO	0.47	1.7			
0.78	ZnO	0.72	3.1			
1.00	ZnO	0.83	4.0	1.9×10^{-6}	4.8×10^{-6}	3×10^{16}
1.24	ZnO	0.93	5.0			
1.00	Li-ZnO		1.0	1.1×10^{-6}	1.1×10^{-6}	2.7×10^{14}
1.00	In-ZnO		<0.1	5.3×10^{-6}	5.3×10^{-6}	1.8×10^{18}

^a The weight of solid maintained in 1 l. of suspension by magnetic stirring. ^b Experimental measure of fraction of light at (310–390 nm) absorbed by suspension of indicated density. ^c ZnO surface area ($\text{m}^2 \text{l}^{-1}$) calculated from area measured by krypton adsorption at -196° . ^d Rate of loss of PNDA molecules in the dark when PNDA was present at an initial concentration of $4 \times 10^{-5} M$ in the suspension. Rates were observed as $\Delta OD \text{ hr}^{-1} 350 \text{ ml}^{-1}$ and converted to mol of PNDA $\text{hr}^{-1} \text{l. of suspension}^{-1}$. ^e Rate of loss of PNDA normalized to rate per unit surface area; mol of PNDA $\text{hr}^{-1} \text{m}^{-2}$. ^f Room temperature concentration of electrons in this zinc oxide after vacuum activation at 350° ; mobile carriers g^{-1} .

mitted light of wavelengths (400–600 nm) too long to be strongly absorbed by the ZnO lattice.

Experimental Evaluation of Light Absorbed by Suspensions. An experimental measure of the light absorbed by the suspensions was sought using the equipment shown in Figure 1 in the following sequence. (i) Uranyl oxalate actinometer solution was placed in the annular compartment, h, usually unoccupied during photoreductions. An experimental value was obtained of the oxalic acid decomposed in unit time, $-\Delta_{ox}$, in that position with the same light as used for photoreduction. This experimental value results from all photons absorbed by samples between 300 and 390 nm for filter A. (ii) An aqueous ZnO suspension was placed in the annular position, g, and kept in suspension by a magnetic stirrer. Uranyl oxalate was placed in outer vessel, h, so that it surrounded the suspension. The number of oxalic acid molecules decomposed per unit time during operation of the lamp in this configuration, $-\Delta'_{ox}$, was then taken as a measure of the light transmitted through the suspension and should include most of the photons which underwent scattering events. The fraction of incident light in the 300–390-nm region which was absorbed by the suspensions was then given by $[(\Delta_{ox}) - (-\Delta'_{ox})]/(-\Delta_{ox})$ and values are given in Table I. A "concentration" of 1 g of ZnO/l. of solution was chosen as the standard condition for this study because it corresponded to strong absorption (82.5%).

Rates of "Dark" and Photoreductions. An aqueous solution (350 ml) of the reagent whose photoreduction was to be studied was introduced into compartment g of the apparatus shown in Figure 1 and flushed vigorously with nitrogen for at least 15 min. Zinc oxide powder (0.35 g) was added and the mixture was continuously purged with N_2 for at least a further 15 min, during which time a magnetic stirrer was activated to produce a uniform suspension. In these conditions

the colored reagents, PNDA, KMnO_4 , and indigo carmine, underwent a slow irreversible loss of absorbance which proceeded whether or not room light was excluded from the system. These slow bleaching effects will be here referred to as "dark" reactions to distinguish them from the much faster bleaching effects noted when the same suspensions were subsequently exposed to uv light. Rate of dark reaction was established in all cases before proceeding to investigate photo rates. (See Table I.) The pH of samples taken from the reaction vessel at this stage and centrifuged was measured with a Radiometer Model 22 meter and lays in the range 7.2–7.6.

The water-cooled medium-pressure mercury lamp (see Figure 1) complete with filter solution was then removed, switched on, and equilibrated in a water bath for 15 min before being introduced into the reaction mixture. This precaution was necessary to ensure a steady light intensity from the beginning of photoreaction. Flushing with nitrogen and stirring with a magnetic stirrer continued in the same manner as prior to illumination. Progress of photoinduced bleaching of colored solutions such as PNDA, KMnO_4 , or indigo carmine was followed by taking samples of approximately 5 ml volume from the reaction mixture with a pipet at suitable time intervals. Samples were centrifuged and absorbance of the clear solution was measured immediately, using a Perkin-Elmer 402 recording spectrophotometer when a full spectrum was required or a Unicam 500 spectrophotometer when absorbance at λ_{max} of the reactant or product sufficed. The pH of centrifuged samples after photolysis, ~ 6 – 7 , decreased relative to those measured prior to illumination (7.2–7.6) but the small magnitude of the pH change made it unsuitable for monitoring rates of the photoreactions. Rate of photoreduction of nitrate was followed by analyzing centrifuged samples for nitrite by a colorimetric method.²⁰

Table II: Quantum Efficiencies of Photoreductions at Uv-Illuminated ZnO-Aqueous Solution Interfaces

I^0_{eq} , quanta/ (sec 350 ml) ^a	Zinc oxide, 0.35 g/350 ml ^b	[Reactant] _{aq} ^c	ϕ_{irr} ^d	ϕ_{α} ^e	η , wrt [R] ^f	Filter solution
1.9×10^{16}	Pure ZnO	$4 \times 10^{-5} M$ PNDA	0.23	0.29	0	A
1.9×10^{16}	Pure ZnO	$3 \times 10^{-4} M$ PNDA	0.29	0.26		A
6×10^{16}	Pure ZnO	$4 \times 10^{-5} M$ PNDA	0.13	0.11		A
1.8×10^{16}	Pure ZnO	$3 \times 10^{-4} M$ PNDA	0.14	0.20	0.18	A
1.8×10^{18}	Pure ZnO	$4 \times 10^{-5} M$ PNDA	0.012	0.009	0.43	A
1.8×10^{18}	Pure ZnO	$3 \times 10^{-4} M$ PNDA	0.021	0.021		A
1.8×10^{18}	Li-ZnO	$4 \times 10^{-5} M$ PNDA	0.0008	0.001		A
1.8×10^{18}	Pure ZnO	$3 \times 10^{-4} M$ PNDA	0.0008	0.001	0	A
1.8×10^{18}	In-ZnO	$4 \times 10^{-5} M$ PNDA	0.0044	0.004	0.22	A
1.8×10^{18}	Pure ZnO	$3 \times 10^{-4} M$ PNDA	0.0082	0.006		A
1.8×10^{18}	Pure ZnO	$7 \times 10^{-4} M$ KMnO ₄	0.058	...		A
1.8×10^{18}	Pure ZnO	$2.5 \times 10^{-4} M$ KMnO ₄	0.037	...		A
1.8×10^{18}	Li-ZnO	$7 \times 10^{-4} M$ KMnO ₄	0.025	...		A
1.8×10^{18}	In-ZnO	$7 \times 10^{-4} M$ KMnO ₄	0.046	...		A
1.8×10^{18}	Pure ZnO	$7 \times 10^{-5} M$ I.C.	0.04	...		A
1.8×10^{18}	Pure ZnO	$5 \times 10^{-1} M$ NaNO ₃	0.0026	...		B

^a I^0_{eq} , light intensity incident on suspension (see text). ^b The same density of zinc oxide, corresponding to 1 g of oxide/l. of suspension, was used in all these runs. ^c Reactant concentration in aqueous suspension before photoreaction. ^d Quantum efficiency of photoreduction determined from initial reaction rate (irr). ^e Quantum efficiency determined at 50% reaction from plots of % reaction, α , vs. time. ^f Order of reaction wrt initial reactant concentrations, determined from $\log t^{1/2}$ vs. \log (concentration) plots.

Actinometry to Determine I^0 and Quantum Efficiencies.

Uranyl oxalate solutions at 0.001 *M* concentration of UO_2^{2+} and 0.005 *M* of oxalate ion were utilized for the majority of actinometry measurements and were placed in the compartment normally occupied by the suspensions. Samples were taken after suitable exposure times and the number of oxalate ions decomposed was determined by a differential absorption procedure²¹ based on reaction of undecomposed oxalate with Ce^{4+} .

The emission spectrum of the lamp in our experimental arrangement contained prominent lines of the mercury arc spectrum at 302, 312, 313, 334, 364, 365, and 366 nm with relative intensities (relative to 100 for the line at 546 nm) of 0.45, 2.3, 2.0, 1.3, 35.7, 19.5, and 11.6, respectively.¹⁰ No other lines of the mercury-arc spectrum were transmitted to any significant extent by the filter solutions employed. A good approximation to I^0 should therefore result by using the values of ϕ and ϵ appropriate to 364–366 nm in the expression

no. of photons absorbed =

$$\frac{-\Delta_{\text{ox}}}{\phi} = I^0 \{1 - \exp(-\epsilon cd)\} \quad (1)$$

The quantum yield for oxalate loss is accepted as 0.49 for light at 366 nm.¹⁹ Beer's law plots yielded a value of $\epsilon = 15 \text{ l. mol}^{-1} \text{ cm}^{-1}$. Values of the flux of photons at wavelengths 300–390 nm, quoted in the text as incident on the suspension, have been calculated by inserting these values and experimentally determined values of $(-\Delta_{\text{ox}})$ into expression 1. It must be noted, however, that the approximations used actually yield values of "equivalent light intensity" I^0_{eq} , i.e., that intensity

of monochromatic light at 365 nm which would have produced the observed change in the uranyl oxalate actinometer. Quantum efficiencies for zinc oxide-promoted photoreductions have been calculated using values of I^0_{eq} derived in this manner, together with the experimentally determined value of the fraction of incident light absorbed by the suspensions (see Tables I and II).

The preceding approximation ignored possible effects of the (less numerous) photons at 302, 312, 313, and 334 nm which would, however, have a disproportionately large effect on $(-\Delta_{\text{ox}})$ because of the much higher values of ϵ at these wavelengths. An experimental measure of the error possibly introduced through neglect of these wavelengths was sought by comparing $-\Delta_{\text{ox}}$, determined with the uranyl oxalate actinometer, with $\Delta_{\text{Fe}^{2+}}$, the number of ferrous ions measured with the potassium ferrioxalate actinometer. The comparison indicated that true values of quantum efficiency would tend to be higher than those based on I^0_{eq} but could not be more than 25% above them.

Effects of Other Solutes on Photoreductions. When the effect of various additives on kinetics and quantum efficiency of PNDA photobleaching was being studied, a similar procedure was followed except that additive was dissolved into PNDA solution before introducing the latter into compartment g of the photolysis equipment. The OD of PNDA at 440 nm was measured before and after mixing in the dark and only additives which did

(20) M. Shinn, *Ind. Eng. Chem., Anal. Ed.*, **13**, 33 (1941).

(21) J. N. Pitts, J. D. Margerum, R. P. Taylor, and W. Brin, *J. Amer. Chem. Soc.*, **77**, 5409 (1955).

not produce a significant and continuing decrease were used.

No appreciable dark reduction of nitrate ion was observed over the zinc oxide. The major product of photoreduction was identified as nitrite ion and was determined by Shinn's colorimetric analysis. For studies of effects of other solutions on nitrite formation the number of suitable additives was limited by interference with this analysis.

Electron Paramagnetic Resonance Studies on Aqueous Suspensions of ZnO. The high sensitivity of electron paramagnetic resonance (epr) spectroscopy, together with literature reports that an electron-excess center in zinc oxide is readily detected by this technique,²²⁻²⁸ led to epr investigations of the ZnO suspensions. It was hoped that this technique would permit direct observation of electron excess centers at the ZnO-H₂O interface in the dark or under illumination.

A Decca X1 epr spectrometer system operating at fixed klystron frequency of 9.27 GHz was used in the homodyne detection mode. A multipurpose rectangular cavity operating in the TE₁₀₂ mode with unloaded *Q* factor of 9000 was used and overall system sensitivity to *ca.* 10¹³ spins was established in calibrations with solutions of DPPH in benzene. Introduction of water and zinc oxides, separately or as a dense suspension, in normal cylindrical epr sample tubes caused such severe dielectric loss through interaction with the electric vector of the microwaves that null balance could not be achieved. It was, therefore, essential to utilize Spectrosil "aqueous solution flat cells" for all ZnO suspensions and these proved to have the additional advantage that dense suspensions once introduced retained their configuration in the narrow space (0.3 mm) between the flat Spectrosil faces. The Decca epr instrument controls provided a method for monitoring the relative values of the cavity *Q* and this allowed signal intensities to be normalized to an arbitrarily chosen system sensitivity. The Mn²⁺-doped MgO powder utilized to calibrate magnetic field positions through the six transitions of Mn²⁺ served also as an additional check on minor variations in system sensitivity caused by uv illumination. Reported intensities have so been corrected and normalized.

Preparation of suspensions and their introduction into the flat cell was achieved using the Pyrex equipment illustrated in Figure 2.

Step A. Zinc oxide powder (0.8 g) was weighed in the sample tube and, using the experimental arrangement shown in Figure 2A, dry, oxygen-free nitrogen gas, additionally purified by a molecular sieve trap at -78°, was passed through the zinc oxide powder. With an external oven, the zinc oxide powder was heated in the flow of nitrogen at 500° for 3 hr, care being taken to agitate the sample and so expose it all to the nitrogen flow. The sample was allowed to cool

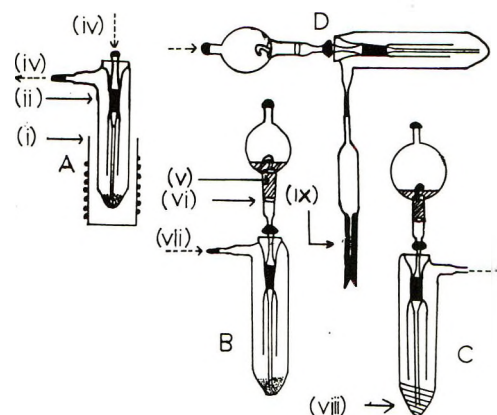


Figure 2. Preparation of dense suspensions of zinc oxide in aqueous solution for epr: A, ZnO activation at 500°: (i) external furnace; (ii) Pyrex vessel containing ZnO at (iii); (iv) direction of flow of prepurified N₂. B, Deoxygenation of aqueous solution; (v) solution of H₂O retained by fritted disk at (vi); (vii) reversed direction of N flow. C, Mixing deoxygenated solutions and activated ZnO to form dense suspension at (viii). D, Introducing dense suspension into aqueous solution flat epr cell (ix).

down to room temperature in the additionally purified nitrogen before the next step.

Step B. An aqueous solution (5 ml) was placed in a solution bulb having a fitted disk which was then assembled as shown in Figure 2B. By reversing the direction of flow, both the activated ZnO powder and solution were flushed with nitrogen for 15–30 min without being mixed. This purged the solution of dissolved oxygen before mixing.

Step C. The experimental arrangement in Figure 2C was used to force the deoxygenated solution through the fritted disk down into the ZnO. Zinc oxide–aqueous suspensions then formed in sample tube (ii) were flushed vigorously by nitrogen gas for an additional 30 min to ensure complete mixing before the next step. Values of 7.8 to 8.2 were measured for the pH of the aqueous phase obtained by centrifuging control samples subjected to steps A, B, and C.

Step D. The flat "aqueous solution cell" was attached to the side arm of sample tube (ii) with polythene tubing, as shown in Figure 2D. It was flushed with nitrogen for 5 min before being filled with the zinc oxide suspension. Both ends of the flat cell were stoppered immediately to prevent contamination with

(22) G. Heiland, E. Mollivo, and F. Stockmann, *Solid State Phys.*, **8**, 191 (1950).

(23) J. Schneider and A. Rauber, *Z. Naturforsch.*, **16**, 713 (1961).

(24) K. A. Nuller and J. Schneider, *J. Phys. Lett.*, **4**, 288 (1963).

(25) R. J. Kokes, *J. Phys. Chem.*, **66**, 99 (1962).

(26) R. J. Kokes, *Proc. Int. Congr. Catal.*, 3rd, Amsterdam 1964, **1**, 484 (1965).

(27) T. Kwan, Symposium on Electronic Phenomena in Chemisorption and Catalysis on Semiconductors, Walter de Gruyter & Co., Berlin, 1968.

(28) M. Setaka, K. M. Sancier, and T. Kwan, *J. Catal.*, **16**, 44 (1970).

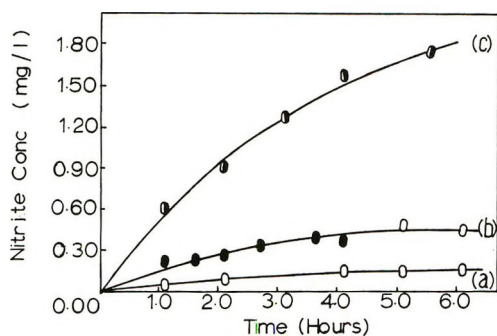


Figure 3. Growth of nitrite product with duration of exposure of dilute ZnO suspensions containing nitrate ions to light of wavelengths >345 nm at I_{eq} of 6.5×10^{16} : (a) data \circ , for ZnO- $\text{NaNO}_3(\text{aq})$ system; (b) data \bullet , for ZnO- $(\text{NaNO}_3 + \text{HCOO}^-(\text{aq}))$ systems; (c) data \ominus , for ZnO- $(\text{NaNO}_3 + \text{C}_2\text{H}_5\text{OH})(\text{aq})$.

atmospheric oxygen. Use of the polythene tubing did not affect the results, as shown by similar results obtained in tests with an all-glass transfer method.

Ultraviolet light from a medium-pressure mercury-arc lamp filtered by appropriate solutions (see A, B, and C above) was passed through the side wall of the cavity to the flat cell containing the suspension. The light beam was focused on the side of the cavity with a quartz lens. A "Blak-ray" uv meter (supplied by U.V. Products Inc., San Gabriel, Calif.) was used to monitor the relative value of the light intensity which was adjusted to a constant value.

Results

Quantum Efficiency of Zinc Oxide Promoted Photoreductions in Deoxygenated Solutions. Photoreduction of Sodium Nitrate-ZnO. Figure 3a illustrates the slow initial rate of appearance of NO_2^- in solution when suspensions of pure ZnO in $0.5 M$ NaNO_3 were illuminated with uv light of wavelengths >345 nm. Measured I_{eq}^0 flux was 6.5×10^{16} photons incident/sec on 350 ml of suspension. Since no nitrite was detected from $\text{NaNO}_3(\text{aq})/\text{ZnO}(\text{s})$ systems maintained in the dark, nor from $0.5 M$ NaNO_3 solutions exposed to the same uv light in the absence of ZnO, this result provided evidence for a zinc oxide promoted photoreduction. The calculated quantum efficiency, $\phi_{\text{NO}_2^-}$ based on the initial rate of appearance of nitrite, was 2.6×10^{-3} . As illustrated in Figure 2a, the apparent quantum efficiency was much lower at long illumination times. Prolonged illumination (>10 hr) removed the nitrite initially produced. Addition of formate ions at $0.1 M$ concentration yielded a higher initial rate of nitrite formation corresponding to $\phi_{\text{NO}_2^-} = 7.6 \times 10^{-3}$ (see Figure 3b) and studies with $\text{NaNO}_2(\text{aq})/\text{ZnO}(\text{s})$ suspensions indicated that formate "protected" nitrite from photoreaction at the ZnO surface. Ethyl alcohol at $1 M$ concentration yielded a still more rapid initial formation of nitrite corresponding to an apparent quantum efficiency of 2.6×10^{-2} .

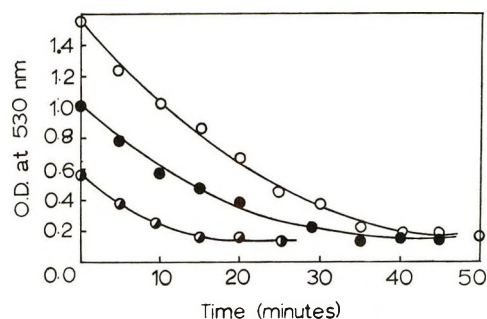


Figure 4. Zinc oxide promoted photobleaching of KMnO_4 solutions. Decrease in MnO_4^- absorbance having λ_{max} at 530 nm with duration of exposure is illustrated for a photon flux of $1.8 \times 10^{18} \text{ sec}^{-1} (350 \text{ ml})^{-1}$ and initial MnO_4^- concentrations of $7 \times 10^{-4} M$ (data points \circ); $4.5 \times 10^{-4} M$ (data \bullet) and $2.5 \times 10^{-4} M$ (data \ominus). Filter solution A was used.

Photoreduction of KMnO_4 Solutions-ZnO. It was convenient to study KMnO_4 solutions of initial MnO_4^- concentrations 2.5×10^{-4} to $6.9 \times 10^{-4} M$, since the extinction coefficient of $2.2 \times 10^3 \text{ l. mol}^{-1} \text{ cm}^{-1}$ for absorption at 550 nm corresponded to solution optical densities of 0.55–1.5. Optical densities of these solutions were lower in the wavelength region of the filtered lamp emission (290–390 nm) but this light caused a slow decrease of OD at 550 nm even in the absence of zinc oxide. A greatly enhanced rate of decrease in OD at 550 nm was observed when zinc oxide was added to the illuminated KMnO_4 solutions. Data illustrating this additional zinc oxide promoted photoreduction were obtained by difference and are illustrated in Figure 4. Apparent quantum efficiencies for loss of KMnO_4 in these systems were 5.8×10^{-2} for pure ZnO, 4.6×10^{-2} for indium-doped ZnO, and 2.5×10^{-2} for lithium-doped zinc oxides, all based on the additional rate of loss of absorbance at 550 nm caused by illumination with $I_{eq}^0 = 1.8 \times 10^{18} \text{ photons sec}^{-1} (350 \text{ ml})^{-1}$. The only observed product of the photolysis of aqueous solutions of KMnO_4 over zinc oxide surface was a dark brown precipitate which was soluble in HCl and appeared to be MnO_2 . Accumulation of this brown precipitate in the suspension as reduction proceeded made this system unsuitable for detailed kinetic study, since it introduced additional light-scattering and absorption, thereby preventing bleaching from proceeding smoothly to completion.

Photoreduction of Indigo Carmine-Zinc Oxide. Figure 5 illustrates the zinc oxide-promoted photobleaching of $7.5 \times 10^{-5} M$ aqueous solution of indigo carmine under illumination by uv photons of wavelengths >345 at $I_{eq}^0 = 6.5 \times 10^{16} \text{ photons sec}^{-1} (350 \text{ ml})^{-1}$. From the observed initial rate of loss of absorbance at 610 nm ($0.105 \text{ OD unit min}^{-1}$) and reported¹⁹ extinction coefficient ($\epsilon = 1.8 \times 10^4$) the quantum efficiency of photobleaching was calculated to be 0.04.

The spectrum of the faintly yellow solution which was obtained from photolysis of the dark blue solutions

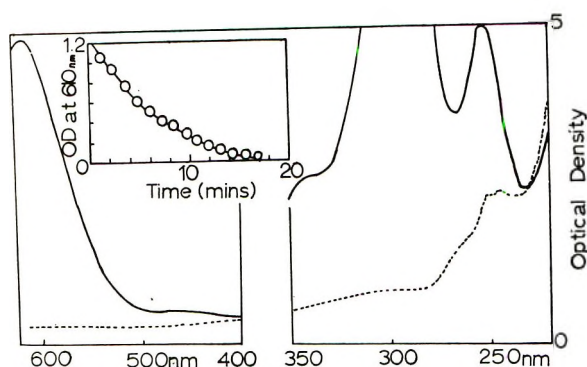


Figure 5. Zinc oxide-promoted photoreduction of an aqueous solution of indigo carmine (IC). Absorption spectra of starting material ($7.5 \times 10^{-5} M$ indigo carmine) is shown as a solid line. Insert illustrates the continuous decrease in absorbance at 610 nm with duration of exposure to a flux of 6.5×10^{18} photons sec^{-1} at wavelengths >345 nm. Broken line shows residual absorbance after bleaching.

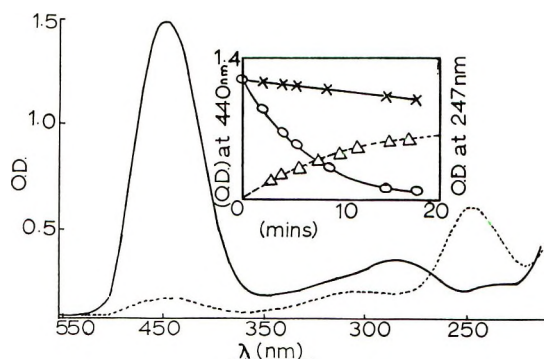


Figure 6. Zinc oxide-promoted reduction of PNDA in ZnO-PNDA(aq) suspensions. Absorption spectra of starting material (solid line) and product are shown. Insert illustrates slow reduction in absorbance at 440 nm in the dark (\times — \times) and accelerated reduction under illumination (\circ — \circ) by photons of wavelengths 300–390 nm at a flux of $1.8 \times 10^{18} \text{ sec}^{-1}$. Insert also illustrates growth of product absorbing at 247 nm (data \triangle — \triangle).

containing indigo carmine over zinc oxide resembled that suggested in the literature²⁹ to arise from a reduced product of the starting material.

Photoreduction of *p*-Nitrosodimethylaniline-Zinc Oxide. Experimental data in Figure 6 illustrates the relative rates of zinc oxide-promoted dark reaction and of photoreaction at room temperature for magnetically stirred deoxygenated suspensions containing 0.35 g of powdered pure zinc oxide per 350 ml of solution with an initial PNDA concentration of $4 \times 10^{-5} M$. The data were taken by measuring the progressive decrease with time in the absorbance at 440 nm, which also is illustrated in Figure 6 together with growth of an absorption band at 247 nm. Quantum efficiency of photobleaching could thus be obtained either from the photo-induced enhancement (relative to the dark rate) of rate of loss of absorbance at 440 nm, *i.e.*, ϕ_{PNDA} , or from the photo-enhanced rate of growth of product absorbance

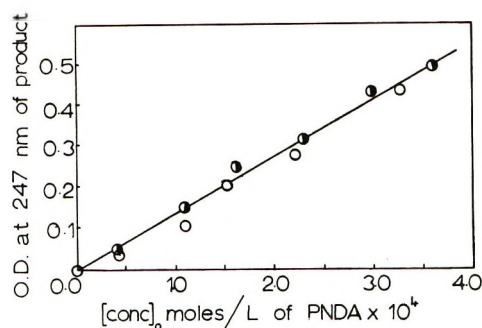


Figure 7. Plot illustrating the correlation between absorbance of zinc oxide-promoted photoproduct (data \circ) from various initial concentrations of PNDA and that obtained by reducing the same PNDA concentrations with zinc dust (data \bullet).

at 247 nm, *i.e.*, ϕ_{247} . For the data in Figure 6 the initial ϕ_{PNDA} value corresponded to 1.2×10^{-2} , using the measured molar extinction coefficient of $3.5 \times 10^4 \text{ l. mol}^{-1} \text{ cm}^{-1}$. The latter was derived from linear Beer's law plots.

Treatment of deoxygenated aqueous PNDA solutions at, or close to, neutral pH with clean zinc powder removed absorbance at 440 nm and produced an absorption band at 247 nm indistinguishable from that present in photobleached PNDA solutions. In Figure 7 a comparison is made between the optical densities experimentally observed at 247 nm when various initial concentrations of PNDA were quantitatively reduced with zinc dust, and the OD values observed when the same PNDA concentrations were completely photobleached. Agreement between both sets of OD values confirms that the photoproduct in deoxygenated solutions was identical with the reduced product obtained with zinc dust and provided a value of $1.4 \times 10^4 \text{ l. mol}^{-1} \text{ cm}^{-1}$ for the extinction coefficient of the reduced product. The value of $\phi_{\text{product}} = 1.2 \times 10^{-2}$ obtained using this value of ϵ and the observed initial rate of growth of absorbance at 247 nm was identical with ϕ_{PNDA} , which is consistent with quantitative conversion of PNDA to reduced product by photobleaching. In the literature,³⁰ reduction of *p*-nitroso compounds with zinc dust leads to corresponding *p*-hydroxylamine compounds. The absorption with λ_{max} at 247 nm and $\epsilon \sim 10^4$ may thus be assigned to *p*-hydroxylamine dimethylaniline (denoted here as PNDA- H_2).

A summary of the quantum efficiencies of these four zinc oxide-promoted photoreductions in various conditions is given in Table II which shows that all values lay between 4×10^{-2} and 8×10^{-4} at high light intensity conditions.

Epr Studies on H_2O -ZnO, PNDA-ZnO, IC-ZnO,

(29) L. Fieser and M. Fieser, "Organic Chemistry," Reinhold, New York, N. Y., 1956.

(30) H. Fever, Ed., "The Chemistry of the Nitro and Nitroso Group," Part I, Interscience, New York, N. Y., 1969.

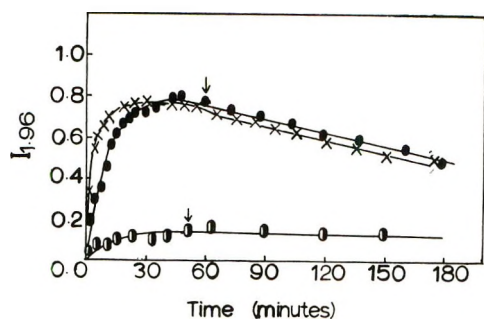


Figure 8. Data illustrating growth of intensity, $I_{1.96}$ of a singlet epr signal with $g = 1.96$ when dense suspensions of preactivated zinc oxide in deoxygenated pure water were illuminated with uv light *in situ* in the epr cavity. Slow decay of the epr signal after illumination ceased (at \downarrow) is also illustrated. Data \bullet , taken with ZnO preactivated 3 hr at 500° ; data \times , with ZnO preactivated 2 hr at 500° , both exposed to photons of λ 300–390 nm; data \circ , taken with ZnO preactivated 3 hr at 500° but exposed to photons of $\lambda > 400$ nm.

and KMnO_4 -ZnO. No epr signal with $g = 1.96$ was observed prior to illumination from suspensions of pure zinc oxide in deoxygenated triply distilled water. A weak broad signal with $g \sim 2.00$ was observed from suspensions if the zinc oxide was not sufficiently well outgassed at temperatures $< 500^\circ$. Investigations of photoproduced epr signals were only made on H_2O -ZnO or D_2O -ZnO systems free from this signal with $g = 2.00$, which probably originated from O_2^- or HO_2 on the zinc oxide surface.

Under illumination with light of wavelengths 290–390 nm while held in the aqueous flat cell *in situ* in the epr cavity, H_2O -ZnO suspensions yielded a singlet epr signal with $g = 1.96$ for spectrometer settings identical with those which failed to yield a signal prior to illumination. Typical growth curves for the intensity $I_{1.96}$ of the signal with $g = 1.96$ under illumination are shown in Figure 8, where it will be noted: (i) that under steady illumination, $I_{1.96}$ required *ca.* 30 min to attain a limiting value; (ii) that this limiting value was reproducible within $\pm 25\%$ for H_2O -ZnO suspensions prepared and illuminated on different days; (iii) that the rate of approach to the limiting value was affected by residual adsorbed species on the zinc oxide surface; (iv) that decay of photo-generated signal intensity $I_{1.96}$ was very slow after illumination ceased; and (v) that illumination with a comparable total photon flux lacking photons of wavelengths inside the zinc oxide band edge (385 nm) produced limiting values of $I_{1.96}$ which were much lower than for photons of wavelengths 290–390 nm.

When suspensions of zinc oxide were prepared in similar manner but with aqueous solutions of PNDA, or indigo carmine, or KMnO_4 or NaNO_3 rather than pure water, no epr signal at $g = 1.96$ was detected in any suspension prior to illumination. As illustrated in Figure 9 for PNDA(aq)/ZnO(s) suspensions, illumination did produce an epr signal with $g = 1.96$ but the

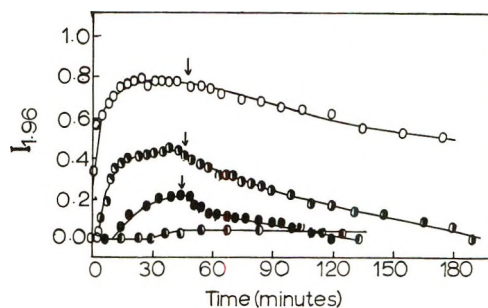


Figure 9. Growth and decay of intensity $I_{1.96}$ of epr signal with $g = 1.96$ compared for dense ZnO- H_2O suspensions and ZnO suspensions in solutions containing various concentrations of PNDA: data \circ , for ZnO- H_2O ; data \bullet , for suspensions $\{\text{PNDA}\} = 1.5 \times 10^{-4} M$; data \bullet , in $\{\text{PNDA}\} = 3 \times 10^{-4} M$; data \bullet , in $\{\text{PNDA}\} = 6 \times 10^{-4} M$. Illumination commenced at $t = 0$ and ceased at arrow in each case.

presence of any of these solutes affected the rate of growth, the limiting value, and the rate of decay of $I_{1.96}$. Effects very similar to those shown in Figure 9 were obtained with indigo carmine, notably that the rate of growth and limiting intensity were greatly reduced whereas the rate of decay of $I_{1.96}$ after illumination was increased. The effect of KMnO_4 was more pronounced and prevented appearance of any readily measurable $I_{1.96}$ value, even when present at only $10^{-5} M$ concentration. Since, indigo carmine, PNDA, and KMnO_4 were indicated in the preceding section to undergo zinc oxide-promoted photoreduction, and since previous workers had assigned the epr singlet with $g = 1.96$ to conduction band electrons or to donor centers in equilibrium with the conduction band, a reasonable working hypothesis was that these solutes acted to provide more rapid and efficient pathways for removal of electron-excess centers produced at the ZnO- H_2O interface by uv illumination.

Epr results with illuminated $\text{NaNO}_3(\text{aq})$ -ZnO suspensions are illustrated in Figure 10a and appeared to be at variance with this working hypothesis, since NO_3^- increased the steady-state value of $I_{1.96}$. The assumption that zinc oxide-promoted photoreduction of NO_3^- to NO_2^- (see Figure 2) proceeded *via* interaction of NO_3^- with electron-excess centers at the interface leads to a predicted decrease in $I_{1.96}$ in the presence of NO_3^- . The origin of this anomaly was further investigated by investigating the influence of NO_3^- upon the rate of photoreduction of PNDA.

Competition-Kinetic Studies. Figure 10b illustrates that the effect of added NO_3^- upon PNDA-ZnO photoreduction was to increase the rate of photoreduction. Nitrate thus appeared to interact at the illuminated H_2O -ZnO interface with some species other than the electron-excess centers responsible for the epr signal and for PNDA photoreduction. Further information on the nature of these additional "active" species at the illuminated interface and on the identity of the centers responsible for PNDA photoreduction

Table III: Relative Reactivities of Solutes in Aqueous Solutions and ZnO Suspensions at pH ≈ 7

Literature values ^a of			Solute	Concentration to achieve ($I^c - I^0$)/($I^0 + I^c$) = $\pm 0.33^b$		Concentration to achieve ($\phi^c - \phi^0$)/($\phi^0 + \phi^c$) = $\pm 0.33^c$	
k_{S+e}	k_{S+H}	k_{S+OH}		Concn, M	Effect	Concn, M	Effect
3.4×10^{10}		1.8×10^{10}	PNDA	1.5×10^{-4}	-0.33		
			IC	$\sim 3 \times 10^{-4}$	-0.33		
3.3×10^{10}			MnO_4^-	$< 10^{-5}$	-0.33		
$< 10^5$	2.5×10^8	2.5×10^9	$HCOO^-$	$\sim 9 \times 10^{-3}$	+0.33	5×10^{-3}	+0.33
9.6×10^9	8×10^6		NO_3^-	$\sim 2 \times 10^{-2}$	+0.33	4×10^{-2}	+0.33
$< 10^5$	1.1×10^9	1.6×10^7	C_2H_5OH	~ 1	+0.33	1	+0.33
		8.5×10^9	I^-	$\sim 5 \times 10^{-4}$	-0.33	3×10^{-5}	-0.33
3.4×10^{10}	10^8	7.6×10^9	Tl^+	$\sim 8 \times 10^{-4}$	-0.33	5×10^{-5}	-0.33
4.6×10^9	2.4×10^9	3.6×10^9	NO_2^-	...	-0.33	4×10^{-4}	-0.33
$< 10^6$		3×10^8	CO_3^{2-}	$\sim 5 \times 10^{-2}$	-0.33	1×10^{-2}	-0.33
5.6×10^9			N_2O	$\sim 10^{-3}$	-0.18
1.9×10^{10}		1.2×10^{10}	O_2			$\sim 10^{-3}$	0

^a Data mainly from ref 16 in units of $M^{-1} \text{ sec}^{-1}$ are rate constants for reaction of indicated solute with $e^-(\text{aq})$, $H(\text{aq})$, or $OH(\text{aq})$.

^b I^0 refers to intensity of esr signal with $g = 1.96$ in a ZnO-H₂O system; I^c to intensity in presence of concn C of a single additive. Photon flux of 6×10^{16} photons incident on sample in esr cell. ^c ϕ^0 refers to quantum yield of PNDA photoreduction for suspensions containing only PNDA_{aq} at $1.5 \times 10^{-4} M$; ϕ^c refers to quantum yield of PNDA photoreduction in the presence also of concn C of the indicated second additive. Photon flux of 6×10^{16} photons incident on suspensions.

was sought by placing solutes other than NO_3^- into competition against PNDA. Solute were selected for their known high rate constants (see Table III) for reaction with electrons, or H atoms, or OH radicals, since the electron, holes, and excitons generated directly in ZnO by uv photons may give rise to surface species resembling e_{aq}^- , H, or OH at the ZnO surface, which is strongly hydroxylated in our conditions.³¹

Inhibiting Additives. Figure 11 illustrates a typical sequence of rates of photobleaching obtained with aqueous suspensions all of the same initial PNDA concentration and ZnO concentration but having various concentrations of iodide ion. Similar "families" of rate plots, showing the PNDA photobleaching rate decreasing as additive concentration, $\{A\}$, increased, were obtained with Tl^+ , CO_3^{2-} or NO_2^- as second additives. For each of these additives, data such as those in Figure 11a were tested, in the conventional manner, for agreement with the requirements of a model envisaging competition between PNDA and the additive for the same reactive intermediate produced by illuminating the ZnO-aq solution interface. Extent of agreement with relationship 2 is illustrated in

$$R_0/R_A = 1 + \frac{k_A\{A\}}{k_{\text{PNDA}}\{\text{PNDA}\}} \quad (2)$$

Figure 11b for iodide as the competing additive (here R_A and R_0 denote the observed initial rates of disappearance of PNDA in the presence or absence of additive at concentration $\{A\}$, k_{PNDA} is the rate constant for reaction of PNDA with radiation-produced intermediate and k_A relates to reaction of A with the same intermediate). Plots similar to those of Figure 11b were obtained for NO_2^- , CO_3^{2-} , and Tl^+ and linear relationship between R_0/R_A and $\{A\}/\{\text{PNDA}\}$ held only over a small range of concentration ratios. Lack

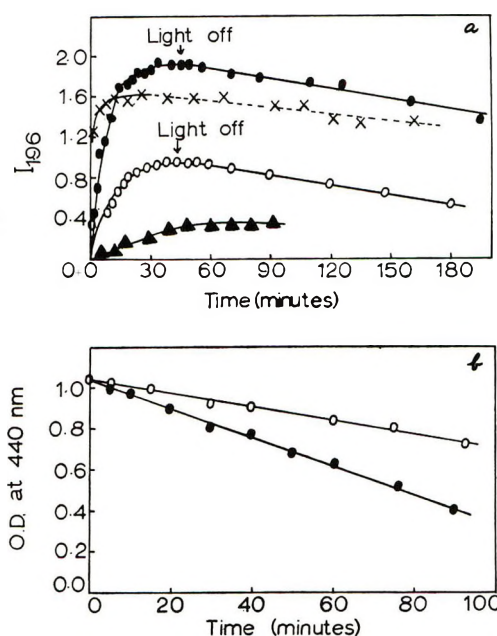


Figure 10. a, Comparison of steady-state intensity $I_{1.96}$ of singlet esr signal with $g = 1.96$ attained under identical uv illumination for a ZnO-pure H₂O dense suspension (data ○), and for a ZnO suspension in NaNO₃ (aq) at $2 \times 10^{-2} M$, (data ●); for a ZnO suspension containing $8 \times 10^{-3} M HCOO^-$ (data ×) and for ZnO suspension containing $1.6 \times 10^{-3} M I^-$ (data △). b, Initial rate of PNDA photoreduction with photons $> 345 \text{ nm}$ in the absence of other additive (data ○) and with $4 \times 10^{-2} M NO_3^-$ (data ●).

of exact agreement with (2) was not unexpected, since the PNDA photobleaching data did not obey first- (nor second-) order kinetics in the absence of other additives. Relative rate constants for reactivity

(31) (a) *Discuss. Faraday Soc.*, **52**, 1 (1971); (b) K. Atherton, G. Newbold, and J. A. Hickey, *ibid.*, **52**, 33 (1971); (c) H. P. Boehm, *ibid.*, **52**, 264 (1971).

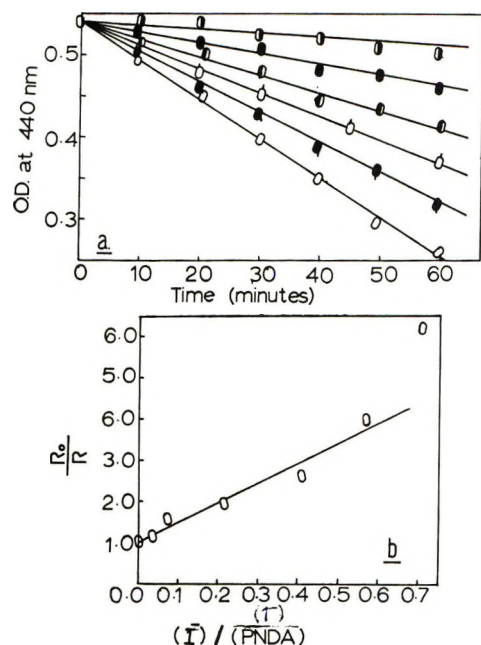


Figure 11. Competition between PNDA and I^- for species generated in ZnO by uv light. a, Data illustrating reduced initial rates of PNDA photobleaching ($1.5 \times 10^{-4} M$) in the presence of various concentrations of I^- : \circ , for $\{I^-\} = 0$; \bullet , for $\{I^-\} 1 \times 10^{-6}$; \circ , for $\{I^-\} 3.1 \times 10^{-6}$; \bullet , for $\{I^-\} 5.7 \times 10^{-6}$; \bullet , for $\{I^-\} 7.9 \times 10^{-6}$ and \circ , for $\{I^-\} 10^{-4} M$. Data all taken with photon flux of $5.9 \times 10^{16} \text{ sec}^{-1}$. b, Rates from Figure 11a tested against competition kinetic expression 2 in text.

toward the intermediate reducing PNDA at the illuminated ZnO-aqueous solution interface were derived from plots similar to those of Figure 11b and were in the ratio, $I^-:Ti^+ : NO_2^- : CO_3^{2-} = 1.0:0.63:0.13:0.003$.

These additives were also tested for their effects upon the saturation value of the epr signal produced by illuminating ZnO- H_2O suspensions in the flat cell. Each of the additives, I^- , Ti^+ , NO_2^- and CO_3^{2-} reduced the saturation intensity of the singlet epr signal with $g = 1.96$ and Figure 10a illustrates this effect for dense ZnO- H_2O suspensions prepared with I^- present. The approximate concentration of additive required to reduce the saturation intensity by 50% relative to ZnO-pure H_2O suspensions were 5×10^{-4} for I^- , 8×10^{-4} for Ti^+ , and 5×10^{-2} for CO_3^{2-} . It may be noted from curves a and b of Figure 9 that $1.5 \times 10^{-4} M$ is the PNDA concentration needed to reduce $I_{1.96}$ by 50% relative to ZnO-pure H_2O suspension similarly illuminated in the flat cell. Data on the concentrations needed to halve the intensity of the steady-state epr signal are summarized in Table III in the column headed $(I^c - I^0)/(I^c + I^0)$. These may be compared with $(\phi^c - \phi^0)/(\phi^c + \phi^0)$ values, which are the concentrations needed to halve the initial rate of photobleaching of $1.5 \times 10^{-4} M$ PNDA solutions.

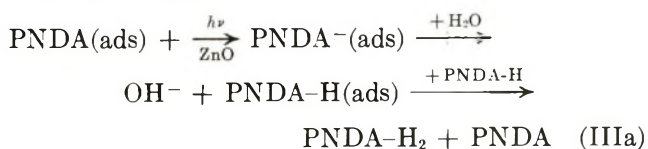
Promoting Additives. In contrast to effects noted above with I^- , Ti^+ , NO_2^- , and CO_3^{2-} additives, an

increase in rate of PNDA photobleaching and an increase in $I_{1.96}$ was observed when ethyl alcohol, formate ion, or nitrate ion was present in the illuminated zinc oxide suspensions. The promoting effect on epr was illustrated for nitrate as additive in Figure 10a where it was noted that an NO_3^- concentration of $2 \times 10^{-2} M$ approximately doubled $I_{1.96}$. Figure 10b illustrated the promoting effect of nitrate on rate of PNDA photobleaching and $4 \times 10^{-2} M NO_3^-$ approximately doubled the rate. In other studies with initial PNDA concentration of $3 \times 10^{-4} M$, relative efficiency of these additives as rate promoters increased in the sequence $C_2H_5OH < NO_3^- < HCOO^-$, as indicated by the concentration needed to double the rate of photobleaching of dilute ZnO-PNDA suspension ($\sim 1 M$ for C_2H_5OH , $4 \times 10^{-2} M$ for NO_3^- , and $\sim 5 \times 10^{-3} M HCOO^-$).

Additives with Minor Effect. Within the $\pm 20\%$ limits of reproducibility in rate of PNDA photobleaching (in a sequence of experiments extending over a 3-month period) no significant increase or reduction in rate was effected by the presence of Cl^- or SO_4^{2-} at concentrations $< 10^{-3} M$. Neutral, electron-attaching molecules, O_2 or CH_3I , present at their limiting solubilities (*ca.* $10^{-3} M$) likewise failed to effect significant changes in rate of PNDA photobleaching. A marginal reduction of 30% in photobleaching rate was noted for ZnO-PNDA(aq) suspension bubbled with N_2O instead of N_2 . Gaseous additives could not be introduced to dense suspensions in the epr flat cell but the presence of CH_3I did not reduce $I_{1.96}$ relative to that in dense ZnO- H_2O suspensions.

Discussion

Comparison of present results with published work on zinc oxide promoted photosynthesis of H_2O_2 in oxygenated aqueous solutions^{2,7} suggested that the observed photoreduction of PNDA to PNDA- H_2 at the ZnO- H_2O interface proceeds, at least in part, *via* mechanism IIIa, *viz.*



In this mechanism, adsorbed PNDA molecules in deoxygenated solution undergo successive processes of: first, electron attachment; second, proton transfer from H_2O ; and third, disproportionation. This sequence is suggested in the literature for adsorbed O_2 molecules at oxygenated H_2O -ZnO interfaces exposed to uv illumination.²⁻⁷ A sequence of steps very similar to that in (IIIa) has been proposed^{13b} by Baxendale and Khan to explain their results on pulse radiolysis of deoxygenated solutions of PNDA at neutral pH. They identified the spectrum of an intermediate of type PNDA-H and obtained evidence for reappearance of

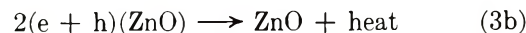
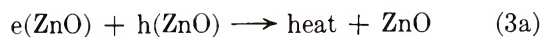
PNDA by disproportionation. In their work, reduction of PNDA to PNDA-H₂ in deoxygenated neutral solutions was initiated by interaction with H atom or e_{aq}⁻ intermediate produced in water by pulses of ionizing radiation. Mechanism (IIIa) above likewise identifies interaction of PNDA with electrons as the step initiating reduction at uv illuminated PNDA(aq)/ZnO interfaces, but these electrons originate from interaction of radiation with the zinc oxide particles rather than with the solution. The following features of the observed results may also be understood in terms of mechanism IIIa.

(i) *Dark Reaction.* The observed specific rates of reduction of PNDA at dark H₂O-ZnO interfaces (see Table I) increase in the sequence Li-ZnO < ZnO < In-Zn, as expected if dark reaction proceeds *via* interaction of adsorbed PNDA with conduction band electrons whose density is greatest in In-ZnO and least in Li-ZnO. Since thermal equilibration of electrons normally occurs at room temperature between conduction-band states and shallow donors such as Zn_i⁰ or Zn_i⁺, the observed similarity between reduction effected by zinc dust and that by dark (or photo-) reaction over ZnO, can be attributed to the reactivity of "Zn⁰-like" states at H₂O-ZnO and H₂O-Zn interfaces.

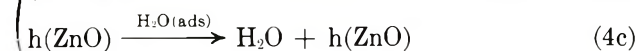
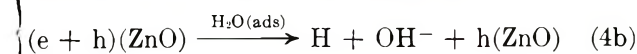
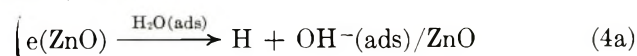
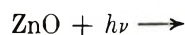
(ii) *Enhanced Quantum Efficiency.* It was proposed previously that the process of electron localization was slow and rate determining at ZnO-N₂O(g) and ZnO-CD₃I(g) interfaces because of negative surface potential produced in prior dark reaction.⁹⁻¹¹ However, at the solution pH values of 7-8 encountered in present studies of the ZnO-H₂O interface, H⁺(ads) ions predominate over OH⁻(ads) on the ZnO surface, because solution pH of ca. 9.5 is required to achieve zero point of charge.³¹ The greatly enhanced quantum efficiency of photoreaction at the ZnO-H₂O interface (see Table II) relative to ZnO-gas interfaces may therefore be understood to result, at least in part, from existence of a positive rather than a negative surface potential. Positive surface potential would accelerate step 1 of mechanism IIIa.

Solvent molecules at the H₂O-ZnO interface may also play an important role in enhancing quantum efficiency above that found previously at interfaces between gaseous N₂O or CH₃I and the same zinc oxides as are used in the present study. Thus any interaction which increased the lifetime or reactivity of electrons produced when ZnO absorbs a uv photon should enhance the probability for reaction *via* step 1 of mechanism IIIa, as opposed to dissipation of the energy *via* radiative or radiationless electron-hole decay in zinc oxide. Data in Table II for quantum efficiencies of photoreduction in PNDA-ZnO at various intensities show conclusively that much dissipation of radiation energy *via* electron-hole decay was occurring in our "high intensity" ($I_0 \sim 10^{18}$) conditions. Thus the quantum efficiency of photoreduction of PNDA is there seen to

increase as incident intensity decreased (from $\phi = 1.2 \times 10^{-2}$ at $I_{eq}^0 = 1.8 \times 10^{18}$, to $\phi = 0.13$ at $I_{eq}^0 = 6 \times 10^{16}$, and finally to $\phi = 0.23$ at $I_{eq}^0 = 1.9 \times 10^{16}$ quanta sec⁻¹ 350 ml⁻¹). Such strong dependence of efficiency upon intensity has been attributed in other irradiated solids³² to increasing probability of radiationless bimolecular quenching processes at higher intensities. In the zinc oxide system these would take the form of (3a) or (3b).



Summarized under eq 4 are possible modes of interaction of solvent molecules with electrons, excitons or holes present at H₂O-ZnO interfaces under uv illumination. Process 4a corresponds to dissociative electron



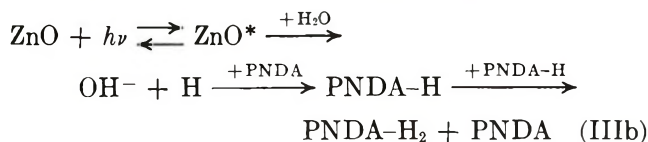
attachment to H₂O, and a rate constant ca. 16 l. mol⁻¹ sec⁻¹ has been measured for this process when it involved fully hydrated electrons in pulse radiolysis experiments with pure water.¹⁴ Ionization of an exciton by encounter with surface H₂O (process 4b), lacks direct experimental support but appears energetically feasible in view of the small energy (ca. 0.1 eV) "binding" the electron and hole in ZnO excitons.¹⁵ The net effect of (4a) and (4b) would be to convert into H atoms some fraction of those electrons or excitons which reach the H₂O-ZnO interface. Evidence supporting this representation of photoreducing action at H₂O-ZnO interfaces as resulting, in part, from H-atom formation come from the previously reported formation of H₂(g), albeit with $\phi_{\text{H}_2} \approx 10^{-5}$, in the H₂O-ZnO system under intense uv illumination.¹² Data in the following section may also be interpreted on this basis.

(iii) *Effects of Inhibiting Additives.* Table III summarizes the parallel effects which the additives I⁻, Tl⁺, NO₂⁻, and CO₃²⁻ had in reducing the rate of PNDA photoreduction and in decreasing the steady-state value of the epr signal with $g = 1.96$ (cf. entries of -0.33 in Table III). Conflicting interpretations in the literature²²⁻²⁵ have assigned this epr signal either to electrons in the conduction band of ZnO or to electron-excess donor centers, *viz.*, Zn_i⁺, in sub-surface layers, or to electrons trapped at surface states such as anion vacancies. Present results do not resolve this dispute, since the observed reduction in the steady-state value of $I_{1.96}$ effected by PNDA, MnO₄⁻, or indigo carmine can be accounted for on mechanism IIIa simply in terms

(32) D. Pooley, *Proc. Phys. Soc. London*, **89**, 723 (1966).

of competition by these species for the electrons needed to yield any of these electron-excess centers.

Concentrations of PNDA for the majority of competition kinetic experiments was that ($1.5 \times 10^{-4} M$) seen in Table III to reduce $I_{1.96}$ by 50%. Consequently some 50% of the primary radiation produced intermediates capable of yielding electron-excess centers escaped reaction with PNDA and were free to yield, *via* (4a) or (4b), species resembling hydrogen atoms at the H_2O -ZnO interface. Chemisorption of hydrogen onto zinc oxide can produce surface configurations, $>Zn-H$ or $>Zn-O-H$, depending on the site of adsorption. Inhibiting effects of I^- , Tl^+ , NO_2^- , and CO_3^{2-} and their relative magnitudes are most readily understood on the basis that they compete against PNDA for secondary reducing sites with the latter configuration. Such sites have similarities to OH radicals at the interface and all the inhibiting additives have high rate constant for reaction with OH radicals (*cf.* Table III where the sequence of relative reactivities from published rate constants is ($I^-(1.00) > Tl^+(0.9) > NO_2^-(0.4) \gg CO_3^{2-}(0.03)$). This can account qualitatively for the relative rate constants here deduced from competition-type plots, *viz.*, $I^-(1.00) > Tl^+(0.63) > NO_2^-(0.13) \gg CO_3^{2-}(0.003)$). Incorporation of processes 4a and/or 4b into mechanism III as alternative pathways to the PNDA-H intermediate thus seem fully consistent with the enhanced quantum efficiency of the aqueous solution-ZnO interface and with effects of inhibiting additives. The mechanism of photo-reduction thus modified is summarized by



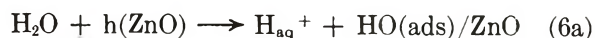
Oxidative Processes. Although type III mechanisms can thus account for several features of the results, they represent only the reducing properties of the illuminated surface, whereas a complete account of photo-produced processes at the H_2O -ZnO interfaces must also describe the *oxidative* properties of the illuminated interface. The need for compensating oxidative process(es) can be clearly seen from the fact that solution pH did not change markedly (ΔpH typically $\sim 7.2 \rightarrow 6.8$) during photobleaching of 10^{-3} mol of PNDA, whereas (IIIa) would require that 2×10^{-3} mol of OH^- be produced and that a large potential build up on the ZnO particles. Elovich-type kinetics should ultimately result if the surface potential attained large values, but the kinetic data presented in this paper could not be fitted to the integrated form of the Elovich expression 5 with any reasonable choice of the adjust-

$$\Delta\{PNDA\} = \log(t + t_0) + D \quad (5)$$

able parameter t_0 . Instead first-order kinetics were

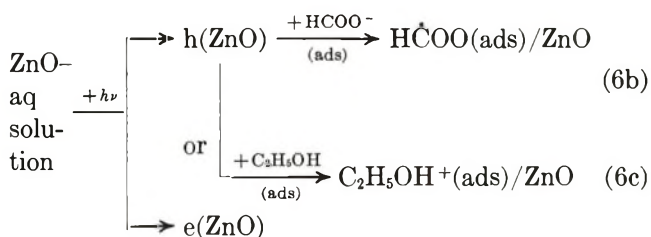
observed when pH was accurately controlled; as will be shown in a later paper.³³

Detailed discussion of the nature of oxidative processes is outside the scope of the present paper but it should be noted that process 4c provides a possible hole-localizing mechanism for ZnO suspensions in additive-free systems. If (4c) is followed by proton loss from the H_2O near which the hole is localized in ZnO, *viz.*



this could explain the small photo-induced decreases in system pH noted here and by previous workers^{2,34} for H_2O -ZnO suspensions. Work is in progress in these laboratories³³ to compare this model of the oxidative process against that recently advanced by Dixon and Healy.³⁴

Additives Which Enhanced Photoreduction and $I_{1.96}$. Several electrochemical studies^{35,36} of photovoltaic and photocurrent effects at illuminated ZnO electrodes have shown that formate ion or alcohols interacted with holes when the ZnO electrode was anodically biased during illumination of the ZnO- H_2O interface. It is reasonable to conclude, therefore, that formate or alcohol present at ZnO- H_2O interfaces in aqueous ZnO suspensions studied in this work increased $I_{1.96}$ by interacting with holes as in (6b) or (6c), thereby reducing the number of type 3a ineffective electron-hole recombinations.



The overall stoichiometry of these processes requires that one electron escapes recombination for each hole trapped at the surface by formate or alcohol. Since the intermediates, $\dot{H}COO$ and $C_2H_5OH^+$, produced by hole-trapping have been shown to be strongly and quantitatively reducing toward organic molecules^{2b-7} including PNDA,^{13b} a correlation is implied between increased intensity of the epr signal and increased rate of PNDA photoreduction. Data in Table III on enhancing additives $HCOO^-$, C_2H_5OH , and NO_3^- are not inconsistent with such a correlation, since the concentration of each additive needed to double the intensity of the epr signal differs by less than a factor of 2 from the concentration of additive needed to double the rate

(33) J. Cunningham and S. Corkery, *Trans. Faraday Soc.*, in press.

(34) D. R. Dixon and T. W. Healy, *Aust. J. Chem.*, **24**, 1193 (1971).

(35) S. R. Morrison and T. Freund, *J. Chem. Phys.*, **47**, 1543 (1967).

(36) W. P. Gomes, T. Freund, and S. R. Morrison, *J. Electrochem. Soc.*, **115**, 818 (1968).

of PNDA photoreduction, despite the very great differences in the two techniques.

Conclusions

From these considerations of reducing and oxidizing processes at ZnO-H₂O interfaces under uv illumination, it appears that present results on extent and quantum efficiency of photoreduction, on lack of large pH changes and on effects of inhibiting and promoting additives, can be qualitatively accounted for by an overall mechanism combining (IIIa) or (IIIb) with oxidative steps. Further detailed investigation of the dependence of photoreaction and $I_{1.96}$ upon solution pH and additives

are needed to establish which oxidative processes best correlate with the varying magnitude of the epr signal and with kinetics of photoreaction. Such investigations are in progress in these laboratories.³³

Acknowledgments. The authors are grateful to J. Kelly, A. Penny, M. Donovan, and M. Nowlan for experimental assistance and to J. Thompson for loan of photolysis equipment. Stimulating discussions with J. Clarke and W. Mehl are also acknowledged. Financial and equipment support from AFOSR greatly assisted the study and H. Z. is grateful to University of Bagdad for a grant.

Radiolysis of Liquid 2,2,4-Trimethylpentane. Kinetics of Scavenging Processes¹

by Stefan J. Rzad* and Krishan M. Bansal

Radiation Research Laboratories and Center for Special Studies, Mellon Institute of Science, Carnegie-Mellon University, Pittsburgh, Pennsylvania 15213 (Received January 27, 1972)

Publication costs assisted by the U. S. Atomic Energy Commission

The methyl radical yield observed upon electron scavenging by methyl bromide in γ -irradiated 2,2,4-trimethylpentane can be quantitatively described by an empirical model similar to that proposed for cyclohexane, $G(\text{CH}_3) = G_{fi} + G_{gi} \sqrt{\alpha_{\text{CH}_3\text{Br}}[\text{CH}_3\text{Br}]/(1 + \sqrt{\alpha_{\text{CH}_3\text{Br}}[\text{CH}_3\text{Br}]})}$. This model was also found to be a good description of data from other scavengers—ethyl bromide and sulfur hexafluoride—in 2,2,4-trimethylpentane. The following parameters were obtained by treating the results in this manner: $G_{fi} = 0.3$, $G_{gi} = 4.54$, $\alpha_{\text{CH}_3\text{Br}} = 24.7 \text{ M}^{-1}$, $\alpha_{\text{SF}_6} = 65 \text{ M}^{-1}$, $\alpha_{\text{C}_2\text{H}_5\text{Br}} = 5 \text{ M}^{-1}$. From the analysis of the scavenging data it is concluded that (1) the characteristic thermalization length in 2,2,4-trimethylpentane is $\sim 50\%$ longer than that in cyclohexane and (2) the rate constant of electron scavenging by CH₃Br as well as the constant λ , representing the recombination rate of geminate ions, are approximately ten times higher in 2,2,4-trimethylpentane than in cyclohexane. The analysis of the nitrogen yields from N₂O-2,2,4-trimethylpentane solutions allows one to estimate that the reaction of the secondary ion produced upon electron capture by N₂O proceeds at a diffusion-controlled rate.

Introduction

Although the radiation chemistry of *n*-alkanes (e.g., *n*-hexane) and cycloalkanes (e.g., cyclohexane) has been studied extensively, much less attention has been focused on branched hydrocarbons.² Recent charge scavenging studies indicated that ionic processes play an important part in product formation in cyclohexane radiolysis.³ These charge scavenging studies are amenable to quantitative interpretation⁴⁻⁶ in terms of an empirical model previously proposed. Physical methods⁷⁻⁹ substantiated by chemical studies^{4-6,10} have shown that in *n*-alkanes and cycloalkanes most ions (geminate ions) generated by radiation recombine very rapidly ($<10^{-9}$ sec), and only a small fraction ($\sim 5\%$) escapes geminate recombination and becomes homogeneously distributed throughout the medium

(free ions). Furthermore, the physical methods also indicated that the yield of ions escaping geminate recombination^{8,9} increased with increasing branching in the hydrocarbons. In addition, the electron mobility

- (1) Supported in part by the U. S. Atomic Energy Commission.
- (2) For a review see, for example, T. Gütmann and J. Hoigne, Ed., "Aspects of Hydrocarbon Radiolysis," Academic Press, New York, N. Y., 1968.
- (3) For a review see J. M. Warman, K.-D. Asmus, and R. H. Schuler, *Advan. Chem. Ser.*, **No. 82**, 25 (1968).
- (4) J. M. Warman, K.-D. Asmus, and R. H. Schuler, *J. Phys. Chem.*, **73**, 931 (1969).
- (5) K.-D. Asmus, J. M. Warman, and R. H. Schuler, *ibid.*, **74**, 246 (1970).
- (6) K. M. Bansal and R. H. Schuler, *ibid.*, **74**, 3924 (1970).
- (7) A. Hummel and A. O. Allen, *J. Chem. Phys.*, **44**, 3426 (1966).
- (8) W. F. Schmidt and A. O. Allen, *ibid.*, **52**, 2345 (1970).
- (9) P. H. Tewari and G. R. Freeman, *ibid.*, **49**, 4394 (1968).

has been found to increase with increased branching^{9,11} (e.g., *n*-hexane, $G_{fi} = 0.131$,⁸ $\mu_e = 0.09 \text{ cm}^2 \text{ V}^{-1} \text{ sec}^{-1}$;¹¹ 2,2,4-trimethylpentane, $G_{fi} = 0.332$,⁸ $\mu_e = 7 \text{ cm}^2 \text{ V}^{-1} \text{ sec}^{-1}$;¹¹ and neopentane, $G_{fi} = 0.857$,⁸ $\mu_e = 55 \text{ cm}^2 \text{ V}^{-1} \text{ sec}^{-1}$).¹¹ This very interesting fact prompted two recent studies, the electron scavenging by methyl bromide in 2,2,4-trimethylpentane¹² and by N_2O in neopentane,¹³ in an attempt to correlate the kinetic parameters with the electron mobility. The study in 2,2,4-trimethylpentane indicated that the distribution of thermalization distances is closely similar in branched and linear chain hydrocarbons, in contradiction to the longer distances necessary to explain the high free ion yield in branched hydrocarbons. Freeman, on the other hand, presented arguments¹³ to the fact that the distribution of the thermalization distances is different in neopentane and linear chain hydrocarbons.¹³ These discrepancies prompted us to restudy the electron scavenging in 2,2,4-trimethylpentane.

Experimental Section

Phillips research grade 2,2,4-trimethylpentane was passed through a column of activated silica gel before use. Methyl bromide, trifluorobromomethane, methyl- d_3 bromide, ethyl bromide, sulfur hexafluoride, nitrous oxide, and perdeuterioammonia were outgassed and distilled at -78° and stored on a vacuum line. Methyl- ^{14}C bromide was purified by a method described elsewhere.¹² Radioiodine ($^{131}\text{I}_2$) was prepared in a manner described before.¹⁴

A known amount of 2,2,4-trimethylpentane (5 cm^3) containing radioiodine ($\sim 5 \times 10^{-4} M$) of known specific activity was degassed by freeze-pump-thaw cycles. The desired amount of the solute as determined by pressure-volume measurements was then distilled into the outgassed 2,2,4-trimethylpentane. The sample was sealed off the vacuum line in such a way that the vapor volume was $\sim 0.5 \text{ cm}^3$. The samples were irradiated in a tubular ^{60}Co γ -ray source at a dose rate in 2,2,4-trimethylpentane of $6 \times 10^{16} \text{ eV}/(\text{cm}^3 \text{ min})$. The dose rate was determined by Fricke dosimeter and corrected for the appropriate electron density differences. After irradiation, 0.5 cm^3 of the sample was chromatographed, the various radioactive alkyl iodide fractions were collected separately, and the total activity in each of the fractions was determined by a method similar to that reported in the studies of the scavenging of methyl radicals.¹⁴

For samples containing methyl- ^{14}C bromide, 1 cm^3 of 2,2,4-trimethylpentane dried over sodium mirror was used. The samples were irradiated at a dose rate of $3 \times 10^{17} \text{ eV}/(\text{cm}^3 \text{ min})$. The radiogas chromatographic method of analysis has been described elsewhere.^{10,12}

For experiments involving the measurements of gases noncondensable at liquid nitrogen temperature, 5 cm^3

of outgassed 2,2,4-trimethylpentane containing a known amount of the scavenger was irradiated at a dose rate of $3 \times 10^{17} \text{ eV}/(\text{cm}^3 \text{ min})$. Unless otherwise stated, the samples received a total dose of $3 \times 10^{18} \text{ eV}/\text{cm}^3$. After irradiation, the products volatile at liquid nitrogen temperature were collected in a Toepler-McLeod apparatus and subsequently analyzed by mass spectrometry. In few experiments, 2,2,4-trimethylpentane was dried over sodium mirror and the dissolved CO_2 was removed by pumping at room temperature. The results obtained with this 2,2,4-trimethylpentane did not differ from those obtained with samples treated in the manner described above.

Results and Discussion

(A) *Electron Scavenging by CH_3Br , $\text{C}_2\text{H}_5\text{Br}$, and SF_6 .* It has been shown previously that in the radiolysis of hydrocarbon-methyl bromide solutions, methyl radicals are produced as a result of the dissociative electron capture by methyl bromide.^{3,4} In a saturated hydrocarbon solvent, RH, methyl radicals may abstract a hydrogen atom to form methane or combine with other radicals to give CH_3R . Therefore, the sum of the yields of CH_4 and CH_3R would give a quantitative measurement of the yield of methyl radicals and in turn that of scavenged electrons, provided there is no source of methyl radicals other than the dissociative electron capture reaction. In most hydrocarbons considerable yields of methyl radicals are formed directly from the pure hydrocarbon.¹⁴ It is, therefore, necessary to discriminate between these different sources. This can be achieved using carbon-14-labeled methyl bromide and radiochromatographic detection of C-14-containing products.¹² In 2,2,4-trimethylpentane it is found that the fraction of $^{14}\text{CH}_3\cdot$ radicals giving rise to $^{14}\text{CH}_3\text{R}$ is essentially constant and equal to 0.05. The concentration dependence of the total yield of $^{14}\text{CH}_3$ is illustrated in Figure 1. The yields obtained at concentrations of $\text{CH}_3\text{Br} \leq 10^{-3} M$ agree very well with those reported previously.¹² At higher concentrations, however, they are higher (3.03 as opposed to 2.21 at $0.1 M \text{ CH}_3\text{Br}$). The reason for this discrepancy is not obvious at the present time.¹⁵

(10) See, for example, F. Williams, *J. Amer. Chem. Soc.*, **86**, 3954 (1964); S. J. Rzed and R. H. Schuler, *J. Phys. Chem.*, **72**, 228 (1968); S. J. Rzed and J. M. Warman, *J. Chem. Phys.*, **49**, 2861 (1968).

(11) W. F. Schmidt and A. O. Allen, *ibid.*, **52**, 4788 (1970).

(12) J. M. Warman and S. J. Rzed, *ibid.*, **52**, 485 (1970).

(13) K. Horacek and G. R. Freeman, *ibid.*, **53**, 4486 (1970).

(14) R. H. Schuler and R. R. Kuntz, *J. Phys. Chem.*, **67**, 1004 (1963).

(15) Similar behavior has been observed in *n*-hexane: G. Bakale and S. J. Rzed, unpublished results. One possibility is the presence of impurities in the CH_3Br used previously. At low concentrations, one uses $^{14}\text{CH}_3\text{Br}$ of full activity purified by gas chromatography. At concentrations higher than 10^{-3} , the "hot" $^{14}\text{CH}_3\text{Br}$ is diluted with "cold" CH_3Br for practical reasons. This "cold" CH_3Br is purified by low-temperature distillation. If an impurity capable of scavenging electrons (e.g., HBr , HI) was present in the CH_3Br used in the earlier work, one would expect an effect such as the one ob-

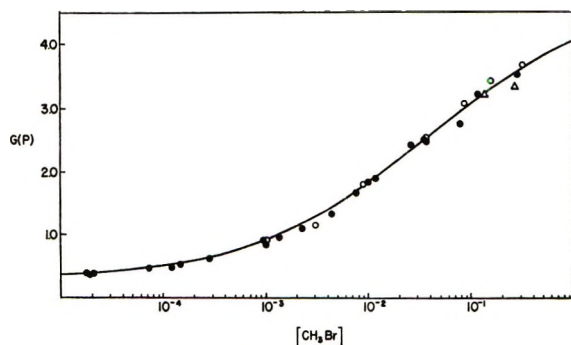


Figure 1. Concentration dependence of the methyl radical yield as a function of methyl bromide concentration: (●) $^{14}\text{CH}_3 = ^{14}\text{CH}_4 \times 1.05$ (to account for the 5% in the CH_3R products), (○) $\text{CH}_3^{131}\text{I}$ corrected for a yield of 0.73 from the solvent, (Δ) $\text{CD}_3\text{H} \times 1.05$. Solid line is calculated using eq I and the parameters given in the text.

The yield of methyl radicals generated in the dissociative electron capture process can also be obtained if one scavenges them with radioactive $^{131}\text{I}_2$ (a very efficient alkyl radical scavenger¹⁴) and measures the $\text{CH}_3^{131}\text{I}$ yield. However, with this technique one cannot distinguish between the methyl radical yield from the electron capture and that from the pure solvent. In the radiolysis of 2,2,4-trimethylpentane-iodine solutions a methyl radical yield of $G(\text{CH}_3) = 0.69$ has been reported.¹⁴ One must, therefore, understand the mode of formation of this yield of methyl radicals prior to correcting the yield of $\text{CH}_3^{131}\text{I}$ from $\text{CH}_3\text{Br}-^{131}\text{I}_2$ -2,2,4-trimethylpentane solutions if one wants to obtain the true yield of the electron capture reaction.

Using the $^{131}\text{I}_2$ scavenging method in pure 2,2,4-trimethylpentane a yield of 0.73 for methyl iodide was obtained in the present work. The agreement between this value and the reported value of 0.69¹⁴ is very good. This methyl radical yield ($G(\text{CH}_3) = 0.73$) remains unaffected in the presence of charge scavengers.¹⁶ These results indicate that the excited states produced directly in the radiolysis of 2,2,4-trimethylpentane are the precursors of methyl radicals. Therefore, in the studies of methyl bromide- $^{131}\text{I}_2$ -2,2,4-trimethylpentane, we have subtracted a constant yield of $G(\text{CH}_3) = 0.73$ from the total methyl radical yield. The residual methyl radical yield ($G(\text{CH}_3) = G(\cdot\text{CH}_3)_{\text{Total}} - 0.73$) is then a true measure of scavenged electrons. The concentration dependence of the yield of methyl radicals obtained in this fashion is illustrated in Figure 1. The agreement between the methyl radical yields obtained by the two different methods is excellent. In two experiments CD_3Br (0.14 and 0.27 M) was used and the yields of $G(\text{CD}_3) = G(\text{CD}_3\text{H}) \times 1.05$ (to allow for the 5% of CD_3 radicals giving rise to CD_3R as in the case of $^{14}\text{CH}_3$ radicals) are also shown in Figure 1 and agree rather well with those obtained by the two previous methods.

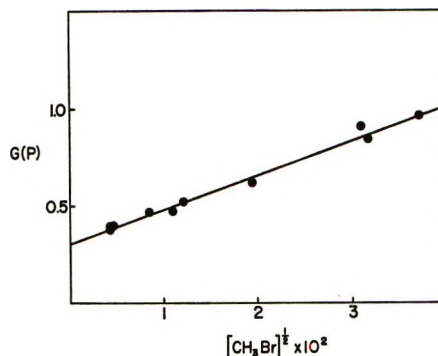


Figure 2. Yield of $^{14}\text{CH}_3$ radicals as a function of the square root of the methyl bromide concentration.

It has been shown previously^{3,4} that the concentration dependence of the yield of a product P produced with unit efficiency in the charge scavenging process is well described in cyclohexane by

$$G(P) = G_{fi} + G_{gi} \frac{\sqrt{\alpha S}}{1 + \sqrt{\alpha S}} \quad (\text{I})$$

where G_{fi} and G_{gi} represent the yields of free and geminate ions, respectively, S is the concentration of the scavenger, and α is a parameter which represents the reactivity of the charged species toward the solute relative to the recombination processes.¹⁷ At low scavenger concentrations eq I reduces to: $G(P) = G_{fi} + G_{gi}(\alpha S)^{1/2}$ and the yield of ions scavenged is proportional to the square root of the solute concentration, with a limiting zero concentration yield equal to the yield of free ions. Such a behavior has been predicted by a theoretical treatment of charge scavenging in irradiated hydrocarbons,¹⁸ and observed in several hydrocarbons for both electron^{4,12,19} and positive ion scavengers.¹⁰ The yields of $^{14}\text{CH}_3\cdot$ obtained in the present experiments at concentrations ranging from 10^{-5} to $\sim 10^{-3}$ M $^{14}\text{CH}_3\text{Br}$ are plotted in Figure 2 as a function of the square root of the methyl bromide concentration. Again, a linear dependence is observed and the intercept of 0.3, so obtained, is identified with the yield of free ions $G_{fi} = 0.3$. This value of the free ion is slightly lower than the values of 0.36¹² and 0.37¹⁹ determined using low concentrations of $^{14}\text{CH}_3\text{Br}$ and C_6F_{12} , respectively. Also values of 0.33⁸ and 0.36²⁰ were determined by the clearing field method and by pulse radiolysis. The overall agreement between these values is rather good. According to eq I, a plot of $[G(P) - G_{fi}]^{-1}$ vs. $S^{-1/2}$ should be linear, with an in-

tercept. We feel that the present data are correct, because no impurity could be detected in the CH_3Br by mass spectrometry or gas chromatography.

(16) K. M. Bansal and S. J. Rzad, *J. Phys. Chem.*, **76**, 2381 (1972).

(17) S. J. Rzad, P. P. Infelta, J. M. Warman, and R. H. Schuler, *J. Chem. Phys.*, **52**, 3971 (1970).

(18) A. Hummel, *ibid.*, **48**, 3268 (1968).

(19) N. H. Sagert and J. A. Reid, *Can. J. Chem.*, **48**, 2429 (1970).

(20) C. Capellos and A. O. Allen, *J. Phys. Chem.*, **73**, 3264 (1969).

tercept equal to G_{gi}^{-1} and slope $(G_{gi}^{-1})(\alpha^{-1/2})$. Using the value of $G_{fi} = 0.3$ determined above, such a plot of the methyl radical yields obtained by $^{14}\text{CH}_3\text{Br}$ and $^{131}\text{I}_2$ methods (above $10^{-2} M$ CH_3Br) is shown in Figure 3. A linear dependence is observed and values of $G_{gi} = 4.54$ and $\alpha_{\text{CH}_3\text{Br}} = 24.7 M^{-1}$ are obtained from a least-mean-squares treatment of the data. Using these three parameters, $G_{fi} = 0.3$, $G_{gi} = 4.54$, and $\alpha_{\text{CH}_3\text{Br}} = 24.7 M^{-1}$, together with eq I one calculates the solid line in Figure 1. Equation I indeed describes the experimental data very well over a wide range of CH_3Br concentrations (10^{-5} – $0.3 M$). The total G of ions obtained in this fashion is $G(\text{ions}) = (4.54 + 0.3) = 4.74$. This value is slightly higher than the value of $G(\text{ions}) \cong 4.4$ obtained in the gas phase assuming a W value of $\sim 23 \text{ eV}$.²¹

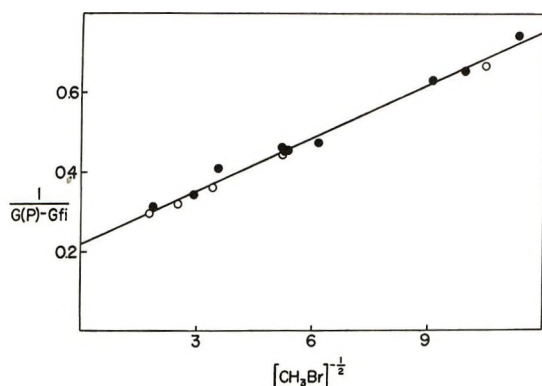


Figure 3. Reciprocal plot of eq I: (●) $^{14}\text{CH}_3$, (○) $\text{CH}_3^{131}\text{I}$.

Electron scavenging studies in 2,2,4-trimethylpentane were also carried out using $\text{C}_2\text{H}_5\text{Br}$ together with the $^{131}\text{I}_2$ technique. In the present experiments the ethyl radicals produced in the electron scavenging process were scavenged by $^{131}\text{I}_2$ and the yield of $\text{C}_2\text{H}_5^{131}\text{I}$ so obtained is a measure of scavenged electrons, since a yield of $\text{C}_2\text{H}_5^{131}\text{I}$ of less than 0.01 was obtained in the radiolysis of pure 2,2,4-trimethylpentane– $^{131}\text{I}_2$ solutions. These ethyl iodide yields are presented in Table I. Using eq I together with the parameters obtained with methyl bromide ($G_{fi} = 0.3$ and $G_{gi} = 4.54$), one can describe the $\text{C}_2\text{H}_5^{131}\text{I}$ yields quite well by using an $\alpha_{\text{C}_2\text{H}_5\text{Br}} = 5 M^{-1}$ (Table I).

One of the most efficient electron scavengers in hydrocarbons is SF_6 .^{3,5} It is, however, difficult to measure its reactivity toward electrons directly as in polar media.^{22,23} One can, however obtain this information from competitive studies.^{3,4,24} The study of the effect of SF_6 on the yield of $^{14}\text{CH}_3$ radicals from $^{14}\text{CH}_3\text{Br}$ –2,2,4-trimethylpentane solutions should give us an α_{SF_6} value. This α_{SF_6} value should be rather reliable because it has been shown recently that in cyclohexane the competition between CH_3Br and SF_6 occurs without any appreciable complications from secondary electron transfer reactions.²⁴ In such an ideal case the

Table I: Yields of Ethyl Iodide from Ethyl Bromide– $^{131}\text{I}_2$ Solutions^a

$[\text{C}_2\text{H}_5\text{Br}]$, mM	$G(\text{C}_2\text{H}_5^{131}\text{I})_{\text{obsd}}$	$G(\text{C}_2\text{H}_5^{131}\text{I})_{\text{calcd}}^b$
5.2	0.78	0.93
12.9	1.23	1.22
46.0	1.76	1.77
82.8	2.01	2.08
113.0	2.53	2.25
317.0	2.67	2.83

^a $^{131}\text{I}_2 = 5.42 \times 10^{-4} M$ in 2,2,4-trimethylpentane. ^b Calculated using eq I with the following parameters: $G_{fi} = 0.3$, $G_{gi} = 4.54$, and $\alpha_{\text{C}_2\text{H}_5\text{Br}} = 5 M^{-1}$.

yield of $^{14}\text{CH}_3$ radicals in the presence of SF_6 should be given by^{4,24}

$$G(^{14}\text{CH}_3)_{\text{SF}_6} = \left[G_{fi} + G_{gi} \frac{\sqrt{\alpha_1 S_1 + \alpha_2 S_2}}{1 + \sqrt{\alpha_1 S_1 + \alpha_2 S_2}} \right] \frac{\alpha_1 S_1}{\alpha_1 S_1 + \alpha_2 S_2} \quad (\text{II})$$

where the symbols have the same meaning as in eq I and the subscripts 1 and 2 refer to $^{14}\text{CH}_3\text{Br}$ and SF_6 , respectively. From the knowledge of $G(^{14}\text{CH}_3)$ in the presence of SF_6 , one obtains a value for α_{SF_6} using eq II. The observed yield of $^{14}\text{CH}_3$ from a $0.012 M$ CH_3Br solution in 2,2,4-trimethylpentane in the presence of SF_6 is given in the second column of Table II. In the third column of Table II are also given the methyl radical yields calculated by eq II, using the parameters obtained above and $\alpha_{\text{SF}_6} = 65 M^{-1}$. The agreement between observed and calculated values is very good.

Table II: Effect of Sulfur Hexafluoride on the $^{14}\text{CH}_3\cdot$ Yield from Methyl Bromide Solutions^a

$[\text{SF}_6]$, mM	$G(^{14}\text{CH}_3\cdot)_{\text{obsd}}$	$G(^{14}\text{CH}_3\cdot)_{\text{calcd}}^b$
	1.89	1.90
11.6	0.73	0.73
35.0	0.37	0.36
38.2	0.34	0.33
332.0	0.07	0.05

^a $[\text{CH}_3\text{Br}] = 0.012 M$ in 2,2,4-trimethylpentane. ^b Calculated with eq II using $G_{fi} = 0.3$, $G_{gi} = 4.54$, $\alpha_{\text{CH}_3\text{Br}} = 24.7 M^{-1}$, and $\alpha_{\text{SF}_6} = 65 M^{-1}$.

(B) $N_2\text{O}$ –2,2,4-Trimethylpentane Solutions. The nitrogen yield from 2,2,4-trimethylpentane are shown

(21) G. G. Meisels, *J. Chem. Phys.*, **41**, 55 (1964). The author reports W values for several saturated hydrocarbons. All are $\sim 23 \text{ eV}$.

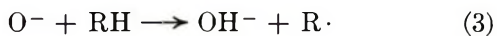
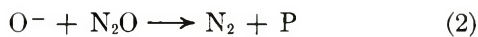
(22) S. J. Rzed and J. H. Fendler, *ibid.*, **52**, 5395 (1970).

(23) K.-D. Asmus and J. H. Fendler, *J. Phys. Chem.*, **72**, 4285 (1968).

(24) P. P. Infelta and R. H. Schuler, *ibid.*, **76**, 987 (1972).

in Figure 4. As can be seen, they agree with the data reported in the literature.^{25,26} However, the yields found in this work are higher than those reported by Holroyd.²⁷

By studying the effect of N_2O on the hydrogen yields an $\alpha_{N_2O} = 6 M^{-1}$ has been obtained¹⁶ and, therefore, if nitrous oxide was producing one nitrogen per electron scavenged, one would expect that the yield of nitrogen be given by eq I together with the parameters derived previously ($G_{fi} = 0.3$, $G_{gi} = 4.54$). The lower dashed line in Figure 4 has been calculated using eq I and indicates clearly that excess nitrogen is produced by secondary ion reaction in 2,2,4-trimethylpentane as well as in cyclohexane.³ On the other hand, if two nitrogen molecules were produced per electron scavenged, one would expect the upper dashed line in Figure 4. This shows that the importance of secondary ionic reactions increases with increasing nitrous oxide concentration. If one considers the following mechanism for the electron scavenging by N_2O in 2,2,4-trimethylpentane²⁸



then, according to the treatment of Infelta and Schuler,²⁹ the yield of nitrogen at a given N_2O concentration is given by

$$G(N_2) = G_{fi} \left(1 + \frac{\beta S}{\beta S + \beta' [RH]} \right) + \left(G_{gi} \frac{\sqrt{\alpha S}}{1 + \sqrt{\alpha S}} \right) \left(1 + \frac{\beta S}{\beta S + \beta' [RH]} \times \left[\frac{\sqrt{\beta S + \beta' [RH]}}{1 + \sqrt{\beta S + \beta' [RH]}} \times \left(1 + \frac{1}{\sqrt{\alpha S + \sqrt{\beta S + \beta' [RH]}}} \right) \right] \right) \quad (III)$$

where S is the N_2O concentration, $\beta = k_2 r_D / \lambda^{29}$ is a parameter representing the reactivity of O^- toward N_2O (reaction 2) relative to its recombination (reaction 4) and $\beta' = k_3 r_D / \lambda^{29}$ is a parameter which represents the efficiency of hydrogen abstraction from the solvent (reaction 3) relative to reaction 4. Although β and β' relate to the geminate ion recombinations, they can be used in the treatment of the free ions because they are involved only as a ratio, i.e., $\beta S / (\beta S + \beta' RH) = k_2 S / (k_2 S + k_3 RH)$. One might think that the fit of eq III to the nitrogen yield is going to be difficult because of the two adjustable parameters β and β' . Fortunately, in 2,2,4-trimethylpentane the O^- reaction with the solvent (reaction 3) seems to be rather unimportant, and as a result β' appears to be very small

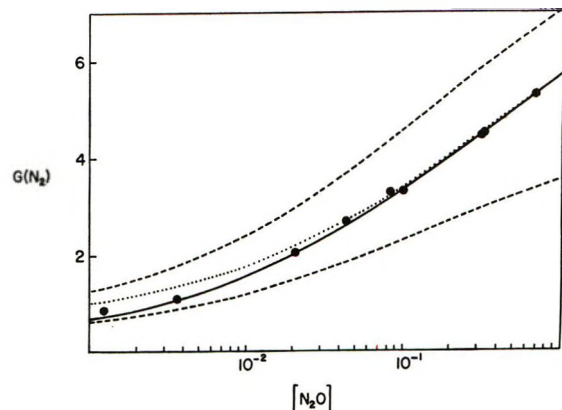


Figure 4. Yields of nitrogen as a function of nitrous oxide concentration. Lower dashed curve calculated using eq I and the parameters given in the text. Upper dashed curve is twice the lower dashed curve. Dotted and solid lines calculated using eq III, the parameters given in the text, and $\beta' = 0$ and $8 \times 10^{-4} M^{-1}$, respectively.

for the following reason. The yields of nitrogen obtained at low concentrations when plotted vs. the square root of the N_2O concentration extrapolate to approximately 1.5 times the free ion yield. At the dose rate used in the present work, the lifetime of the free ions is of the order of milliseconds with respect to recombination. If reaction 3 were very efficient, the extrapolated yield of nitrogen should be equal to the free ion yield. On the other hand, if β' were 0, then this extrapolated yield should be twice the free ion yield. Therefore, at high N_2O concentrations where reaction 3 is negligible, the fit of eq III to the nitrogen yield should give β . The best fit is obtained with $\beta = 0.7 M^{-1}$ and is illustrated as the dotted line in Figure 4. To fit the data at low concentrations of N_2O , one can then introduce a small value for the parameter β' . The best fit is obtained for $\beta' = 8 \times 10^{-4} M^{-1}$ and is illustrated as the solid line drawn through the nitrogen yields in Figure 4.

(C) *General Conclusions.* It has been shown that the parameter α is given by

$$\alpha_x = k_x / \lambda \quad (IV)$$

where k is the rate constant for charge scavenging, λ is a constant for a given solvent and represents the rate of recombination of geminate ions,¹⁷ and the subscript x defines the charge scavenged (n for the electron and p for the positive ion). If in two different solvents k_x is the same, then the ratio of the α values should be

(25) M. B. Muratbekov, S. V. Zatonkii, and V. V. Saraeva, *Khim. Vys. Energ.*, **5**, 134 (1971).

(26) S. Iida, R. Yugeta, and S. Sato, *Bull. Chem. Soc. Jap.*, **43**, 2758 (1970).

(27) R. A. Holroyd, *Advan. Chem. Ser.*, **No. 82**, 48 (1968).

(28) A very general mechanism where a secondary ion produced in the electron scavenging process reacts with nitrous oxide to give excess nitrogen in competition with its recombination and its decay through some process would be described by eq III.

(29) P. P. Infelta and R. H. Schuler, *Int. J. Radiat. Phys. Chem.*, in press.

equal to the inverse ratio of the λ parameters. The rate constant for proton transfer from RH^+ to ND_3 should not change significantly when going from cyclohexane (C) to 2,2,4-trimethylpentane (TMP). This rate constant is a diffusion-controlled process³⁰ and therefore proportional to the diffusion of the positive ion. The ratios of the mobilities of the positive ions as measured in several hydrocarbons by Tewari and Freeman³¹ are identical with the ratios of the self-diffusion in these liquids.³² Since the ratio for the self-diffusion in 2,2,4-trimethylpentane and cyclohexane is expected to be *ca.* unity,³² the rate constants for proton transfer should be quite similar. Hence, the ratio $\alpha_{\text{P}}(\text{C})/\alpha_{\text{P}}(\text{TMP})$ should be equal to $\lambda(\text{TMP})/\lambda(\text{C})$. Since $\alpha_{\text{ND}_3} = 1.00 \text{ M}^{-1}$ ^{30,33} and 0.15 M^{-1} ¹⁶ in cyclohexane and 2,2,4-trimethylpentane, respectively, $\lambda(\text{TMP})/\lambda(\text{C}) = 1.0/0.15 = 6.7$. This would indicate that the recombination processes in 2,2,4-trimethylpentane occur on a time scale which is approximately ten times smaller than in cyclohexane. On the other hand, it has been shown¹² that if the Nernst-Einstein relationship applies to the recombination of the geminate ion pairs α can be expressed quite generally as

$$\alpha_x = 4\pi R_x(D_x + D_s)b^3N/3r_c(D_e + D_+)1000 \quad (\text{V})$$

where x can refer to the positive ion (α_{P} , D_+) or to the electron (α_{N} , D_e), R is the reaction radius for the given diffusion-controlled reaction, N is the Avogadro number, b is the characteristic length of a distribution of thermalization distances $f(r)$, and r_c is the Onsager critical distance ($r_c = e^2/\epsilon kT$). Remembering that $D = \mu kT/e$, the combination of (IV) and (V) gives for λ

$$\lambda = 3(\mu_e + \mu_+)r_c kT/b^3e \quad (\text{VI})$$

and since $\mu_e \gg \mu_+$

$$\lambda = 3\mu_e r_c kT/b^3e \quad (\text{VII})$$

Equation VII leads then to the following

$$\frac{\lambda(\text{TMP})}{\lambda(\text{C})} = \frac{(\mu_e r_c)_{\text{TMP}}}{(\mu_e r_c)_{\text{C}}} \left(\frac{b(\text{C})}{b(\text{TMP})} \right)^3 = 6.7$$

Since all the parameters are known, *i.e.*, $\mu_e(\text{TMP}) = 7 \text{ cm}^2 \text{ V}^{-1} \text{ sec}^{-1}$,¹¹ $\mu_e(\text{C}) = 0.35 \text{ cm}^2 \text{ V}^{-1} \text{ sec}^{-1}$,¹¹ $r_c(\text{TMP}) = 2.91 \times 10^{-6} \text{ cm}$, and $r_c(\text{C}) = 2.79 \times 10^{-6} \text{ cm}$, one gets that $b(\text{C})/b(\text{TMP}) = 0.68$. This value indicates that the characteristic distance b is $\sim 50\%$ longer in 2,2,4-trimethylpentane than in cyclohexane. Such a conclusion has been reached previously by Schmidt and Allen⁸ ($b(\text{C})/b(\text{TMP}) = 0.7$), who fitted the free ion yields in these hydrocarbons by using the Onsager escape probability ($e^{-r_c/r}$) and varying the characteristic length b of a three-dimensional Gaussian distribution. These authors also found that b in neopentane is of the order of three times larger than in cyclohexane.⁸ Such a trend was confirmed by Freeman

who finds that $b(\text{neopentane})$ is *ca.* four to five times larger than in *n*-hexane.¹³

The conclusion reached above does not agree with that reached previously¹²—namely, that the thermalization distances are closely similar in cyclohexane and 2,2,4-trimethylpentane. Such conclusion was obtained by comparing $\alpha_{\text{CH}_3\text{Br}}$ obtained in these two solvents. According to (V), $(\alpha_{\text{N}}(\text{C})/\alpha_{\text{N}}(\text{TMP}))^{1/3} \simeq b(\text{C})/b(\text{TMP})$. Using the value of $\alpha_{\text{CH}_3\text{Br}}$ obtained in this work, 24.7 M^{-1} and that for cyclohexane, $\alpha_{\text{CH}_3\text{Br}} = 16 \text{ M}^{-1}$,^{2,4,24} one calculates $b(\text{C})/b(\text{TMP}) = 0.87$, which indicates again that the thermalization distances are similar within $\sim 10\%$ in the two solvents. Moreover, comparison of the α parameters for N_2O and $\text{C}_2\text{H}_5\text{Br}$ in the two solvents leads to the conclusion that the thermalization length is larger in cyclohexane than in 2,2,4-trimethylpentane. However, the α values obtained for SF_6 , *i.e.*, $\alpha(\text{C}) = 17 \text{ M}^{-1}$ ²⁴ and $\alpha(\text{TMP}) = 65 \text{ M}^{-1}$, give $b(\text{C})/b(\text{TMP}) \sim 0.64$, which agrees very well with the value of 0.68 obtained above from the α values for α_{ND_3} . Since SF_6 is one of the best electron scavengers known,^{3,5,34} one would expect it to react with electrons on every collision and hence with a diffusion-controlled rate describable by the Smoluchowski equation ($k_{\text{SF}_6} = 4\pi RD$). The discrepancies obtained with CH_3Br , N_2O , and $\text{C}_2\text{H}_5\text{Br}$ arise then from a change in some factor for the reaction with electrons when going from cyclohexane to 2,2,4-trimethylpentane. That there is a factor involved is evident since the electron capture reactions are essentially diffusion controlled (see below) and yet the α values which are directly proportional to the rate constants of scavenging vary: in cyclohexane²⁴ $\alpha_{\text{SF}_6} = 17 \text{ M}^{-1} > \alpha_{\text{CH}_3\text{Br}} = 16 \text{ M}^{-1} > \alpha_{\text{N}_2\text{O}} = 10 \text{ M}^{-1} > \alpha_{\text{C}_2\text{H}_5\text{Br}} = 8 \text{ M}^{-1}$; in 2,2,4-trimethylpentane $\alpha_{\text{SF}_6} = 65 \text{ M}^{-1} > \alpha_{\text{CH}_3\text{Br}} = 24.7 \text{ M}^{-1} > \alpha_{\text{N}_2\text{O}} = 6 \text{ M}^{-1} > \alpha_{\text{C}_2\text{H}_5\text{Br}} = 5 \text{ M}^{-1}$. Moreover, the same α values are obtained from single and competitive experiments,^{4,24} indicating that the factor involved is not in the efficiency of product generation. In some cases this factor³⁵ makes the electron reactions with CH_3Br , N_2O , and $\text{C}_2\text{H}_5\text{Br}$ not truly diffusion controlled and hence should be taken into account when comparing α values from two different solvents, *i.e.*, $b(\text{C})/b(\text{TMP})$ should be given by $[(\alpha_{\text{N}}(\text{C})/\alpha_{\text{N}}(\text{TMP}))(f(\text{TMP})/f(\text{C}))]^{1/3}$, where f is the factor under consideration for a given solute in the given solvent. This fact indi-

(30) S. J. Rzed, Abstracts, 158th Meeting of the American Chemical Society, New York, N. Y., Sept 1969, p 239.

(31) P. H. Tewari and G. R. Freeman, *J. Chem. Phys.*, **49**, 4394 (1968).

(32) D. W. McCall, D. C. Douglass, and E. W. Anderson, *ibid.*, **31**, 1555 (1959).

(33) K.-D. Asmus, *Int. J. Radiat. Phys. Chem.*, **3**, 419 (1971).

(34) R. W. Fessenden and K. M. Bansal, *J. Chem. Phys.*, **53**, 3468 (1970).

(35) The theory of electron reactions in dielectric liquids is sufficiently tenuous to cast some doubt on any speculation as to the exact nature of this factor.

cates that one has to exercise extreme caution in comparing α parameters obtained for one scavenger in two different solvents, as was done previously with CH_3Br .¹² Information on several scavengers both of electrons and positive ions is necessary for a valid comparison. From the arguments given above $f(\text{C}) \simeq f(\text{TMP}) \simeq 1.0$ for SF_6 . Since $\alpha_{\text{CH}_3\text{Br}} \simeq \alpha_{\text{SF}_6}$ in cyclohexane, $f(\text{C}) \simeq 1.0$, while $f(\text{TMP}) \simeq 24.7/65 \sim 0.4$ for methyl bromide. Similarly, using the values given for the parameter α above, it is found that $f(\text{C}) \sim 0.6$ and 0.5 and $f(\text{TMP}) \simeq 0.1$ and 0.08 for N_2O and $\text{C}_2\text{H}_5\text{Br}$, respectively.

It has been shown recently, from the application of charge scavenging kinetics to the formation of excited states in cyclohexane, that $\lambda = 2 \times 10^{11} \text{ sec}^{-1}$.³⁶ Such a value would indicate that $\lambda(\text{TMP}) \simeq (2 \times 10^{11})(6.7) \sim 1.3 \times 10^{12} \text{ sec}^{-1}$, and hence while half of the electrons recombine in $\sim 3 \times 10^{-12} \text{ sec}$ in cyclohexane, they recombine in $\sim 5 \times 10^{-13} \text{ sec}$ in 2,2,4-trimethylpentane. Using these values of λ together with eq VII allows us to calculate the parameter b as 72 \AA and 106 \AA in cyclohexane and 2,2,4-trimethylpentane, respectively. These values agree surprisingly well with the values of 66.1 and 95 \AA obtained by Schmidt and Allen.⁸ It should be pointed out here that eq VII has been derived for a general distribution of thermalization distances $f(r)$.¹² It is a general property of the Laplace transformation used that the explicit form of $f(r)$ is not necessary for the calculation of λ . It is then interesting to note the similarity between the value obtained for the parameter b in this work and that obtained by Schmidt and Allen who assumed a three-dimensional Gaussian distribution, *i.e.*, $f(r) = 4r^2/\pi^{1/2}b^3 \exp(-r^2/b^2)$. The value of $\lambda \sim 1.3 \times 10^{12} \text{ sec}^{-1}$ in 2,2,4-trimethylpentane allows us to obtain the different rate constants for scavenging, since $k_n = \lambda\alpha_n$; thus $k_{\text{SF}_6} \sim 8 \times 10^{13}$, $k_{\text{CH}_3\text{Br}} \sim 3 \times 10^{13}$, $k_{\text{N}_2\text{O}} \sim 8 \times 10^{12}$, and $k_{\text{C}_2\text{H}_5\text{Br}} \sim 7 \times$

$10^{12} \text{ M}^{-1} \text{ sec}^{-1}$. Since the electron mobility is $7 \text{ cm}^2 \text{ V}^{-1} \text{ sec}^{-1}$ ¹¹ and $f(\text{TMP}) \simeq 1.0$, the reaction radius R in the case of SF_6 comes out to be $\sim 6 \text{ \AA}$, which is of the order of magnitude of a molecular diameter. Evidently, when taking into account the factors obtained previously, $R \sim 6 \text{ \AA}$ for CH_3Br , N_2O , and $\text{C}_2\text{H}_5\text{Br}$.

Upon addition of an electron scavenger, the lifetime of the ion pairs is increased as a result of the conversion of high-mobility electrons to more massive negative ions. To account quantitatively for cyclopropane positive ion reactions in cyclohexane in the presence of an electron scavenger, a model was proposed in which it was assumed that upon electron capture the residual lifetime of the ion pair was increased by a constant factor $\tau_D (=17)$.³⁷ This factor was identified with the ratio of the mutual ion mobility before and after scavenging. At infinite scavenger concentration, *i.e.*, scavenging at time = 0, the time scale is extended by τ_D , *i.e.*, the characteristic constant λ becomes λ/τ_D . Since τ_D is essentially proportional to the electron mobility, the value of $\lambda/\tau_D \sim (1.3 \times 10^{12})(0.35)/(17)(7) \sim 4 \times 10^9 \text{ sec}^{-1}$ in 2,2,4-trimethylpentane. This value allows an estimate of the rate constants of the O^- reactions 2 and 3. According to Infelta and Schuler,²⁹ $\beta = k_2\tau_D/\lambda$ and $\beta' = k_3\tau_D/\lambda$. Since $\beta = 0.7 \text{ M}^{-1}$ and $\beta' = 8 \times 10^{-4} \text{ M}^{-1}$, then $k_2 \sim 3 \times 10^9 \text{ M}^{-1} \text{ sec}^{-1}$ and $k_3 \sim 3 \times 10^6 \text{ M}^{-1} \text{ sec}^{-1}$. Although k_2 is of the order of magnitude one would expect for a diffusion-controlled process, k_3 is smaller than the values reported for O^- reactions in aqueous systems, *e.g.*, $k_{\text{O}^- + \text{CH}_3\text{OH}} = 5.8 \times 10^8 \text{ M}^{-1} \text{ sec}^{-1}$ and $k_{\text{O}^- + \text{C}_2\text{H}_5\text{OH}} = 11.3 \times 10^8 \text{ M}^{-1} \text{ sec}^{-1}$.²⁸

(36) S. J. Rzad, *J. Phys. Chem.*, in press.

(37) S. J. Rzad, R. H. Schuler, and A. Hummel, *J. Chem. Phys.*, **51**, 1369 (1969).

(38) R. Wander, B. L. Gall, and L. M. Dorfman, *J. Phys. Chem.*, **74**, 1819 (1970).

Radiolysis of Liquid 2,2,4-Trimethylpentane. Effect of Charge

Scavengers on Product Formation¹

by Krishan M. Bansal and Stefan J. Rzed*

Radiation Research Laboratories and Center for Special Studies, Mellon Institute of Science, Carnegie-Mellon University, Pittsburgh, Pennsylvania 15213 (Received January 27, 1972)

Publication costs assisted by the U. S. Atomic Energy Commission

Electron scavengers are found to depress the hydrogen yield and have only a slight effect on the methane yield. The effects of these electron scavengers are quantitatively described by the empirical equations proposed earlier for cyclohexane. It is concluded that in 2,2,4-trimethylpentane only 30 and 5% of the ionic neutralization processes produce hydrogen and methane, respectively. Although some hydrogen atoms originate in ion recombination processes, this is not the case for methyl radicals, which originate exclusively from excited states produced directly by radiation. Methyl radicals are found to be scavenged by ethylene, and a value of 33 is obtained for the ratio of the rate constant for the addition of methyl radicals to ethylene to that for abstraction of hydrogen from the solvent. From the effect of N_2O and ND_3 on the hydrogen yield in 2,2,4-trimethylpentane, values of $\alpha_{N_2O} = 6 M^{-1}$ and $\alpha_{ND_3} = 0.15 M^{-1}$ are obtained.

Introduction

Recent interest in the radiation chemistry of branched hydrocarbons showed that, as in cyclohexane,²⁻⁴ charge scavenging has an effect on the products generated by radiolysis.⁵⁻⁷ However, no systematic study has been made to account for the quantitative contribution of ionic processes in the radiation chemistry of 2,2,4-trimethylpentane. Recently the kinetics of the charge scavenging processes have been studied in 2,2,4-trimethylpentane⁸ and it has been shown that as in cyclohexane^{2,9} the yield of a product P produced with unit efficiency in the charge scavenging process can be very well described by

$$G(P) = G_{fi} + G_{gi} \frac{\sqrt{\alpha S}}{1 + \sqrt{\alpha S}} \quad (I)$$

where G_{fi} and G_{gi} are the yields of free and geminate ions, respectively, S is the concentration of the scavenger, and α is a parameter which represents the reactivity of the solute toward the charged species relative to the recombination process.¹⁰ Parameters pertinent to eq I have been obtained for several scavengers in 2,2,4-trimethylpentane.⁸ With this information at hand, the present work has been undertaken in order to study the importance of the contribution of ionic processes to the formation of hydrogen and methane in the γ -radiolysis of 2,2,4-trimethylpentane.

Experimental Section

Most materials and their purification have been described previously.⁸ Phillips research grade benzene and absolute ethanol from Rossville Gold Shield were used without further purification and were added with a syringe before outgassing the 2,2,4-trimethylpentane.

Irradiations and experimental procedure have been described previously.⁸

Results and Discussion

(A) *Effect of Charge Scavengers on the Hydrogen Yield.* (a) *Electron Scavengers.* The hydrogen yield from the γ -radiolysis of pure 2,2,4-trimethylpentane was found to be 2.44 and independent of dose over the narrow range of 1.5×10^{18} – 6×10^{18} eV/cm³.¹¹ As previously noted,¹² the hydrogen yield decreases at higher doses. An almost identical value of 2.45 has been reported for low doses of γ -irradiation of 2,2,4-trimethylpentane.¹² All the other values quoted are lower: $G(H_2) = 2.2^{6,13-15}$ and $G(H_2) = 2.1^{16}$. These

(1) Supported in part by the U. S. Atomic Energy Commission.

(2) J. M. Warman, K.-D. Asmus, and R. H. Schuler, *Advan. Chem. Ser.*, **No. 82**, 25 (1968).

(3) K.-D. Asmus, J. M. Warman, and R. H. Schuler, *J. Phys. Chem.*, **74**, 246 (1970).

(4) K. M. Bansal and R. H. Schuler, *ibid.*, **74**, 3924 (1970).

(5) M. Muratbekov, S. V. Zatonskii, and V. V. Saraeva, *Khim. Vys. Energ.*, **5**, 134 (1971).

(6) S. Iida, R. Yugeta, and S. Sato, *Bull. Chem. Soc. Jap.*, **43**, 2758 (1970).

(7) K. Horacek and G. R. Freeman, *J. Chem. Phys.*, **53**, 4486 (1970).

(8) S. J. Rzed and K. M. Bansal, *J. Phys. Chem.*, **76**, 2374 (1972).

(9) J. M. Warman, K.-D. Asmus, and R. H. Schuler, *ibid.*, **73**, 931 (1969).

(10) S. J. Rzed, P. P. Infelta, J. M. Warman, and R. H. Schuler, *J. Chem. Phys.*, **52**, 3971 (1970).

(11) K. M. Bansal and S. J. Rzed, *J. Phys. Chem.*, **74**, 3486 (1971).

(12) R. H. Schuler and R. R. Kuntz, *ibid.*, **67**, 1004 (1963).

(13) J. A. Knight, R. L. McDaniel, R. C. Palmer, and F. Sicilio, *ibid.*, **67**, 2273 (1963).

(14) T. Kudo and S. Shida, *ibid.*, **67**, 2871 (1963).

(15) T. Kudo, *ibid.*, **71**, 3681 (1967).

(16) V. I. Pichuzhkin, V. V. Saraeva, and N. A. Bakh, *Khim. Vys. Energ.*, **4**, 317 (1970).

Table I: Effect of Electron Scavengers on the Yields of Hydrogen and Methane from the γ -Radiolysis of 2,2,4-Trimethylpentane

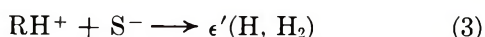
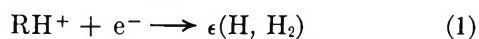
S	[S], mM	$G(\text{H}_2)_{\text{obsd}}$	$G(\text{H}_2)_{\text{calcd}}^a$	$G(\text{CH}_4)_{\text{obsd}}$		
				Total	From solvent ^b	$G(\text{CH}_4)_{\text{calcd}}^c$
...	...	2.44	2.44	...	1.21	1.21
CH_3Br	2.7	2.09	2.07	2.33	1.16 ^b	1.15
	8.4	1.97	1.92	2.93	1.29	1.12
	36.8	1.77	1.69	3.48	1.08	1.08
	137.0	1.50	1.47	4.33	1.24	1.05
	139.0	1.48	1.47	4.26	1.17	1.05
	187.0	1.53	1.42	4.46	1.22	1.04
	317.0	1.32	1.35	4.45	0.98	1.03
SF_6	127.0	1.46	1.34		1.01	1.03
	304.0	1.26	1.24		0.97	1.00
$\text{C}_2\text{H}_5\text{Br}$	136.0	1.65	1.73		1.16	1.09
	250.0	1.44	1.63		1.12	1.08
N_2O	1.2	2.39	2.24		1.25	1.18
	3.6	2.25	2.18		1.22	1.17
	20.6	2.04	2.00		1.19	1.14
	43.4	1.92	1.89		1.21	1.12
	83.3	1.79	1.79		1.17	1.11
	100.0	1.73	1.76		1.17	1.10
	312.0	1.45	1.56		1.10	1.07
	328.0	1.49	1.55		1.04	1.07
	680.0	1.32	1.44		1.04	1.05

^a Calculated using eq II and the following parameters: $\epsilon = 0.3$, $G_{\text{fi}} = 0.3$, $G_{\text{gi}} = 4.54$, $\alpha_{\text{CH}_3\text{Br}} = 24.7 M^{-1}$, $\alpha_{\text{SF}_6} = 65 M^{-1}$, $\alpha_{\text{C}_2\text{H}_5\text{Br}} = 5 M^{-1}$, $\alpha_{\text{N}_2\text{O}} = 6 M^{-1}$. ^b For methyl bromide solutions this yield was obtained by subtracting from the observed yield of methane the contribution of methane originating in electron scavenging as calculated by eq I with the pertinent parameters as given in footnote a. ^c Calculated using eq II, $\epsilon = 0.05$, and the other parameters as given in footnote a.

lower values were obtained at doses much greater ($\geq 10^{20}$ eV/cm³) than in the present work and, since the $G(\text{H}_2)$ is somewhat dose dependent, one would expect a lower yield.

In order to understand the mode of formation of hydrogen, the effect of various electron scavengers was investigated and the results are presented in Table I. One can see that the hydrogen decreases with increasing scavenger concentration. Since the four electron scavengers studied here neither react with hydrogen atoms nor undergo energy transfer other than electron capture,^{2,3,17} one can safely assume that some of the hydrogen has ionic precursors. In 2,2,4-trimethylpentane such a decrease of the hydrogen yield with increasing electron scavenger concentration (SF_6 and N_2O) has been already observed by Iida, *et al.*⁶

As previously shown,³ the hydrogen production by ionic processes can be represented by the following scheme



where ϵ and ϵ' are efficiencies for production of hydrogen from reactions 1 and 3 because the hydrogen atoms produced finally give hydrogen by abstracting a hydrogen atom from the solvent. In the case of cyclohexane,

it has been shown that the efficiency of hydrogen production from reaction 3, *i.e.*, ϵ' , is zero or nearly so.³ Since hydrogen production from 2,2,4-trimethylpentane is a much less efficient process than from cyclohexane ($G(\text{H}_2) = 2.44$ and 5.67 , respectively), it should be expected that ϵ' would be equal to zero in 2,2,4-trimethylpentane. Therefore, one can calculate the hydrogen yield in the presence of various charge scavengers according to the following equation³

$$G(\text{H}_2) = G(\text{H}_2)_0 - \epsilon \left[G_{\text{fi}} + G_{\text{gi}} \frac{\sqrt{\alpha S}}{1 + \sqrt{\alpha S}} \right] \quad (\text{II})$$

where $G(\text{H}_2)_0$ is the yield of hydrogen in the absence of the scavenger ($=2.44$). Since all the parameters are known from electron scavenging studies⁸ ($G_{\text{fi}} = 0.3$, $G_{\text{gi}} = 4.54$, $\alpha_{\text{CH}_3\text{Br}} = 24.7 M^{-1}$), one can fit eq II to the experimental yields of hydrogen observed in the presence of CH_3Br in order to obtain ϵ . The best fit was obtained for $\epsilon = 0.3$ (Table I). Using this value and the parameters pertinent to sulfur hexafluoride and $\text{C}_2\text{H}_5\text{Br}$ as obtained previously⁸ ($\alpha_{\text{SF}_6} = 65 M^{-1}$, $\alpha_{\text{C}_2\text{H}_5\text{Br}} = 5 M^{-1}$), one calculates the values given in the fourth column of Table I. The overall agreement is rather good. In the case of N_2O , however, one does not know the value of the parameter α , since the yield

(17) The treatment of the hydrogen yields given in this work is essentially the one proposed for cyclohexane in ref 3.

of nitrogen does not represent directly the yield of scavenged electrons. This is due to complications arising from secondary reactions of the anions produced in the electron scavenging process.^{2,8,18} One can, however, use eq II to obtain an estimate of this value, since one knows all the other parameters necessary for the calculation. The best fit (fourth column of Table I) was obtained for an $\alpha_{N_2O} = 6 M^{-1}$. Again the overall description by eq II of the hydrogen yield in the presence of electron scavengers is very good. A value of $\epsilon = 0.3$ implies that a hydrogen yield of 1.45 G units ($G_{ions}(\epsilon)$) originates from ionic processes and, hence, a $G(H_2) = 0.99$ comes from nonionic processes. It should be pointed out here that Horacek and Freeman⁷ found that 36% of ionic recombination processes lead to hydrogen formation in the γ -radiolysis of neopentane- N_2O solutions.

Table II: Effect of Electron Scavengers on the Yield of Ethyl Iodide from Ethylene- $^{131}I_2$ Solutions^a

S	[S], mM	$G(C_2H_5^{131}I)_{obsd}$	$G(C_2H_5^{131}I)_{calcd}^b$
...	...	0.81 ^c	0.81
SF ₆	12	0.67	0.63
	35	0.64	0.59
	89	0.54	0.55
	160	0.55	0.53
N ₂ O	105	0.63	0.64
	335	0.51	0.59

^a $[C_2H_4] = 0.11 M$, $^{131}I_2 = 5.2 \times 10^{-4} M$ in 2,2,4-trimethylpentane. ^b Calculated using eq III and the following parameters: $G_{fi} = 0.3$, $G_{gi} = 4.54$, $f = 0.09$, $\alpha_{SF_6} = 65 M^{-1}$, $\alpha_{N_2O} = 6 M^{-1}$, and $(k_{abs}/k_{add})[RH] = 0.026 M$. ^c Value interpolated from the data in Figure 1 of ref 11.

It is interesting to probe further the hydrogen originating from ionic processes in order to obtain information as to what extent these processes produce thermal hydrogen atoms and molecular hydrogen. It has been shown recently from the study of 2,2,4-trimethylpentane- $^{131}I_2$ -ethylene solutions¹¹ that the yield of thermal hydrogen atoms is $G(H)_0 = 1.0$. Ethylene, which does not interfere with ionic processes in 2,2,4-trimethylpentane,¹¹ competes with the solvent for the hydrogen atoms to produce ethyl radicals, which in turn are scavenged by radioiodine to give ethyl iodide. A measure of the ethyl iodide yield gives a measure of the yield of scavenged hydrogen atoms. Extrapolation to infinite concentration of ethylene gives the yield of thermal hydrogen atoms produced in the γ -radiolysis of 2,2,4-trimethylpentane. The study of such a system in the presence of electron scavengers, which interfere with reaction 1, should give information on the yield of hydrogen atoms produced in this reaction with an efficiency f . The results of such experiments involving SF₆ and N₂O as electron scavengers are presented in

Table II for an ethylene concentration of 0.11 M . At this concentration $\sim 80\%$ of the thermal hydrogen atoms are scavenged by ethylene. As can be seen in Table II, $G(C_2H_5^{131}I)$ decreases with increasing electron scavenger concentration, indicating that indeed reaction 1 is the source of some thermal hydrogen atoms. One can extend to 2,2,4-trimethylpentane the kinetic model recently proposed for cyclohexane.³ In this model, for a given ethylene concentration, the electron scavenger concentration dependence of the yield of ethyl radicals (measured as ethyl iodide) is given by

$$G(C_2H_5\cdot)_{[C_2H_4]} = \left[G(H)_0 - f \left(G_{fi} + G_{gi} \frac{\sqrt{\alpha S}}{1 + \sqrt{\alpha S}} \right) \right] \frac{1}{1 + \frac{k_{abs}[RH]}{k_{add}[C_2H_4]}} \quad (III)$$

where $G(H)_0$ is the yield of thermal hydrogen atoms in the pure 2,2,4-trimethylpentane ($=1.0$). f , as mentioned above, is the efficiency of producing a thermal hydrogen atom upon electron-ion neutralization (reaction 1) and k_{abs}/k_{add} is the ratio of the rate constant for the abstraction of hydrogen atom from the solvent (k_{abs}) to that for the addition to ethylene (k_{add}). The value of k_{abs}/k_{add} was found to be 0.0043.¹¹ $[RH]$ is the molarity of 2,2,4-trimethylpentane = 6.06 M . The other parameters have been defined previously. In eq III the only unknown parameter is f . From the best fit of this equation to the experimental data, one obtains $f \simeq 0.09$. The last column in Table II gives the values calculated with eq III and $f = 0.09$. The general agreement between the calculated and experimental values is fairly good. The value of $f \simeq 0.09$ shows that a yield of $G = 0.44$ [$f(G_{ions})$] or 44% of the thermal hydrogen atoms come from ion-electron neutralization processes (reaction 1). The remaining yield of $G(H) = 0.56$ comes from direct excitation of 2,2,4-trimethylpentane. With the knowledge of the yields of hydrogen and thermal hydrogen atoms originating from ionic processes, one can estimate the contribution of various processes to the total hydrogen (Table III).

Table III: Estimated Yields of Hydrogen and Methane According to the Different Sources from Which They Originate

	—Molecular—		Atomic/radical		—Total—	
	H ₂	CH ₄	H	CH ₃	H ₂	CH ₄
Ionic	1.01	~ 0.24	0.44	0	1.45	0.24
Nonionic	0.43	~ 0.24	0.56	0.73	0.99	0.97
Total	1.44	0.48	1.00	0.73	2.44 ^a	1.21 ^a

^a These two values are the experimentally determined yields of hydrogen and methane.

(18) P. P. Infelta and R. H. Schuler, *J. Phys. Chem.*, **76**, 987 (1972).

(b) ND_3 . From a study of ND_3 -cyclohexane solutions, Williams has shown that although $G(H_2)$ decreases with increase in ND_3 concentration, the total hydrogen yield remains constant.¹⁹ Since in cyclohexane ion-electron recombination results in hydrogen formation with unit efficiency, this indicated that the neutralization of the secondary ions, produced by proton transfer from cyclohexane positive ion to ammonia, also results in hydrogen formation with unit efficiency. This has been further confirmed recently.^{3,20} On the other hand, in systems where the efficiency of hydrogen production from the electron-ion neutralization is less than unity, the total hydrogen should increase with added ammonia, since the efficiency of hydrogen production from the neutralization of the secondary ion in the ammonia system is higher than that in the pure solvent. As expected, the addition of ND_3 to 2,2,4-trimethylpentane results in an increase in the hydrogen yield, as is illustrated in Figure 1. (The total yield of hydrogen is $G(H_2)_{total} = 3.00$ at $0.3 M ND_3$.) This increase of the total hydrogen yield represents actually a constant $G(H_2)$ and a production of $G(HD)$ (dashed circles in Figure 1.) The reaction scheme leading to these products consists of the proton-transfer reaction (4) in competition with reaction 1 followed by the neutralization reaction (5)



The hydrogen or deuterium atoms produced in reaction 5 with the statistical weights of one-fourth and three-fourths, respectively, will abstract a hydrogen atom from the solvent to give H_2 or HD . Since only the yield $G(HD)$ is measured, one obtains the yield of reaction 5 and, hence, the yield of ND_3H^+ produced by multiplying the $G(HD)$ by $4/3$ to correct for the hydrogen atoms produced.^{19,20} In turn, one has to subtract from the yield of $G(H_2)$ a yield equal to $1/3 G(HD)$ to account for the hydrogen originating in the neutralization of ND_3H^+ . These corrected yields of $G(HD)$ and $G(H_2)$ are shown in Figure 1. Since the equations presented so far are also applicable to positive ion scavengers, the total hydrogen yield at any concentration of ND_3 should be given by an equation such as eq II with $-\epsilon$ being replaced by $(\epsilon_{ND_3} - \epsilon)$, where ϵ_{ND_3} is the efficiency of producing hydrogen from ND_3H^+ neutralization (reaction 5) and ϵ is the efficiency of producing hydrogen upon ion-electron neutralization in the pure solvent. We will refer to this equation as eq II'. Since $\epsilon_{ND_3} \simeq 1.0$ and $\epsilon = 0.3$, one has $\epsilon_{ND_3} - \epsilon = 0.7$. In eq II' all the parameters are known but α_{ND_3} and a fit of this equation to the total hydrogen yields should give an estimate of this value. However, total hydrogen changes from $G(H_2) = 2.44$ to $G(H_2) = 3.00$ at $0.3 M ND_3$, and one can very readily see that one cannot fit the yields of hydrogen with eq II' unless $G_{fi} = 0$.

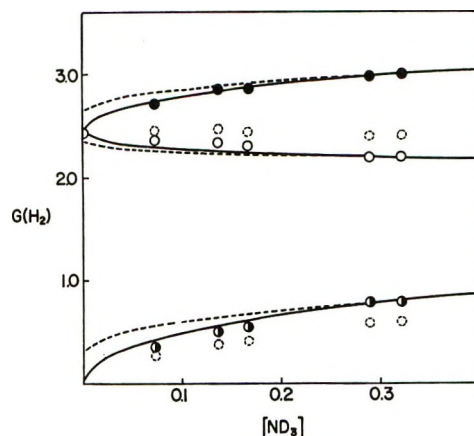


Figure 1. Hydrogen yields as a function of ND_3 concentration: (●) $G(\text{total hydrogen})$, (upper ○) $G(H_2)$, (lower ○) $G(HD)$; (○) $G(H_2)(\text{corr})$ (see text), (●) $G(HD)(\text{corr})$ (see text). Lines are calculated using eq II', II, and I for $G(\text{total hydrogen})$, $G(H_2)$, and $G(HD)$, respectively, with the parameters given in the text. Dashed lines refer to the case where $G_{fi} = 0.3$ and solid lines to $G_{fi} = 0$.

If $G_{fi} = 0.3$, the free ion contribution to the total yield of hydrogen would be 0.21, and α_{ND_3} should be close to zero in order to explain the yield of total hydrogen $G(H_2) = 2.71$ at $0.073 M ND_3$. If free ions were contributing to the yield of HD , the best fit of eq II' to the total yield of hydrogen would be that illustrated as the uppermost dashed line in Figure 1 ($\alpha_{ND_3} = 0.05 M^{-1}$). Assuming that there is no contribution of free ions to the yield of HD ,²¹ the solid line drawn through the total hydrogen yields is calculated with eq II' and the following parameters: $G(H_2)_0 = 2.44$, $\epsilon_{ND_3} = 1.0$, $\epsilon = 0.3$, $G_{fi} = 0$, $G_{gi} = 4.54$, and $\alpha_{ND_3} = 0.15 M^{-1}$. One can calculate $G(HD)$ and $G(H_2)$ by using eq I and II. This is illustrated as the dashed ($G_{fi} = 0.3$) and the solid lines ($G_{fi} = 0$) drawn through the HD and H_2 yields. The agreement between the calculated solid lines and the experimental data is gratifying, indicating again that ND_3 does not react with the free ions. It should be pointed out here that the determination of α_{ND_3} is independent of the correction of $4/3$ applied to the HD yields. Therefore, the good agreement obtained between the calculated and corrected experimental HD yields supports the assumptions made in applying such a correction, i.e., (1) there is very little deuterium exchange between ND_3 and ND_3H^+ to give ND_4^+ , (2) there is no isotope effect in producing H or D in the neutralization of ND_3H^+ (and, therefore, they are produced according to their statistical weights). Muratbekov, *et al.*,⁵ reported a total yield of hydrogen $G(H_2) = 3.2$ from a solution of $1 M NH_3$ in 2,2,4-tri-

(19) F. Williams, *J. Amer. Chem. Soc.*, **86**, 3954 (1964).

(20) K.-D. Asmus, *Int. J. Radiat. Phys. Chem.*, **3**, 419 (1971).

(21) One reason can be that free ions do not react with ND_3 . Another suggested by a referee is that traces of an electron scavenging impurity in the ND_3 would convert free electrons to free anions and as a result no hydrogen would be produced upon neutralization.

methylpentane. Using the above parameters and eq II', one calculates a total hydrogen yield $G(\text{H}_2) = 3.3$ at this concentration. The agreement is again satisfactory.

(B) *Methane.* (a) *Effect of Charge Scavengers.* The methane yield from the γ -radiolysis of pure 2,2,4-trimethylpentane was found to be 1.21 ± 0.05 and independent of dose in the range of 1.5×10^{18} – 6×10^{18} eV/cm³. This value agrees with the yields of 1.12,¹² 1.1,^{6,13,16} 1.25,¹⁴ and 1.27¹⁵ reported in the literature. Using the ¹³¹I₂ scavenging technique in pure 2,2,4-trimethylpentane, a yield of 0.73 for methyl iodide was obtained in the present work. This indicates that the methane yield originates from methyl radicals, $G(\text{CH}_3) = 0.73$, and molecular methane, $G(\text{CH}_4)_M = 1.21 - 0.73 = 0.48$. Similar values have been reported in the literature for $G(\text{CH}_3)$ and $G(\text{CH}_4)_M$, respectively: 0.69 and 0.50,¹² 0.69 and 0.56,¹⁴ 0.70 and 0.57.¹⁵ This methyl radical yield ($G(\text{CH}_3) = 0.73$) remains unaffected in the presence of charge scavengers as indicated in Table IV. These results indicate that the excited states produced directly in the radiolysis of 2,2,4-trimethylpentane are the precursors of methyl radicals. However, the presence of electron scavengers decreases slightly the total yield of methane, as shown in Table I. The yields of methane from CH₃Br solutions when corrected for the methane originating in the electron scavenging process as calculated by eq I are also presented in Table I and indicate a decrease of $G(\text{CH}_4)$ with increasing CH₃Br concentration. A similar decrease of the methane yield has been observed by Iida, *et al.*,⁶ who used N₂O and SF₆ as scavengers. Equation II, which has been used above in the case of hydrogen, can be extended to methane provided one replaces $G(\text{H}_2)_0$ by $G(\text{CH}_4)_0 = 1.21$ and ϵ by ϵ'' , the efficiency of producing methane upon electron-ion recombination. Since the effect of electron scavengers is relatively small, the calculation is rather insensitive to small variations of ϵ'' . The last column of Table I shows the yields of methane calculated by eq II with the parameters obtained previously and $\epsilon'' = 0.05$. The agreement is sufficiently good, especially in view of the experimental errors involved in the measurement of methane. Bearing in mind that the $G(\text{CH}_3)$ originates only from direct excitation of the 2,2,4-trimethylpentane, one can now, as for hydrogen, estimate the contribution of various processes to the yield of methane (Table III). The effect of positive ion scavengers, namely ND₃ and ethanol, is smaller than the effect of electron scavengers: $G(\text{CH}_4) = 1.15$ and 1.13 at 0.14 and 0.32 M ND₃ and $G(\text{CH}_4) = 1.17$ at 0.1 and 0.3 M ethanol, respectively. Such a smaller effect is expected, since the value of $\alpha_{\text{ND}_3} = 0.15 \text{ M}^{-1} \cong \alpha_{\text{EtOH}}$,²² is much smaller than, for instance, $\alpha_{\text{N}_2\text{O}} = 6 \text{ M}^{-1}$. It should be pointed out here that Iida, *et al.*,⁶ found a yield of 0.2 of molecular methane originating from non-ionic processes. This value should be compared with

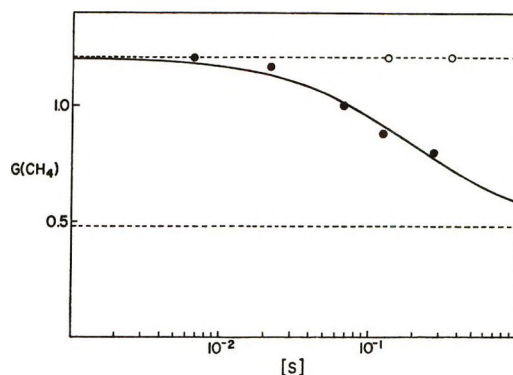


Figure 2. Yield of methane as a function of solute concentration: (●) $[S] = \text{C}_2\text{H}_4$, (○) $[S] = \text{c-C}_3\text{H}_6$. Solid line calculated using eq IV and the parameters given in the text. The upper and lower dashed lines refer to the total (= 1.21) and molecular (0.48) yield of methane from the radiolysis of pure 2,2,4-trimethylpentane.

Table IV: Effect of Charge Scavengers on the Yield of Methyl Iodide from ¹³¹I₂-2,2,4-Trimethylpentane Solutions^a

S	[S], mM	$G(\text{CH}_3^{131}\text{I})$
...	...	0.73
SF ₆	107	0.73
	293	0.76
CF ₃ Br	320	0.75
C ₂ H ₅ Br	300	0.72
C ₂ H ₅ OH	120	0.77
C ₆ H ₆	135	0.75

^a ¹³¹I₂ = $5.4 \times 10^{-4} \text{ M}$.

the value of 0.24 obtained in the present work (Table III).

(b) *Effect of Ethylene.* In a series of experiments the effect of C₂H₄ on the yield of methane has been investigated, and the results are shown in Figure 2. The yield of methane decreases with increasing ethylene concentration. However, it is unaffected by the presence of cyclopropane (Figure 2). Since it has been shown previously that ethylene as well as cyclopropane do not interfere with the reactions of positive ions in 2,2,4-trimethylpentane,¹¹ the decrease in the methane yield should then be due to the reaction of CH₃ radicals with ethylene in competition with the hydrogen atom abstraction from the solvent in a manner similar to that occurring with CF₃ radicals in ethylene-cyclohexane solutions.^{23,24}

If such competition represents the effect of ethylene, then the yield of methane at any given concentration of ethylene should be given by

(22) S. J. Rząd, Abstracts, 158th Meeting of the American Chemical Society, New York, N. Y., Sept 1969, p 239. It has been shown that in cyclohexane $\alpha_{\text{ND}_3} = 1.0 \text{ M}^{-1}$ and $\alpha_{\text{EtOH}} = 1.2 \text{ M}^{-1}$.

(23) P. P. Infelta and R. H. Schuler, *J. Phys. Chem.*, **73**, 2083 (1969).

(24) R. A. Weir, P. P. Infelta, and R. H. Schuler, *ibid.*, **74**, 2596 (1970).

$$G(\text{CH}_4) = G(\text{CH}_4)_M + \frac{G(\text{CH}_3)}{1 + \frac{k'_{\text{add}} [\text{C}_2\text{H}_4]}{k'_{\text{abs}} [\text{RH}]}} \quad (\text{IV})$$

where $G(\text{CH}_4)_M$ and $G(\text{CH}_3)$ are the yields of molecular methane ($=0.48$) and of methyl radicals ($=0.73$), respectively, in pure 2,2,4-trimethylpentane. $k'_{\text{add}}/k'_{\text{abs}}$ is the ratio of the rate constant for the addition of methyl radicals to ethylene to that for hydrogen abstraction from the solvent. According to this equation a plot of $G(\text{CH}_3)/(G(\text{CH}_4) - G(\text{CH}_4)_M)$ vs. $[\text{C}_2\text{H}_4]$ should be a straight line with an intercept of one and slope of $k'_{\text{add}}/k'_{\text{abs}}[\text{RH}]$. Such a linear relationship is indeed observed and a slope of $5.5 M^{-1}$ is obtained. Since $[\text{RH}] = 6.06 M$, $k'_{\text{add}}/k'_{\text{abs}} = 33.3$. With $k'_{\text{abs}} \simeq 20 M^{-1} \text{sec}^{-1}$,¹² $k'_{\text{add}} \simeq 665 M^{-1} \text{sec}^{-1}$. The

value of 33.3 agrees very well with the value of $k'_{\text{add}}/k'_{\text{abs}} = 34$ obtained at 65° in 2,2,4-trimethylpentane by Szwarc and coworkers.²⁵ The order of magnitude of $k'_{\text{add}} \simeq 665 M^{-1} \text{sec}^{-1}$ is in accord with the results obtained in the present work that the yield of methyl iodide is unaffected by the addition of ethylene (in the range of 3.53×10^{-3} – $0.22 M$) to solutions of $5 \times 10^{-4} M$ I_2 in 2,2,4-trimethylpentane (for example, $G(\text{CH}_3\text{I}) = 0.74$ at $0.22 M$ C_2H_4).²⁶ Using eq IV and the rate constants determined above, one calculates the solid line through the points in Figure 2.

Acknowledgment. The authors wish to thank Mr. G. K. Buzzard for the mass spectrometric analyses.

(25) R. P. Buckley and M. Szwarc, *Proc. Roy. Soc., Ser. A*, **240**, 396 (1957).

(26) The rate of reaction of $\text{CH}_3 + \text{I}_2$ to give CH_3I has been estimated to be $3 \times 10^8 M^{-1} \text{sec}^{-1}$.¹²

The Production of Halide Ion in the Radiolysis of

Aqueous Solutions of the 5-Halouracils¹

by Krishan M. Bansal, Larry K. Patterson, and Robert H. Schuler*

Radiation Research Laboratories, Center for Special Studies, and Department of Chemistry, Mellon Institute of Science, Carnegie-Mellon University, Pittsburgh, Pennsylvania 15213 (Received March 2, 1972)

Publication costs assisted by Carnegie-Mellon University and the U. S. Atomic Energy Commission

The radiation chemical production of halide ion from aqueous solutions of 5-fluoro-, 5-chloro-, and 5-bromouracil has been examined by conductometric pulse radiolysis and ion-selective electrode methods. The conductometric studies indicate that on the time scale of 10^{-3} to 10^{-2} sec approximately 15, 50, and 80% of the hydrated electrons produced in the irradiation react to form F^- , Cl^- , and Br^- from the respective halouracils while attack by $\cdot\text{OH}$ radicals gives hydrogen halide with corresponding efficiencies of 75, 65, and 55%. In these latter cases the yields of hydrogen halide presumably result from addition of $\cdot\text{OH}$ at the 5 position followed by dehydrohalogenation of the resulting radical. About 50% of the H atoms produce Br^- from bromouracil but the contribution is small in the case of the fluoro and chloro compounds. Steady-state experiments in which the halide ion was determined after γ radiolysis show that long-term processes are responsible for significant additional yields of halide ion. In particular it is shown that each of the halouracils is subject to attack by organic radicals arising from the uracil itself or produced from other solutes present in the system. In 5-chloro- and 5-bromouracil solutions containing added isopropyl alcohol a chain mechanism leads to the production of large yields of Cl^- and Br^- .

In recent years there has been considerable interest in the radiation chemistry of 5-bromouracil (BrUr) and related compounds as a result of the observed increase in the radiation sensitivity of DNA in which thymine has been partially replaced by BrUr .² The mechanism of this effect is not wholly understood, but it seems likely that dehalogenation following attack on DNA- BrUr by radicals produced in the irradiation is im-

portant.³ A number of pulse radiolysis studies have been carried out on aqueous solutions of BrUr ⁴ and

(1) Supported in part by the U. S. Atomic Energy Commission.

(2) See J. E. Zimbrick, J. F. Ward, and L. S. Myers, Jr., *Int. J. Radiat. Biol.*, **16**, 505 (1969), for a summary of previous work on this subject.

(3) G. E. Adams, "Current Topics in Radiation Research," Vol. III, M. Ebert and A. Howard, Ed., Wiley, New York, N. Y., 1967, p 35.

recently Neta⁵ has examined the esr spectrum during irradiation. Although several authors have investigated certain aspects of product formation^{2,3,6-8} only Adams³ and Schulte-Frohlinde and coworkers^{8b} have measured the production of Br⁻. Except for the pulse radiolysis⁴ and esr⁵ studies carried out parallel to the present investigation, no radiation chemical studies have, as yet, been reported on the other 5-halouracils. With the availability of ion-selective electrode and conductometric pulse radiolysis methods the radiation damage to these compounds, as monitored by halide ion formation, can be readily examined. We wish to present here a summary of the results of our studies on BrUr and also on 5-chlorouracil (ClUr) and 5-fluorouracil (FUr).

Experimental Section

The 5-fluorouracil and 5-bromouracil were obtained from Sigma Chemical Co. and the 5-chlorouracil from Calbiochem. These compounds were used without further purification.

Production of HX on the 10^{-5} to 10^{-2} sec time scale was determined by conductometric pulse radiolysis experiments of the type described by Beck⁹ and previously used in these laboratories to examine the radiation chemistry of SF₆,¹⁰ CH₃Cl,¹¹ and other simple halogen-containing compounds¹² in aqueous solution. These experiments involve the examination of the current in the conductivity cell with an a.c. amplifier; hence only differences in conductivity produced by the irradiation are measured. Observations at long times (>10 msec) are limited by the a.c. response of the amplifier and at short times (<10 μ sec) by recovery of the amplifier from the electron burst.

All studies were made on deaerated solutions initially in the pH range of 5-6. The observed conductivity changes were determined as a function of dose. Dosimetry of the conductometric experiments was based on an HCl yield of 3.14 from oxygen-free solutions saturated with CH₃Cl at atmospheric pressure (0.13 M).¹¹ Solutions of the halouracils (10^{-3} M) were deaerated by bubbling with N₂ or, where desired to convert e_{aq}⁻ into \cdot OH, with N₂O. The samples flowed through the irradiation cell and were replenished between pulses. Pulse durations were varied from 0.1 to 1 μ sec and beam current densities from 1 to 50 mA/cm². Total doses were less than 2×10^{17} eV/g in all cases. With these doses product concentrations did not exceed 10^{-5} M so that the pH at the end of the pulse was never less than 5.

The observed conductivity changes in the halouracil systems are interpreted here in terms of the formation of HF, HCl, and HBr. The equivalent conductance of each of these acids is approximately the same since the conductance of H⁺ represents $\sim 80\%$ of that of the product ions. Direct comparison of results from ClUr and BrUr systems with those from CH₃Cl are

possible since the equivalent conductances of HCl and HBr differ by less than 1%. A 7% correction was made in the case of FUr to take into account the difference in equivalent conductances of HF and HCl (395 and 425 mhos/equiv, respectively).

The production of halide ion over long periods of time was determined by ion-selective electrode methods similar to those used in the study of SF₆,¹³ CH₃Cl,¹¹ and related compounds. The production of F⁻ from FUr was determined with an Orion Model 94-09 ion-selective electrode, Cl⁻ from ClUr with a Model 94-17 electrode, and Br⁻ from BrUr with a Model 94-35 electrode. A Model 90-02 double junction reference electrode was used in conjunction with each of the above and electrode potentials were determined with an Orion 701 digital pH/mV meter capable of measuring the emf of the cell to 0.1 mV. The electrode system was calibrated with appropriate reference solutions before and after each set of measurements. Most measurements were made at pH 7 with both irradiated samples and calibration solutions containing 10^{-3} M phosphate buffer. The electrodes used here permit fluoride and bromide ion concentrations to be measured readily down to 5×10^{-6} M. The chloride electrode is less sensitive, and measurements were limited to concentrations above 1×10^{-4} M. The reference solutions gave good Nernst plots with slopes of ~ 59 mV/decade in the regions of interest.

Solutions of the 5-halouracils in the range 5×10^{-4} to 10^{-2} M were outgassed on a vacuum line by the usual freeze-pump-thaw method, and the samples were sealed. Nitrous oxide, where desired, was added after outgassing. The amounts of nitrous oxide added were determined from *P-V* measurements and concentrations were corrected for the fraction in the gas phase using a Bunsen coefficient of 0.59. The dose rate in these steady-state experiments was 4.2×10^{-8} eV g⁻¹ hr⁻¹. Total doses $\sim 1.5 \times 10^{18}$ eV/g were used in the case of the FUr solutions. Doses for BrUr solutions were usually a factor of ~ 2 lower and for ClUr solutions a factor of 2-3 higher. Fresh solutions

(4) L. K. Patterson and K. M. Bansal, *J. Phys. Chem.*, **76**, 2392 (1972). See this article for references to previous pulse radiolysis studies.

(5) P. Neta, *ibid.*, **76**, 2399 (1972).

(6) H. Walker, H. Dellweg, and D. Weinblum, *J. Mol. Biol.*, **3**, 787 (1961).

(7) H. Rueschl, *Z. Naturforsch. B*, **21**, 643 (1966).

(8) (a) E. Gilbert, O. Volkert, and D. Schulte-Frohlinde, *ibid.*, **22**, 477 (1967); (b) O. Volkert, W. Borst, and D. Schulte-Frohlinde, *ibid.*, **22**, 480 (1967).

(9) G. Beck, *Int. J. Radiat. Phys. Chem.*, **1**, 361 (1969).

(10) K.-D. Asmus, W. Grunbein, and J. H. Fendler, *J. Amer. Chem. Soc.*, **92**, 2625 (1970).

(11) T. I. Balkas, J. H. Fendler, and R. H. Schuler, *J. Phys. Chem.*, **74**, 4497 (1970).

(12) T. I. Balkas, J. H. Fendler, and R. H. Schuler, *ibid.*, **75**, 455 (1971).

(13) K.-D. Asmus and J. H. Fendler, *ibid.*, **72**, 4285 (1968).

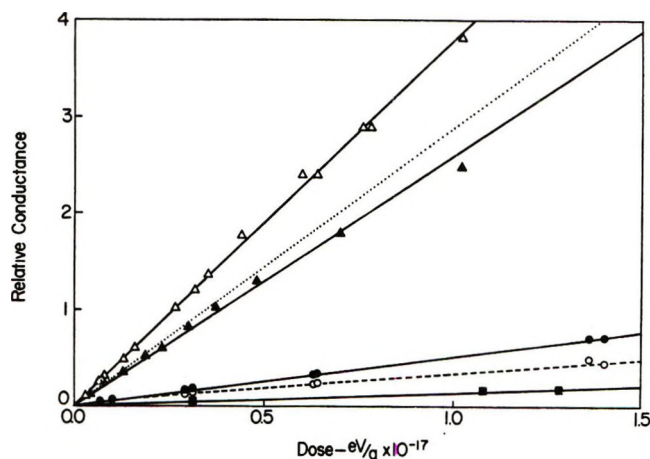


Figure 1. Relative conductivity increments observed as a function of dose for solutions (▲) of 5-fluorouracil and for solutions containing in addition (Δ) N_2O saturated at atmospheric pressure, (●) and (○) 0.5 *M* *tert*-butyl alcohol and (■) both N_2O and *tert*-butyl alcohol. The solid circles are the changes observed at 50 μ sec and open circles at 1 msec. The results from the reference CH_3Cl solutions fall along the dotted line indicated in the figure. The increase in the conductivity yield on saturation of the solution with N_2O was observed in a number of experiments and demonstrates quite directly the fact that attack on the uracil by $\cdot OH$ produces HX with a considerably greater efficiency than does attack by e_{aq}^- .

were prepared for each set of experiments. The extent of hydrolysis was low in each case and was measurable only for the fluoro and bromo compound ($\sim 5 \times 10^{-6}$ *M* for solutions $\sim 10^{-3}$ *M* in solute). Corrections were made in these cases. In the case of the chloride, hydrolysis was below the sensitivity limits of the electrode and no correction was made. Because of the higher doses used, the correction would amount to only 1–2% if the hydrolysis rate is similar to that of the other compounds.

Conductometric Pulse Radiolysis Studies

Pulse irradiation of 5-halouracil solutions results in a stepwise change in conductivity which is, for the most part, similar to that observed for methyl chloride.¹¹ In studies such as these quantitative interpretation is possible only after careful consideration of the stoichiometry and reaction rates of all of the ionic species involved. In general, one expects that the changes observed for solutions of halogen-containing organic compounds will be relatively simple since the formation of halide ion effectively removes the anion from reaction and in acid solutions fixes the product as HX. Assuming this to be the case the radiolysis of these solutions results in HX production with yields in the range of 2.4 to 4.6. Nitrous oxide and/or *tert*-butyl alcohol were added to isolate the contributions from e_{aq}^- , $H\cdot$, and $\cdot OH$. Plots of the changes observed in FUr solutions are given in Figure 1 as a function of dose, and the results with all of the halouracils are summarized in Table I.

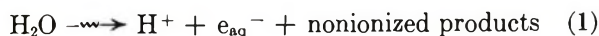
Table I: Yields of HX as Determined from the Increase in Conductivity Observed 50 μ sec after an Irradiation Pulse^a

Additional solute	Reactants	5-Fluorouracil	5-Chlorouracil	5-Bromouracil
None	$e_{aq}^- + H\cdot + \cdot OH$	3.0	3.4	4.6
0.5 <i>M tert</i> -butyl alcohol	$e_{aq}^- + H\cdot$	0.5	1.6	2.6
0.02 <i>M N</i> ₂ O ^b	$H\cdot + \cdot OH^c$	4.4	3.8	3.3
0.5 <i>M tert</i> -butyl alcohol + 0.02 <i>M N</i> ₂ O ^b	$H\cdot$	0.1	0.1	0.3

^a Measured for 1 *mM* solutions relative to a yield in HCl of 3.14 from a saturated solution of CH_3Cl (see ref 11). Average yields measured from slope of plots such as those given in Figure 1. All slopes corrected for the background conductance change observed for water saturated with N_2O which corresponds to a yield ~ 0.1 . ^b System saturated with N_2O at atmospheric pressure. ^c The $\cdot OH$ radical yield is approximately twice that in the absence of N_2O as a result of the conversion of e_{aq}^- to $\cdot OH$.

Reactions of the Hydrated Electron. We will first consider reactions occurring in systems containing *tert*-butyl alcohol. From the rate constants of the $\cdot OH$ reactions^{4,14} it is estimated that for 10^{-3} *M* halouracil in the presence of 0.5 *M tert*-butyl alcohol $\sim 98\%$ of the $\cdot OH$ radicals are scavenged by the alcohol so that effectively only the hydrated electrons and residual H atoms are available for reaction with the halouracils. Pulse irradiation of solutions of BrUr and ClUr containing *tert*-butyl alcohol results in a stepwise change in conductivity similar to that observed for methyl chloride (see ref 10) but of a magnitude corresponding to HX yields of 2.6 and 1.6, respectively. The conductivity increment at short times for FUr corresponds to an HF yield of only 0.5. A decrease in conductivity on the 100- μ sec time scale, as is shown in Figure 2b, indicates a complication in this system. These results show that a major fraction of the anions produced from the chloro and fluoro compounds do not rapidly give halide ion as a result of attack by e_{aq}^- .

The initial ionic species produced in the irradiation are, of course, H^+ and e_{aq}^-



The mechanism for the reaction of the hydrated electrons certainly includes as the next step



In these experiments the period of reaction 2 is known from the pulse radiolysis studies⁴ to be $\sim 10^{-7}$ sec. At submicrosecond times neutralization reactions cannot, however, occur at the pH's involved, and one expects

(14) R. L. Willson, C. L. Greenstock, G. E. Adams, R. Wageman, and L. M. Dorfman, *Int. J. Radiat. Phys. Chem.*, **3**, 211 (1971).

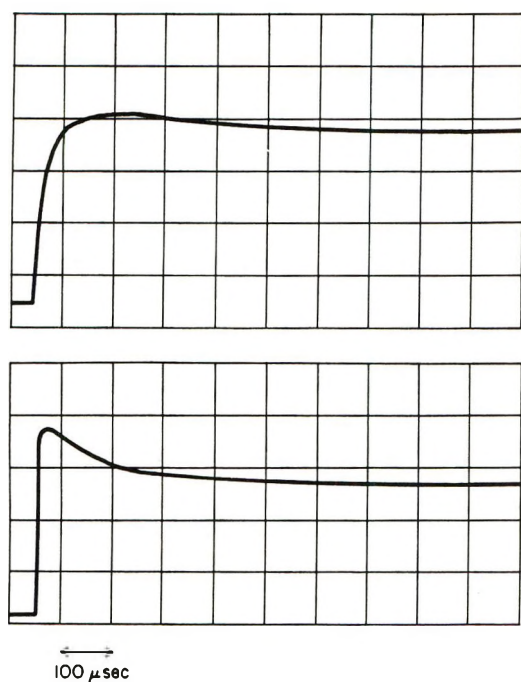
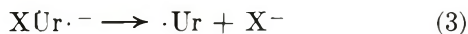
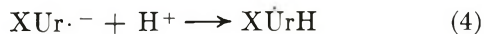


Figure 2. Conductivity as a function of time after a 1- μ sec irradiation of 10^{-3} *M* 5-fluorouracil containing 0.5 *M* *tert*-butyl alcohol to scavenge the OH radicals. Dose delivered (a) 2×10^{16} eV/g, (b) 2×10^{17} eV/g.

a proton and an anion to be present in solution. One possible explanation for the production of the observed conductivity is direct elimination of halide ion from the halouracil electron adduct



The fact that the hydrated electrons do not quantitatively produce halide indicates that processes competing with reaction 3 must be important. The two most likely competing reactions are neutralization



and hydrolysis



Theard, *et al.*,¹⁵ have found a rate constant of 6×10^{10} $M^{-1} \text{ sec}^{-1}$ for the neutralization of thymine radical anion and the rate constant for reaction 4 should be comparable. At the pH of these experiments a period of $\sim 5 \mu\text{sec}$ is expected for the decay of the conductivity if reaction 4 is important. Such a decay should be observable, particularly in the experiments on FUr solutions, but no such decay was, in fact, found for any of these systems. Theard, *et al.*,¹⁵ have also shown that the electron adduct of thymine hydrolyses with a rate constant $\sim 1.3 \times 10^4 M^{-1} \text{ sec}^{-1}$. One would expect the halogen derivatives of the uracil anion to react at least as fast so that a period of $\sim 1 \mu\text{sec}$ is expected for reaction 5. Reaction 5 will be followed by neutralization of H^+ and OH^- ions ($k_{\text{H}^+ + \text{OH}^-} = 1.4 \times 10^{11}$

$M^{-1} \text{ sec}^{-1}$)¹⁴ with a period (of 1–2 μsec) which would not be observable in the present experiments.

From the above arguments reactions 1, 2, and 4, or 5 will lead to no net conductivity at times $\sim 10 \mu\text{sec}$ or longer. It is, of course, possible that the radical produced in reactions 4 and 5 can subsequently react to give HX. In the case of BrUr a stepwise change which corresponds nearly to the number of electrons produced in the system is observed. In the pulse radiolysis experiments on BrUr no transient absorption corresponding to the anion present in the FUr and ClUr systems was found.⁴ It seems therefore that dehalogenation is very rapid and probably proceeds by reaction 3. The yields are lower in the case of FUr and ClUr indicating that in these cases the other reaction paths are considerably more important. Elimination of HCl from ClUr anion appears to be only $\sim 60\%$ efficient. As mentioned above the conductivity results on FUr are complicated by a time-dependent decay. As is illustrated in Figure 2a, the period of this decay is much longer at lower doses. The period appears to be inversely proportional to the dose indicating that a second-order radical reaction is involved. At the higher dose a radical concentration $\sim 10^{-5} M$ is produced. Assuming a combination rate constant of $10^9 M^{-1} \text{ sec}^{-1}$, a median radical lifetime of $\sim 100 \mu\text{sec}$ is estimated. This period is in reasonable agreement with the observed decay. This decay can be explained if a product of radical–radical combination reacts with an ionic product and effectively acts as a buffer. We have therefore taken the maximum observed at times $\sim 50 \mu\text{sec}$ as the proper measure of HF formation although complications can certainly be present in this interpretation.

Reaction of OH Radicals. Pulse irradiation of nitrous oxide saturated solutions shows for each of the halouracils a stepwise increase in conductivity although in the case of FUr a small ($\sim 10\%$) decrease from its value at short times was observed on the msec time scale. These results show very directly the importance of $\cdot\text{OH}$ reactions with the halouracils since pulse irradiation of water saturated with N_2O shows only a negligibly small net conductivity at times longer than $10 \mu\text{sec}$. The hydrated electrons react with N_2O within a period of $< 10^{-7} \text{ sec}$ to produce equivalent quantities of $\cdot\text{OH}$ and OH^- , *i.e.*, reaction 1 is rapidly followed by

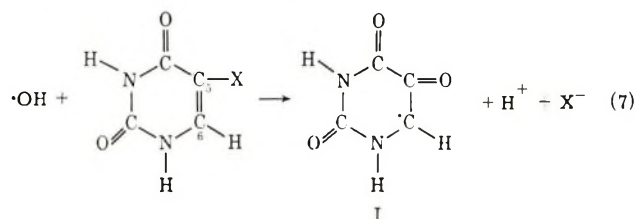


In the absence of secondary reactions of $\cdot\text{OH}$ with a solute, the only ionic species present on the microsecond time scale will be H^+ and OH^- and because of the rapid neutralization of the latter, as discussed above, no net conductivity is expected (or observed). From the measured rate constants for $\cdot\text{OH}$ reactions with the

(15) L. M. Theard, F. C. Peterson, and L. S. Myers, Jr., *J. Phys. Chem.*, **75**, 3815 (1971).

halouracils⁴ the period for attack is submicrosecond. The yields of ionized product at short times for FUr are illustrated in Figure 2 as a function of dose. If, in addition to the N₂O, *tert*-butyl alcohol is added to scavenge the OH radicals, then the residual conductivities are again very small. Values of the conductivity yield, after a small correction has been made for ~10% of the electrons scavenged by the uracil rather than by the N₂O, are given in Table I. Dividing this by a total yield of 5.6 (the sum of a direct ·OH yield of 2.8 and 90% of a yield of 3.1 produced from e_{aq}⁻ + N₂O) one obtains the fractional yields from ·OH given in the table.

The experiments in the presence of N₂O appear to be relatively free from complications and show that ·OH reacts with each of the halouracils to produce conducting species within the response time of the instrument. The most likely reaction seems to be addition at the site of the halogen atom followed by rapid dehydrohalogenation. This suggestion, which was also made



by Schulte-Frohlind and coworkers,^{8b} is confirmed by the esr observations of Neta⁵ in which a common spectrum attributable to radical I was observed during the irradiation of all three of the 5-halouracils. Since the efficiencies for production of HX are less than unity, it is assumed that attack of ·OH at the 6 position (or elsewhere) does not produce a radical which eliminates HX on the time scale of the conductivity experiments.

Reactions of H Atoms. From the conductivities observed in N₂O-saturated systems containing 0.5 M *tert*-butyl alcohol the yields of HX produced by attack of residual H atoms on the halouracils appears to be quite small. Only in the case of the bromo compounds is any significant yield observed and this amounts to ~50% of the residual yield of H·.

Summary of the Conductivity Results. As indicated in Table II the results of the conductivity experiments can be summarized by the statement that 15, 50, and 80% of the electrons and 75, 65, and 55% of the OH radicals produce HX by attack, respectively, on the fluoro, chloro, and bromo derivatives of uracil. As is indicated in Figure 1 saturation of FUr solutions with N₂O results in an increase in the conductivity increment. This fact indicates very directly that OH radical produces HX more efficiently than does e_{aq}⁻. A similar but considerably smaller increase is noted with ClUr while the opposite is true for BrUr where conversion of e_{aq}⁻ to ·OH is found to result in a decrease in the overall efficiency for HX production. In general, organic

fluorides do not appear to give fluoride ion by direct attack of e_{aq}⁻ on the fluorine atom¹² so that the low yield observed in the case of FUr is not surprising. From the fact that methyl chloride reacts quantitatively with e_{aq}⁻¹¹ one might expect that the reaction would also be quantitative in the case of the other two halouracils. This is certainly not true in the case of chlorouracil and probably not in the case of bromouracil so that reaction paths other than dehalogenation seem to be open to the radical anions produced. The decreased efficiency of ·OH in going from the fluoride to the bromide can conceivably result from steric effects which make attack at the 5 position less favored in the case of the bromide. Hydrogen atom attack produces negligibly small yield in the case of the fluoro and chloro derivatives and only a partial yield in the case of the bromo compounds. From the fractional efficiencies given in Table II, the yields predicted for the solutes in the absence of electron or radical scavengers are, respectively, 2.6, 3.3, and 4.1. Measurements on de-aerated solutions in the absence of added solutes gave yields which are 0.4, 0.1, and 0.5 units higher so that these efficiencies should be regarded as possibly being low by 10–20%.

Table II: Percentage Yields of HX Estimated from Conductometric Experiments^a

Reactants	5-Fluoro-uracil	5-Chloro-uracil	5-Bromo-uracil
e _{aq} ⁻	15	50	80
·OH	75	65	55
H·	15	15	50

^a Efficiency of e_{aq}⁻ estimated from yields observed in the presence of *tert*-butyl alcohol and of ·OH from the yields observed in the presence of N₂O. The ·OH efficiencies estimated from the decrease in yield observed upon addition of *tert*-butyl alcohol to the neat solution would be 90, 65, and 70%, respectively.

Steady-State Experiments

The results of the steady-state experiments, in which yields of halide ion produced at low dose rates over periods of minutes were measured, are reported in Table III. All experiments gave yields somewhat larger than those determined in the conductivity experiments. In general, one finds that halide ion yields increase in the solute concentration region of 10⁻³ to 10⁻² M. Results from experiments with each of the solutes in the absence of electron or radical scavengers are reported in Figure 3. A dependence for BrUr similar to that in this figure has been reported by Adams.³ It is seen that the concentration dependences for BrUr and FUr are small and that a reasonable extrapolation to low solute concentrations can be made. The extrapolated limits are reported in Table III. In

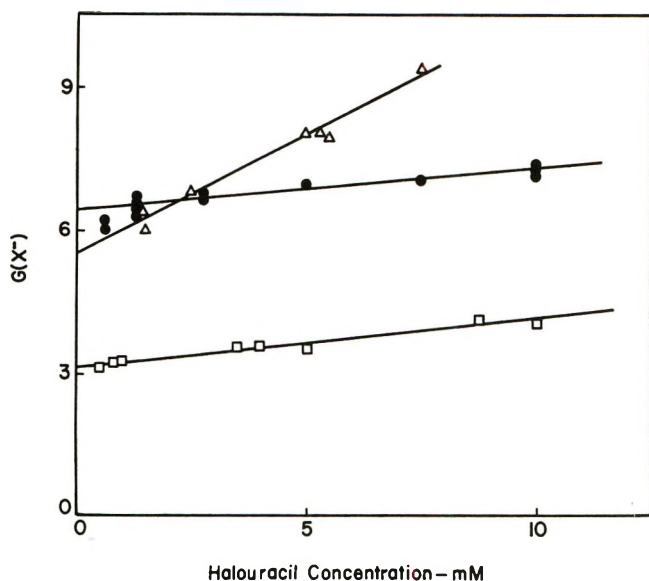


Figure 3. Concentration dependence of the halide ion yield in γ -ray experiments at a dose rate of 4.2×10^{18} eV g⁻¹ hr⁻¹: \square , fluorouracil; Δ , chlorouracil; and \bullet , bromouracil. No scavengers were present in these experiments.

the case of ClUr the concentration dependence is very pronounced, and extrapolation is subject to considerable uncertainty. Addition of *tert*-butyl alcohol and N₂O to the ClUr system to scavenge, respectively, the OH radicals and the hydrated electrons shows that the observed concentration dependence results principally from secondary reactions of the electron adduct.

Table III: Yields of Halide Ion Determined after γ Irradiation^{a,b}

Additional solute	5-Fluorouracil	5-Chlorouracil	5-Bromouracil
None	3.1	5.5	6.4
0.2 M <i>tert</i> -butyl alcohol	1.8	3.0	4.0
0.02 M N ₂ O	5.1	6.1	4.8
0.2 M <i>tert</i> -butyl alcohol + 0.02 M N ₂ O	1.7	2.0 ^c	0.9
0.02 M H ₂ O ₂	5.4	...	5.2
0.2 M isopropyl alcohol	1.7	14 ^c	33
0.2 M acetone	2.8	3.4	3.5

^a Yields are dependent on concentration. Unless otherwise indicated the yields have been extrapolated to low concentration ($\sim 10^{-4}$ M) of 5-halouracil. ^b Experiments at pH 7. Dose rates 4.2×10^{18} eV g⁻¹ hr⁻¹. ^c Determined at 5×10^{-3} M 5-chlorouracil.

The extrapolated fluoride yield of 3.1 observed for FUr in the absence of radical scavengers is in good agreement with that indicated by the conductivity experiments. However, it is very striking that on the addition of *tert*-butyl alcohol the yield was reduced

only to 1.75. A considerably greater reduction is expected from the results of the conductivity experiments. Irradiation of FUr in the presence of both N₂O and *tert*-butyl alcohol also gave an unexpectedly large yield ($G(F^-) = 1.7$). Under similar conditions the yield in the conductivity experiments is negligible (see the lowest curve in Figure 1). It seems that the radicals produced from the alcohol attack FUr to give product halide ion which is observable at times beyond the range of the conductivity experiments. At the dose rates of these experiments the mean radical lifetime is of the order of seconds, ample time for secondary reactions to occur. The yields of fluoride measured in the solutions to which N₂O or H₂O₂ had been added to convert the hydrated electrons into OH radicals indicate that $\cdot OH$ attacks FUr to give F⁻ with $\sim 90\%$ efficiency over the long term. While this result is in reasonable agreement with that from the conductivity experiments, it does indicate that a fraction of the OH radicals may add at the 6 position and ultimately give fluoride. The addition of acetone or isopropyl alcohol, from which the radical (CH₃)₂ $\dot{C}OH$ is produced, respectively, by electron addition or H-atom abstraction, indicates that this latter radical attacks FUr to give F⁻. An attempt to determine the yield from e_{aq}^- by scavenging the OH radicals with sodium azide gave a fluoride yield of 4.1. Complications are obviously also present in this case. A similar experiment with ethylene gave a yield of 3.4. It is clear from these various experiments that at low dose rates many different types of radicals can attack 5-fluorouracil over the relatively long radical lifetime involved.

All of the yields determined in the steady-state experiments on ClUr are substantially above those expected from the results of the conductivity experiments. It is obvious from the pronounced dependence on the concentration of ClUr indicated in Figure 3 that complications are present and that good correlation with the short-term yields determined conductometrically cannot be expected. In this case the very high yields observed in the presence of isopropyl alcohol can only be explained in terms of a chain propagation of the dehalogenation step.² Presumably the radical (CH₃)₂ $\dot{C}OH$, which can be regenerated by hydrogen atom abstraction from the isopropyl alcohol, is the propagating intermediate. In the experiments where acetone has been added, the same radical is produced by reaction of e_{aq}^- with the acetone, but it cannot be regenerated and relatively low yields are observed.

The case of BrUr is somewhat more simple than the above example in that both the reduction in Br⁻ produced by the addition of *tert*-butyl alcohol and the yield observed in the presence of N₂O indicate that about 80–85% of the OH radicals ultimately produce Br⁻. This fraction is slightly greater than that indicated by the conductivity experiments. If we subtract one-half the yield from the N₂O solutions from that ob-

served in deaerated solutions, we obtain a net Br^- yield of 3.9 for reaction of e_{aq}^- and $\text{H}\cdot$. This yield is $\sim 25\%$ more than expected if the reactions of the latter species are not increased by some multiplicative step. A short radical chain seems to be important here. The very high yield of Br^- observed if isopropyl alcohol is added indicates the importance of a chain similar to that present in the ClUr system. One series of experiments at pH 1 gave a Br^- yield of 3.7. If the $\cdot\text{OH}$ contribution is subtracted from this latter yield, the 1.3 residue indicates that 30–40% of the H atoms give Br^- .

In summary, the results of the steady-state experi-

ments are complicated and cannot be interpreted solely in terms of elementary reactions of the radicals initially produced in the water. These results do, however, demonstrate that all of the halouracils are readily attacked by organic radicals in secondary reactions. Zimbrick, *et al.*,² have suggested similarly that various organic radicals can attack bromouracil by both abstraction and electron-transfer processes. This behavior must be taken into account in interpretation of the results of biologically oriented studies and may well be an important source of the high radiosensitivity indicated in the introduction for the DNA-BrUr system.

Pulse Radiolysis Studies of 5-Halouracils in Aqueous Solutions¹

by L. K. Patterson* and K. M. Bansal

Radiation Research Laboratories and Center for Special Studies, Mellon Institute of Science, Carnegie-Mellon University, Pittsburgh, Pennsylvania 15213 (Received March 2, 1972)

Publication costs assisted by Carnegie-Mellon University and the U. S. Atomic Energy Commission

Pulse radiolysis studies of 5-fluorouracil, 5-chlorouracil, and 5-bromouracil have been carried out in argon and N_2O -saturated aqueous systems. Rate constants for attack by e_{aq}^- and $\cdot\text{OH}$ were found to be insensitive to the character of the halogen substituent. The second-order rate constant for attack on the halouracil by e_{aq}^- is $(1.4 \pm 0.2) \times 10^{10} \text{ M}^{-1} \text{ sec}^{-1}$ and by $\cdot\text{OH}$ is $(5.4 \pm 0.2) \times 10^9 \text{ M}^{-1} \text{ sec}^{-1}$ at pH 7. The stability of the halouracil radical anion or its protonated analog was found to be, however, markedly affected by altering the halogen at the C-5 position. Upon reaction with hydrated electrons the fluoro and chloro compounds gave similar spectra though differing in intensities (λ_{max} $335 \pm 5 \text{ nm}$). No significant optical absorption by the bromouracil anion was observed within the time resolution of the apparatus used here. Rates of decay associated with the species produced from reaction with e_{aq}^- followed the order: bromo- \gg chloro- $>$ fluoro-uracil. The dehalogenated intermediates from bromo- and chlorouracil appeared to give hydrolysis products with λ_{max} $360 \pm 5 \text{ nm}$. Reactions of these intermediates with *tert*-butyl alcohol were also indicated. Reactions with $\cdot\text{OH}$ produced very similar transient spectra in all three cases with λ_{max} at $330 \pm 5 \text{ nm}$ and a broad band in the region 400–425 nm. Loss of a halide ion following attack at the C-5 position appeared to be very rapid in all cases with $\cdot\text{OH}$ attachment as the rate-determining step. Spectra associated with H-atom reactions at pH 1 are included and show similar optical absorptions for FUr and ClUr systems ($\lambda_{\text{max}} \sim 370 \text{ nm}$). The BrUr intermediate exhibited an additional absorption at lower wavelengths. All results are in reasonable agreement with the findings of conductometric pulse radiolysis studies on comparable systems.

Pyrimidine bases and related compounds have been shown, by pulse radiolysis studies, to react rapidly with hydrated electrons and hydroxyl radicals in aqueous solutions.^{2–13} In several cases, the optical absorption spectra for various intermediates resulting from e_{aq}^- , $\cdot\text{OH}$, and H atom interaction with such compounds have been measured and structural assignments suggested. Also, rates of radical–radical recombination and of other secondary processes have been determined. Studies on 5-bromouracil indicate, however, that the inclusion of a halogen atom in the pyrimidine system markedly alters the radiation chemistry from that observed in related nonhalogenated systems.^{3,5,14} Con-

ductometric pulse radiolysis measurements have shown that reactions with primary radicals, e_{aq}^- , $\cdot\text{OH}$, and $\cdot\text{H}$, may yield halide ions from 5-fluoro-, chloro-, and

(1) Supported in part by the U. S. Atomic Energy Commission.

(2) G. Scholes, P. Shaw, and R. L. Wilson, "Pulse Radiolysis," M. Ebert, *et al.*, Ed., Academic Press, New York, N. Y., 1965, p 151.

(3) R. M. Danziger, E. Hayon, and M. E. Langmuir, *J. Phys. Chem.*, **72**, 3842 (1968).

(4) G. L. Greenstock, M. Ng, and J. W. Hunt, *Advan. Chem. Ser.*, **No. 81**, 397 (1968).

(5) J. D. Zimbrick, J. F. Ward, and L. S. Myers, Jr., *Int. J. Radiat. Biol.*, **16**, 505 (1969).

(6) B. Cercek, *Nature (London)*, **223**, 491 (1969).

(7) E. Hayon, *J. Chem. Phys.*, **51**, 4881 (1969).

bromouracil with efficiencies dependent on the nature of the halogen atom involved.¹⁵ In the same work steady-state investigations carried out at low dose rates revealed that halide ions may be produced from a variety of secondary processes. Further, direct identification of radicals resulting from $\cdot\text{OH}$ attack on the halouracils has been made by esr methods.¹⁶ To examine fully the kinetics of reactions with primary radiolytically generated radicals as well as to characterize the complementary species involved in the production of halide ions, we have carried out pulse radiolysis studies in aqueous solutions of 5-fluorouracil (FUr), 5-chlorouracil (ClUr), and 5-bromouracil (BrUr). It is observed that variation of the halogen atom at the C-5 position may have a marked influence on the overall reaction mechanism of the substituted uracil. A summary of these studies is reported here.

Experimental Section

A Van de Graaff generator giving 0.1–1.0- μsec pulses of 2.8-MeV electrons was utilized in this work. Doses of 200–700 rads were deposited in a 2-cm quartz cell perpendicular to the monitoring light beam. The relative dose in each pulse was monitored by integrating the current with an electrometer circuit.

Monitoring light from an Osram 450-W XBO xenon lamp was focused on a mirror behind the cell such that the beam made a double pass through the cell. This source was flashed from a bank of capacitors to increase the light output for a period of ~ 1 msec. Triggering of the Van de Graaff generator was synchronized with the maximum of the flash which, over a period of about 100 μsec , varied by less than 1%. The intensity of the flash was also reproducible to within 1%.

The light beam was then focused onto the entrance slit of a Bausch and Lomb monochromator which has a focal length of 500 cm and a bandwidth of about 2 nm. As a light detector we used an EMI 9558 QC photomultiplier wired to amplify through only the first six dynodes. These were decoupled by capacitors to assure linear response at high light levels over the period of the flash. A shutter isolated the solution and detector from the light beam between monitoring flashes. A flow system replenished the solution between measurements. For measurements of extinction coefficient, normalized absorbance values were calibrated against $(\text{CNS})_2^-$ values obtained from pulse radiolysis of a $4 \times 10^{-3} M$ CNS^- solution bubbled with N_2O . The extinction coefficient at λ_{max} was taken to be $7100 M^{-1} \text{cm}^{-1}$.¹⁷

Complementary hydrogen atom reactivity data were obtained by the isopropyl alcohol- d_7 competition technique described by Neta, *et al.*¹⁸ Samples (10 cm^3) containing aqueous solutions of isopropyl alcohol- d_7 , halouracil, and $10^{-4} M$ acetone to scavenge electrons were deaerated by the standard freeze-thaw process and irradiated in a ^{60}Co γ cell 220 at a dose rate of $6 \times$

10^{19} eV/g-hr . Total absorbed doses were $6 \times 10^{18} \text{ eV/g}$. After irradiation, gases noncondensable at liquid N_2 temperatures were analyzed mass spectrometrically for H_2 and HD content. Details of rate constant calculations are available in the literature.¹⁸

5-Fluorouracil and 5-bromouracil from Sigma Chemical Co. and 5-chlorouracil from Calbiochem were used as supplied. Solutions were deaerated by bubbling with J. T. Baker ultra pure N_2 ; N_2O also supplied by J. T. Baker was used, where desired, to convert e_{aq}^- into $\cdot\text{OH}$. Buffers for adjustment of solution to pH 7 were prepared from monobasic (Baker Analyzed reagent) and dibasic (Fisher Certified ACS grade) sodium phosphate. Both $\text{Na}_2\text{B}_4\text{O}_7$ for buffering of solutions at pH 7 and sodium sulfate for maintaining ionic strength were Baker Analyzed reagents. Mallinckrodt (analytical grade) *tert*-butyl alcohol was used to scavenge hydroxyl radicals.

Kinetic Studies

Reactions of Hydrated Electrons. Pseudo-first-order rate constants for the reactions of e_{aq}^- with FUr, ClUr, and BrUr at pH 7, 9, and 11 in deaerated solutions were measured by monitoring the decay of e_{aq}^- absorption at 600 nm as a function of solute concentration. In each of these systems the total ionic strength was held constant at 0.05 with Na_2SO_4 , and *tert*-butyl alcohol was added to scavenge hydroxyl radicals. Rate constants were calculated in the standard manner¹⁹ from

$$k_{\text{e}_{\text{aq}}^- + \text{XUr}} = \frac{0.693}{[\text{XUr}]} \left[\frac{1}{\tau_{\text{obsd}}} - \frac{1}{\tau_{\text{H}_2\text{O}}} \right] \quad (1)$$

where τ_{obsd} and $\tau_{\text{H}_2\text{O}}$ are the half-lives in the presence and absence of solute at the concentration $[\text{XUr}]$. The results are summarized in Table I. Values were also obtained for $k_{\text{uracil} + \text{e}_{\text{aq}}^-}$, in good agreement with those previously reported.^{2,4}

(8) C. L. Greenstock, J. W. Hunt, and M. Ng, *Trans. Faraday Soc.*, **65**, 3279 (1969).

(9) C. L. Greenstock, *ibid.*, **66**, 2541 (1970).

(10) L. S. Myers, Jr., and L. M. Theard, *J. Amer. Chem. Soc.*, **92**, 2868 (1970).

(11) L. S. Myers, Jr., A. Warnick, M. L. Hollis, J. D. Zimbrick, L. M. Theard, and F. C. Peterson, *ibid.*, **92**, 2871 (1970).

(12) L. S. Myers, Jr., M. L. Hollis, L. M. Theard, F. C. Peterson, and A. Warnick, *ibid.*, **92**, 2875 (1970).

(13) L. M. Theard, F. C. Peterson, and L. S. Myers, Jr., *J. Phys. Chem.*, **75**, 3815 (1971).

(14) M. E. Langmuir and E. Hayon, *J. Chem. Phys.*, **51**, 4893 (1969).

(15) K. M. Bansal, L. K. Patterson, and R. H. Schuler, *J. Phys. Chem.*, **76**, 2602 (1972).

(16) P. Neta, *ibid.*, **76**, 2604 (1972).

(17) G. E. Adams, J. W. Boag, J. Currant, and B. D. Michael, "Pulse Radiolysis," M. Ebert, *et al.*, Ed., Academic Press, New York, N. Y., 1965, p 117.

(18) P. Neta, G. R. Holdren, and R. H. Schuler, *J. Phys. Chem.*, **75**, 449 (1971).

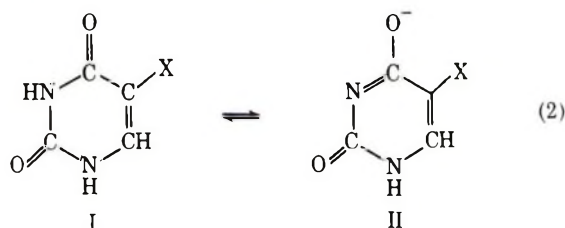
(19) E. J. Hart and M. Anbar, "The Hydrated Electron," Wiley-Interscience, New York, N. Y., 1970, p 218.

Table I: Rate Constants for Reactions of e_{aq}^- with 5-Halouracils

Halogen substituent	$k_{e_{aq}^- + \text{Xuracil}} \times 10^{-9}, M^{-1} \text{ sec}^{-1}$			pK's (reaction 2)
	pH 7	pH 9	pH 11	
F	12	5.7	5.0	
Cl	15	6.3	5.5	7.9 ^a
Br	16	8.2	7.0	8.1 ^c
	(26) ^c			
	19 ^d			
Uracil ^e	15	10	3.5	9.4
	14			

^a J. H. Fendler (private communication). ^b Reference 3. ^c Reference 5. ^d Reference 6. ^e Reference 4.

The observed pH dependence parallels that reported by Greenstock, Ng, and Hunt for uracil (HUr) over a similar pH range.⁴ They assigned the observed decrease in rate constant partly to electrostatic repulsion between e_{aq}^- and the negatively charged HUr at pH's above the pK and partly to a reactivity change accompanying keto-enol tautomerization of the carbonyl groups in the ionized form (II)



That the pronounced drop in $k_{XUr + e_{aq}^-}$ occurs between pH 7 and 9 rather than 9 and 11 as in the case of HUr simply reflects the lower pK's for halouracils. Also, the value of $1.6 \times 10^{10} M^{-1} \text{ sec}^{-1}$ at pH 7 of BrUr obtained in this work is somewhat smaller than the published values of 2.6×10^{10} and $1.9 \times 10^{10} M^{-1} \text{ sec}^{-1}$.^{5,6} However, in unbuffered systems at low ionic strength a value of $2.2 \times 10^{10} M^{-1} \text{ sec}^{-1}$ was found in the present study. It may be seen that substitution of a halogen at the C-5 position has little direct effect on the reactivity of e_{aq}^- toward the uracil ring system.

Reactions of $\cdot\text{OH}$ and $\cdot\text{H}$. Reactivity of the 5-halouracils toward $\cdot\text{OH}$ at pH 7 was measured both by competition with CNS^- and by monitoring the time-dependent buildup in optical absorption at 340 nm associated with $\cdot\text{OH}$ attachment (see next section) as a function of solute concentration. The competition experiments were carried out in the conventional way⁸ taking $k_{\text{OH} + \text{CNS}^-} = 1.1 \times 10^{10} M^{-1} \text{ sec}^{-1}$.⁹ Results from both these methods are given in Table II. Comparison of our values for $k_{\text{OH} + \text{BrUr}}$ with those previously reported shows reasonable agreement.^{5,20} Again, it may be seen that the substitution of a halogen at the 5 position has no dramatic effect on $k_{\text{OH} + \text{XU}}$. Unlike

e_{aq}^- , the reactivity of $\cdot\text{OH}$ toward these compounds is unaffected by raising the pH above the pK. This behavior parallels that of HUr which exhibits a change only in the pH region above 12 where the primary oxidizing species becomes O^- . Indeed, Greenstock, *et al.*,⁴ report a slight increase in $k_{\text{OH} + \text{XUr}}$ between pH 5 and 10.5. This is not inconsistent with our findings in which the differences in values between pH 7 and 11 are within experimental error. We have no data at present for $\cdot\text{OH}$ reactions at lower pH.

Table II: Rate Constants for the Reactions of $\cdot\text{OH}$ and $\cdot\text{H}$ with 5-Halouracils

Halogen substituent	$k_{\text{OH} + \text{XUr}} \times 10^{-9}, M^{-1} \text{ sec}^{-1}$ CNS ⁻ competition	$k_{\text{Adduct buildup}} \times 10^{-9}, M^{-1} \text{ sec}^{-1}$		$k_{\text{H} + \text{XUr}} \times 10^{-9}, M^{-1} \text{ sec}^{-1}$
		pH 7	pH 11	
F	5.2	5.5	6.0	0.18 ^e
Cl	5.2	5.5	5.8	0.16 ^e
				0.22 ^f
Br	4.0	5.6	5.8	0.22 ^e
	3.6 ^a			
	3.6 ^b			
Uracil	5.0 ^c	6.5	~6 ^d	0.24 ^f
	5.0			0.28 ^e

^a Reference 5. ^b Reference 20. ^c Reference 8. ^d Reference 4. ^e Reference 21. ^f Data obtained by the *d*-isopropyl alcohol competition technique at pH 7.

The rate constants for H-atom reactions with these compounds have recently been measured by Neta and Schuler using an esr technique²¹ and reveal a small decrease in the rate constant upon halogen substitution at the C-5 position of uracil. Although these esr measurements were made at pH 1, there is general agreement between rate constants at low pH for pyrimidines and those measured at pH 7.²² Their H-atom rate constants are given in Table II for purposes of comparison along with $k_{\text{H} + \text{HUr}}$ and $k_{\text{H} + \text{ClUr}}$ obtained in our laboratory by *d*-isopropyl alcohol competition methods,¹⁸ which serve to further corroborate the agreement in the two pH regions. No attempts to determine $k_{\text{H} + \text{XUr}}$ pulse radiolytically were made as experimental difficulties often produce rate constants that are too large.²³

Optical Absorption Spectra of the Transients

Spectra of transients produced by the pulse radiolysis of 5-halouracil were measured between 310 and 550 nm at solute concentrations of $4 \times 10^{-4} M$ in solutions ad-

(20) I. Kraljic, "The Chemistry of Ionization and Excitation," G. R. A. Johnson and G. Scholes, Ed., Taylor and Francis Ltd., London, 1967, p 305.

(21) P. Neta and R. H. Schuler, *Radiat. Res.*, **47**, 612 (1971).

(22) G. Scholes and M. Simic, *Biochem. Biophys. Acta*, **166**, 255 (1968).

(23) P. Neta, *Accounts Chem. Res.*, submitted for publication.

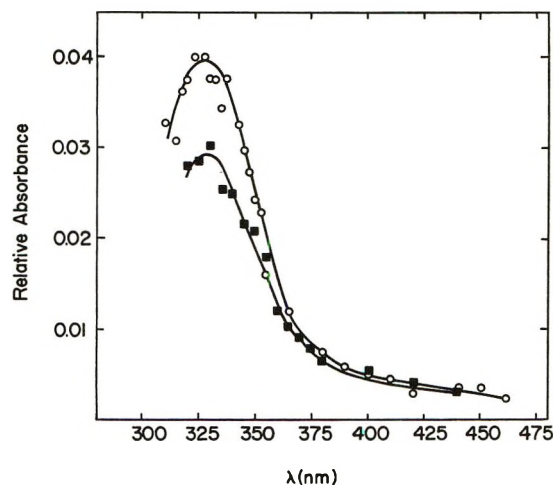


Figure 1. Transient absorption spectra produced by the pulse radiolysis of $4 \times 10^{-4} M$ FUr (O) and ClUr (■) in N_2 -saturated aqueous solutions containing $0.5 M$ *tert*-butyl alcohol. Optical densities were measured at peak absorption after the pulse.

justed to pH 7 by means of $10^{-3} M$ phosphate buffer. Ground-state absorption of these compounds limited measurements to wavelengths above 300 nm. In each system a spectrum was taken on an N_2 -saturated solution. This spectrum may be attributed principally to reaction products of XUr with e_{aq}^- and $\cdot OH$. From measurements at pH 1, described below, it is concluded that the contribution from H-atom adducts in this wavelength region is very small.

In the presence of N_2O , e_{aq}^- was converted into $\cdot OH$ by the reaction



with a rate constant for reaction 3 of $5.6 \times 10^9 M^{-1} \text{sec}^{-1}$.²⁴ However, there is a competition between N_2O and XUr for e_{aq}^- which dictates that about 6% of e_{aq}^- reacts with XUr. Also taking into account the increase in yield which results from scavenging of electrons from the spurs²⁵ in a system $2 \times 10^{-2} M$ in N_2O , one may assume that $G(OH)$ is essentially 5.7 or twice that in oxygen-free solutions.

Intermediates from e_{aq}^- Reactions. The spectra of e_{aq}^- related transients may be found in two ways: (1) by removing $\cdot OH$ with some efficient scavenger which does not affect e_{aq}^- such as *tert*-butyl alcohol or HCO_2^- ; (2) by difference, subtracting at each wavelength one-half the absorbance measured in N_2O -saturated solutions from that obtained in deaerated or N_2 -saturated solution. In this study both methods were employed and produced markedly different results in time-dependent behavior of the absorption signals.

Spectra taken in deaerated solutions of FUr and ClUr containing $0.5 M$ *tert*-butyl alcohol are shown in Figure 1 and may be seen to be of similar shape ($\lambda_{max} \sim 330 \text{ nm}$) though differing in apparent extinction coefficient, ϵ_a [*i.e.*, assuming $G(OH)$ or $G(e_{aq}^-)$ equals $G(\text{transient})$].

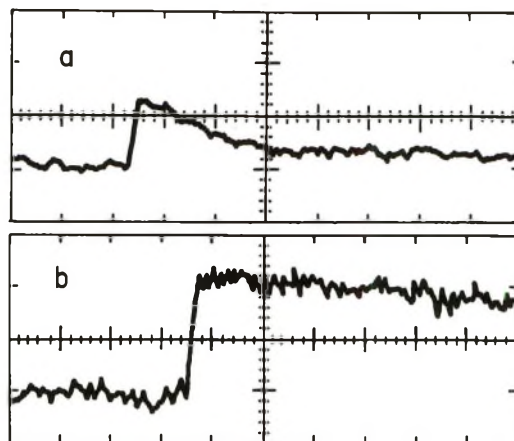


Figure 2. Oscillogram traces of transient absorption at 335 nm following pulse radiolysis of $4 \times 10^{-4} M$ (a) ClUr and (b) FUr in N_2 -saturated aqueous solutions containing $0.5 M$ *tert*-butyl alcohol. The horizontal axis corresponds to $5 \mu\text{sec}$ per major division. Vertical displacements correspond to decreased transmittances of (a) 2% and (b) 1.7% per major division.

At concentrations above $0.2 M$ *tert*-butyl alcohol, the transient from ClUr decays with a $\tau_{1/2}$ of about $5 \mu\text{sec}$ as may be seen from the oscillogram given in Figure 2a. Over the same time region, the transient produced from FUr is shown to decay very little (Figure 2b). In agreement with the findings of Langmuir and Hayon,¹⁴ we observed no significant transient absorption for the BrUr system which indicates that any intermediate formed has a very short lifetime.

Conductivity experiments carried out in these systems have shown that reactions with e_{aq}^- lead to dehalogenation from FUr, ClUr, and BrUr with efficiencies of approximately 15, 50, and 80%, respectively.¹⁵ Such percentage yields, when compared to the stabilities of the intermediates as reflected by their transient decays, suggest that a major reaction path for these species is dehalogenation. No spectra which might be assigned to secondary transients were observed in any of the systems containing *tert*-butyl alcohol. Further, no transient absorption was seen when these systems were bubbled with N_2O , demonstrating that the presence of the *tert*-butyl alcohol radical does not interfere with the observations.

Several comparisons may be made between the above results and those from systems in which spectra were taken by difference as described. Although N_2O -saturated solutions gave stepwise absorption following the pulse for all three cases (see next section), deaerated solutions of ClUr and BrUr exhibited, in a region centered at $\sim 360 \text{ nm}$, an initial rise followed by a further slow growth in absorption. This behavior, suggesting the presence of a secondary species, is illustrated

(24) P. Neta and M. Anbar, *Int. J. Appl. Radiat. Isotopes*, **18**, 493 (1967).

(25) T. I. Balkas, J. H. Fendler, and R. H. Schuler, *J. Phys. Chem.*, **74**, 4497 (1970).

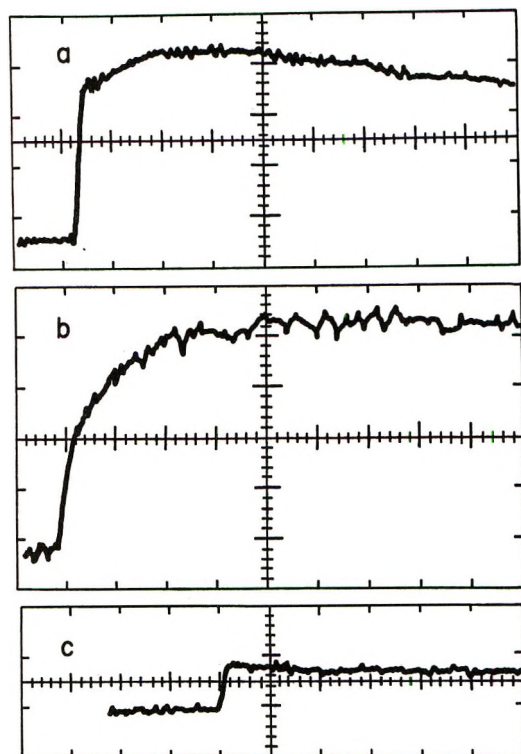


Figure 3. Oscillogram traces of transient absorption at 365 nm following pulse radiolysis of $4 \times 10^{-4} M$ (a) CIUr, (b) BrUr, and (c) FUr in N_2 -saturated aqueous solutions. The horizontal axis corresponds to (a) 10 μ sec, (b) 2 μ sec, and (c) 5 μ sec per major division. Vertical displacements correspond to decreased transmittances of (a) 1.4%, (b) 1.5%, and (c) 3.0% per major division.

in Figures 3a and b. The periods of growth may be seen to be about the same in both systems. CIUr absorption may be seen to give a pronounced step in which the change in optical density remains small for an interval of 4–5 μ sec before further growth. Such behavior suggests the compensatory growth and decay of two different species during this period. This interval is similar to that for the decay of the CIUr intermediate observed in the presence of *tert*-butyl alcohol. On the other hand, FUr absorption after the pulse rises sharply and then remains constant with no ensuing growth (Figure 3c). Figure 4 illustrates, for each of the halouracils, the transient spectra produced in de-aerated and N_2O solutions *immediately* after the pulse along with a difference spectrum for each system except BrUr which, within experimental error, shows none. For FUr and CIUr, the difference spectra are seen to be of similar structure to those spectra taken in *tert*-butyl alcohol solutions. The λ_{max} and long wavelength values of the CIUr species are subject to some uncertainty because of the small difference readings. Again, the apparent extinction coefficient of the CIUr transient is less than that for FUr although in de-aerated solutions both are less by about a factor of 2 than in the presence of *tert*-butyl alcohol.

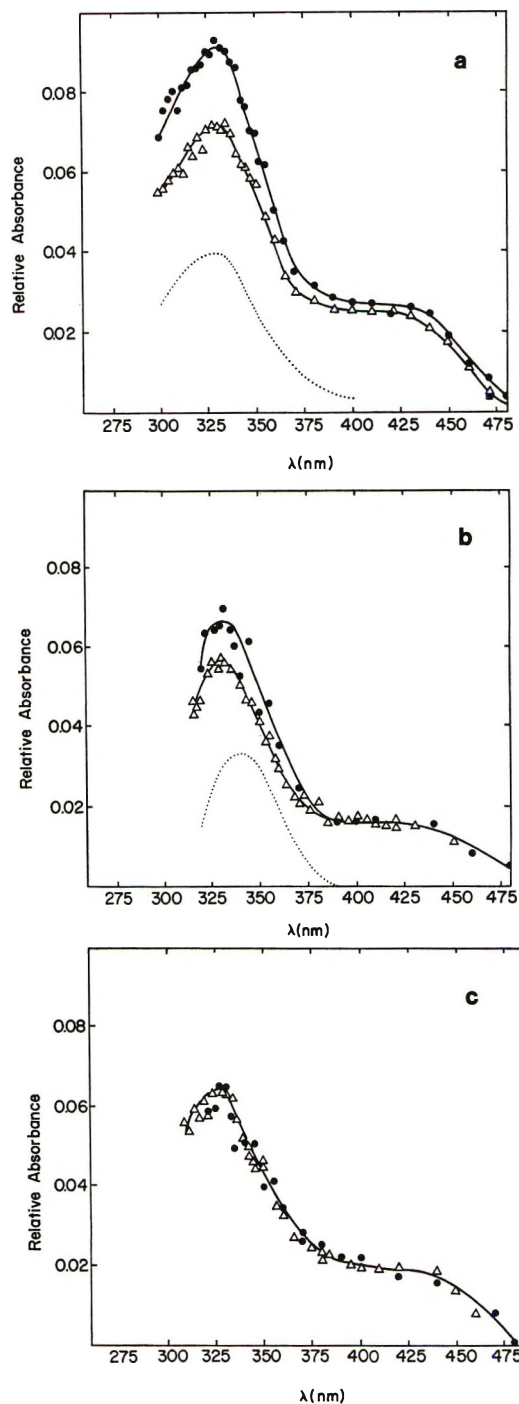


Figure 4. Transient absorption spectra from pulse radiolysis of $4 \times 10^{-4} M$ aqueous solutions of (a) FUr, (b) CIUr, and (c) BrUr each saturated with N_2 (●) and N_2O [relative absorbances corrected to $G(OH) = 2.8$] (Δ). The relative absorbances of the difference spectra (····) were multiplied by a factor of 2 for FUr and 3 for CIUr. Optical densities were measured at times corresponding to peak absorption in N_2O -saturated solutions.

Transient spectra from reactions of HUr with e_{aq}^- measured by both methods and giving spectra quite similar in profile to those found here showed no such discrepancy in ϵ_a . Some interaction between *tert*-butyl alcohol and XUr^- may be indicated. In both

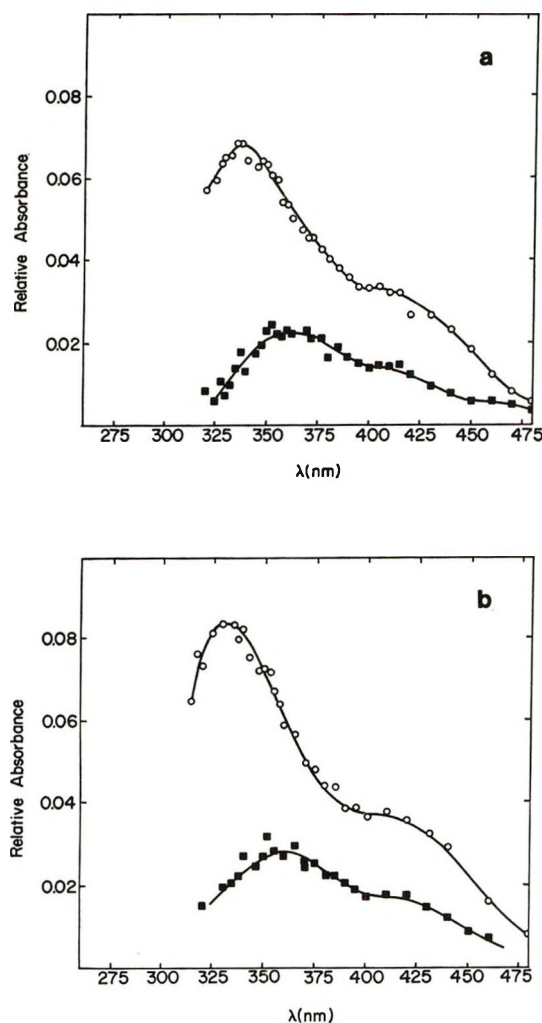


Figure 5. Transient absorption spectra obtained on pulse radiolysis of (a) $4 \times 10^{-4} M$ ClUr and (b) $4 \times 10^{-4} M$ BrUr in N_2 -saturated solution (O). The difference spectra (■) are also given. Optical densities were measured at times corresponding to maximum absorption in the N_2 -saturated solution.

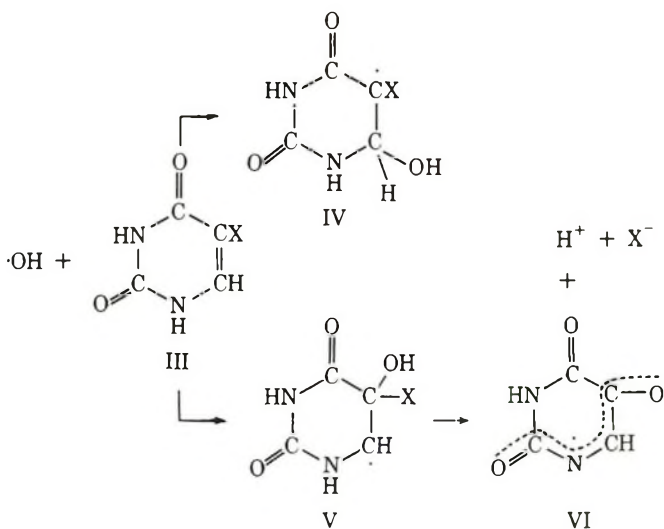
sets of experiments with each XUr, however, there is evidence that the initial radicals have about the same stability: FUr gave long-lived intermediates; the initial ClUr transients in both cases appeared to decay with a half-life of about 5 μsec ; BrUr produced no initial absorption related to the reaction with e_{aq}^- in either deaerated or *tert*-butyl alcohol containing systems. Also it was shown in the conductivity studies¹⁵ that yields of halide ion from reactions of $XUr + e_{\text{aq}}^-$, when measured in deaerated solutions containing 0.5 *M tert*-butyl alcohol gave good agreement with yields taken by difference from deaerated and N_2O -saturated solution data. These findings, taken together, indicate that interactions with *tert*-butyl alcohol have limited effect on the mechanism of the dehalogenation proceeding from XUr $^-$.

The species observed optically are probably protonated, at least in part. Theard, Peterson, and Myers¹³ have found that the electron adduct of thy-

mine, 5-methyluracil, may protonate either by reaction with H^+ ($k_{H^+ + Thy^-} = 6 \times 10^{10} M^{-1} \text{sec}^{-1}$) or by hydrolysis ($k_{H_2O - Thy^-} \sim 10^4 M^{-1} \text{sec}^{-1}$). Both species, protonated and unprotonated, gave similar spectra though differed in extinction coefficient. The halouracils would be expected to behave in similar fashion.

Spectra from deaerated solutions of ClUr and BrUr at the *maximum* intensity are given in Figure 5 along with corresponding difference spectra which take into account the small decay in the transients produced in N_2O -saturated solutions. These show that very similar intermediates with $\lambda_{\text{max}} \sim 360 \text{ nm}$ appear over about the same time interval in both systems. The apparent extinction coefficient in ClUr is about 15% lower than in BrUr. As this intermediate appears only for ClUr and BrUr systems, it seems reasonable that the precursor is the dehalogenated radical which itself has no absorption in the 300–550-nm region and that the slow growth at 350 nm is due to some hydrolysis of this radical. The relative peak absorption for the dehalogenated radical in BrUr and ClUr are in qualitative agreement with findings in the conductivity experiment that BrUr is more efficiently dehalogenated than ClUr by reactions with e_{aq}^- . In *tert*-butyl alcohol containing systems, the dehalogenated species appears to lead to no product with absorption over the wavelength region examined.

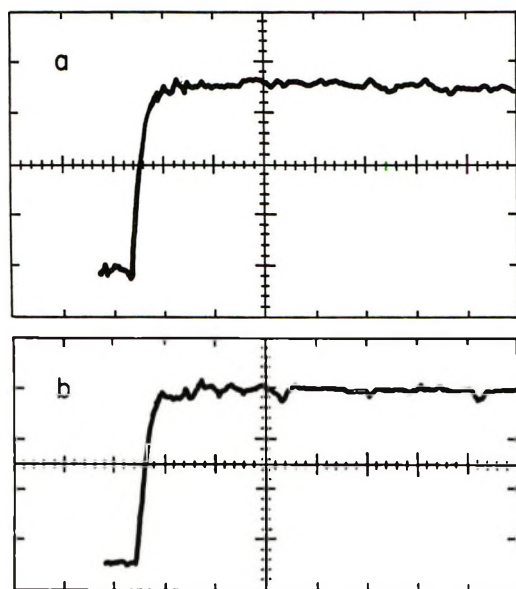
Intermediates from $\cdot OH$ Reactions. The transient absorption spectra obtained in N_2O -saturated solutions have already been given in Figure 4. From these data it is clear that in all three systems the profiles ($\lambda_{\text{max}} \sim 325 \text{ nm}$) and apparent extinction coefficients are similar (see Table III). Hydroxyl radicals may add to the double bond at the C-5 and C-6 positions to produce species IV and V.



It has been found by conductometric pulse radiolysis¹⁵ that for all three halouracils at $10^{-3} M$, attack by $\cdot OH$ yields halide within the response time of the instrument and with 65–75% efficiency. The radical VI has been observed in all three systems by Neta using esr tech-

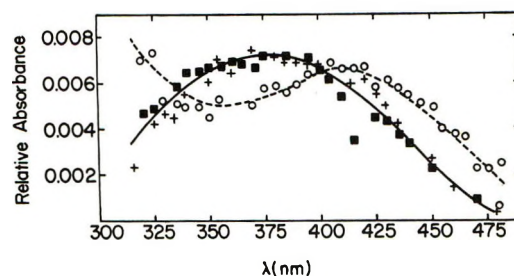
Table III: Second-Order Decay Data from Transient Species Produced in N_2O -Saturated Solutions of $4 \times 10^{-4} M$ Halouracils

Halogen substituents	λ , nm	$2k/\epsilon \times 10^{-5}$, $cm \ sec^{-1}$	$\epsilon_{app} \times 10^{-3}$, $M^{-1} \ cm^{-1}$	% OH adduct ^a undergoing dehalogenation	$\epsilon_{cor} \times 10^{-3}$, $M^{-1} \ cm^{-1}$	Absolute rate $(2k)^b \times 10^{-9}$, $M^{-1} \ sec^{-1}$
F	330	1.2	6.4	0.75	8.5	1.0
	425	4.3	2.1		2.8	1.2
Cl	330	1.8	5.0	0.65	7.7	1.4
	425	5.4	1.4		2.2	1.2
Br	330	2.4	5.6	0.55	10	2.4
	425	6.1	1.7		3.1	1.9

^a Reference 15. ^b Calculated on the basis of ϵ_{cor} .**Figure 6.** Oscillogram traces of transient absorption at 325 nm following pulse radiolysis of $1.5 \times 10^{-3} M$ (a) BrUr and (b) ClUr in N_2O -saturated aqueous solutions. The horizontal axis corresponds to $2 \mu sec$ per major division. Vertical displacements correspond to decreased transmittances of 4% per major division.

niques,¹⁶ and presumably this species is produced by dehydrohalogenation of V. Optical absorption of the $\cdot OH$ adduct of HUr has been found to be weak compared to that of the intermediate arising from its halogenated analogs³ (i.e., apparent extinction coefficients in a ratio of $\sim 1:5$) though somewhat similar in structure. This would suggest, then, that radicals IV and V make a limited contribution to the overall spectrum compared to VI, the dehalogenated radical. The optical absorption exhibits a stepwise growth corresponding to k_{OH+XUr} over all regions of the spectrum even at $1.5 \times 10^{-3} M$ XUr indicating that $\cdot OH$ attachment is the rate-determining step for the dehalogenation process (see Figure 6).

The decay in all three systems obeyed second-order kinetics both at 330 and 425 nm. These data are summarized in Table III. Our results for BrUr are comparable with those of Danziger, *et al.*³ ($2k/\epsilon = 2.3 \times$

**Figure 7.** Transient absorption spectra obtained on pulse radiolysis of $4 \times 10^{-4} M$ FUr (■), ClUr, (+), and BrUr (○) in N_2 -saturated aqueous solutions containing $0.5 M$ *tert*-butyl alcohol at pH 1. Optical densities were measured at times corresponding to maximum absorption.

$10^5 \ cm \ sec^{-1}$ at 330 nm) and Zimbrick, *et al.*⁵ ($2k/\epsilon = 4 \times 10^5 \ cm \ sec^{-1}$ at 408 nm). The absolute values of $2k$ will, of course, depend on the proper choice of ϵ . As it has been argued here that the transient spectrum is predominantly due to the dehalogenated species, correction of ϵ apparent may be made taking into account the efficiency of dehalogenation of the $\cdot OH$ adducts found in the conductivity experiments.¹⁵ The results of this correction along with corresponding values of the second-order decay rate constants are included in Table III. No attempt has been made to correct the rate constants for the cross reactions between halogenated and dehalogenated species.

Intermediates from H-Atom Reactions. Spectra were taken of transients found in deaerated solutions containing $0.5 M$ *tert*-butyl alcohol at pH 1 (see Figure 7). Similar absorption bands with $\lambda_{max} \sim 370$ nm were observed with FUr and ClUr. BrUr, which in the conductivity studies was the only halouracil to show significant dehalogenation from reaction with $\cdot H$ at pH 7, shows some absorption to the low wavelength side of this band. The apparent extinction coefficient at 370 nm was calculated to be about $450 \ M^{-1} \ cm^{-1}$ assuming a total reaction of H atoms with XUr and taking $G(H)$ at pH 1 to be 3.4. This low value of ϵ suggests that little error will result from ignoring any contributions of $\cdot H$ adducts to the difference spectrum at pH 7 where $G(H) = 0.6$.

Summary

Reactivities of HUr toward $\cdot\text{OH}$ and e_{aq}^- were shown to be essentially unchanged by the presence of a halogen atom. This behavior may be compared to an earlier study involving reactivity toward H atoms in which the halogen was seen to have a limited influence.²¹ However, the stability of XUr^- , or its protonated analog, toward loss of a halide ion does depend strongly on the nature of the halo substituent. Time dependences of optical absorption ($\lambda_{\text{max}} 335 \pm 5 \text{ nm}$) indicate these stabilities to be in the order $\text{FUr}^- > \text{ClUr}^- \gg \text{BrUr}^-$. The dehalogenated species proceeding from XUr^- gave evidence of forming a secondary intermediate ($\lambda_{\text{max}} 360 \pm 5 \text{ nm}$) probably by hydrolysis, over a period of 15–20 μsec . Dehydrohalogenation

following attack by hydroxyl radicals appeared to proceed with $\cdot\text{OH}$ attachment as the rate-determining step and gave comparable spectra ($\lambda_{\text{max}} 330 \pm 5 \text{ nm}$) in all three halouracils. Only the efficiencies of dehydrohalogenation were affected by varying the halogen. Closely related transients with broad absorption bands ($\lambda_{\text{max}} \sim 370 \text{ nm}$) were observed for reactions of $\cdot\text{H}$ with FUr and ClUr. The corresponding spectrum involving BrUr displayed an additional absorption at lower wavelengths which may be associated with the observation that only from BrUr is there significant halide ion produced from reactions with H atoms.

Acknowledgment. The authors wish to acknowledge the many helpful comments and suggestions given by Professor R. H. Schuler.

Electron Spin Resonance Study of Radicals Produced in

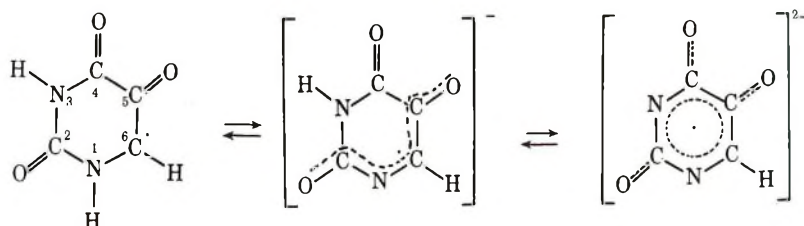
Irradiated Aqueous Solutions of 5-Halouracils¹

by P. Neta

Radiation Research Laboratories and Center for Special Studies, Mellon Institute of Science, Carnegie-Mellon University, Pittsburgh, Pennsylvania 15213 (Received March 2, 1972)

Publication costs assisted by Carnegie-Mellon University and the U. S. Atomic Energy Commission

Radicals produced in irradiated aqueous solutions of 5-halouracils have been studied using the *in situ* radiolysis steady-state esr method. The radicals produced by the reaction of OH with fluoro-, chloro-, and bromouracil were found to be identical. The spectrum observed in alkaline solution shows two nitrogen splittings and one proton splitting, that in neutral solution contains two proton splittings, and the spectrum in acid solution shows three. The parameters determined from the spectra suggest these acid-base forms of the radical



These radicals are formed by addition of OH to position 5 followed by elimination of hydrogen halide. The corresponding radicals from 5-bromouracil and 5-chlorouracil were also observed. The radicals produced by reactions of e_{aq}^- with 5-halouracils were not observed because they rapidly abstract a hydrogen atom from the formate used as a scavenger for OH.

Introduction

The radiation chemistry of the 5-halouracils has been recently studied in this laboratory.^{2,3} The rate constants for the reactions of these compounds with H, OH, and e_{aq}^- were found to be of the order of 10^8 , 10^9 ,

and $10^{10} \text{ M}^{-1} \text{ sec}^{-1}$, respectively. The mechanism of these reactions was studied both by the conductometric

(1) Supported in part by the U. S. Atomic Energy Commission.

(2) K. M. Bansal, L. K. Patterson, and R. H. Schuler, *J. Phys. Chem.*, **76**, 2386 (1972).

pulse radiolysis technique and by determination of the yield of halide ions formed during steady-state radiolysis.² It was concluded that the reaction of OH radicals brings about dehalogenation to a major extent in all 5-halouracils whereas the reaction of e_{aq}^- is largely dependent on the halogen, *i.e.*, dehalogenation by e_{aq}^- is 80% efficient with 5-bromouracil but only ~10% with 5-fluorouracil.²

To further examine the mechanisms suggested for these reactions it seemed desirable to undertake an esr study of the intermediate radicals present during irradiation of solutions of 5-halouracils. A similar study of the radicals from uracil, thymine, orotic acid, and several other uracil derivatives has been recently completed,⁴ and the results can be used for the identification of the radicals studied in the present work.

Experimental Section

5-Fluorouracil and 5-bromouracil were obtained from Sigma Chemical Co., 5-chlorouracil from Calbiochem, 5-bromoorotic acid from Cyclo Chemical Co., and 5-chlorobarbituric acid from Aldrich. Water was doubly distilled. Solutions were buffered with Baker Analyzed sodium tetraborate or sodium phosphates. Alkaline (pH >11) solutions were prepared with potassium hydroxide. Solutions were deoxygenated by bubbling with nitrogen or were saturated with N_2O . The irradiation with 2.8-MeV electrons was carried out directly in the esr cavity while the solution flowed through a flat silica cell. All the other details of this technique have been described previously.⁵

Results and Discussion

The esr spectra recorded with irradiated solutions (pH 6–10) of the three 5-halouracils studied are shown in Figure 1. The spectrum of identical radicals was obtained with N_2O -saturated solutions of 5-fluorouracil at pH 7.4 (Figure 1a), 5-chlorouracil at pH 6.1 (Figure 1b), and 5-bromouracil at pH 6.4, 8.8, and 9.9 (Figure 1c). The stick spectrum in Figure 1 shows the relationship of the lines. The spectrum was analyzed in terms of two hydrogen hyperfine splittings of 4.96 and 0.20 G and two nitrogen splittings of 2.21 and 1.105 G. No halogen splitting was observed. The g factor is 2.00470. These parameters resemble those determined previously⁴ for radicals produced by addition of OH to position 5 of uracil and other related pyrimidines.

The spectra recorded with irradiated alkaline solutions (pH >12) of 5-chloro- and 5-bromouracil (Figure 2) are again identical. They differ from the spectrum in neutral solution by the absence of the small proton splitting and slight changes in the nitrogen splittings. The spectra recorded with irradiated solutions of 5-bromouracil at pH 2.5 and 2.9 consisted of 72 lines of equal intensities. The signal-to-noise ratio was much smaller than that in Figure 1, but all the lines were observable and the spectra could be analyzed. The g

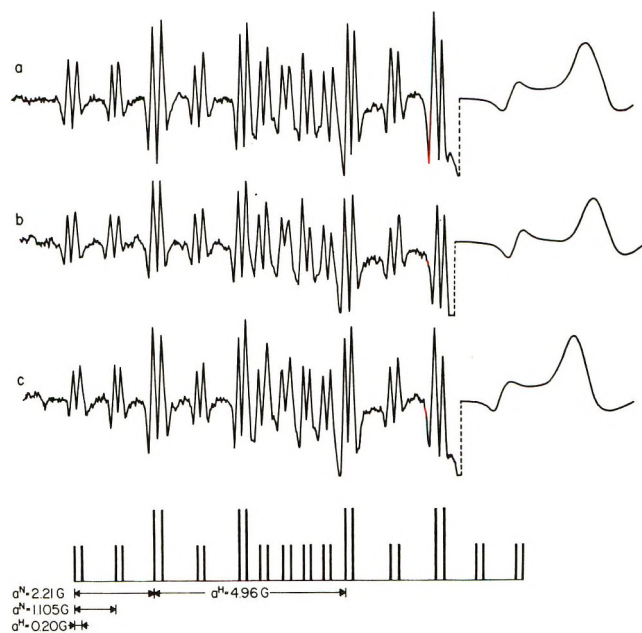


Figure 1. Second derivative esr spectra recorded with neutral solutions of 5-halouracils (0.003 M) saturated with N_2O and buffered with phosphate during irradiation with 2.8-MeV electrons. Magnetic field increases to the right. The stick spectrum shows the relationship of the lines. The large signal from the silica cell is seen above the center of the spectrum and is recorded at a gain 100 times less than the other portions: a, 5-fluorouracil, pH 7.4; b, 5-chlorouracil, pH 6.1; c, 5-bromouracil, pH 9.9 (similar spectra were observed at pH 6.4 and 8.8).

factor remains similar to that in neutral solution. However, the large proton splitting is larger by almost a factor of 2, and an additional 3.4-G proton splitting is observed.

The esr parameters determined and the suggested radical structures are summarized in Table I. The high g factors observed for these radicals are reasonable for radical structures with a carbonyl group at position α to the unpaired electron.^{4,6,7} The hyperfine constants resemble those determined for various radicals derived from uracil and substituted uracils.⁴ The suggested structures are also supported by the absence of any halogen splitting and by the fact that the fluoro-, chloro-, and bromouracil all gave the same radical. The assignment of the larger proton splitting to that at position 6 is based on comparison to the case of bromoorotic acid where this hydrogen is replaced by a carboxyl group (see below). The assignment of the other proton splittings to those at positions 1 and 3 as given in Table I is based on the expected order of their dissociation and on the magnitude of the splittings. The

(3) L. K. Patterson and K. M. Bansal, *ibid.*, **76**, 2392 (1972).

(4) P. Neta, *Radiat. Res.*, **49**, 1 (1972).

(5) K. Eiben and R. W. Fessenden, *J. Phys. Chem.*, **75**, 1186 (1971).

(6) H. Zeldes and R. Livingston, *J. Chem. Phys.*, **45**, 1946 (1966).

(7) R. Livingston and H. Zeldes, *J. Amer. Chem. Soc.*, **88**, 4333 (1966).

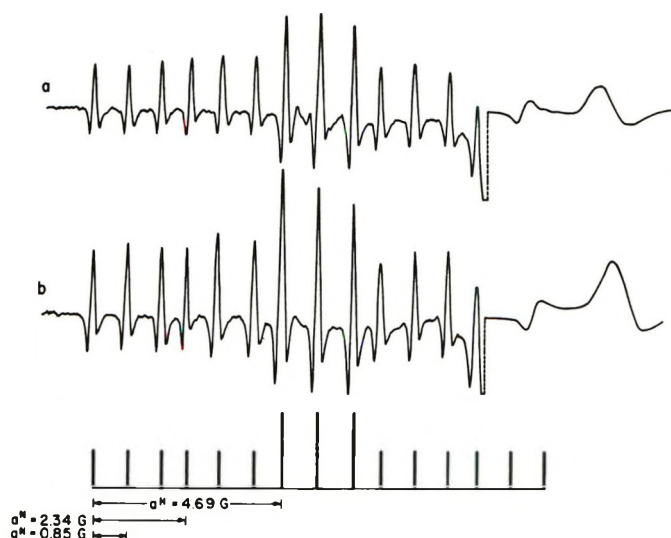
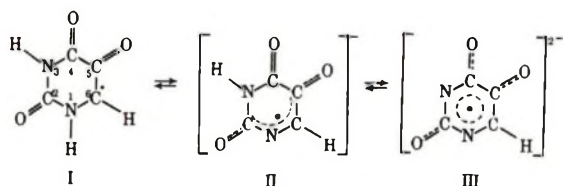


Figure 2. ESR spectra recorded with alkaline solutions of 5-halouracils (0.003 *M*) saturated with N_2O during irradiation. The signal from the cell is recorded at a gain 50 times less than the other portions: a, 5-chlorouracil, pH 13.7; b, 5-bromouracil, pH 12.4.

assignment of the nitrogen splittings is based only on the assumption that the nitrogen with the larger splitting would be closer to the unpaired electron and bear the proton with the larger splitting.

Table I: ESR Parameters and Suggested Structures for Radicals Produced by the Reaction of OH with 5-Halouracil^a

pH 2-3	pH 6-10	pH 12-14
$g = 2.00482$	2.00470	2.00461
$a_1^N = 1.88$	2.21	2.34
$a_3^N = 0.77$	1.105	0.85
$a_1^H = 3.41$
$a_3^H = 0.19$	0.20	...
$a_6^H = 9.67$	4.96	4.69



^a The g factors are measured relative to the peak from the silica cell and are accurate to ± 0.00005 . Hyperfine constants are given in Gauss and are accurate to ± 0.03 G.

The formation of halide ions from all these compounds by the reaction of OH radicals has been observed,² and the mechanism is most probably

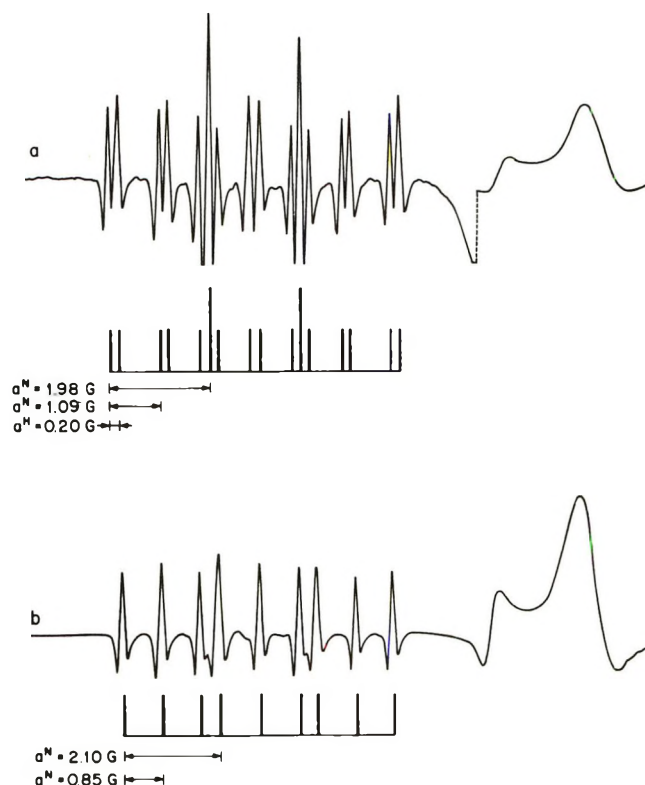
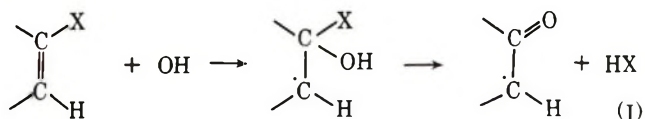


Figure 3. ESR spectra recorded with irradiated solution of 5-bromoorotic acid (0.003 *M*) saturated with N_2O : a, pH 5.9, buffered with phosphate, the signal from the cell is recorded at a gain 20 times less than the other portions; b, pH 12.3, all portions of the spectrum recorded at the same gain.

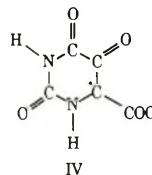
The second step in this mechanism could be catalyzed by acid or base. However, it must be relatively fast, and the esr results suggest that it is complete within a millisecond at all pH values examined.

The spectra obtained with irradiated solutions of 5-bromoorotic acid in neutral and alkaline solutions are shown in Figure 3. Except for the absence of the larger hydrogen splitting the parameters determined in this case are similar to those for the 5-halouracils and similar structures can be suggested for the radicals, formed *via* the same mechanism of dehalogenation by OH radicals. The esr parameters and the suggested radical structures are given in Table II. The resemblance of the g factors and hyperfine splittings for the radicals derived from 5-halouracil (Table I) and for those derived from 5-bromoorotic acid (Table II) is striking, except for the one hydrogen which is replaced by a carboxyl group and thus identifies the splitting constant assigned to this hydrogen (Table I).

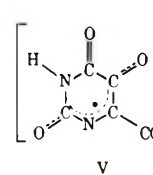
It should be noted in Figure 3 that the line intensities of the spectra obtained with bromoorotic acid are much higher than those of the spectra obtained with the halouracils. This is clearly the effect of the dissociated carboxyl group in decreasing the radical-radical reaction rate constants through electrostatic repulsion and thus increasing the steady-state concentration of the

Table II: ESR Parameters and Suggested Structures for Radicals Produced by the Reaction of OH with 5-Bromoorotic Acid^a

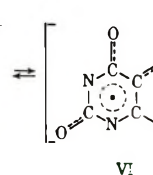
pH 3	pH 6	pH 12
$g = 2.00488$	2.00479	2.00466
$a_1^N = 1.98$	1.98	2.10
$a_3^N = 0.69$	1.09	0.85
$a_1^H = 3.50$
$a_3^H = 0.17$	0.20	...



IV



V

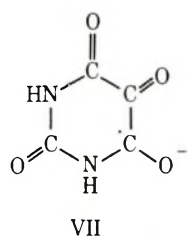


VI

^a The g factors are measured relative to the peak from the silica cell and are accurate to ± 0.00005 . Hyperfine constants are given in Gauss and are accurate to ± 0.03 G.

radicals. The difference between the triply charged compared to the doubly charged species is much greater than that between the latter and the singly charged species. Similar findings were noted previously (ref 4 and references within).

The reaction of OH radicals with 5-chlorobarbituric acid according to mechanism I should yield radical VII



which resembles that formed by one electron reduction of alloxan.⁸ The esr spectra recorded with irradiated solutions of 5-chlorobarbituric acid at pH 2.4 and 9.9 in the presence of N_2O both consisted of seven equally spaced lines with relative intensities of 1:4:8:10:8:4:1. This sequence could result from two equivalent nitrogens and two equivalent hydrogens which accidentally had very similar hyperfine constants. The splitting measured was 0.45 G and the g factor 2.00488. These parameters are in good agreement with those reported for the alloxan radical⁸ and, therefore, support the

identification of radical VII and the suggested mechanism I.

The radicals observed with irradiated solutions of all halouracils studied are those formed *via* OH addition to position 5 (mechanism I). Although it has been found^{2,3} that OH radicals add to position 6 also, no such adducts were detected. This failure must be owing to the lower yield of the latter radicals and also to their probably shorter lifetimes. Both effects cause lower steady-state concentrations as compared to those of the radicals observed. Furthermore, the number of lines in the esr spectra of radicals produced by OH addition to position 6 is expected to be larger than in the case of the observed radicals, and this again results in a decrease in line intensity.

An attempt was made to observe the radicals formed by reaction of e_{aq}^- with 5-bromouracil and 5-bromoorotic acid. This reaction was found to cause quantitative debromination.² To eliminate the formation of radicals by reaction with OH, formate was used as a scavenger for the OH radicals. This method has been proved successful in the experiments with orotic and isoorotic acid⁴ where the electron adducts were observed. In the present study no spectrum was observed with bromouracil, and a weak spectrum was detected in the case of bromoorotic acid. However, the parameters determined did not agree with the radical expected to be formed by direct debromination with e_{aq}^- . Instead, the spectrum observed with solution of bromoorotic + formate was identical with that observed with solution of orotic + formate.⁴ The interpretation of this result is clear. The radical formed by the reaction of e_{aq}^- with bromoorotic acid reacts very rapidly with formate to abstract a hydrogen atom and produce a molecule of orotic acid. This type of reaction was found to take place in the case of bromouracil and thus cause a chain reaction of the debromination of this compound in the presence of formate⁹ or isopropyl alcohol.² A similar reaction in the case of bromoorotic acid is expected. The irradiated solution then becomes a mixture of bromoorotic and orotic acid. The hydrated electrons can then react with both compounds ($k \approx 10^{10} M^{-1} sec^{-1}$),² but the product of orotic acid reacts more slowly with formate⁴ and accumulates at a steady-state concentration sufficient to give an observable esr spectrum.

(8) J. K. Dohrmann, R. Livingston, and H. Zeldes, *J. Amer. Chem. Soc.*, **93**, 3343 (1971).

(9) J. D. Zimbrick, J. F. Ward, and L. S. Myers, *Int. J. Radiat. Biol.*, **16**, 505 (1969).

Nitrogen-14 Nuclear Magnetic Resonance Study of 1,5-Disubstituted Tetrazoles

by Edward B. Baker and Alexander I. Popov*¹

Chemistry Department, Michigan State University, East Lansing, Michigan 48823 and
Dow Chemical Company, Midland, Michigan 48640 (Received December 20, 1971)

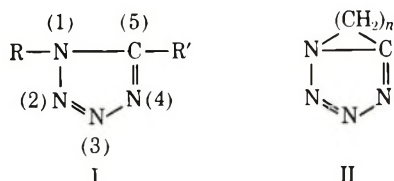
Publication costs assisted by the National Institutes of Health

Nitrogen-14 nmr spectra were obtained for a number of 1,5-disubstituted tetrazoles as well as for some substituted triazoles. The spectrum of the trimethylenetetrazole was resolved into four bands corresponding to the four nitrogen atoms in the ring. The assignments of the resonances are discussed. The spectra of other cyclopolymethylenetetrazoles and 1,5-dimethyltetrazole are compared.

Introduction

Most of 1,5-disubstituted tetrazoles have been noted for their strong stimulating action on the central nervous system.^{2,3} Since it is entirely possible that the neurological activity is related to the physicochemical properties of these compounds, a thorough investigation of the chemistry of physiologically active tetrazole derivatives has been initiated in this laboratory some time ago.

It has been previously shown that 1,5-disubstituted tetrazoles (I) as well as cyclic polymethylenetetra-



zoles (II) can act as unidentate ligands towards transition metal ions and Lewis acids such as the halogens.² Crystal structure of pentamethylenetetrazole-iodine monochloride complexes,⁴ as well as of dichlorobis(1-methyltetrazole)zinc(II)⁵ and of bis[nitratobis(pentamethylenetetrazole)silver(I)]⁶ complexes showed that the bonding occurs through the nitrogen atom in the 4 position, although in the latter case one of the tetrazoles in the unit cell acts as a bridging ligand through 3- and 4-nitrogen atoms. The coordination site, of course, can be quite different when the complexation reaction takes place in solutions. Investigation of 1,5-dimethyltetrazole-silver complex using proton nmr gave rather inconclusive results.⁷ It seemed reasonable to assume that ¹⁴N nmr spectra of the tetrazole ring will be more sensitive to the change in the environment of the nitrogen atoms upon complexation. This paper reports some of the preliminary results obtained with this technique.

Experimental Section

The nmr spectrometer used⁸ has a superconducting solenoid (61 kG) and is frequency swept with a software program in a HP 2115 computer. The computer

is interfaced (HP 2759 A) to HP 5105 A and HP 5102 A synthesizers. A sweep width of 16 kHz and sweep time of 20 sec were used for all spectra with about 300 sweeps averaged. Time-sharing modulation⁹ at 18 kHz gave absorption mode signals directly. Spinning 8-mm sample tubes were used. The NO₃⁻ line of acidified NH₄NO₃ was used as external reference by sample interchange.

Reagents. Pentamethylenetetrazole was obtained from Knoll Pharmaceutical Co. and was purified by recrystallization from ether. Cyclopolymethylenetetrazoles and 1,5-dimethyltetrazole, as well as other heterocyclic amines, were prepared and purified by previously described techniques.^{7,10,11}

Results and Discussion

The ¹⁴N spectrum of 1.5 M trimethylenetetrazole (Figure 1) exhibits four partially resolved peaks of line width ranging from 320 Hz to perhaps 900 Hz. Assignments of these peaks to the four nitrogens in the molecule were made by comparison to the spectra of some triazoles and diazoles (Figure 1). All of these compounds were examined as saturated water solutions, except for pyrazole, which had higher solubility in acetone.

It is evident that there is rapid proton exchange be-

(1) To whom correspondence should be addressed at Michigan State University.

(2) A. I. Popov, *Coord. Chem. Rev.*, **4**, 463 (1969).

(3) W. E. Stone, *Pharmacology*, **3**, 367 (1970).

(4) N. C. Baenziger, A. D. Nelson, A. Tulinsky, J. H. Bloor, and A. I. Popov, *J. Amer. Chem. Soc.*, **89**, 6462 (1967).

(5) N. C. Baenziger and R. J. Schultz, *Inorg. Chem.*, **10**, 661 (1971).

(6) R. L. Bodner and A. I. Popov, *ibid.*, **11**, 1410 (1972).

(7) D. M. Bowers, R. H. Erlich, S. Policec, and A. I. Popov, *J. Inorg. Nucl. Chem.*, **33**, 81 (1971).

(8) E. B. Baker, Abstracts of 1970 Experimental Nuclear Magnetic Resonance Conference (ENC); L. M. Huber, Abstracts of 1971 ENC.

(9) E. B. Baker, L. W. Burd, and G. N. Root, *Rev. Sci. Instrum.*, **10**, 1495 (1965).

(10) F. M. D'Itri and A. I. Popov, *J. Amer. Chem. Soc.*, **90**, 6476 (1968).

(11) D. M. Bowers, Ph.D. Thesis, Michigan State University, 1971.

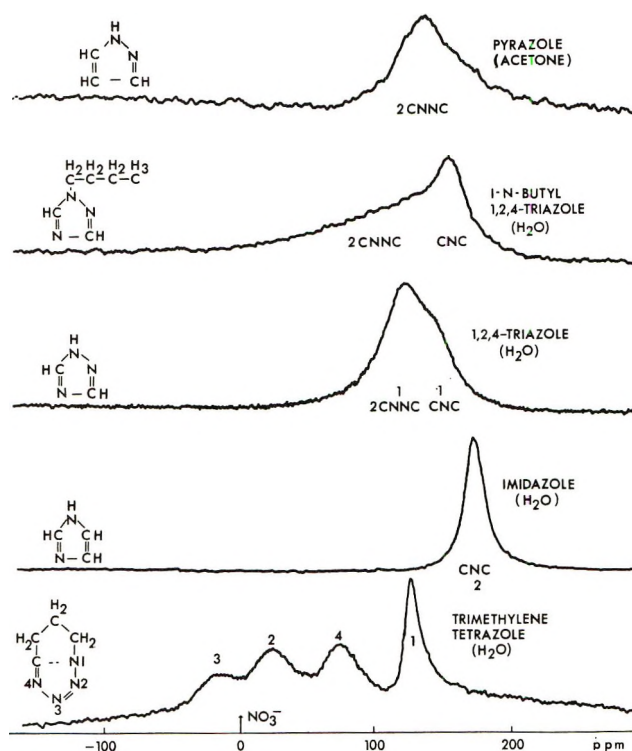


Figure 1. Comparison of ^{14}N spectra of trimethylenetetrazole with those of triazoles and of pyrazole.

tween the two nitrogens in imidazole, resulting in a single line at +171.9 ppm relative to NO_3^- in the reference. Each of these nitrogens is attached to two carbons, and this chemical shift is the highest upfield of any in the spectra shown.

On this basis the high field lines in 1,2,4-triazole and 1-*n*-butyl-1,2,4-triazole are assigned to the nitrogen attached to two carbons.

The pair of adjacent nitrogens ($-\text{CNNC}-$) in 1,2,4-triazole, 1-*n*-butyl-1,2,4-triazole, and pyrazole are downfield from $-\text{CNC}-$. The trimethylenetetrazole highest field peak is, therefore, assigned to the nitrogen in the 1 position ($-\text{CNC}-$), but since this nitrogen is also bonded to another nitrogen, it is downfield from $-\text{CNC}-$ in the diazoles and triazoles. The second line downfield in trimethylenetetrazole is assigned to the 4 position, since this nitrogen is attached to one carbon and another nitrogen. The remaining two nitrogens, at the 2 and 3 positions are tentatively assigned as shown in Figure 1.

A comparison of 1.5 *M* trimethylene-, pentamethylene-, and hexamethylenetetrazoles and saturated 1,5-dimethyltetrazole in aqueous solutions are shown in Figure 2. Only the trimethylenetetrazole has four peaks. In the others, the peak assigned to the 3 position has presumably moved upfield and merged with that assigned to the 2 position, although the intensities are not correct, except for the saturated solution of 1,5-dimethyltetrazole. The above results may

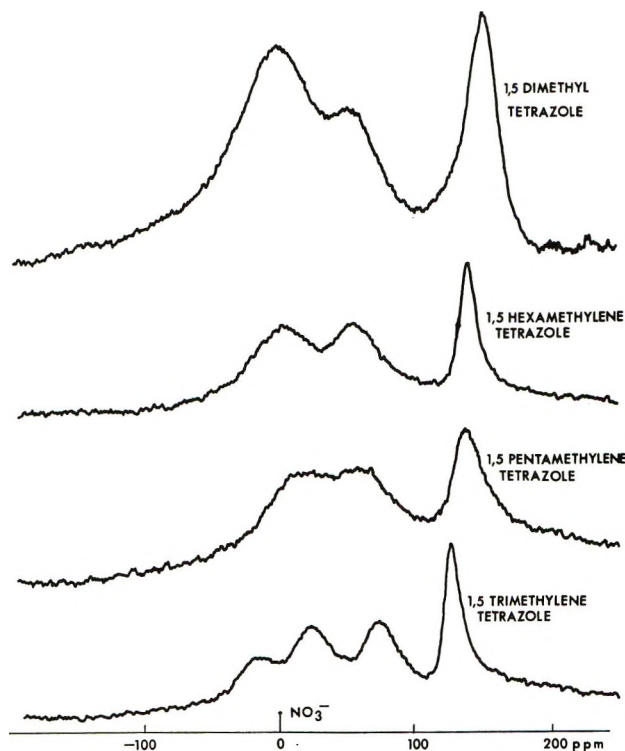


Figure 2. Comparison of ^{14}N spectra of trimethylenetetrazole with those of other cyclopolymethylenetetrazoles.

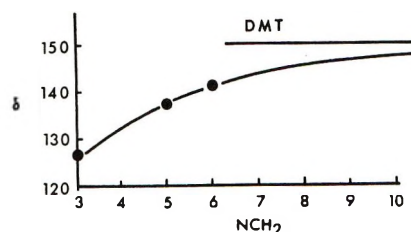


Figure 3. ^{14}N chemical shifts (relative to NO_3^-) of N(1) nucleus in cyclopolymethylenetetrazoles as a function of the number of carbons in the polymethylene chain. The shift of the 1,5-dimethyltetrazole is shown as the horizontal line.

possibly be due to partial saturation of the signals in the more dilute solutions.

The line assigned to the 1 position is not as broad as the other lines and is shifted upfield in going from trimethylenetetrazole to longer methylene chains. These shifts are plotted in Figure 3, which depicts the shift of 1,5-dimethyltetrazole as a limiting case involving no strain at the 1-nitrogen due to the methylene chains. There are no double bonds on the 1-nitrogen; it may have some sp^3 character and thus a smaller quadrupole coupling constant than the sp^2 nitrogens with the double bonds.

Acknowledgment. The authors gratefully acknowledge partial support of this work by a research grant (NS 69061) from the National Institutes of Health.

Intermolecular Charge-Transfer Studies. Thioamide-Iodine System

by R. Abu-Eittah* and A. El-Kourashy

Chemistry Department, Faculty of Science, Cairo University, Giza, Egypt, U. A. R. (Received October 12, 1971)

Publication costs borne completely by The Journal of Physical Chemistry

The intermolecular charge-transfer spectra of 1,3-diphenylthiourea and ethylenethiourea (as donors) and iodine (as an acceptor) were studied in the visible-ultraviolet region. The numerical values of the equilibrium constants of thioamide-iodine complexation were computed at different temperatures. Some thermodynamic properties of the complexes were investigated. Ionization potentials of the donors were calculated from the energies of the charge-transfer transitions.

Introduction

Benzene and its derivatives, when mixed with some sorts of Lewis acids, form a large group of relatively unstable molecular complexes. These complexes may either be π or n complexes.¹⁻³ The most extensively studied group of these complexes is probably the benzene (and alkylbenzene)-iodine complexes.⁴⁻⁸

The donor properties of sulfur-containing organic compounds are not yet extensively studied. Drago, *et al.*,⁹ investigated the donor properties of some sulfides, sulfones, and sulfites. The effect of ring size on the donor properties of cyclic ethers and sulfides has been investigated.¹⁰ The charge-transfer complexes of some five-membered heteroaromatics with iodine, chloranil, tetracyanoethylene, and maleic anhydride have been studied.¹¹⁻¹⁴

Drago, *et al.*,¹⁵ studied the charge-transfer interaction of tetramethylthiourea with iodine. Complexes of some derivatives of thiourea with transition metals have been investigated.¹⁶ The donor-acceptor interactions of alkylthioureas, thiocarbanilides, and thioacetamides with halogens have been reported.^{17a-c}

In this work an attempt is made to study the complexes of some thioamides with halogens in view of the limited information available on these systems in the literature. The donating properties of sulfur are expected to be pronounced since its ionization potential is relatively small. The charge-transfer interaction of 1,3-diphenylthiourea and ethylenethiourea with iodine was studied by electronic spectroscopy. Equilibrium constants, standard enthalpies, and entropies of formation are computed. Finally an estimate of the ionization potentials of the donors was obtained from the charge-transfer studies. The donor site in the studied molecules was identified.

Experimental Section

A. Solvents. Chloroform and carbon tetrachloride are analar grade reagents and were used without further purification.

B. Compounds. 1,3-Diphenylthiourea was prepared by the conventional methods found in literature.¹⁸

Ethylenethiourea was provided by Aldrich Chemical Co. Samples were purified by repetitive crystallization.

C. Apparatus. Measurement of absorption spectra were carried out on a Beckman DK-1 spectrophotometer using 1.0-cm fused silica cells. Solutions were thermostated in a Metrimbex Neo-thermostat.

Results and Discussion

A. 1,3-Diphenylthiourea-Iodine System. 1. Equilibrium Studies. When 1,3-diphenylthiourea (DPT) (A) solution is mixed with that of iodine (B), using carbon tetrachloride as a solvent, the following equilibrium exists assuming that only one molecular complex (1:1) is formed



- (1) I. Omura, H. Baba, K. Higasi, and Y. Kanaoka, *Bull. Chem. Soc. Jap.*, **30**, b33 (1957).
- (2) K. Higasi, I. Omura, and H. Baba, *J. Chem. Phys.*, **24**, 263 (1956).
- (3) M. A. El-Sayed, M. Kasha, and Y. Tanaka, *ibid.*, **34**, 334 (1961).
- (4) R. S. Mulliken, *J. Amer. Chem. Soc.*, **74**, 811 (1952).
- (5) H. A. Benesi and J. H. Hildebrand, *ibid.*, **71**, 2703 (1949).
- (6) L. J. Andrews, *Chem. Rev.*, **51**, 713 (1954).
- (7) N. S. Ham, H. R. Platt, and H. McConnell, *J. Chem. Phys.*, **19**, 1301 (1951).
- (8) R. M. Keefer and L. J. Andrews, *J. Amer. Chem. Soc.*, **77**, 2164 (1955).
- (9) R. S. Drago, B. Wayland, and R. L. Carlson, *ibid.*, **86**, 388 (1964).
- (10) M. Tamres and S. Searles, Jr., *J. Phys. Chem.*, **66**, 1099 (1962).
- (11) R. P. Lang, *J. Amer. Chem. Soc.*, **84**, 4438 (1962).
- (12) R. Zahradnik and C. Parkanyi, *Coll. Czech. Chem. Commun.*, **30**, 195 (1965).
- (13) A. R. Cooper, C. W. Crowne, and P. G. Farrell, *Trans. Faraday Soc.*, **62**, 18 (1966).
- (14) Z. Yoshida and T. Kobayashi, *Tetrahedron*, **26**, 267 (1970).
- (15) R. J. Niedzieiski, R. S. Drago, and R. L. Middaugh, *J. Amer. Chem. Soc.*, **86**, 1694 (1964).
- (16) T. J. Lane, A. Yamaguchi, J. V. Quagliano, J. A. Ryan, and S. Mizushima, *ibid.*, **81**, 3824 (1959).
- (17) (a) K. R. Bhaskar, R. K. Gosavi, and C. N. R. Rao, *Trans. Faraday Soc.*, **62**, 29 (1966); (b) A. F. Grand and M. Tamres, *J. Phys. Chem.*, **74**, 208 (1970); (c) A. F. Grand and M. Tamres, *Inorg. Chem.*, **8**, 2495 (1969).
- (18) "Practical Organic Chemistry," A. I. Vogel, 3rd ed, Longmans and Green, London, 1967.

$$K_{AB} = \frac{C_{AB}}{C_A C_B} = \frac{C_{AB}}{(C_A^\circ - C_{AB})(C_B^\circ - C_{AB})} \quad (1)$$

where C_{AB} is the concentration of the complex $DPT \cdot I_2$, C_A° is the original concentration of DPT, and C_A is the concentration of noncomplexed DPT; similar designations are applied to iodine (component B). For small concentrations of A and B

$$\frac{C_A^\circ C_B^\circ}{C_{AB}} = \frac{1}{K_{AB}} + (C_A^\circ + C_B^\circ) - K_{AB} C_A^\circ C_B^\circ \quad (2)$$

If the absorbance D , at a specific wavelength (410 nm in case of $DPT \cdot I_2$ complex), is only due to the charge-transfer complex AB, then

$$D = \epsilon_{AB} C_{AB} \quad (3)$$

Substituting by (3) in (2), one gets

$$\frac{C_A^\circ C_B^\circ}{D} = \frac{1}{K_{AB} \epsilon_{AB}} + \frac{C_A^\circ + C_B^\circ}{\epsilon_{AB}} - \frac{K_{AB} C_A^\circ C_B^\circ}{\epsilon_{AB}} \quad (4)$$

If C_A° and C_B° are small and $C_A^\circ \gg C_B^\circ$, eq 4 is reduced to

$$\frac{C_A^\circ C_B^\circ}{D} = \frac{1}{K_{AB} \epsilon_{AB}} + \frac{C_A^\circ}{\epsilon_{AB}} \quad (5)$$

Equation 5 is the Scott's¹⁹ form of Benesi-Hildebrand⁵ relation. If C_A° and C_B° are equal (a usual procedure followed in the charge-transfer study) or are of the same order of magnitude and both are small, then the last term in eq 4 can be neglected. Hence, a plot $C_A^\circ C_B^\circ / D$ against $(C_A^\circ + C_B^\circ)$ will not be completely linear. According to Scott, the best straight line is drawn through the experimental points. From the slope and intercept ϵ_{AB} and K_{AB} are computed.

Figure 1 shows the absorption spectra of solutions, in carbon tetrachloride, of pure iodine ($5.500 \times 10^{-4} M$), pure DPT ($4.665 \times 10^{-4} M$) and mixtures of both. Concentration of iodine is constant in all mixtures but that of DPT varied between 4.665×10^{-4} and $1.166 \times 10^{-4} M$. Iodine solution in carbon tetrachloride has an absorption maximum at 512 nm and a very low absorbance in the 440–350-nm region. Absorption of DPT is also negligibly small in this spectral region. For mixed solutions of iodine–DPT, there is a definite and discrete absorption band with λ_{max} at 410 nm. The pink color of iodine solution changes to pale orange on addition of the colorless solution of DPT.

Figure 1 indicates clearly the following experimental results: (i) a blue shift of the iodine 512-nm maximum which increases with the increase of the DPT concentration; (ii) a decrease in the absorbance of the 512 nm of iodine, which also increases with the increase of the DPT concentration; (iii) a new absorption band appears at ~ 410 nm; intensity of this band increases with the concentration of DPT; (iv) the presence of an isosbestic point at 482 nm is quite clear. These

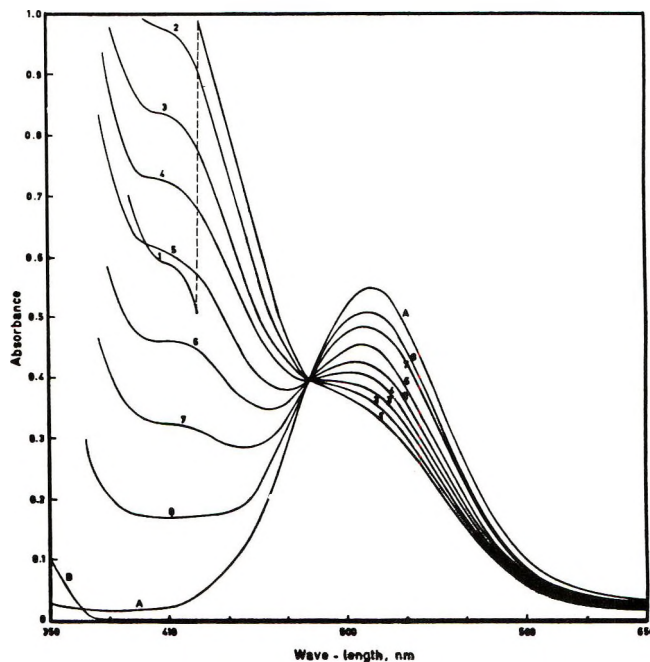
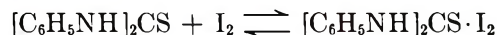


Figure 1. Absorption spectra of pure iodine (A) ($5.500 \times 10^{-4} M$), pure diphenylthiourea (B) ($4.665 \times 10^{-4} M$) and their mixed solutions at 29° . The concentrations of DPT are (1) $4.665 \times 10^{-4} M$, (2) $4.082 \times 10^{-4} M$, (3) $3.499 \times 10^{-4} M$, (4) $2.915 \times 10^{-4} M$, (5) $2.332 \times 10^{-4} M$, (6) $1.749 \times 10^{-4} M$, (7) $1.166 \times 10^{-4} M$.

results clearly indicate the formation of a charge-transfer complex on mixing iodine and DPT solution, which has an absorption band of its own with λ_{max} at ~ 410 nm.

The blue shift of the iodine visible band, on mixing with an electron donor, has been interpreted by Mulliken²⁰ to be due to repulsive interaction between the two components of the charge-transfer complex. In our case, the charge-transfer attraction originates from interaction between the σ_u MO of iodine and, most probably, the nonbonding orbital of sulfur atom of DPT. As a result, the σ_u MO of iodine will be raised while the energy of the nonbonding orbital of the donor will be lowered. This leads to the observed blue shift of the iodine visible band.

To begin with, we tried to apply the Benesi-Hildebrand relation to evaluate the equilibrium constant for



However, such a procedure was not applicable. When the concentration of the donor was increased much more than that of iodine, the pink color of iodine turned to pale yellow. This indicates a very strong interaction between the two partners of the charge-transfer complex. This led us to use small concentrations of the donor and, as shown, this procedure was successful.

(19) R. L. Scott, *Recl. Trav. Chim. Pays-Bas*, **75**, 787 (1956).

(20) R. S. Mulliken, *ibid.*, **75**, 845 (1956).

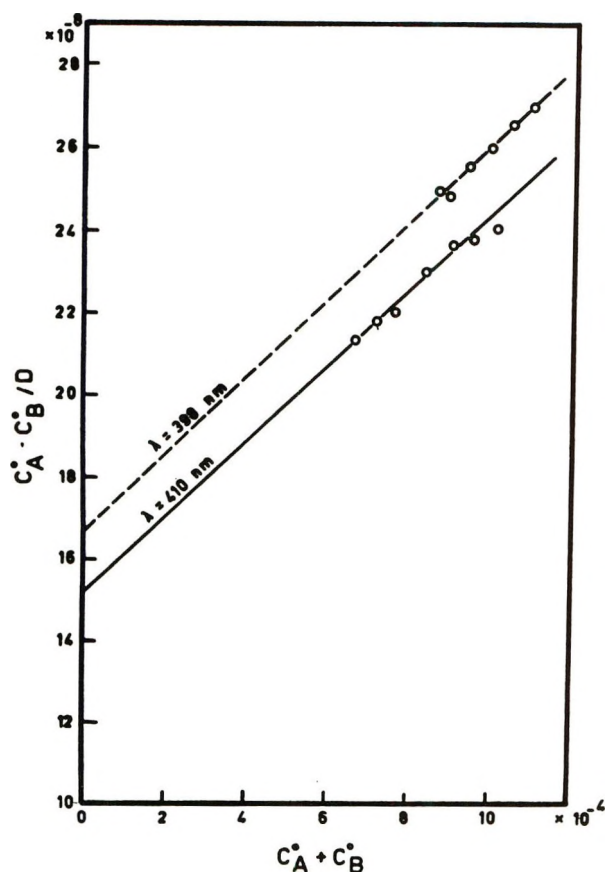


Figure 2. Relation between $C_A^0 C_B^0 / D$ and $C_A^0 + C_B^0$ at 29°: —, diphenylthiourea-iodine system; ---, ethylenethiourea-iodine system.

Equation 4 was used to evaluate the equilibrium constant and the molar extinction coefficient of the charge-transfer complex. Plots of $C_A^0 C_B^0 / D$ against $C_A^0 + C_B^0$ were drawn at different wavelengths in the charge-transfer absorption region, one of which is shown in Figure 2. An average value of 622 is computed for the stability constant of "DPT·I₂" charge-transfer complex at 29° (Table I).

Table I: Equilibrium Constants and Molar Extinction Coefficients of DPT-Iodine Charge-Transfer Complex

Temp. °C	Wave-length, nm	K_{AB}	ϵ
25	416	888	9,700
	410	898	10,262
	404	875	10,140
	Av	885	
29	416	622	10,501
	410	620	10,807
	404	624	10,770
	Av	622	
32	416	494	11,111
	410	484	11,904
	404	467	11,764
	Av	481	

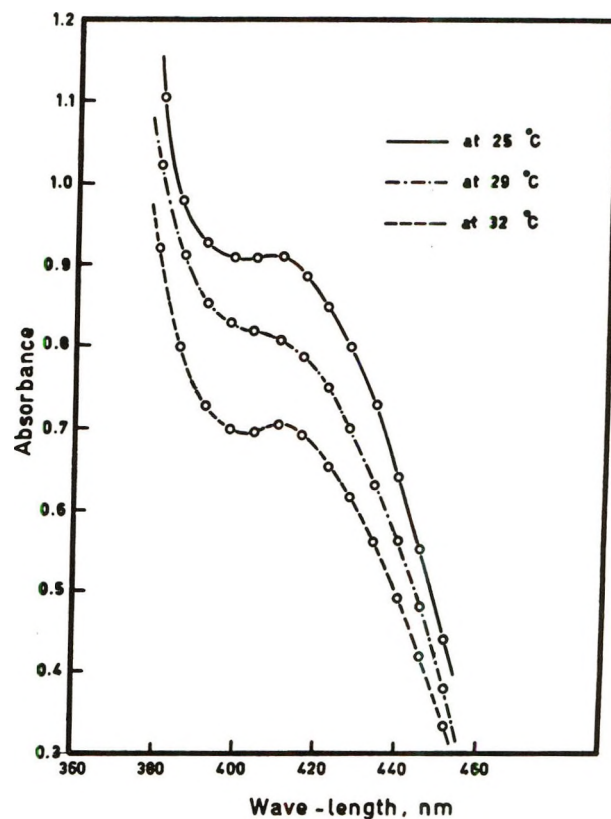


Figure 3. Variation of absorbance of the diphenylthiourea-iodine charge-transfer complex with temperature ($[I_2] = 5.500 \times 10^{-4} M$, $[DPT] = 3.499 \times 10^{-4} M$).

Auterly, *et al.*,²¹ and Buckles, *et al.*,²² have indicated that the I₃⁻ ion has an absorption maximum at 365 and 295 nm. The slight variation of K_{AB} with wave-length is attributed to the presence of a small concentration of I₃⁻.

2. *Thermodynamic Properties.* To get an estimate of the enthalpy and entropy of formation of the DPT·I₂ charge-transfer complex, the equilibrium constants were determined at different temperatures. Absorption spectra of mixtures of "iodine-DPT" solutions were studied at 25 and 32° (in addition to those at 29°). Features of the spectra were very much similar to those presented in Figure 1. Equilibrium constants were also calculated and results are presented in Table I. In Figure 3 the spectra (in charge-transfer region) of one of the studied DPT-iodine solutions, at different temperatures, are presented.

The relation between $R \ln K_{AB}$ vs. $1/T$ is plotted, and a straight line was drawn to fit the points as well as possible (Figure 4). The heats of formation (ΔH°) and the entropy of formation of the complex (ΔS°) are obtained from the slope and intercept with abscissa, respectively, and are presented in Table II.

(21) A. D. Auterly and R. E. Gonnick, *J. Amer. Chem. Soc.*, **73**, 1842 (1951).

(22) R. E. Buckles, J. P. Yuk, and I. Popov, *ibid.*, **74**, 4379 (1952).

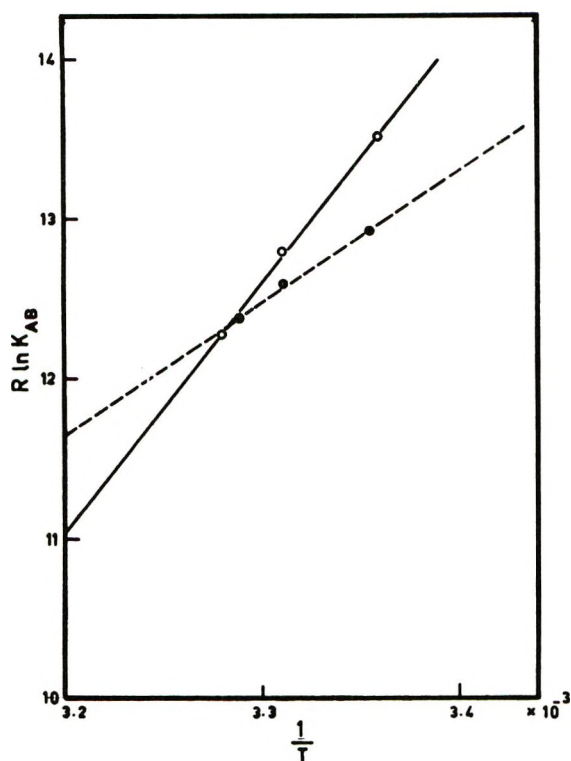


Figure 4. The relation between $R \ln K_{AB}$ and $1/T$: —, diphenylthiourea-iodine system; ---, ethylenethiourea-iodine system.

Table II: Comparison of the Physical Constants of Some Thio Compounds-Iodine Charge-Transfer Complexes

Donor	K_{AB} at 29°	$-\Delta H^\circ$	$-\Delta S^\circ$
Diphenylthiourea	622	15.2 ± 0.4	37.5 ± 0.9
Ethylenethiourea	558	8.1 ± 0.3	14.4 ± 0.5
Di- <i>tert</i> -butylthiourea ^a		18.6	39.8
Tetramethylthiourea ^a		9.5	12.3

^a Reference 17.

The values obtained for K_{AB} are too large for a π charge-transfer complex. The equilibrium constants of some π complexes of benzene, toluene, and hexamethylbenzene vary between 0.13 and 1.35.^{23,24} Hence we conclude that the obtained charge-transfer complex is an "n" one. The donor site in DPT is expected to be the sulfur atom. This has been confirmed by ir studies on thiourea-iodine system.¹⁷

3. *Position of the Charge-Transfer Absorption Band of DPT-Iodine System and Ionization Potential of the Donor.* Figure 5 shows the charge-transfer absorption band of DPT-iodine complex at 29°. The Breigleb²⁵ equation is, usually, used to get an estimate of the ionization potential of the donor, when the acceptor is iodine, as

$$E_{CT} = I_D - 5.2 + 1.5/(I_D - 5.2)$$

Energy of the charge-transfer transition for DPT-iodine complex is 3.02 eV. Using this value one gets 7.59 eV as the ionization potential for DPT. The first ionization potential of tetramethylthiourea has been found to be 8.12 eV by electron impact method.¹⁷ This value is quite comparable with the value obtained for DPT by charge-transfer studies.

B. *Ethylenethiourea-Iodine System.* To get a fairly complete idea about the nature of the charge-transfer complex between "thioamides" as donors and "iodine" as the acceptor, we chose ethylenethiourea (ETU) as the second donor in this study. The absorption spectra of free iodine ($7.930 \times 10^{-4} M$), free ETU ($3.102 \times 10^{-4} M$), and mixtures of both were investigated. All spectra were scanned using chloroform as the solvent and blank since the solubility of ETU in carbon tetrachloride is very low. Features of the spectra are very much similar to those of the DPT-iodine solutions. That is, one isosbestic point, a characteristic charge-transfer band whose intensity is proportional

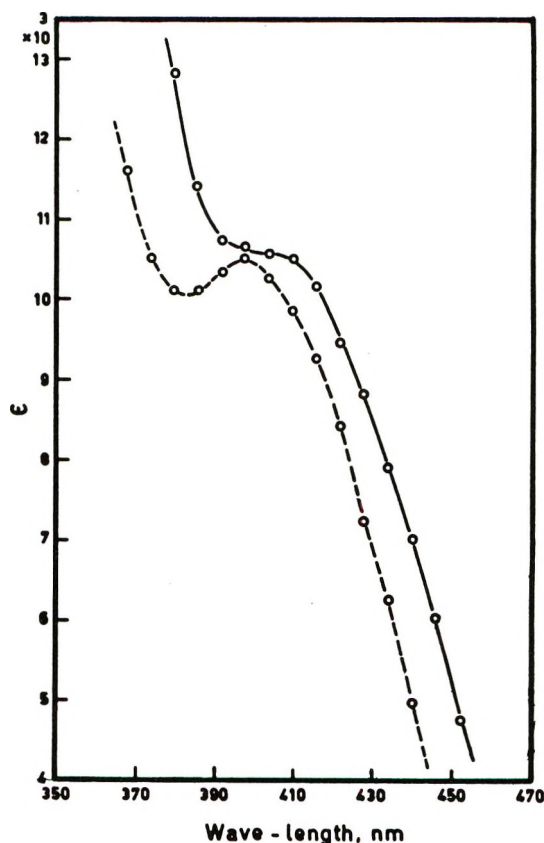


Figure 5. Charge-transfer absorption bands: —, diphenylthiourea-iodine system; ---, ethylenethiourea-iodine system.

(23) L. J. Andrews and R. M. Keefer, *J. Amer. Chem. Soc.*, **74**, 4500 (1952).

(24) N. W. Blake, H. Winston, and J. A. Patterson, *ibid.*, **73**, 4437 (1951).

(25) G. Breigleb, "Electrom Donator-Acceptor Komplexe," Springer-Verlag, West Berlin, 1961.

to the donor concentrations and the blue shift of iodine visible maximum on mixing with the donor were the experimental results for the ETU-iodine system.

Proceeding as before, values of K_{AB} , ΔH° , and ΔS° were computed. The average K_{AB} is found to be 558 at 29° (less than that of DPT-iodine complex). Table II compares the values of ΔH° and ΔS° for complexation of some thioamides and iodine. Enthalpy as well as entropy of formation of ETU-iodine complex

are much less than those of DPT-iodine complex. This goes along with the low enthalpy and entropy of formation of tetramethylthiourea-iodine complex as compared with those of di-*tert*-butylthiourea-iodine complex.¹⁷ In fact we expect ETU to be a weaker donor than tetramethylthiourea. The Breigleb equation was used to get an estimate of the ionization potential of ETU. A value of 7.71 eV was obtained for its first ionization potential.

An Ultrasonic Shear Wave Study of the Mechanical Properties of a Nematic Liquid Crystal

by Y. S. Lee, Sherman L. Golub, and Glenn H. Brown*

*Liquid Crystal Institute, Department of Chemistry, and Department of Physics,
Kent State University, Kent, Ohio 44242 (Received November 15, 1971)*

Publication costs assisted by the Air Force Office of Scientific Research

The dynamic shear properties of *p*-methoxybenzylidene-*p*-*n*-butylaniline (MBBA) in its nematic and isotropic states are studied in the temperature range 25 to 65° using a shear reflectance technique. Shear wave frequencies from 2.75 to 10 MHz are used, and three orientations of the preferred direction of the molecular axis with respect to the direction of polarization of the shear wave are considered. The anisotropy ratio for the dynamic viscosity is about 2; the ratio for the shear modulus is highly frequency dependent, being as large as 3.5. Approximations are made which allow the Leslie-Ericksen coefficients to be calculated.

Introduction

Liquid crystals differ from isotropic liquids and crystalline solids in that they have special structural characteristics. The intermolecular relationship in liquid crystals is not yet completely known. To understand the structural characteristics of the liquid crystal on a molecular scale, the application of wave techniques with ultrasonic vibrations seems to be most appropriate.

It is the purpose of this work to use the ultrasonic shear wave technique to study the mechanical properties of a nematogenic compound *p*-methoxybenzylidene-*p*-*n*-butylaniline (MBBA) in both its nematic and isotropic states. The compound as used had a nematic-isotropic transition temperature of $44.0 \pm 0.5^\circ$. We report the calculated values of the anisotropic dynamic viscosity and shear storage modulus of the compound.

There have been several previous studies of the viscosity of nematic liquid crystals.¹⁻³ These involved macroscopic flow techniques. Because flow has an orienting effect on the molecules of an anisotropic fluid, these techniques yield viscosity for definite molecular

orientations only with extreme difficulty. The classic measurements of Miesowicz on *p*-azoxyanisole were, of course, for three definite orientations. Ultrasonic shear techniques overcome this difficulty. The first application of this latter technique to nematic liquid crystals has been recently reported by Candau and Martinoty.⁴

Theoretical Background

Earlier attempts at the application of the ultrasonic technique to liquid crystal studies involved mostly the use of longitudinal waves. Some of the interesting observations^{5,6} are the anomalous variation in the velocity and absorption of ultrasound in *p*-azoxyanisole

(1) M. Miesowicz, *Nature (London)*, **136**, 261 (1935); **158**, 27 (1946).

(2) R. S. Porter, J. F. Johnson, and E. M. Barrall, *J. Chem. Phys.*, **45**, 1452 (1966).

(3) J. Fisher and A. G. Frederickson, *Mol. Cryst., Liquid Cryst.*, **8**, 267 (1969).

(4) P. Martinoty and S. Candau, *ibid.*, **14**, 243 (1971).

(5) W. H. Hoyer and A. W. Nolle, *J. Chem. Phys.*, **24**, 803 (1956).

(6) I. Gabrielli and L. Verdini, *Nuovo Cimento*, **2**, 426 (1955).

and cholesteryl benzoate at and on both sides of their mesomorphic-isotropic transition points.

The viscous flow of a fluid is a shearing process. The propagation of a compressional wave involves a combination of shear and compressional moduli. Therefore, to obtain mechanical properties of the nematic liquid crystal, such as the anisotropic dynamic viscosity and the anisotropic stiffness, it is necessary to study the liquid crystal system with shear waves. Due to the fact that ordinary liquids have no static shear modulus, one would expect a shear wave to be rapidly damped as it enters a liquid. Therefore, instead of measuring the attenuation and velocity directly from the transmitted wave, as is done for the longitudinal wave, the reflected shear ultrasound wave is studied.^{7,8}

Shear Mechanical Parameters. When a liquid crystal is disturbed with a mechanical wave of ultrasonic frequency, it will respond viscoelastically. The mechanical properties of a viscoelastic system are described in terms of complex quantities known as the mechanical impedance, Z_m , and its real and imaginary components called, respectively, the mechanical resistance, R_m , and the mechanical reactance, X_m .⁹ If the quartz delay line or impedometer of the type used by Mason, *et al.*,⁷ is used, in which the polarization of the shear wave is parallel breadthwise to the reflecting upper surface of the bar, the complex mechanical impedance of a viscoelastic system can be determined by the following relation^{7,8}

$$Z_m = R_m + iX_m = Z_q \cos \phi \left(\frac{1 - r^2 + i2r \sin \theta}{1 + r^2 + 2r \cos \theta} \right) \quad (1)$$

where Z_q is the shear mechanical impedance of fused quartz and is a constant ($8.3 \times 10^5 \Omega_m/\text{cm}^2$), ϕ is the angle of incidence of the ultrasonic wave to the normal of the reflecting quartz bar surface (77° for the delay line used in this work), r and θ are, respectively, the absolute reflection coefficient and the phase shift (or delay) of the ultrasonic wave reflected at the liquid-fused quartz boundary.

The complex modulus $G^* = G' + i\omega\eta'$ can then be determined and, in particular, the dynamic viscosity, η' , and the shear storage modulus or stiffness, G' , of a liquid can be calculated, respectively, from the relations

$$\eta' = \frac{2R_m X_m}{\rho\omega} \quad (2)$$

and

$$G' = \frac{R_m^2 - X_m^2}{\rho} \quad (3)$$

From eq 2 and 3, it is seen that determinations of the dynamic viscosity and shear storage modulus of a liquid depends on the success of the measurements of both

the absolute reflection coefficient, r , and the phase shift, θ .

Liquid crystals are anisotropic liquids and, therefore, are anisotropic in viscosity¹ and diffusion.^{10,11} Their mechanical properties should depend distinctively on the orientation of the molecules with respect to the direction of disturbance. In this work, three different orientations of the molecules with respect to the direction of polarization of the ultrasonic shear wave are considered. These three orientations are (a) molecular orientation A—long axes of the molecules lie parallel to both the reflecting bar surface and the direction of polarization, (b) molecular orientation B—long axes of the molecules lie perpendicular to both the reflecting bar surface and the direction of polarization, and (c) molecular orientation C—long axes of the molecules lie parallel to the reflecting bar surface but perpendicular to the direction of polarization of the shear wave. Consequently, in applying eq 2 and 3 to the differently oriented nematic liquid crystals on the reflecting surface of the impedometer, three values for the anisotropic viscosity and three values for the anisotropic shear storage modulus can be obtained under a definite condition.

Absolute Reflection Coefficient. For nematic liquid crystals, as for ordinary low viscosity liquids, the absolute reflection coefficient is quite close to unity. Technically, it was found more reliable to determine the absolute reflection coefficient for low viscosity liquids by considering the amplitudes of a single echo with and without the liquid on the reflecting bar surface. It can be shown that the absolute reflection coefficient, r , can be extracted from any echo in the reflected echo train using the equation

$$r = \left(\frac{h_n'}{h_n} \right)^{1/(2n-1)} \quad (4)$$

where h_n' and h_n are, respectively, the amplitudes of the reflected echo with and without the liquid, and n is the number of the echo in the exponential echo train of the reflected ultrasonic wave observed on the oscilloscope.

Phase Shift. The small shift in phase of the ultrasonic wave upon reflection at the liquid crystal-quartz delay line interface is difficult to measure, partly because the phase shift is very small and partly because the time delay in the fused quartz impedometer is very sensitive to small temperature fluctuation. Previous workers^{4,12} have made the approximation that the

(7) W. P. Mason, W. O. Baker, H. J. McSkimin, and J. H. Heiss, *Phys. Rev.*, **75**, 976 (1949).

(8) H. T. O'Neil, *ibid.*, **75**, 928 (1949).

(9) J. Blizt, "Fundamentals of Ultrasonics," 2nd ed, Plenum Publishing Co., New York, N. Y., 1967, p 8.

(10) T. Svedberg, *Kolloid-Z.*, **22**, 68 (1918).

(11) C. K. Yun and A. G. Fredrickson, *Mol. Cryst., Liquid Cryst.*, **12**, 73 (1970).

(12) S. V. Letcher and A. J. Barlow, *Phys. Rev. Lett.*, **26**, 172 (1970).

real and the imaginary parts of the complex mechanical impedance of liquids are equal. This allows the dynamic shear viscosity of a liquid to be estimated from a measurement of only the absolute reflection coefficient, but implies a vanishingly small shear storage modulus. The viscoelastic behavior of a liquid in the ultrasonic field is frequency dependent. At high frequency, the shear storage modulus of the liquid is quite sizable and the approximation that R_m and X_m are equal might result in too large an estimated value of the dynamic viscosity of the liquid. We have found that the interpretation of our data using this assumption leads to a qualitative error in the frequency dependence of the viscosity.

It is essential to develop a method to determine accurately the small phase shift of liquid crystals with the quartz delay line used in this work. The method used in this work is as follows.

A signal from the signal generator is fed to two divided paths. In the first path, the signal goes directly to a double balanced mixer; this is the continuous (cw) signal. In the second path, the pulse which is produced by the gating unit is delayed, mostly by the quartz delay line, and goes then to the mixer. The mixer functions in such a way that it will give a zero output voltage resulting in a nullity on the oscilloscope when the two signals, respectively, from the first and the second paths are exactly 90° out of phase.

Assume that the pulse arrives at the mixer at a time t after the portion of the cw signal which initiated the pulse. The condition for which the cw and the pulse are 90° out of phase is

$$(m \pm 1/4) \frac{1}{f} = t \quad (5)$$

where m is any integer and f is the frequency of the cw. If t is increased slightly to $t + \delta t$, then, to preserve a nullity, the frequency must be changed to $f - \delta f$. One can show that, for small δf , the phase shift corresponding to δt is given by

$$\frac{\delta f}{f - f'} \times 360^\circ$$

where f' is the frequency at which the next nullity occurs or the frequency corresponding to 360° phase shift, *i.e.*

$$(m \pm 1 \pm 1/4) \frac{1}{f'} = t \quad (6)$$

We assume no dispersion in the velocity of the signal over the small variation of the frequency. The frequency variation can be read from the frequency counter. Therefore, the change in frequency equivalent to 1° shift in the phase can be calculated. With the quartz delay line used in this work, it was found that 102-Hz change in frequency is equivalent to 1°

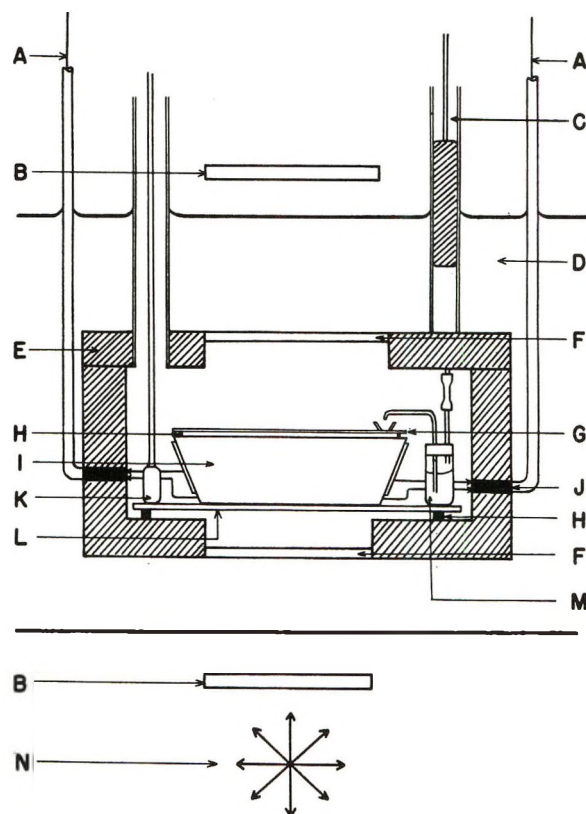


Figure 1. The quartz delay line assembly: A, coaxial cable; B, polarizer; C, syringe; D, water bath; E, aluminum box; F, glass window; G, cover glass; H, spacer; I, quartz delay line; J, connector; K, quartz thermometer; L, glass supporter; M, sample; N, light source.

shift in the phase. This frequency-phase shift relation is then used to interpret the delay of a reflected pulse as the phase shift.

Experimental Details

In determining the absolute reflection coefficient, r , the unloaded quartz delay line was kept in the constant temperature bath for 3 hr to establish equilibrium. The equilibrium temperature was constant to within $\pm 0.002^\circ$ for a period of 0.5 hr which was long enough for making the amplitude and frequency readings. The amplitudes of the second and third echoes in the exponential echo train were read. These values are h_n ($n = 2, 3$). The sample at the same temperature as the quartz delay line (see Figure 1) was then placed on the reflecting surface of the quartz delay line. When the molecules of the sample assumed their final equilibrium orientation, as determined by examination between crossed polarizers, the readings for the amplitudes were again taken. The values are h'_n ($n = 2, 3$). All the measured amplitudes for the h and h' were normalized with respect to a standard input signal amplitude. The precision of reading the echo amplitudes was better than 0.5% even for the lowest amplitude echo observed in this experiment.

Any echo in the exponential echo train on the oscilloscope can be used for the phase shift measurement. This method required a highly constant temperature of the quartz delay line, because the velocity of the ultrasonic shear wave is temperature dependent.

Orientation of the Molecules of MBBA. To obtain the anisotropic properties of the nematic liquid crystal, molecules of MBBA are aligned in three different orientations with respect to the polarization of the shear wave. To align the molecules parallel to the reflecting surface of the quartz bar, the method of Chatelain¹³ was adopted. The reflecting surface of the quartz bar and the cover glass were cleaned with chromic acid. The clean surfaces were rubbed with Kimwipes wipers. The molecules will line up perfectly on these rubbed surfaces with their long axes parallel to the direction of rubbing. To align the molecules perpendicular to the reflecting surface of the quartz bar, both the reflecting quartz bar surface and the cover glass were coated with a thin layer of lecithin. A dilute solution of 0.1% by weight of lecithin in petroleum ether (boiling range 30–60°) was prepared. An artist oilpaint brush was used to apply a thin coat of the solution on the clean surface by one single stroke. The petroleum ether vaporized away rapidly leaving a thin film of lecithin on the surface. The thickness of the lecithin coat so prepared was found to be less than 0.04 μ . The surfaces give perfect vertical orientation for MBBA. It was also found that the thin lecithin coat on the reflecting bar surface has no detectable effect on the amplitudes of the reflected echoes in the quartz delay line.

The orientations of the molecules were examined in polarized light between crossed polarizers (Figure 1).

Results and Discussion

To verify that our apparatus gives results for isotropic liquids in agreement with those of other workers, the dynamic viscosity of diethyl phthalate was determined. Results obtained by this verification experiment agree well with what McSkimin and Andreatch have reported.¹⁴ The viscosity of MBBA for molecular orientation A agrees closely with the capillary viscometry data of Candau and Martinoty.⁴ This is to be expected as the flow of the liquid in the capillary tends to align the molecules in the direction of flow, perpendicular to the shear gradient as in orientation A.

The input voltage to the transducers was varied over two orders of magnitude to verify that the results were insensitive to amplitude.

Absolute Reflection Coefficient. Results of the absolute reflection coefficient measurements for MBBA are summarized in Table I. They cover both the nematic and the isotropic states of the compound. The subscript for each r represents a molecular orientation in the nematic state, while in the isotropic state, the

Table I: Measured Absolute Reflection Coefficients of MBBA at 10 MHz and at Various Temperatures from the Nematic State through the Isotropic State; Sample Thickness = 0.2 mm

Temp. °C	r_A	r_B	r_C	State
25.0	0.9660	0.9642	0.9544	Nematic
30.0	0.9699	0.9682	0.9608	
32.5	0.9719	0.9704	0.9633	
37.5	0.9749	0.9736	0.9679	
40.0	0.9753	0.9739	0.9699	
43.0	0.9747	0.9734	0.9715	
44.0 ^a	0.9696(I)	0.9722(N)	0.9700(I)	Transition
49.0	0.9730	0.9731	0.9726	Isotropic
53.0	0.9753	0.9748	0.9752	
56.2	0.9762	0.9763	0.9762	

^a (I) and (N) indicate, respectively, that the compound was observed to exist in the isotropic and the nematic states.

subscripts represent the preparation of the surfaces of the quartz bar and the cover glass. The standard deviation in the determination of the reflection coefficient, r , is less than ± 0.0007 .

Phase Shift. The measurements of the phase shift of MBBA for various orientations and at different temperatures are summarized in Table II. The subscripts have the same meaning as for the absolute reflection coefficients. The phase shift measurements were made at the same time and under identical conditions as the measurement of the absolute reflection coefficients. The standard deviation in the phase shift measurements is $\pm 0.02^\circ$.

Table II: Measured Phase Shifts of MBBA in Degree per Reflection at 10 MHz and Various Temperatures from the Nematic State through the Isotropic State; Sample Thickness = 0.2 mm

Temp. °C	θ_A	θ_B	θ_C	State
25.0	1.86	1.95	2.32	Nematic
30.0	1.67	1.71	2.07	
32.5	1.56	1.63	1.98	
-37.5	1.46	1.50	1.73	
40.0	1.42	1.44	1.64	
43.0	1.38	1.42	1.48	
44.0	1.42(I)	1.45(N)	1.43(I)	Transition
49.0	1.29	1.29	1.30	Isotropic
53.0	1.18	1.17	1.15	
56.2	1.13	1.13	1.12	

Real and Imaginary Components of Complex Mechanical Impedance. The real and the imaginary components of the complex mechanical impedance are

(13) P. Chatelain, *Acta Crystallogr.*, **1**, 315 (1947).

(14) H. J. McSkimin and P. Andreatch, Jr., *J. Acoust. Soc. Amer.*, **42**, 248 (1967).

Table III: Shear Mechanical Impedances of MBBA in Ω_m/cm^2 at 10 MHz and at Various Temperatures; Sample Thickness = 0.2 mm

Temp, °C	R_{m_A}	R_{m_B}	R_{m_C}	X_{m_A}	X_{m_B}	X_{m_C}	State
25.0	3228	3404	4358	3031	3177	3799	Nematic
30.0	2854	3019	3737	2721	2786	3373	
32.5	2661	2805	3489	2542	2657	3226	
37.5	2395	2499	3049	2379	2445	2819	
40.0	2336	2469	2854	2314	2347	2672	
43.0	2395	2518	2701	2249	2314	2412	Transition
44.0	2884(I)	2632(N)	2844(I)	2314(I)	2363(N)	2362(I)	
49.0	2557	2548	2592	2102	2102	2119	Isotropic
53.0	2307	2380	2346	1923	1907	1874	
56.2	2248	2238	2248	1841	1841	1825	

calculated with the data tabulated in Tables I and II. Table III summarizes the results of these calculations.

Density of MBBA. To calculate the dynamic viscosity and the shear storage modulus of MBBA, the density of MBBA must be known. The density was obtained by comparing the weight of an ampoule submerged in MBBA with the weight of the ampoule submerged in distilled water at the same temperature. The data of Kell were used for the density of water.¹⁵ These results are summarized in Table IV.

Table IV: Density of MBBA at Various Temperatures in the Temperature Range 25.5–54.5°

Temp, °C	ρ , g/cm ³	State
25.5	1.042	Nematic
29.5	1.040	
35.0	1.037	
41.0	1.034	
48.0	1.028	Isotropic
50.5	1.027	
54.5	1.025	

Dynamic Viscosity of MBBA. Figure 2 represents the anisotropic dynamic viscosity of MBBA calculated from the measured data of r and θ according to eq 2. The possible error in the calculated dynamic viscosity, η' , arising from the standard deviations of the measured values of r and θ , is $\pm 3\%$.

From Figure 2, the anisotropy in the dynamic viscosity of MBBA in the nematic state can be clearly seen. Discontinuities of the dynamic viscosity-temperature curves, particularly obvious for the orientations A and B, were observed at the nematic-isotropic point of the compound. It was also observed that the dynamic viscosities of the compound were not much different for the orientations A and B, but η_B' was at all temperatures in the nematic state higher than η_A' at the corresponding temperatures. However, in the

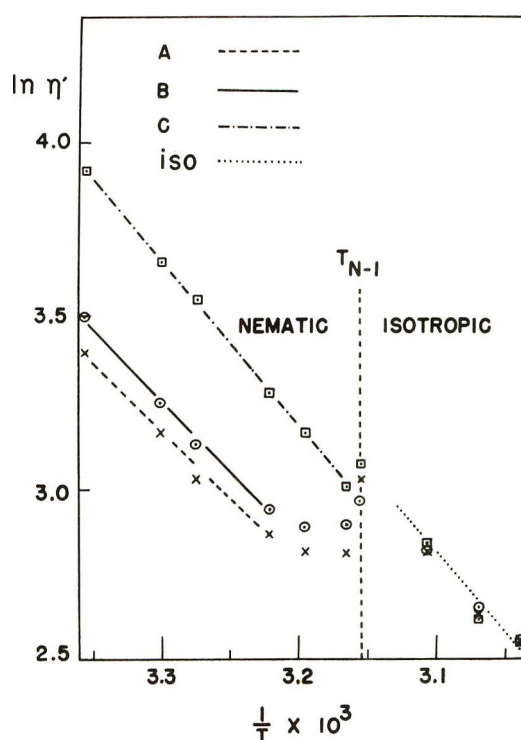


Figure 2. Dynamic viscosity of MBBA at 10 MHz for three orientations. T_{N-I} is the nematic-isotropic transition temperature.

nematic state, the dynamic viscosity for the molecular orientation C was distinctly higher than for the other two molecular orientations at the same temperatures. After the nematic-isotropic point, the dynamic viscosity anisotropy of the compound disappeared, as can be seen by the superposition of the curves for different preparations of the bar surfaces.

It seems appropriate to discuss some of the features of the viscosity anisotropy of MBBA in terms of the dynamic theory of anisotropic liquids by Erickson and Leslie.¹⁶⁻¹⁸ In Figure 3, N is a unit vector representing

(15) G. S. Kell, *J. Chem. Eng. Data*, **12**, 67 (1967).

(16) J. L. Erickson, *Arch. Ration. Mech. Anal.*, **9**, 371 (1962).

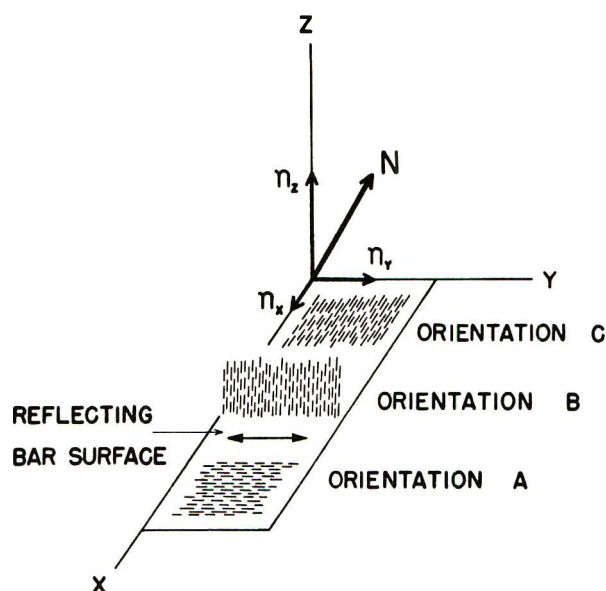


Figure 3. Shear flows in the nematic liquid. The arrow in the plane of the reflecting bar surface represents the direction of displacement. Short lines represent long axes of molecules of MBBA.

the preferred direction of molecules in a nematic liquid crystal. n_x , n_y , and n_z are, respectively, the components of N in the x , y , and z directions. If the shear flow or the direction of shear is parallel to the y axis, a relation between the dynamic viscosity and the vector components of the preferred direction of molecules has been deduced by Papoular¹⁹ from the viscosity function formulated by Ericksen and Leslie in their dynamic theory of anisotropic liquids. The relation is

$$\eta' = \frac{1}{2}[\alpha_4 + (\alpha_5 - \alpha_2)\overline{n_x^2} + (\alpha_6 + \alpha_3)\overline{n_y^2} + 2\alpha_1\overline{n_x^2 n_y^2}] \quad (7)$$

where η' is the dynamic viscosity. α_i ($i = 1, 2, \dots, 6$) are the six coefficients appearing in Ericksen and Leslie's stress-strain rate relation in their dynamic treatment of anisotropic liquid systems. They have, according to Newton's law of viscosity, the dimension of viscosity. The bars on the vector components indicate thermal averaging.

In the isotropic phase, there is no preferred direction of the molecules. Therefore

$$\overline{n_x^2} = \overline{n_y^2} = \overline{n_z^2} = \frac{1}{3} \quad (8)$$

The viscosity in the isotropic phase, η_0' , is then

$$\eta_0' = \frac{1}{2}\alpha_4 + \frac{1}{6}(\alpha_6 + \alpha_3) + \frac{1}{6}(\alpha_6 - \alpha_2) + \frac{1}{9}\alpha_1 \quad (9)$$

With the further use of the relations²⁰

$$\alpha_6 - \alpha_5 = \alpha_2 + \alpha_3 \quad (10)$$

and

$$\alpha_6 - \alpha_5 \approx \alpha_2 - \alpha_3 \quad (11)$$

it is possible to solve for the six coefficients in terms of the measured viscosities. They are found to be

$$\alpha_1 = 9(\eta_0' - \eta_B') - 3(\eta_A' - 2\eta_B' + \eta_C') \quad (12a)$$

$$\alpha_2 \approx \eta_A' - \eta_C' \quad (12b)$$

$$\alpha_3 \approx 0 \quad (12c)$$

$$\alpha_4 = 2\eta_B' \quad (12d)$$

$$\alpha_5 \approx \eta_A' - 2\eta_B' + \eta_C' \quad (12e)$$

$$\alpha_6 \approx 2(\eta_A' - \eta_B') \quad (12f)$$

Equation 12a involves the viscosities of both the nematic and the isotropic states. It would seem then, that since the dynamic viscosity is a function of temperature, α_1 can be evaluated only at T_{N-I} . However, one can replace η_0' by η_C' for a reasonable approximation, since the discontinuity of the viscosity-temperature curve (Figure 2) is small when the sample of molecular orientation C goes from the nematic to the isotropic state. Extrapolation of the isotropic viscosity curve into the nematic region will give a theoretical supercooled isotropic viscosity curve closely following the η_C' curve. With such an approximation, α_1 may be expressed for all temperatures in the nematic state as

$$\alpha_1 = 9(\eta_C' - \eta_B') - 3(\eta_A' - 2\eta_B' + \eta_C') \quad (13)$$

The anisotropic viscosity now enables us to calculate all the Leslie-Ericksen viscosity or friction coefficients, the α 's, in the nematic state of MBBA through the use of eq 12 and 13. These calculated values are collected in Table V.

Table V: The Leslie-Ericksen Viscosity or Friction Coefficients of MBBA in the Nematic State in cP

Temp, °C	α_1	α_2	α_3	α_4	α_5	α_6
25.0	113.1	-20.4	0	66.1	14.1	-6.30
30.0	82.9	-14.8	0	51.5	10.9	-3.94
32.5	76.4	-13.8	0	45.7	9.5	-4.24
37.5	49.6	-8.9	0	37.5	6.4	-2.52
40.0	37.6	-6.8	0	35.7	4.4	-2.40
43.0	16.9	-3.5	0	35.9	0.77	-2.72

The accuracy of the calculated values of α_1 depends on the validity of the approximation that

$$\eta_0' (\text{supercooled}) = \eta_C'$$

in the nematic temperature range of the compound. One way to test the validity of the above approximation is to determine the viscosity in the isotropic state

(17) F. M. Leslie, *Quart. J. Mech. Appl. Math.*, **19**, 357 (1966).

(18) F. M. Leslie, *Arch. Ration. Meth. Anal.*, **28**, 265 (1968).

(19) M. Papoular, *Phys. Lett.*, **30A**, 5 (1969).

of a nematic liquid crystal doped with a small amount of an appropriate impurity. Note that a small amount of an impurity may depress the nematic-isotropic point of a liquid crystal considerably without appreciably changing its mechanical properties. That is, the curve is displaced with very little change in shape. The isotropic curve can in this sense be extrapolated to lower temperatures. Papoular¹⁹ notes that in general η_C' is expected to decrease at T_{N-I} . This is not implied by eq 7 and in fact the relative value of η_0' seems to depend on α_1 . Observation of the sample in polarized light indicated excellent mode C orientation. At this point we should explain that the paucity of data in the immediate vicinity of T_{N-I} is due to the lack of reproducibility of data between samples. This is likely due to the sensitivity of T_{N-I} to small amounts of impurities.

It has been pointed out by Papoular that, in most cases, α_1 is expected to be small. In the present investigation, it was found that α_1 is not necessarily small, but the term containing α_1 in the expression for η_0' (eq 9) might be relatively small.

The value $\alpha_3 \approx 0$ results from eq 10 and 11. It should be noted that the viscosity coefficients of PAA as evaluated by the Orsay Group²¹ from quasielastic Rayleigh scattering data give $|\alpha_3|$ to be of the same order as α_2 .

Shear Storage Modulus of MBBA. From Table III, it is seen that the real and the imaginary components of the complex shear mechanical impedance of MBBA at 10 MHz are not equal. At all temperatures, the real component is larger than the imaginary one, implying that in the ultrasonic field, the system has certain characteristic stiffness. The anisotropic shear storage modulus of MBBA is calculated from eq 3. The temperature dependence of the modulus of MBBA in the nematic and isotropic states is shown in Figure 4.

Besides the anisotropic nature of the shear storage modulus observed, the modulus appeared higher in the isotropic state than in the nematic state near the nematic-isotropic point. This appears rather peculiar.

Anomalous absorption and velocity of ultrasonic longitudinal waves have been observed and explained in terms of structural relaxation or reorientation of molecular groups near and at the liquid crystal-isotropic transition temperature.^{5,22,23}

Experiments have shown that other physical properties (e.g., optical) of the system near the transition temperatures are different from those of the nematic or isotropic phases. These anomalies are often referred to as pretransition effects.

It seems clear that there are structural changes in the system near the transition temperatures giving rise to physical properties considerably different from either phase. One model proposed to explain this phenomenon is that of heterophase fluctuations.^{24,25} Further ultrasonic experiments may help to resolve

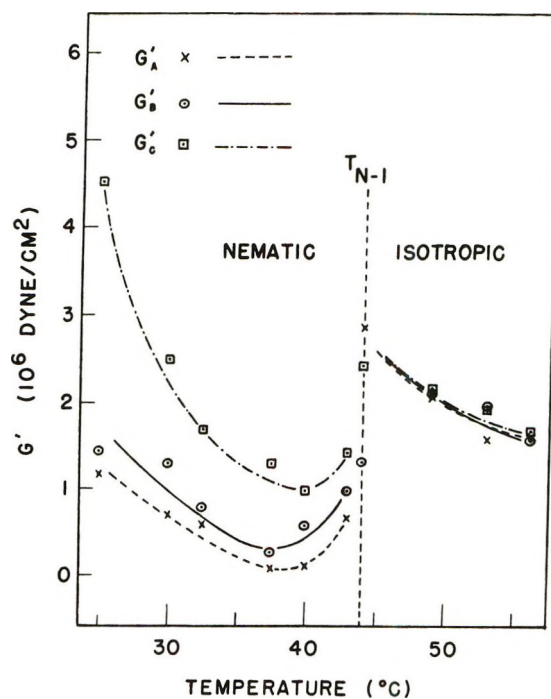


Figure 4. Shear storage modulus of MBBA at 10 MHz.

this question. In particular, it would be interesting to see whether structural relaxation effects appear in the stiffness.

The Dependence of Mechanical Properties of MBBA on the Frequency of the Ultrasonic Shear Wave. In measuring the phase shift, the techniques used in this work involve a slight variation of the frequency of the ultrasonic shear waves to nullify the signals resulting from mixing the reflected echoes and the continuous waves. We also made the phase shift measurement at four frequencies corresponding to four successive nullities of the second echo in the reflected echo train in the quartz delay line. At the frequency of 10 MHz, the difference in frequency from one nullity to a successive nullity for the second echo was about 3.7×10^4 Hz. To obtain four successive nullities for the second echo, the total frequency variation was about 1.1×10^5 Hz. It was observed that this frequency fluctuation did not result in a fluctuation in the measured values of either the absolute reflection coefficient or the phase shift.

It is the purpose of this section to illustrate how the variation of the frequency of ultrasonic shear waves in a large range, say, at various odd harmonics of the

(20) O. Parodi, *J. Phys. (France)*, **31**, 581 (1970).

(21) Orsay Liquid Crystal Group in "Liquid Crystals and Ordered Fluids," J. Johnson and R. Porter, Ed., Plenum Publishing Co., New York, N. Y., 1970, p 447.

(22) G. E. Zvereva, *Sov. Phys.-Acoust.*, **11**, 212 (1965).

(23) A. P. Kapustin and G. E. Zvereva, *Sov. Phys.-Crystallogr.*, **10**, 603 (1966).

(24) J. Frenkel, *J. Exp. Theor. Phys.*, **9**, 952 (1939).

(25) J. Frenkel, "Kinetic Theory of Liquids," Oxford University Press, London, 1946.

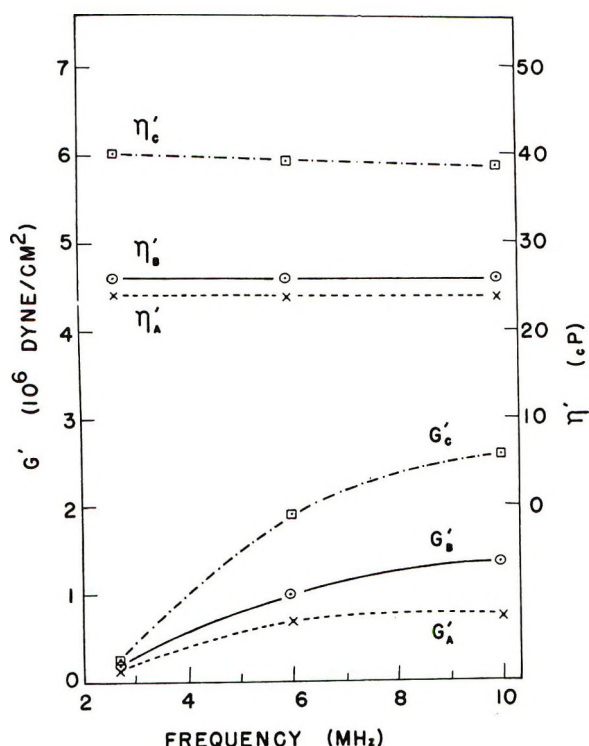


Figure 5. Frequency dependence of the dynamic viscosity and the shear storage modulus of MBBA at 30°.

fundamental frequency of the transducer, will affect the measured values for the absolute reflection coefficients and the phase shifts. This might consequently provide information about the dispersion of the calculated mechanical properties of MBBA.

The frequencies chosen for the dispersion study were 2.75, 6, and 10 MHz. Dispersion investigations were done on the nematic MBBA for all three orientations of the molecules at 30°. Results of these investigations are summarized in Table VI. Both R_m and X_m for the three orientations vary with the frequency and tend to converge to a common frequency. This results in the frequency dependence of G' presented in Figure 5. The convergence of each pair of R_m and X_m predicts that G' goes to zero at about 2 MHz for all three orientations.

Although all other mechanical parameters were frequency dependent, the dynamic viscosity of MBBA was found to show only a very slight continuous decrease with frequency in the frequency range of 2.75–10 MHz at 30.0° (Figure 5). If we calculate the viscosity assuming $X_m = R_m$, the viscosity shows a maximum in this frequency region.

Although the absolute reflection coefficient and the phase shift are both frequency dependent, the error introduced in reporting them by taking the average measured data from four successive nullities of the second echo is still within experimental error, only about 0.01° in phase shift (experimental error $\pm 0.02^\circ$) and 0.0003 in the absolute reflection coefficient (experimen-

Table VI: The Dependence of the Mechanical Properties of MBBA on the Frequency of Ultrasonic Shear Waves at 30.0° for Molecular Orientations A, B, and C; Sample Thickness 0.2 mm

Parameter	2.75 MHz	6 MHz	10 MHz
$R_{mA}, \Omega_m/\text{cm}^2$	1504	2258	2854
$X_{mA}, \Omega_m/\text{cm}^2$	1450	2086	2721
η_A', cP	24.27	23.92	23.77
$G_A', \text{dyn/cm}^2$	0.16×10^6	0.7×10^6	0.74×10^6
$R_{mB}, \Omega_m/\text{cm}^2$	1562	2366	3019
$X_{mB}, \Omega_m/\text{cm}^2$	1500	2151	2786
η_B', cP	26.08	25.96	25.74
$G_B', \text{dyn/cm}^2$	0.19×10^6	0.97×10^6	1.35×10^6
$R_{mC}, \Omega_m/\text{cm}^2$	1945	2949	3737
$X_{mC}, \Omega_m/\text{cm}^2$	1874	2607	3373
η_C', cP	40.57	39.22	38.58
$G_C', \text{dyn/cm}^2$	0.27×10^6	1.90×10^6	2.59×10^6

tal error ± 0.0007). Actually, the variation of the frequency to obtain four successive nullities for the second echo is not a necessity as far as the measuring techniques for the absolute reflection coefficient and the phase shift are concerned. It was used in this work only for monitoring the accuracy of the measurements and for the detection of mode conversion of the shear wave.

The mode conversion that might take place in the present experiment is due to the slight misorientation or tilting of the transducers on the quartz delay line in such a way that the direction of polarization of the shear wave will be at an angle to the reflecting surface of the quartz bar. A small portion of the acoustic pressure will be converted into a longitudinal wave at the quartz-liquid boundary. The longitudinal wave will propagate through the liquid and be reflected by the cover glass to the reflecting bar surface, where mode conversion might take place again with the production of a shear wave. This shear wave may propagate to the transducers and interfere with the primary reflected shear wave. Depending on its amplitude and phase relative to the reflected shear wave, this may cause considerable error in the phase-shift measurement.

Mode conversion will also interfere with the absolute reflection coefficient measurement, depending on the additive or subtractive effect of the converted signal on the reflected shear-wave signal amplitude. The detailed nature of the influence of mode conversion on the impedometric technique is being investigated.

From the shear storage modulus curves in Figure 5, it can be seen that for MBBA at 30°, when the frequency of the ultrasonic shear wave is below 2 MHz

$$R_m = X_m \quad (14)$$

From eq 1, it can be seen that R_m depends primarily

on the absolute reflection coefficient, r . Therefore, at 30° and below 2 MHz, only r needs to be measured to calculate the dynamic viscosity of MBBA. This is significant as it is much more difficult to measure the phase shift, θ , than to measure r . At frequencies higher than 2 MHz, the same approximation of the equality of R_m and X_m may lead to a calculated dynamic viscosity that is too high.

The Activation Energy for Viscous Flow of MBBA. Eyring²⁶ and Glasstone, Laidler, and Eyring²⁷ developed the relationship of viscosity and temperature

$$\eta = Be^{E_{vis}/RT} \quad (15)$$

where η is the steady flow viscosity, B is a constant, E_{vis} is the activation energy for viscous flow, R is the gas constant, T is the absolute temperature, and e is the base for the natural logarithm.

Since viscous flow is a shearing process comparable to the interaction of a liquid with shear waves, the dynamic viscosities determined for MBBA should also vary exponentially with $1/T$ or

$$\ln \eta' \propto \frac{1}{T}$$

Accordingly, from the slopes of the plots of $\ln \eta'$ vs. $1/T$ for various molecular orientations, the anisotropic activation energy for the dynamic viscosity of MBBA can be evaluated. Let this activation energy be E'_{vis} . The prime is used to indicate that the activation energy is evaluated from the dynamic viscosity-temperature relations. The data for η' are presented in this format, usually called the Arrhenius plots, in Figure 2. The straight line in each of the Arrhenius plots was drawn using the least-squares method. The four data from 25 to 40° were used.

The activation energies (E'_{vis}) for the three molecular orientations and for the isotropic structure are

$$E'_{vis(A)} = 7.5 \text{ kcal/mol-deg, ERMS} = 0.04$$

$$E'_{vis(B)} = 7.6 \text{ kcal/mol-deg, ERMS} = 0.03$$

$$E'_{vis(C)} = 9.4 \text{ kcal/mol-deg, ERMS} = 0.03$$

and

$$E'_{vis(iso)} = 10.0 \text{ kcal/mol-deg}$$

The letters appearing in parentheses with each E'_{vis} indicate molecular orientations; "iso" represents isotropic structure.

When the temperature of the nematic liquid crystal systems approaches the nematic-isotropic point, the Arrhenius plots for the molecular orientations A and B deviate from linearity and eq 15 fails to describe the behavior of these systems in flow. This may be explained by the temperature dependence of the order parameter.

The Arrhenius plot for the molecular orientation C holds its linearity until the nematic-isotropic point of the compound is reached. This seems to point out that in the ultrasonic field in the present case, MBBA in the molecular orientation C has the highest ability to retain the structure of the nematic liquid crystal. The activation energy for viscous flow of the compound in the molecular orientation C is almost equal to that in its isotropic state. This might also be because the viscous response of the two systems to some high frequency shear is very similar, and the fluctuation of the order parameter in molecular orientation C near the transition temperature results in no corresponding viscosity fluctuation.

Acknowledgment. This research was supported in part by Contract No. F44620-69-C-0021 from the Air Force Office of Scientific Research and in part from the U. S. Army Electronics Command, Night Vision Laboratory under Contract No. DA-44-009-AMC-1074(T).

(26) H. Eyring, *J. Chem. Phys.*, **4**, 283 (1936).

(27) S. Glasstone, K. J. Laidler, and H. Eyring, "The Theory of Rate Processes," McGraw-Hill, New York, N. Y., 1941, pp 480-484.

Some Comparisons of the RRK and RRKM Theories of Thermal Unimolecular

Reaction. Energy Distributions and the s Parameter^{1a}

by Gordon B. Skinner^{1b} and B. S. Rabinovitch*

Department of Chemistry, University of Washington, Seattle, Washington 98195 (Received March 1, 1972)

Publication costs assisted by the Air Force Office of Scientific Research

Some comparisons are drawn between the classical RRK and RRKM theories in regard to unimolecular rate behavior. The position of the fall-off curves with respect to pressure, the detailed shapes of the fall-off curves, the rate constants as a function of energy (k_E), and the energy distributions $T(E)$ of reacting molecules were calculated by the two theories. Both a specific comparison, for the cis-trans isomerization of 2-butene at several temperatures, and more general comparisons are made. The value of the Kassel s value that gives the correct pressure fit for fall-off differs from that which correctly describes the shape of the fall-off curve; in general, s is a double-valued function of the shape. For values of the RRK s quantity, $s > b/3$, the proposal⁶ that s is given by $s = C_{vib}/R$ may be used to find the approximate pressure region for fall-off. However, under virtually all conditions the numerical values of k_E and $T(E)$ given by the RRK theory are far from realistic, and no unique value of the RRK s value exists for a given reaction which summarizes all aspects of rate behavior.

Introduction

An interest in the use of the classical Rice-Ramsperger-Kassel (RRK)² theory and the Marcus-Rice formulation (RRKM)³ for correlating kinetic data on unimolecular reactions led us earlier⁴ to make some detailed comparisons of the two theories. A recent paper by Golden, Solly, and Benson⁵ (GSB) has compared the two theories for several different model molecules, but only on the basis of pressure region of the fall-off (k/k_∞) behavior. In recent years, also, more information on unimolecular reaction behavior has become available over a wide range of temperatures due mainly to shock-wave work. This has prompted us to examine several of the quantities involved in the theoretical calculations, with particular emphasis on the energy distribution of the reacting molecules and on the magnitudes and characteristics of the Kassel s quantity. Some new and useful insights into the similarities and differences of the two theoretical models are reported here for some sample model systems and conditions. They emphasize the fact that there is no unique s value which can reproduce the several aspects of thermal unimolecular reaction behavior. The most striking illustrations, first, are that the s values which give the approximate pressure region of onset of fall-off are in general quite different from those that describe the shape of the fall-off curve; and second, even the s values that successfully describe either the pressure region or shape of fall-off do not give the correct microscopic values of k_E , compensating errors being involved in their limited successes.

Calculations

Both RRK and RRKM expressions can for practical

purposes be written as an integral of the general Lindemann form

$$k_{uni} = \int_{E_0}^{\infty} \frac{B(E)k_E dE}{1 + k_E/\omega} \quad (1)$$

where E_0 is the zero-point activation energy for reaction; $B(E)$ is the Boltzmann distribution function for active vibrational and internal rotational energy E ; k_E is the microscopic rate constant for reaction at energy E ; and ω is the deactivation collision rate per second, on the basis of the strong collision assumption whose correctness is not directly relevant here.

$B(E)$ and k_E are formulated differently in the two treatments. For the RRKM theory

$$B(E) = N(E)e^{-E/RT}/Q$$

where $N(E)$ is the density of active rotational and vibrational states of the molecule at energy E , and Q is the corresponding partition function

$$k_E = \frac{C}{h} \frac{G^+(E)}{N(E)} \quad (2)$$

where C is related to the ratio of the overall moments of inertia of the activated complex, Z^+ , and energized molecule, Z , respectively, and will be approximated

(1) (a) Part of this work was supported by the Air Force Office of Scientific Research Air Force Systems Command, Grant No. AFOSR F-44620-70-C0012. (b) Department of Chemistry, Wright State University, Dayton, Ohio 45431.

(2) L. S. Kassel, *J. Phys. Chem.*, **32**, 225 (1928).

(3) R. A. Marcus, *J. Chem. Phys.*, **20**, 359 (1952).

(4) D. W. Placzek, B. S. Rabinovitch, G. Z. Whitten, and E. Tschui-kow-Roux, *ibid.*, **43**, 4071 (1965).

(5) D. M. Golden, R. K. Solly, and S. W. Benson, *J. Phys. Chem.*, **75**, 1333 (1971).

as such;⁶ it also includes any statistical factor for reaction path degeneracy. $G^+(E)$ is the sum of states for the activated complex up to energy $E - E_0$.

In the classical Kassel description

$$B(E) = \frac{(E)^{s-1}}{(RT)^s} \frac{e^{-E/RT}}{(s-1)!} \quad (3)$$

where s is the number of effective oscillators present in the molecule

$$k_E = \nu(E - E_0/E)^{s-1} \quad (4)$$

ν is an empirical constant which is conventionally of the order of magnitude of a vibrational frequency. With the substitutions

$$x = (E - E_0)/RT \text{ and } b = E_0/RT \quad (5)$$

then

$$B(x) = \frac{(b+x)^{s-1} e^{-(b+x)}}{RT(s-1)!}$$

$$k_x = \nu(x/(b+x))^{s-1}$$

$$dE = RTdx$$

These expressions for $B(x)$ and k_x may be substituted into eq 1. Since we wish to emphasize the role of the individual constituents of eq 1, we will not write down the full equations. We note only that at high pressure ($\omega \rightarrow \infty$) the RRKM theory gives

$$k_\infty = \frac{1}{h} \frac{Z^+}{Z} \frac{1}{Q} \int_0^\infty G^+(E) e^{-E/RT} dE$$

which is identical³ with the absolute reaction rate theory expression, so we may write

$$k_\infty = A(T) e^{-E_0/RT}$$

where A has some temperature dependence. The RRK theory gives

$$k_\infty = \nu e^{-E_0/RT}$$

One may arbitrarily provide an estimate of ν by setting it equal to the ART-RRKM pre-exponential factor;⁵ this will be done for purposes of comparison of the two treatments.

At low pressures ($\omega \rightarrow 0$), for both theories

$$k_0 = \omega \int_{E_0}^\infty B(E) dE$$

so that the energy distribution for the reacting molecules is the Boltzmann distribution above E_0 .

Results

A Particular Comparison. We first compare the two theories for a particular illustrative reaction—the cis-trans isomerization of *cis*-2-butene. This reaction has been studied at low^{7,8} and high^{9,10} temperatures. The best overall Arrhenius equation appears to be $k_\infty = 10^{13.15} e^{-62.9/RT}$. All of the data are reasonably well

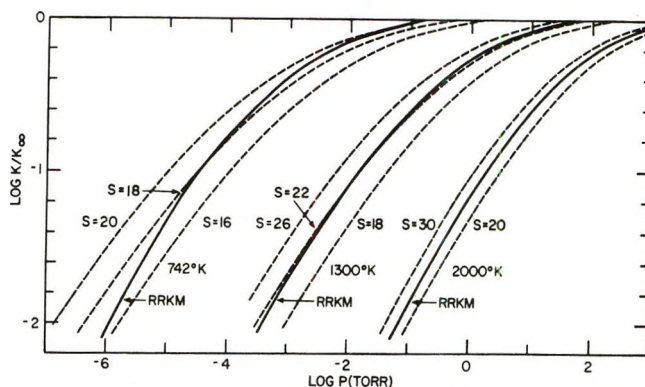


Figure 1. Comparison of RRKM and RRK fall-off curves for the isomerization of *cis*-2-butene at 742°K ($k_\infty = 2.4 \times 10^{-6}$ sec⁻¹, $b = 41.3$), 1300°K ($k_\infty = 1.6 \times 10^3$ sec⁻¹, $b = 23.6$), and 2000°K ($k_\infty = 7.0 \times 10^6$ sec⁻¹, $b = 15.3$). See Table I for molecular data. Consideration of reversibility would move all curves along the pressure axis by less than a factor of 2.

Table I: Constants Used in the Calculations for the Reaction of *cis*-2-Butene

Frequencies (cm ⁻¹) and degeneracies ^{a-c}	
Molecule	Complex
2980 (8)	2980 (8)
1670 (1)	1030 (1)
1400 (8)	1400 (8)
995 (7)	995 (7)
626 (2)	626 (2)
350 (2)	304 (1)

Moments of inertia of molecule: 6.00, 14.24, 19.19 $\times 10^{-39}$ g cm² ^a

Moments of inertia of complex: 6.00, 16.38, 22.07 $\times 10^{-39}$ g cm² ^d

Reduced moments of inertia of methyl groups (assumed equal for both molecule and complex): 5.0×10^{-40} g cm² ^a

Potential barrier for internal rotation assumed to be zero: actual value 260 cm⁻¹ ^{e,f}

Total symmetry number product of both molecule and complex: 18

Reaction path degeneracy: 2

Collision diameter: 5.0 Å

^a J. E. Kilpatrick and K. S. Pitzer, *J. Res. Nat. Bur. Stand.*, **37**, 163 (1946). ^b J. E. Kilpatrick and K. S. Pitzer, *ibid.*, **38**, 191 (1947). ^c Vibrations of approximately the same frequency were grouped. ^d Assuming the C=C bond stretched from a typical double bond length (1.35 Å) to a typical single bond length (1.54 Å). ^e T. N. Sarachman, *J. Chem. Phys.*, **49**, 3146 (1968). ^f S. Kondo, Y. Sakurai, E. Hirota, and Y. Morino, *J. Mol. Spectrosc.*, **34**, 231 (1970).

(6) We have not included the corrections for centrifugal effects described by E. V. Waage and B. S. Rabinovitch, *Chem. Rev.*, **70**, 377 (1970), and *J. Chem. Phys.*, **52**, 5581 (1970), because the corrections would be applied equally to both theories and would add complexity with no effect in the comparison.

(7) B. S. Rabinovitch and K. W. Michel, *J. Amer. Chem. Soc.*, **81**, 5065 (1959).

(8) R. B. Cundall and T. F. Palmer, *Trans. Faraday Soc.*, **57**, 1936 (1961).

(9) A. Lifshitz, S. H. Bauer, and E. L. Resler, Jr., *J. Chem. Phys.*, **38**, 2056 (1963).

(10) P. Jeffers and W. Shaub, *J. Amer. Chem. Soc.*, **91**, 7706 (1969).

Table II: Matching of RRK s to RRKM Calculations for *cis*-2-Butene Isomerization

Log k/k_∞	742°K		1300°K		2000°K	
	Position comparison	Shape comparison	Position comparison	Shape comparison	Position comparison	Shape comparison
-0.02	20.5	11.8 ^a	23.5	14.0 ^b	26	32 ^c
-0.05	20.0	11.7 ^a	23.3	13.8 ^b	26	32 ^c
-0.1	19.5	11.5 ^a	23.1	13.6 ^b	25	31 ^c
-0.2	19.1	11.1 ^a	22.9	13.2 ^b	25	31 ^c
-0.5	18.5	10.0	22.5	12.2	24	30
-1.0	17.8	8.3	22.0	11.0	24	30
-1.5	17.2	6.7	21.5	10.2	24	30
-2.0	16.6	5.2	21.0	9.6	24	29
-3.0	15.6	3.2	20.1	8.5	24	29
-4.0	14.6	2.4	19.2	6.5	23	29
-5.0	13.8	~2	18.2	3.8	23	29
b	41.3		23.6		15.3	
C_{vib}/R	14.6		21.0		24.4	
E_{vib}/RT	8.0		12.9		16.8	

^a Redundant value of $s(\text{shape})$ (see text) is $s > 100$. ^b Redundant value of $s(\text{shape})$ (see text) is $s \sim 60$. ^c Redundant value of $s(\text{shape})$ (see text) is $s = 10$.

correlated¹¹ by an RRKM calculation, with use of the thermal and molecular constants given in Table I. Figure 1 shows RRKM plots of $\log k/k_\infty$ vs. \log pressure at 742, 1300, and 2000°K, along with several RRK curves which fall nearby. As indicated in Table II, the best RRK s values with regard to pressure fit of the high end of the fall-off curve ($0.01 \leq k/k_\infty \leq 0.9$) match well with C_{vib}/R for the two highest temperatures, verifying Golden, Solly, and Benson's⁵ findings in these instances.

Figure 1 clearly reveals a marked discrepancy at 742° between the shape of the RRKM fall-off and that of the RRK curves ($s = 16$ –20) of best position fit; the discrepancies at higher temperatures are smaller. The extent of agreement of the shapes of the fall-off curves can be seen much more clearly if the slopes of the fall-off curves, $d \log k/k_\infty / d \log p$, are plotted vs. $\log k/k_\infty$, as is done in Figure 2 for the 1300°K data ($b = 23.6$). The shape of the RRKM curve does not match that for $s = 22$ (the value that gives the best match with respect to the position of the fall-off curve in Figure 1) and in fact does not match any RRK curve closely. However, it does come fairly close to matching the RRK curve with $s = 11$ in the range $0.01 < k/k_\infty < 0.9$.

Figure 3 shows RRKM k_x and $B(x)$ curves for the 2-butene reaction at 1300°K as a function of x , along with their product $T(x)$, the distribution of reacting molecules, which by eq 1 provides the terms in the summation for k_∞ . The steady-state population distribution factor $F(x)$ is seen to fall below the Boltzmann curve at a lower pressure. The $F(x)$ and $T(x)$ curves provide a quantitative illustration of the fact that, since k_x increases with x , the steady-state concentrations of higher-energy reacting molecules drop off before the lower-energy ones are significantly affected, thereby weighting the average energy of the reacting molecules

to lower energies. However, the contribution to reaction from energies which are only a few RT above E_0 is still small at values of k/k_∞ as low as 0.02.

This latter effect is seen to be much accentuated when the RRK curves for $s = 22$ are examined (Figure 4), and even more so when plots of $T(x)$ vs. x , for $p = \infty$, are compared directly (Figure 5). For the RRK model, no appreciable fraction of molecules with energies less than $10RT$ (26 kcal) above E_0 react at pressures above 10^{-3} Torr. The RRK curve of Figure 5 is displaced by about 9 units of x to the right of the RRKM curve, although the curves are otherwise quite similar in shape. This displacement comes about from two sources. First, the use of the classical model for k_x causes the RRK k_x to go to 0 at $x = 0$ (rather than remaining finite as in the quantum statistical theory) and to remain very small until x has attained a fairly large value (compare Figures 3 and 4). Second, for a given b value, the k_x 's must have approximately equal values at comparable points on the $T(x)$ curves to give equal degrees of fall-off. For example, in Figure 3 it is indicated that, at high pressure, $\log k_x$ is about 6.3 at the maximum of the $T(x)$ curve. This also happens, as shown in Figure 4, for the RRK $s = 22$ curve. For smaller s , $\log k_x$ is greater than 6.3 at the maximum in $T(x)$, while for larger s , $\log k_x$ is smaller at the maximum.

The basic similarity of the $T(x)$ and k_x curves, over a limited region of x near the maximum in $T(x)$, leads to comparable degrees of fall-off as the pressure

(11) The fit of the model with the fall-off data of ref 7 is excellent if it is assumed that the rate data at 2 mm still suffer from approximately 30% acceleration due to (a second order) radical catalysis which is clearly exhibited at still higher pressure; previously, Rabinovitch and Michel had hopefully concluded that radical acceleration was significant only above 2 mm. For present purposes, reversibility is ignored.

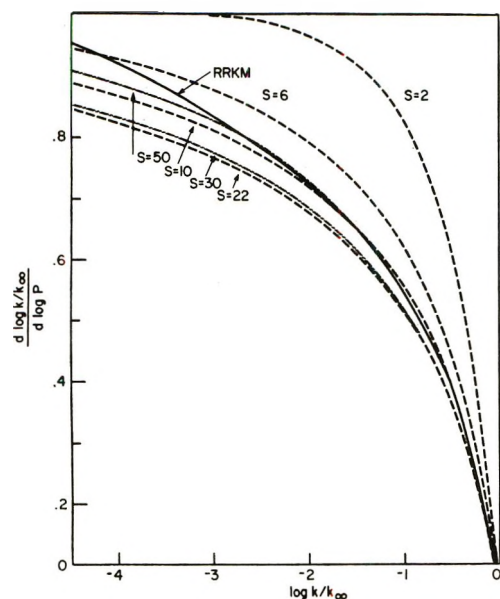


Figure 2. Comparison of RRKM and RRK fall-off curves based on the slopes of the curves for a given degree of fall-off (shape curves), for the isomerization of *cis*-2-butene at 1300°K.

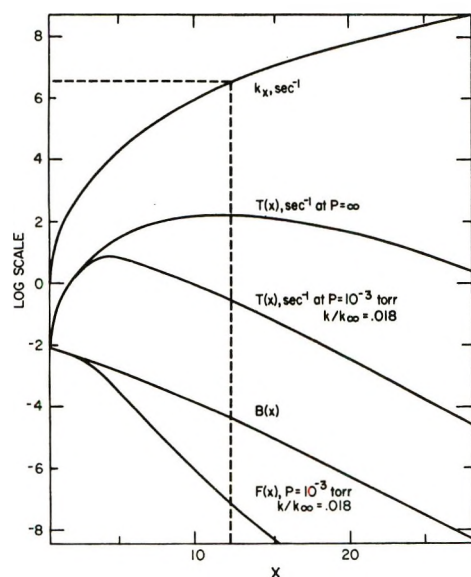


Figure 3. Energy dependence of k_x , $B(x)$, $T(x)$, and $F(x)$ according to the RRKM calculation for the isomerization of *cis*-2-butene at 1300°K.

is lowered moderately, as shown in Tables II and III. At still lower pressures, however, the fall-off curves differ markedly as the RRKM behavior approaches second order (the matching s values decreasing in every case as the pressure is lowered). This comes about because of the marked difference in shape at lower values of x between the k_x curve for $s = 22$ and the RRKM k_x curve, and because of the different steady-state population distributions $F(x)$ (Figures 3 and 4). The RRK distribution curve has a substantial lower energy component of the reactive molecule population which suffers no depletion until very low pressures.

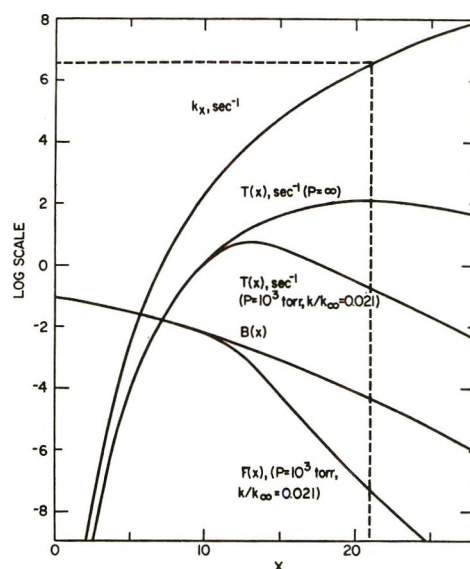


Figure 4. Energy dependence of k_x , $B(x)$, $T(x)$, and $F(x)$ according to the RRK calculation ($s = 22$, $b = 23.6$ for the isomerization of *cis*-2-butene at 1300°K).

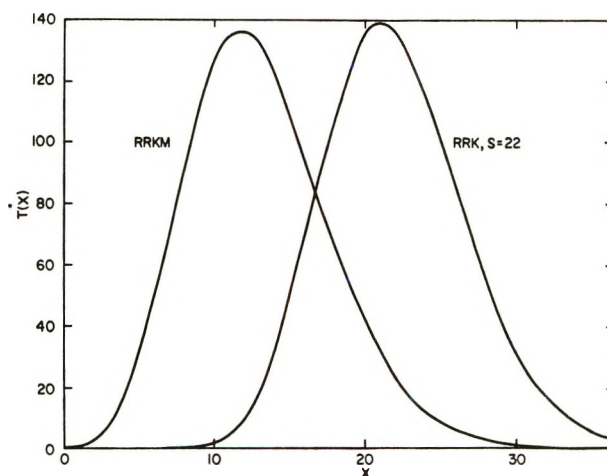


Figure 5. Comparison of RRKM and RRK energy dependencies of $T(x)$ at high pressure for the isomerization of *cis*-2-butene at 1300°K.

Indeed, the RRK model with $s = 22$ does not quite predict the second-order region even at a pressure of 10^{-23} Torr and a k/k_∞ of 10^{-20} !

General Comparisons. The following discussion is based on RRK and RRKM calculations, analogous to those for *cis*-2-butene, for two other molecules, ethylene and 4-octene. We have also studied the effect of modifying the fundamental frequencies of Table I that were assumed for the transition state for *cis*-2-butene isomerization, so as to increase k_∞ by up to 2×10^3 . In addition, we have drawn upon RRKM calculations we have made in connection with kinetic studies involving methane, ethane, ethyl radical, sulfur hexafluoride, methyl isocyanide, and ethyl isocyanide; and the comparisons of Golden, Solly, and

Table III: Comparison of RRKM and RRK ($s = 22$) Fall-Off Behavior and Energy Distribution for *cis*-2-Butene at 1300°K

Log P , Torr	RRKM				RRK			
	k/k_∞	Average z	z at max	Half- width ^a	k/k_∞	Average z	z at max	Half- width ^a
∞	1.000	12.97	11.8	10.9	1.000	22.00	21.00	10.8
0	0.550	10.31	10.0	7.7	0.522	19.14	19.0	7.6
-1	0.249	8.43	7.8	6.0	0.240	17.25	16.9	6.1
-2	0.079	6.63	5.8	4.9	0.080	15.40	14.7	5.2
-3	0.018	5.12	4.0	4.2	0.021	13.74	12.9	4.5
-4	3.4×10^{-3}	3.94	2.5	3.6	4.3×10^{-3}	12.30	11.2	4.0
-5	5.1×10^{-4}	3.08	1.5	3.2	7.7×10^{-4}	11.02	9.8	3.8
-6	6.2×10^{-5}	2.71	0.7	2.6	1.2×10^{-4}	10.01	8.6	3.6
-9	6.9×10^{-8}	2.44	0.1	2.1	3.1×10^{-7}	7.77	5.9	3.5
-15	7.0×10^{-14}	2.42	0.0	1.9	7.0×10^{-13}	5.48	3.0	3.5
-19	7.0×10^{-18}	2.42	0.0	1.9	8.9×10^{-17}	4.73	1.5	3.5
-23					1.0×10^{-20}	4.29	1.2	3.5
$-\infty$					0	3.54	0	3.5

^a Width of the energy distribution curve (Figure 5) at half-height, in units of z .**Table IV:** Comparative Values of Several Reaction Properties for Four Reactions with $E_0 = 60.9$ kcal

Property	Molecule ^b	T , °K		
		742	1300	2000
Log k_∞ , sec ⁻¹ (RRKM)	C ₂	-4.5	3.4	7.0
	C ₄	-4.6	3.2	6.8
	C ₈	-4.7	3.1	6.8
	C ₄ , mod.	-2.2	6.3	10.3
Log $p_{1/2}$, ^a Torr (RRKM)	C ₂	1.1	2.2	3.3
	C ₄	-2.7	-0.2	1.9
	C ₈	-5.7	-1.6	0.9
	C ₄ , mod.	0.6	3.4	5.5
RRK s , position fit (for $0.01 \leq k/k_\infty \leq 0.5$)	C ₂	7 (6) ^c	9 (9)	10 (10)
	C ₄	18 (15)	22 (21)	24 (24)
	C ₈	36 (33)	46 (48)	52 (56)
	C ₄ , mod.	15 (15)	18 (21)	20 (24)
$\langle E - E_0 \rangle_\infty / RT$, RRKM	C ₂	3.0	4.9	6.6
	C ₄	8.0	12.9	16.8
	C ₈	16.3	27.4	36.5
	C ₄ , mod.	11.1	15.0	18.3
$\langle E - E_0 \rangle_\infty / RT$, RRK	(same as RRK s values above)			
$\langle E - E_0 \rangle_0 / RT$, RRKM	C ₂	1.2	1.4	1.8
	C ₄	1.6	2.4	4.6
	C ₈	2.3	7.1	20.9
	C ₄ , mod.	1.6	2.4	4.6
$\langle E - E_0 \rangle_0 / RT$, RRK ^d	C ₂	1.2	1.4	1.9
	C ₄	1.6	3.5	8.9
	C ₈	3.8	22.4	36.7
	C ₄ , mod.	1.5	2.6	5.8

^a $p_{1/2}$ is the pressure at which $k/k_\infty = 0.5$. ^b C₄ is *cis*-2-butene, with molecular quantities given in Table I. C₄, mod. is *cis*-2-butene, with the seven 995-cm⁻¹ frequencies of the complex reduced to 250 cm⁻¹ to produce higher rate constants; C₂ and C₈ are essentially ethylene and 4-octene, with transition states comparable to that of C₄. ^c Parenthetical number is $s(C_{\text{vib}})$, rounded; principal number is best-fit s value. ^d s value employed is best position fit value.

Benson⁵ and some earlier calculations¹² have also been useful. In Table IV we provide numerical reaction parameters for three molecules, with two different transition states for one of them, to further clarify the comparison of the two treatments.

The Kassel-related curves display some general characteristics which will now be described.

The maximum value of $B(x)$ occurs at $x = s - b - 1$. This is negative, of course, for $s < b + 1$, so for this situation the maximum number of reacting molecules at low pressure comes at $x = 0$. For $s > b + 1$, the maximum number of reacting molecules at low pressure occurs at the nonzero value of $x = s - b - 1$. The maximum high-pressure value of $T(x)$ occurs at $x = s - 1$. This means that in a family of curves of increasing s with given b , the numerical change in x_{max} in going from high to low pressures equals $s - 1$, for all s up to the value $s = b + 1$, and remains constant at $\Delta x_{\text{max}} = b$ for higher s .

For the region of s in which the change in x_{max} increases, the range of k/k_∞ needed for the reaction to convert from first into second order increases, as may be seen in Figure 2. But the range reaches a maximum for s values near $b + 1$, where the change in x_{max} becomes constant, and decreases for higher s . As s becomes very large compared to b , either because of a low activation energy, high temperature or a large number of degrees of freedom in the molecule, then $k/k_\infty \rightarrow \omega/(\omega + c\nu)$, where c is a constant (unity for $T \rightarrow \infty$, e^{-b} for $s \rightarrow \infty$) which gives the same fall-off curve shape that applies for the "Hinshelwood case," $s = 1$, for any b . The reason for this behavior is evident from the term, $(x/(b + x))^{s+1}$, in the denominator of eq 1 (see eq 6), and the fact that as x_{max} increases

(12) B. S. Rabinovitch and D. W. Setser, *Advan. Photochem.*, **3**, 1 (1964).

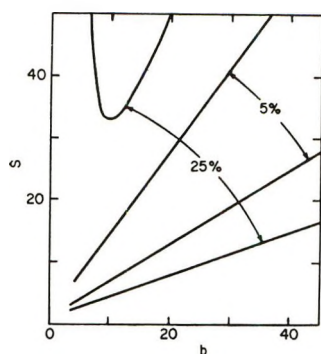


Figure 6. Extent of region around $s = b + 1$ for which fall-off curve shapes differ by less than 5 and 25%, according to the criterion given in the text.

with s , then $x_{\max} \gg b$ at all pressures; then $\lim_{s \rightarrow \infty} (x/(b + x))^{s+1}$ is a constant. Accordingly, the curves of Figure 2 go through a cycle of increasing and decreasing fall-off ranges as s increases without limit. RRKM calculations give the same effect if one considers a given reaction for a certain molecule over a wide range of temperatures,¹³ or else over a series of molecules of increasing size at a given temperature.

One result of this behavior is that the fall-off shape of any RRKM curve can be matched at a given degree of fall-off by *two* RRK curves. The appropriate one can be selected in a given instance by making comparisons at a series of increasing temperatures; the second may correspond to a physically impossible value of s . For the *cis*-2-butene example, the s values for the shape comparison in Table II are on the lower s family of curves for 742 and 1300°K, and on the upper family at 2000°K, the change-over occurring at about 1700°K. We do not intend in any of the above to imply practical physical accessibility of fall-off features at large s values.

Another result is that the fall-off shapes of all the curves for s values near $b + 1$ become similar and experimentally indistinguishable. We may adduce the quantitative connotations of this statement by finding the range of s for which fall-off curves do not deviate by more than 5% over the range, $0.01 < k/k_{\infty} < 0.9$, if they are matched at $k/k_{\infty} = 0.1$; this is probably the present day limit of very good experimental accuracy. The results of this calculation are shown in Figure 6 together with the range for 25% deviation which represents mediocre accuracy. Since the range of shapes becomes quite limited for small b , the 25% curve barely comes onto the figure on the upper side.

The relative separation of the RRK curves of Figure 2 for smaller s values becomes less as b decreases. This fact, coupled with the folding back of the shape curves at $s = b + 1$, means that the total range of useful experimental discrimination of curve shapes diminishes with decreasing b , *i.e.*, with increasing temperature for a given reaction. Accordingly, the most sensitive region for testing and comparing fall-off theories is

the low-temperature one, with fall-off data obtained over a wide range, say down to $k/k_{\infty} \simeq 0.01$, or less, since the curves are spread out most in the range $k/k_{\infty} < 0.1$. From the experimental point of view, this can be done most easily with smaller molecules for which the fall-off occurs at higher pressures.

We turn now to the generalization of Golden, Solly, and Benson⁵ that for values of $k_{\text{uni}} \geq 10^{-4} \text{ sec}^{-1}$, the RRK theory gives an adequate representation of thermal unimolecular fall-off if the s parameter is evaluated as $s = C_{\text{vib}}(T)/R$, and if $s \geq 5$ or 6. These authors also questioned our earlier conclusion⁴ that a single s value could not provide an adequate representation of the diverse aspects of unimolecular reaction systems.

It is clear from the preceding presentation that the RRK s value that gives the best pressure position fit to an RRKM fall-off curve is greater than the value that corresponds to the average energy of the reacting molecules, *i.e.*, $s = E_{\text{vib}}(T)/RT$, and less than the total number of vibrational degrees of freedom of the molecule. The value, $s(C_{\text{vib}})$, invariably falls within this range. As may be seen from Figure 1, for a middle-sized or large molecule the value of s may be varied by several units without changing k/k_{∞} by more than a factor of 2 to 3 (the accuracy claimed by GSB for their generalization). As long as s is approximately equal to or greater than $b/3$, their generalization may be expected to hold well, with some exceptions in both directions, and to be useful for rough and ready estimation of rates, if A is known or can be estimated. The concomitant error in the pressure estimate of the position of fall-off, for k/k_{∞} in the range 0.1–0.9, may be considerable—of the order of a factor of 10 to 100. For smaller s , but not always as small as 5 or 6, the RRK position curves spread out, the shapes do not match well, and the approximation can break down further. This generalization does not apply to a substantial body of data obtained in conventional static studies at moderate temperatures in which $k_{\text{uni}} < 10^{-4} \text{ sec}^{-1}$.

From the point of view of unimolecular rate studies *per se*, in which the greatest possible insight into the molecular processes involved is desired, a method of correlating rate data which involves inconsistencies with a more complete theory as large as a factor of 2 is inadequate. The difference between $s(\text{shape})$ and $s(\text{fall-off position})$ is frequently, and most usefully, quite significant with respect to theory, and especially so for the smaller molecules excluded by the generalization of GSB. The calculations of our paper confirm that, in general, no single RRK s can correlate all of the quantities—position of fall-off, shape of fall-off curve, average energy, k_E , and $B(E)$ —that are important for a complete description of the kinetics of a unimolecular reaction.

(13) F. W. Schneider and B. S. Rabinovitch, *J. Amer. Chem. Soc.*, **84**, 4215 (1962).

Finally, we turn to a common unjustified custom that springs from resort to the RRK classical treatment. Even though a fall-off curve has been well matched by some RRK curve, with ν and b determined from an Arrhenius plot of the high-pressure rate constants, the calculated $B(E)$, average energy and most importantly, k_E , will usually differ greatly from those of the real molecules and from the k_E values given by RRKM or other more realistic treatment. The custom of estimating k_E values for nonthermal systems by use of the Kassel eq 4, with insertion of the relevant E values and with employment of s values deduced from thermal

data, invites catastrophe. Thus, in the *cis*-butene case at 1300°K, for some arbitrary energy, say 90 kcal mol⁻¹, as might arise in a chemical activation or photon activation system, Figures 3 and 4 show that the calculated k_E values ($x \simeq 10$) are $\sim 10^6$ sec⁻¹ (RRKM) and $\sim 10^2$ sec⁻¹ (RRK, $s = 22$). The "correct" $s(k_E)$ in this instance is $s \simeq 17$; thus a better estimate from thermal data of the correct s for use in the classical Kassel k_E expression is found as $s(k_E) \simeq \frac{1}{2}[s(C_{\text{vib}}) + s(E_{\text{vib}})]$. Of course, $s(k_E)$ is not a fixed value; in the case of *cis*-2-butene at 1300°K, it rises to $s = 19$ for $x = 30$ and drops to $s = 13$ for $x = 5$; also, the correct $s(k_E)$ at given x also depends on temperature.

CNDO-CI Studies of the Effects of Multiple Substitution on the Electronic Spectrum of *p*-Benzoquinone

by Philip E. Stevenson

Department of Chemistry, Worcester Polytechnic Institute, Worcester, Massachusetts 01609 (Received December 20, 1971)

Publication costs borne completely by The Journal of Physical Chemistry

The CNDO-CI method of Del Bene and Jaffé has been used to calculate the uv spectra of *p*-benzoquinone and all its methyl derivatives. The uv-visible absorption spectrum of *p*-benzoquinone is qualitatively well represented, although the two $\pi-\pi^*$ transitions are calculated to be about 8 kK higher than observed. The calculated orbital energies agree reasonably well with the photoelectron spectrum. The substituent induced changes in the uv spectrum are quite well reproduced by the calculation, but there seems to be no simple way to relate the parameters of this MO approach to the parameters used in the phenomenological description of substituent effects.

Introduction

The relationship between the uv spectra of derivatives of *p*-benzoquinone (PBQ) and the structure of these derivatives has been studied by a perturbation theory approach.¹⁻⁴ The observed spectrum of PBQ was taken as the solution to the unperturbed problem, and the substituents were represented as perturbations to the excited states. The formalism of the second-order perturbation equations⁵ divides the substituent effect into two kinds: a conjugative (or mesomeric⁶) effect where excited states of the substituents mix with the excited states of the PBQ; and an inductive effect where the substituents cause the PBQ states to mix with each other. The conjugative effect depends only on the numbers and types of substituents, while the inductive effect depends on the relative positions of substitution as well as on the numbers and types of substituents. Simple formulas for frequency and

intensity shifts of the two $\pi-\pi^*$ transitions in PBQ and its derivatives were derived, and inductive and conjugative parameters for a number of substituents were obtained from spectra.² Spectra of other derivatives were successfully predicted from the parametrized formulas.

The perturbation approach works well only for weak substituents such as CH₃ and Cl and breaks down for strong substituents such as NH₂ and NO₂ which substantially expand the π system. However, the strong substituents can, in principle, be treated by the Pariser-

- (1) L. E. Orgel, *Trans. Faraday Soc.*, **52**, 1172 (1956).
- (2) P. E. Stevenson, *J. Mol. Spectrosc.*, **17**, 58 (1965).
- (3) P. E. Stevenson, *J. Chem. Phys.*, **43**, S27 (1965).
- (4) P. E. Stevenson, *J. Mol. Spectrosc.*, **23**, 191 (1967).
- (5) J. Petruska, *J. Chem. Phys.*, **34**, 1111 (1961).
- (6) J. N. Murrell, "The Theory of the Electronic Spectra of Organic Molecules," Wiley, New York, N. Y., 1963, p 211.

Parr-Pople method.⁷ For CH₃ though, it is difficult to define and parametrize an addition to the π system of a parent compound. Moreover it is likely that a substituent perturbs both the σ and π systems of the parent compound. Finally it is now possible to perform calculations which take into account all the valence electrons in a molecule, both σ and π .⁸

The work described in this paper consists of calculations on PBQ and all six of its methyl derivatives with the intent of predicting the electronic spectrum of each of the seven compounds. The modified CNDO method of Del Bene and Jaffé with configuration interaction was chosen for these calculations.⁹ This method has been used successfully to predict the spectra of a number of aromatic compounds and some of their mono-substituted derivatives, as well as some small molecules. The formulas and parametrization employed in this study are given in the original references except that the two-electron, two-center integrals were calculated by the Mataga approximation¹⁰ instead of the Pariser formula.¹¹ It was hoped that this work would show the relationship between the orbital and perturbation approaches to prediction of electronic spectra, but it will be seen below that this hope has only been realized in part.

Details of the Calculations

The MO-CI calculations were performed with the program CNDO/S-CI.¹² Coordinates for PBQ were obtained from the work of Robertson.¹³ Methyl groups were assumed to have the geometry shown in Figure 1. The methyl carbon was assumed to have tetrahedral geometry. The angles of the C-C bond with the ring were assumed to be the same as those of the C-H bond in PBQ. Cartesian coordinates were calculated with the time-sharing version of COORD.¹⁴ The number of configurations taken for CI was in each case equal to the number of orbitals, or 36 plus 6 for each methyl group.

The Spectrum of *p*-Benzoquinone

The electronic spectrum of PBQ (Figure 2) is well known¹⁵ and consists of three absorption bands in the visible and near-uv. The lowest energy band ($\nu = 20$ –25 kK, $\epsilon = 20$, $f = 0.0004$) arises from $n-\pi^*$ absorption and is labeled ${}^1A-{}^1U$ in the Platt notation. The other two bands ($\nu = 36$ kK, $\epsilon = 300$, $f = 0.0008$; and $\nu = 41$ kK, $\epsilon = 20,000$, $f = 0.4$) arise from $\pi-\pi^*$ transitions. The assignment of these two transitions, based on substituent perturbations, are ${}^1A_{1g}-{}^1B_{1g}$ and ${}^1A_{1g}-{}^1B_{3u}$, respectively.¹ For the purpose of discussing the spectra of derivatives of PBQ where the symmetry is lower, an alternate notation has been proposed which labels the two transitions as ${}^1A-{}^1K$ and ${}^1A-{}^1J$, respectively.²

The CNDO-CI calculation (Table I) reproduces the observed spectrum of PBQ quite well except that the

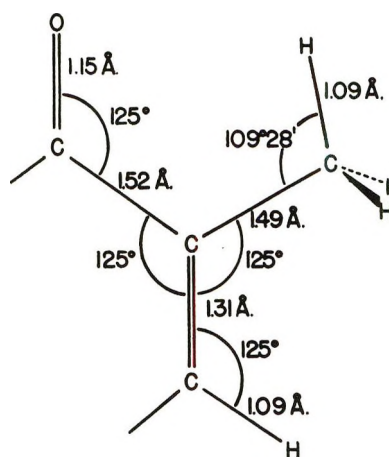


Figure 1. Geometry of methyl-*p*-benzoquinone used in calculations.

${}^1A-{}^1J$ and ${}^1A-{}^1K$ transition energies are overestimated by about 8 kK (1 eV). The $n-\pi^*$ absorption is predicted to occur right where it is observed. Moreover, the calculation shows that this absorption arises from two transitions, there being two oxygen lone-pair orbitals from which $n-\pi^*$ transitions can arise. A third $n-\pi^*$ transition (${}^1A_g-{}^1B_{1u}$) is calculated to occur at 40.8 kK, below the first calculated $\pi-\pi^*$. However, one would not expect to observe it, since its calculated energy is greater than that of the observed ${}^1A-{}^1K$ transition (${}^1A_g-{}^1B_{3g}$) which has considerably more intensity than would be expected from $n-\pi^*$ absorption.

Table I: The Electronic Spectrum of *p*-Benzoquinone

Transition	Symmetry	ν^a		f^b	
		Obsd	Calcd	Obsd	Calcd
${}^1A-{}^1U$	${}^1A_g-{}^1B_{3g}$	22	21.1	0	0
	${}^1A_g-{}^1A_u$		23.6		0
${}^1A-{}^1K$	${}^1A_g-{}^1B_{1g}$	36.2	44.3	0	0
${}^1A-{}^1J$	${}^1A_g-{}^1B_{3u}$	41.7	49.2	0.4	0.64

^a Energies in kK. ^b Electronic component of oscillator strength.

(7) R. G. Parr, "Quantum Theory of Molecular Electronic Structure," W. A. Benjamin, New York, N. Y., 1963.

(8) (a) J. A. Pople, D. P. Santry, and G. A. Segal, *J. Chem. Phys.*, **43**, S129 (1965); (b) J. A. Pople and G. A. Segal, *ibid.*, **43**, S136 (1965); (c) J. A. Pople and G. A. Segal, *ibid.*, **44**, 3289 (1966).

(9) J. Del Bene and H. H. Jaffé, *ibid.*, **48**, 1807, 4050 (1968); **49**, 1221 (1968); **50**, 1126 (1969).

(10) K. Nishimoto and N. Mataga, *Z. Phys. Chem. (Frankfurt am Main)*, **12**, 335 (1957); **13**, 140 (1957).

(11) R. Pariser and R. G. Parr, *J. Chem. Phys.*, **21**, 767 (1953).

(12) J. Del Bene, H. H. Jaffé, R. L. Ellis, and G. Kuehnlenz, CNDO-S/CI, program no. 174, Quantum Chemistry Program Exchange, Indiana University (1971).

(13) J. M. Robertson, *Proc. Roy. Soc., Ser. A*, **150**, 106 (1935).

(14) P. E. Stevenson and J. E. Merrill, COORD, program no. 186, Quantum Chemistry Program Exchange, Indiana University (1971).

(15) W. Flaig, Th. Ploetz, and A. Küllmer, *Z. Naturforsch. B*, **10**, 668 (1955).

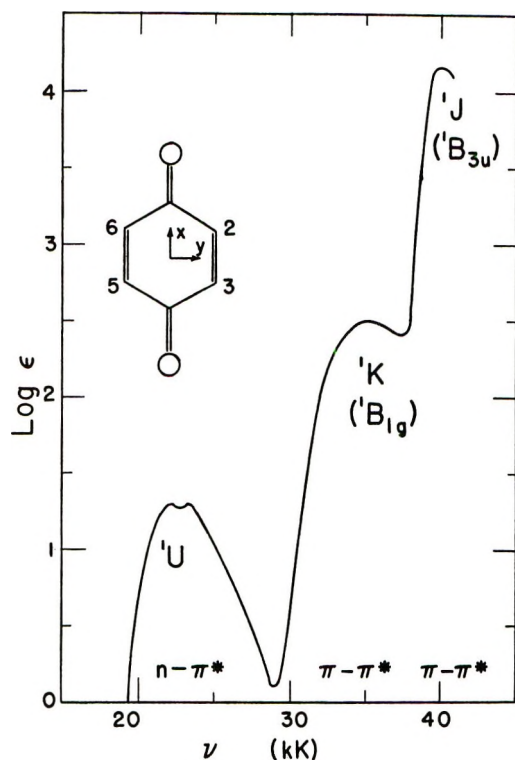


Figure 2. Electronic spectrum of *p*-benzoquinone (from ref 15). The two bumps in the ¹U peak are calculated in this work to arise from two *n*- π^* transitions (into ¹B_{3g} and ¹A_u states).

A prediction of the photoelectron spectrum of PBQ may be made from this calculation. Peaks in photoelectron spectra correspond to vertical ionizations which in turn correspond to calculated molecular orbital energies according to Koopmanns' theorem. The photoelectron spectra of PBQ and its tetrafluoro derivative have been discussed by Brundle, Robin, and Kuebler.¹⁶ Making use of the "perfluoro effect" which stabilizes σ orbitals by *ca.* 5 eV in perfluoro compounds with respect to the unsubstituted parents (π orbitals are stabilized hardly at all), they assigned the ionizations at 10.11 and 11.5 eV to *n* orbitals, the ionizations at 10.41 and 11.06 eV to π orbitals, and the ionization at 13.43 eV to a σ orbital. These assignments are shown in Table II along with assignments made by this author of several other peaks in their spectrum and the corresponding calculated orbital energies. Agreement of the orbital energies with the observed ionizations is quite good. The observed large gap between the fourth and fifth ionization potentials is reproduced (albeit exaggerated) by the calculation; only the position of the *b*_{2u}(*n*) orbital is out of the observed order; and most of the energies agree within a root mean square deviation of ± 0.5 eV. (All agree within ± 1.0 eV.)

Effects of Methyl Substitution

The results of calculations on the methyl derivatives of PBQ are shown in Table III and Figures 3 and 4.

Table II: Molecular Orbitals of *p*-Benzoquinone

Calculated orbitals		Observed photoelectron spectrum ^b	
Energy, eV	Symmetry ^a	Energy, eV	Assignment
-9.92	b _{1g} (<i>n</i>)	10.11	n _g
-10.91	b _{1u} (π)	10.41	π
-11.03	b _{2g} (π)	11.06	π
-10.61	b _{2u} (<i>n</i>)	11.5	n _u
-14.31	a _g (σ)	13.43	σ
-14.98	b _{1g} (σ)	14.3 ^c	σ
-15.05	b _{2g} (π)	14.7 ^c	π
-15.42	b _{3u} (σ)	15.2 ^c	σ
-16.11	b _{2u} (σ)	16.1 ^c	σ
-16.36	b _{1u} (π)	16.6 ^c	π

^a Axes as shown in Figure 2. ^b Reference 16. ^c Energy read from curve in Figure 7, ref 16.

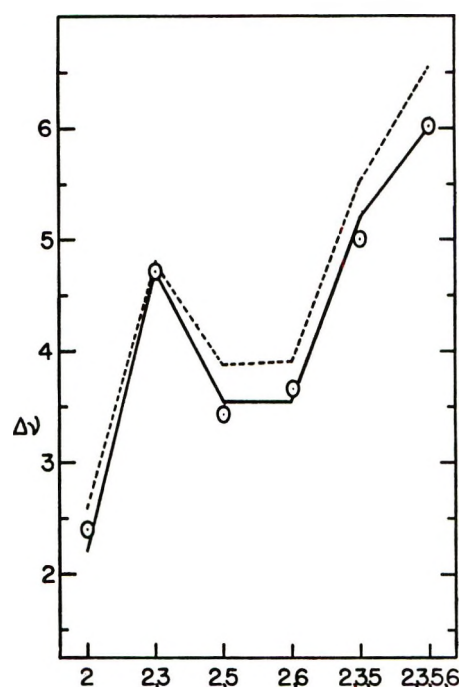


Figure 3. Frequency shifts of the ¹A-¹K transition in the methyl PBQ's: CNDO-CI calculation (---); perturbation treatment (—); observed (○).

The observed changes in transition energies and electronic oscillator strengths in the ¹A-¹K and ¹A-¹J transitions are qualitatively well represented. In particular the calculations predict quite well the way the spectrum of the 2,3 derivative differs from those of the 2,5 and 2,6 derivatives. Quantitative accuracy is not quite as good. The frequency shifts of the ¹A-¹K and ¹A-¹J transitions are overestimated by about 8 and 50%, respectively, and the substituent induced electronic oscillator strengths of the ¹A-¹K transition

(16) C. R. Brundle, M. B. Robin, and N. A. Kuebler, *J. Amer. Chem. Soc.*, **94**, 1466 (1972).

Table III: Effects of Methyl Substitution on the Spectrum of *p*-Benzoquinone

		Methyl groups at positions					
		2	2,3	2,5	2,6	2,3,5	2,3,5,6
		¹ A- ¹ K					
$\Delta\nu^a$	Calcd ^b	2.58	4.78	3.87	3.91	5.52	6.54
	Perturbation ^c	2.20	4.72	3.54	3.54	5.20	6.00
	Obsd ^d	2.41	4.72	3.44	3.66	5.00	6.02
f^e	Calcd	0.048	0.088	0	0.0022	0.020	0
	Perturbation	0.0048	0.019	0	0	0.0048	0
	Obsd	0.0070	0.018	0	0.0012	0.0039	0
		¹ A- ¹ J					
$\Delta\nu$	Calcd	0.81	1.34	2.48	2.62	3.25	4.29
	Perturbation	0.68	0.92	1.56	1.56	2.06	2.76
	Obsd	0.69	1.02	1.51	1.67	1.99	2.76
f	Calcd	0.52	0.34	0.58	0.58	0.50	0.54
	Obsd	0.5	0.3	0.4	0.4	0.4	0.4

^a Frequency shifts (in kK) relative to transition frequency in PBQ. ^b This work. ^c Reference 2. ^d Reference 15. Spectra observed in *n*-C₆H₁₄. ^e Electronic component of oscillator strength.

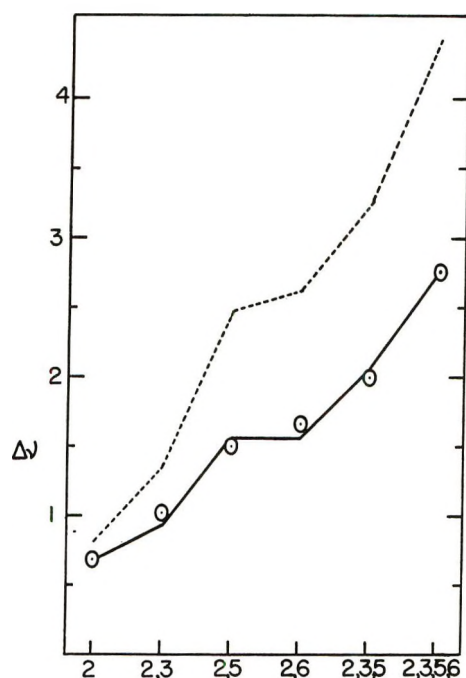


Figure 4. Frequency shifts of the ¹A-¹J transition in the methyl PBQ's: CNDO-Cl calculation (---); perturbation treatment (—); observed (○).

are overestimated by a factor of 5. The predicted shifts in the energies of the two low-lying $n-\pi^*$ transitions are all quite small, agreeing with the observation that the ¹A-¹U band is little affected by substitution.²

Discussion

It is evident from the above calculations that the modified CNDO method with CI⁹ is successful in accounting for the effects of substitution on the electronic spectrum of PBQ. Although the quantitative results are not as good as might be desired, the calculations closely parallel the observed effects of methyl substitu-

tion. This is especially true of the three isomers of dimethyl PBQ where the relative positions of the substituents govern the changes in the spectra. There is a considerably greater red shift and much more intensity in the ¹A-¹K transition of 2,3-dimethyl PBQ than in the ¹A-¹K transitions of the 2,5 and 2,6 isomers, and these differences are rather well predicted by the calculations.

However, in spite of the parallel results of the perturbation method and the molecular orbital method, there seems to be no simple way to identify anything at any stage in the MO procedure as either an inductive or conjugative perturbation. An analysis of the π matrix elements of the Hamiltonians of all seven compounds showed only very small and unsystematic variations among corresponding elements. Average values of these elements with r.m.s. deviations are given in Table IV. The only substituent caused perturbation to the MO Hamiltonian is its enlargement to accommodate the substituent atomic orbitals.

Table IV: π Matrix Elements from the CNDO Hamiltonians of Methyl-Substituted *p*-Benzoquinones (in eV)

Diagonal elements			Off-diagonal elements		
Atom	Position	Value	Bond	Position	Value
C	1	-5.58 ± 0.10	C—C	1-2	-2.54 ± 0.02
C	2	-5.89 ± 0.07	C=C	2-3	-5.41 ± 0.03
O	7	-8.69 ± 0.08	C=O	1-7	-7.29 ± 0.01
C (CH ₃)		-5.70 ± 0.03	C—C (CH ₃)		-2.46 ± 0.01
H (CH ₃)		-7.34 ± 0.03	C—H (CH ₃)		-7.97 ± 0.001

This is not to say that the MO's are not perturbed. In fact the MO's undergo considerable change when methyl groups are introduced. There are some energy

Table V: Calculated Spectra of the Methyl PBQ's—Comparison of Single Configuration Results with Full CI Treatment

		PBQ	2	2,3	2,5	2,6	2,3,5	2,3,5,6
¹ A- ¹ K Transition								
Single configuration	Energy ^a	45.69	44.57	41.59	41.56	41.49	40.82	38.76
	Shift ^b	...	1.12	4.10	4.13	4.19	4.87	6.83
	<i>f</i> ^c	0	0.54	0.44	0.0002	0.0020	0.29	0
CI	Energy ^a	44.28	41.70	39.50	40.41	40.37	38.76	37.74
	Shift ^b	...	2.58	4.78	3.87	3.91	5.52	6.54
	<i>f</i> ^c	0	0.049	0.088	0	0.0022	0.020	0
Observed ^d	Shift ^e	...	2.41	4.72	3.44	3.66	5.00	6.02
	<i>f</i> ^c	0	0.0070	0.018	0	0.0012	0.0039	0
¹ A- ¹ J Transition								
Single configuration	Energy ^a	51.16	48.78	49.43	49.20	48.34	46.78	46.57
	Shift ^b	...	2.38	1.73	1.96	2.82	4.38	4.59
	<i>f</i> ^c	1.34	0.67	0.75	1.23	1.22	0.87	1.18
CI	Energy ^a	49.19	48.38	47.86	46.72	46.58	45.94	44.90
	Shift ^b	...	0.81	1.34	2.48	2.62	3.25	4.29
	<i>f</i> ^c	0.64	0.53	0.34	0.58	0.58	0.51	0.54
Observed ^d	Shift ^e	...	0.69	1.02	1.51	1.67	1.99	2.76
	<i>f</i>	0.4	0.5	0.3	0.4	0.4	0.4	0.4

^a Calculated energies in kK. ^b Shift of energy relative to equivalent stage of PBQ calculation. ^c Electronic component of oscillator strength. ^d Reference 15. Spectra observed in *n*-C₆H₁₄. ^e Shift of transition frequency relative to observed PBQ spectrum.

Table VI: Fraction of Charge Found on the CH₃ Groups in the Spectroscopically Important π -MO's

Orbital		PBQ	2	2,3	2,5	2,6	2,3,5	2,3,5,6
ψ_{-3}	ϵ^a	0.973	1.039	1.081	1.097	1.088	1.135	1.174
	<i>q</i> _{CH₃} ^b	...	0.00	0.00	0.00	0.00	0.00	0.00
ψ_{-2}	ϵ	-0.257	-0.179	-0.107	-0.097	-0.101	-0.030	0.034
	<i>q</i> _{CH₃}	...	0.01	0.02	0.02	0.02	0.02	0.03
ψ_{-1}^c	ϵ	-1.788	-1.715	-1.649	-1.628	-1.642	-1.570	-1.506
	<i>q</i> _{CH₃}	...	0.01	0.01	0.01	0.01	0.02	0.02
ψ_1^d	ϵ	-10.909	-10.426	-10.019	-10.318	-10.318	-9.951	-9.815
	<i>q</i> _{CH₃}	...	0.08	0.10	0.09	0.09	0.14	0.13
ψ_2	ϵ_3	-11.030	-10.913	-10.817	-10.431	-10.420	-10.352	-10.057
	<i>q</i> _{CH₃}	...	0.00	0.00	0.06	0.06	0.07	0.10

^a Orbital energies in eV. ^b Fraction of charge summed over all CH₃ groups. ^c Lowest empty MO. ^d Highest occupied MO.

shifts, of course, but the most notable change is a fairly thorough mixing of the b_{1u} and b_{3g} MO's (the two highest occupied MO's) of PBQ in all the derivatives except tetramethyl PBQ, brought about by the reduction from D_{2h} symmetry.

The fact that the π Hamiltonian elements are nearly invariant from one methyl-substituted PBQ to the next might tempt one to try predicting spectra by use of these elements in a Hückel MO calculation. However, one would still need to compute the two electron integrals necessary for calculation of the energies of excited configurations. Moreover, the energies of the excited configurations of PBQ derivatives do not give good predictions of substituent effects; so one would need to perform a CI calculation as well. In particular, the energies of the lowest excited π - π configurations of the three dimethyl derivatives are nearly identical

(see Table V). It is only when configuration interaction is included that the CNDO method gives its good account of the effects of methyl substituents.

The origins of the inductive and conjugative effects may be qualitatively accounted for by the CNDO-CI calculations. Table VI indicates that the highest two occupied π orbitals are spread out appreciably onto the CH₃ groups of the substituted PBQ's whereas the lowest three empty π MO's are almost completely confined to the ring. Thus there is a significant charge transfer from CH₃ to ring when an electron undergoes a π - π^* excitation. (There follows some amount of rearranging of the charge transfer upon CI mixing.) The CI, however, does not bring about any additional charge transfer, as the configurations which would bring this about are of such high energy as to be of no importance. Thus the conjugative effect

seems to appear on the MO level. On the other hand, the CI seems to contain most of the inductive effect, the clearest evidence for this being the calculations of the three dimethyl isomers (Table V). In the perturbation model, the 2,3 isomer has the largest inductive effect of all the derivatives, while in the 2,5 and 2,6 isomers there is none. Since the CI step is necessary to match these results, the CI must account for much of the inductive effect.

Quantitatively, however, it does not seem possible to relate the inductive and conjugative parameters to such quantities as orbital energies, single configuration energies, CI matrix elements, or CI mixing coefficients. This would be possible if the single configurations corresponded to the unperturbed ring and substituent states of the perturbation method, and if the configurations were essentially the same for all the compounds (as are the ring states in the perturbation treatment). However, since the single configurations are built of MO's and since many of the MO's are different from one compound to the next, the single configurations of one derivative are different from those of the next, and comparison of, say, CI matrix elements for the two derivatives becomes meaningless in terms of calculating perturbation parameters.

Further evidence for the above claim comes from examination of the calculated shifts in energy between PBQ and its methyl derivatives. If the conjugative effect were described entirely by the single configuration energies, and if the inductive effect were described entirely by CI, the configuration energy shifts would be proportional to the number of CH₃ groups. Moreover, the CI would cause additional shifts only for the 2, 2,3, and 2,3,5 derivatives.² Table V shows that this is obviously not the case. Thus the inductive and conjugative effects must both contribute to changes in MO's, excitation, and CI, and there seems to be no simple way to calculate values for the inductive and conjugative parameters from intermediate quantities obtained from the CNDO-CI calculation.

Summary

Introduction of a substituent into the CNDO-CI framework produces (1) an expansion of the Hamiltonian but no important changes in the values of the matrix elements; (2) changes in MO's, MO energies, and configuration energies, and (3) changes in the extent of interaction among configurations; proper account of substituent effects occurs only upon CI. Introduction of a substituent into the perturbation framework produces (1) mixing of the states originally present in the parent compound as measured by the inductive parameter, and (2) mixing of substituent states with parent states as measured by the conjugative parameter. There seems to be no simple way to associate the individual steps of one method with those of the other. Thus there is no direct way of calculating inductive and conjugative parameters within the CNDO-CI method.

Proponents of the perturbation method of handling the effects of substituents on electronic spectra made the point long ago that one should think in terms of electronic states in discussing spectra rather than in terms of molecular orbitals.¹⁷ These calculations reinforce this point. Good account of the substituent effects here is not obtained at either the orbital stage or even the single configuration stage, but only when states have been constructed through configuration interaction.

Acknowledgments. The author would like to thank Professor H. H. Jaffé and Dr. R. L. Ellis for helpful discussions, R. W. Counts for an advance copy of program CNDO-S/CI, Dr. M. B. Robin for a prepublication copy of his photoelectron spectrum of PBQ, and the Worcester Area College Computation Center for a grant of computer time. The comments of an unnamed referee are gratefully acknowledged.

(17) J. R. Platt, personal communication.

Studies of the Ester Group. I. *Ab Initio* Calculations on Methyl Formate

by Håkan Wennerström,*^{1a} Sture Forsén,^{1a} and Björn Roos^{1b}

Division of Physical Chemistry 2, The Lund Institute of Technology, Chemical Center, S-220 07 Lund 7, Sweden, and Institute of Theoretical Physics, University of Stockholm, S-113 46 Stockholm, Sweden (Received February 18, 1972)

Publication costs assisted by The Lund Institute of Technology

Ab initio LCAO-MO-SCF calculations on the s-cis, s-trans, and 90° rotated conformations of methyl formate have been performed. A gaussian basis set of a double- ζ type was used. With possible errors taken into account, the calculations gave the estimates $\Delta H = 8 \pm 3$ kcal/mol and $\Delta H^+ = 13 \pm 2$ kcal/mol for the s-trans \rightleftharpoons s-cis interconversion in the gas phase. In a liquid of high polarity the estimate is $\Delta H = 4 \pm 5$ kcal/mol and $\Delta H^+ = 11 \pm 3$ kcal/mol. All these values are in agreement with experiments. The energy difference between the s-cis and s-trans conformations is interpreted as due to an electrostatic effect. A simple model for calculating such electrostatic contributions to conformational equilibria is proposed and also applied to the conformation problem of some molecules analogous to methyl formate.

Introduction

Methyl formate, the smallest carboxylic acid ester, can in many respects be regarded as a model compound for aliphatic esters. Quantum chemical calculations on methyl formate should accordingly give aspects of the structure of the ester bond. It is the main purpose of the present work to throw light on two phenomena involving this bond: the rotational barrier and the s-trans-s-cis conformation equilibrium.

During recent years a large number of *ab initio* quantum mechanical calculations on different chemical problems have been published. The rapidly developing computer technique has made it possible to perform calculations on increasingly larger molecules.

In the present work we report the results of an *ab initio* LCAO-MO-SCF calculation on the three conformations of the methyl formate molecule shown in Figure 1. Forms I and III possess a plane of symmetry, while II has no symmetry at all. Several experimental determinations and estimates have been made for both ΔH and ΔH^+ for the s-trans-s-cis interconversion reaction $I \rightleftharpoons (II) \rightleftharpoons III$, where II is an assumed approximate description of the transition state (*cf.* Table I). The presence of a rotational barrier is generally recognized as arising from the decrease of the conjugation between one ester oxygen lone pair and the carbonyl group, but the source of the energy difference between the s-cis and s-trans conformations is less well understood. A few suggestions have been put forward on the latter question and one of the aims of present work is to scrutinize these suggestions in the light of the theoretical calculations.

Schwartz, Hayes, and Rothenberg² have recently made an *ab initio* calculation on formic acid very analogous to the one reported here with respect to basis set and general approach to the problem. Their results are very similar to ours, indicating that the

carboxylic group and the corresponding ester group have many properties in common (*cf.* Table I).

Method of Calculation

A single SCF-type calculation was made on each of the three conformations I, II, and III. A computer program, REFLECT,^{3a} which can make computational use of molecular symmetry, was used for I and III, while the calculation for II was accomplished with IBMOL (version IV).^{3b} Details about the gaussian basis set are given in Table II. The basis set chosen gave 76 uncontracted and 48 contracted basis functions.

Recently it has been suggested that molecular optimized orbital exponents and contraction coefficients be used in *ab initio* calculations.⁴ This method was not used, since a test calculation on methanol using a methane optimized set for the carbon and a water optimized set for the oxygen showed that this choice was inferior to an analogous atom optimized set. It seems that one has to limit the use of molecular optimized basis sets to calculations on molecules very similar to those on which the optimization was made.

The long computer times, approximately 2 hr (IBM 360/75) for each calculation, and the restricted computer time at our disposal precluded a full geometry optimization. The geometry used for the s-trans conformation I was taken from the microwave spectroscopic study made by Curl.⁵ The geometries of II and III were obtained by a stiff rotation around the

(1) (a) Lund Institute of Technology; (b) University of Stockholm.

(2) M. E. Schwartz, E. F. Hayes, and S. Rothenberg, *J. Chem. Phys.*, **52**, 2011 (1970).

(3) (a) P. Siegbahn, *Chem. Phys. Lett.*, **8**, 245 (1971); (b) A. Veillard, IBMOL, Version IV, IBM manual.

(4) G. Wipff, U. Wahlgren, E. Kochanski, and J. M. Lehn, *Chem. Phys. Lett.*, **11**, 350 (1971).

(5) R. F. Curl, Jr., *J. Chem. Phys.*, **30**, 1529 (1959).

Table I: Experimental Determinations of ΔH and ΔH° of the s-Trans-s-Cis Conformation Change of Methyl Formate Compared with the Results of Reported Calculations

Method	ΔH , kcal/mol	ΔH° , kcal/mol	Phase	Ref
Ir	>2.7	13.1	Gas	<i>b</i>
Ultrasonic relaxation	2.3	10.1	Liquid	<i>c</i>
Ultrasonic relaxation	0.4	8.2	Liquid	<i>d</i>
Ultrasonic relaxation	6.2	11.9–12.2	Liquid	<i>e</i>
<i>Ab initio</i> calculations ^a	9.0	13.2		This work
<i>Ab initio</i> calculations on formic acid	8.1	13.0		2

^a Estimated errors not taken into account. ^b T. Miyazawa, *Bull. Chem. Soc. Jap.*, **34**, 691 (1961). ^c S. V. Subrahmanyam and J. E. Piercy, *J. Acoust. Soc. Amer.*, **37**, 340 (1965). ^d J. Bailey and A. M. North, *Trans. Faraday Soc.*, **64**, 1499 (1968). ^e K. M. Burundukov and V. F. Jakovlev, *J. Fiz. Chim.*, **42**, 2149 (1968).

Table II: Description of the Basis Set Used in the Calculations

	—Atoms—	
	C, O	H
Uncontracted basis functions	7s, 3p	3s
Contracted basis functions	4s, 2p	2s
Exponents	<i>a</i>	<i>b</i> (with the scale factor 1.34)
Contraction coefficients	<i>a</i>	<i>b</i>

^a From B. Roos and P. Siegbahn, *Theor. Chim. Acta*, **17**, 209 (1970). ^b From S. Huzinaga, *J. Chem. Phys.*, **42**, 1293 (1965).

O₍₂₎–C₍₁₎ bond of 90 and 180°, respectively, with the CH₃ group staggered relative to the O₍₂₎–C₍₁₎ bond.

Results

In Table III the calculated total energy and various other energy components for the three conformations are given. The result of a Mulliken population analysis is shown in Table IV. It should be noted that due to the limited number of hydrogen basis functions the population analysis tends to underestimate the formal populations on the hydrogen atoms. This also leads to an error in the calculated dipole moments. For conformation I this error is expected to approximately cancel, since the C₍₁₎–H₍₄₎ and C₍₂₎–H_(1,2,3) directions are nearly antiparallel. For conformations II and III there is no such cancellation and the calculated dipole moments for these are predicted to be too high. In Table V the electrostatic potentials at the nuclei are summarized. Various calculated one-

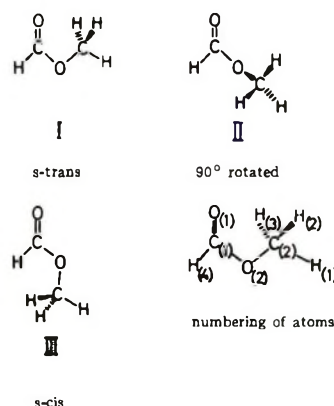


Figure 1. The different conformations of methyl formate on which calculations were made. Included is also the numbering of atoms used in the text. (The cis-trans convention is chosen to be in accordance with the one accepted for esters of larger carboxylic acids.)

electron properties for the s-trans conformation are compared with experimentally determined values and given in Table VI.

Discussion

(A) *Accuracy of the Calculation.* A crucial point in the calculation is the accuracy of the obtained total energies. A chemical interpretation of the obtained results is of course senseless if these have no significance. We have therefore tried to make at least a crude estimate of the errors involved. These can be divided into three kinds as due to: (i) the Hartree-Fock approximation, (ii) the use of a limited basis set, and (iii) the neglect of geometry optimization. As long as one is primarily interested in energy differences between different conformations of the same molecule, recent calculations⁶ have shown that it is possible to reach very good agreement, within less than 1 kcal/mol, with experimental values if a sufficiently large basis set is chosen. The errors of type ii resulting from the use of a limited basis set are more difficult to estimate. In the well-known case of ammonia,⁷ for example, the absence of d orbitals in the basis set has been found to introduce considerable errors owing to symmetry reasons. This particular aspect should, however, not be of importance in the present work. The effect on the total energy of an extension of the basis set may be inferred from other published *ab initio* calculations (for example, cf. ref 2 and 6). In general, calculated total energy differences do not change more than ca. 1 kcal/mol on going from a double- ζ to a larger basis set. There are thus reasons to believe that the method of calculation used gives a good measure of the energy difference between the conformations with the geometries chosen.

(6) See, for example, D. H. Christensen, R. N. Kortzeborn, B. Bak, and J. J. Led, *J. Chem. Phys.*, **53**, 3912 (1970).

(7) A. Rauk, L. C. Allen, and E. Clementi, *ibid.*, **52**, 4133 (1970).

Table III: Calculated Energy Components (au) of Three Conformations of Methyl Formate

Conformation	I	II	III	II - I	III - I
Total energy	-227.4404	-227.4194	-227.4261	0.0210	0.0143
Two-electron energy	203.4825	201.6164	200.5455	-1.8661	-2.9370
One-electron energy	-553.6086	-549.9299	-547.8761	3.6787	5.7325
Potential energy of the nuclei	122.6857	120.8941	119.9045	1.7916	2.7812
Kinetic energy	227.3917	227.4133	227.3751	-0.0216	0.0166
- $V/2T$	1.00011	1.00001	1.00011		

Table IV: Gross Atomic Populations

Nucleus	I	II	III	II - I	III - I
O1	8.52	8.46	8.49	-0.06	-0.03
C1	5.42	5.43	5.39	0.01	-0.03
O2	8.68	8.69	8.68	0.01	0.00
C2	6.24	6.24	6.25	0.00	0.01
H1	0.79	0.77	0.76	-0.02	-0.03
H2, H3	0.78	0.79 ^a	0.79	0.01	0.01
H4	0.79	0.83	0.85	0.04	0.06
Dipole moment, D	1.76	3.55	4.95		

^a A mean value for the two protons.

Table V: The Electrostatic Potential at the Nuclei

Conformation	Nucleus	Total potential	Potential from other nuclei	Potential from electrons
I	O ₍₁₎	-22.289	6.519	-28.807
II		-22.277	6.227	-28.544
III		-22.290	6.097	-28.387
I	C ₍₁₎	-14.557	9.112	-23.669
II		-14.555	9.112	-23.667
III		-14.553	9.112	-23.665
I	O ₍₂₎	-22.233	7.502	-29.735
II		-22.251	7.502	-29.753
III		-22.233	7.502	-29.735
I	C ₍₂₎	-14.640	7.520	-22.159
II		-14.626	7.319	-21.945
III		-14.621	7.211	-21.832
I	H ₍₁₎	-1.074	7.822	-8.896
II		-1.063	7.748	-8.812
III		-1.056	7.696	-8.751
I	H _{(2), H₍₃₎}	-1.079	8.555	-9.634
II		-1.068 ^a	8.298 ^a	-9.366
III		-1.058	8.157	-9.214
I	H ₍₄₎	-1.045	8.477	-9.522
II		-1.049	8.701	-9.750
III		-1.040	9.072	-10.111

^a A mean value for the two protons.

Table VI: Calculated and Experimental One-Electron Properties of the s-Trans Conformation of Methyl Formate

	Calcd	Exptl ^a
Dipole moment, D	1.76	1.77 ± 0.03
Angle with C=O bond, deg	37.5	39 ± 2
Quadrupole Moment in the Principal Axis System of the Moment of Inertia (10 ⁻²⁶ esu cm ²)		
Q_{xx}	4.15	2.3 ± 0.8 ^b
Q_{yy}	-4.77	4.2 ± 1.0 ^b
Q_{zz}	0.62	-6.5 ± 1.3 ^b
Second Moments of the Electron Distribution ^c (same axes as above)		
$\langle x^2 \rangle$	45.8	44.9 ± 1.4
$\langle y^2 \rangle$	19.2	18.2 ± 1.4
$\langle z^2 \rangle$	6.3	7.3 ± 1.4

Calculated Orbital Energies, au

σ symmetry	π symmetry
-20.65	-0.678
-20.60	-0.555
-11.41	-0.455
-11.31	
-1.494	
-1.393	
-0.997	
-0.819	
-0.735	
-0.668	
-0.595	
-0.520	
-0.452	

^a From ref 5. ^b From J. H. S. Wang and W. H. Flygare, *J. Chem. Phys.*, **53**, 4479 (1970). ^c In units of 10⁻¹⁶ cm².

In the calculations, no geometry optimization was carried out and thus the choice of actual geometry introduces a certain arbitrariness when comparison is

made with experiments. As bond lengths and bond angles are those determined experimentally for the s-trans form I, it can be assumed that this choice favors form I in the energy comparison, since *ab initio* calculations give geometries close to the experimentally determined ones. Exploratory calculations using the CNDO/2 method demonstrate that no great steric interactions are introduced when the methyl group is rotated. These calculations give no significant changes (less than 1 kcal/mol) in energy differences on bond length optimization. The *ab initio* results

on formamide in ref 6 show that no dramatic effects were obtained in the geometry optimization. The virial theorem is well fulfilled in the calculation for all three conformations (*cf.* Table III), which also indicates that the calculations have been performed with bond lengths close to equilibrium. As a reasonable estimate of the error in $(E_{II}) - (E_I)$ and $(E_{III}) - (E_I)$ due to uncertainties in the geometries, one can take 1 ± 1 kcal/mol. It should be remembered that the errors given above are the result of semi-empirical considerations and are only crude estimates.

(B) *The Energy Difference between the Trans and Cis Conformations of Aliphatic Esters.* To the summary of experimental determinations on the trans-cis interconversion of methyl formate given in Table I it can be added that there exists negative evidence indicating that the ΔG value of this interconversion process is at least 2.8 kcal/mol. This can be derived from the fact that even in very polar solutions the s-cis form has not been observed either by ir or nmr spectroscopy. The experimental ΔH values determined in solution are without exception smaller than the calculated energy difference ΔE for isolated molecules, even if the errors estimated in the preceding section are taken into account. The change in the trans-cis equilibrium of methyl formate which takes place when going from the gaseous to liquid phase will be primarily dependent on the difference in dipole moment of the two conformers and on the dielectric constant of the liquid medium. Onsager⁸ was one of the first to treat solute dipole-solvent interactions with some success. The Onsager model has been extended by several workers.⁹ These more elaborate models have the virtue of giving better agreement with experiments but have the drawback of being so complicated that they can be applied only to rather simple molecules. The Onsager theory⁹ gives, for the stabilization energy E_s of a molecule with dipole moment μ

$$E_s = \frac{\mu^2 (\epsilon - 1)}{a^3 (2\epsilon + 1)} \quad (1)$$

where a^3 is the molecular volume of the (spherical) solute and ϵ is the dielectric constant of the solvent. Although eq 1 contains many approximations, we feel that it gives a reasonably good measure of the factors influencing the gain in dipole stabilization energy when a molecule is brought from the gas phase into a dielectric medium.

As discussed above, the calculated dipole moment of I should be reliable, while those of II and III are expected to be overestimated. The bond moment method gives for III 3.04,¹⁰ 3.54,¹¹ or 4.6¹² D and the dipole moment of butyrolactone, where ring formation locks the ester in a cis type conformation, is 4.18 D.¹² If the dipole moment of III is taken as 4.1 D in eq 1, one obtains for the difference in stabilization energy between III and I, $E_s^{III} - E_s^I = 4.0$ kcal/mol in a

liquid of high polarity ($\epsilon > 30$). Owing to the uncertainties in the method and in the dipole moment of III, this figure has an estimated error of ± 2 kcal/mol.

Few experimental tests have been made of the influence of solvent polarity on the ΔH of the reaction $I \rightleftharpoons III$ and related reactions with other esters. Oki and Nakanishi¹⁰ obtained very solvent-dependent peaks in the ir spectrum of *tert*-butyl formate which they assigned to the s-cis form of the ester. If a $(\epsilon - 1)/(2\epsilon + 1)$ dependence of E_s is assumed, their experimental values give a crude estimate of 2.1 kcal/mol for $E_s^{cis} - E_s^{trans}$ for *tert*-butyl formate in a highly polar liquid.

In summary, we can say that the vapor-phase methyl formate exists practically exclusively in the s-trans form I, and that the high energy difference between I and III is only partially reduced when the molecule is brought into a liquid phase. The calculations give the estimate $(E_{III}) - (E_I) = 8 \pm 3$ kcal/mol in the gas phase and $(E_{III}) - (E_I) = 4 \pm 5$ kcal/mol in a liquid with $\epsilon > 30$. The mean values of the energy difference agree well with experiments, especially with those of ref 13 and 14 (see Table I), which indicates that the calculations have a greater accuracy than could be predicted without reference to experiments.

Several suggestions have been put forward to explain the energy difference between the s-trans and s-cis conformations of aliphatic esters. For a recent summary, see ref 10. Bailey and North¹⁵ conclude that the most important effect is the steric repulsion between the carbon chains in the alcohol and in the carboxylic acid forming the ester. For esters other than formate this is certainly an important factor, but for formates it is doubtful. The bulky *tert*-butyl formate, for example, has a higher population of the s-trans form than less bulky formates.¹⁰ The population analysis and the electron density maps furthermore show that the electron density increases on O₍₁₎ and H₍₄₎ when the methyl group is in their vicinity. The effect of a steric repulsion should be the reverse. Owen and Sheppard¹⁶ suggest that oxygen lone-pair repulsion is an important factor in the determination of the most stable conformation. Since lone pair-lone

(8) L. Onsager, *J. Amer. Chem. Soc.*, **58**, 1486 (1936).

(9) See, for example, R. J. Abraham, L. Cavalli, and K. G. R. Pachler, *Mol. Phys.*, **11**, 471 (1966).

(10) M. Oki and H. Nakanishi, *Bull. Chem. Soc. Jap.*, **43**, 2558 (1970).

(11) R. J. B. Marsden and L. E. Sutton, *J. Chem. Soc.*, 1383 (1936).

(12) E. Bock, *Can. J. Chem.*, **45**, 2761 (1967).

(13) T. Miyazawa, *Bull. Chem. Soc. Jap.*, **34**, 691 (1961).

(14) S. V. Subrahmanyam and J. E. Piercy, *J. Acoust. Soc. Amer.*, **37**, 340 (1965).

(15) J. Bailey and A. M. North, *Trans. Faraday Soc.*, **64**, 1499 (1968).

(16) L. Owen and N. Sheppard, *Proc. Chem. Soc. London*, 264 (1963).

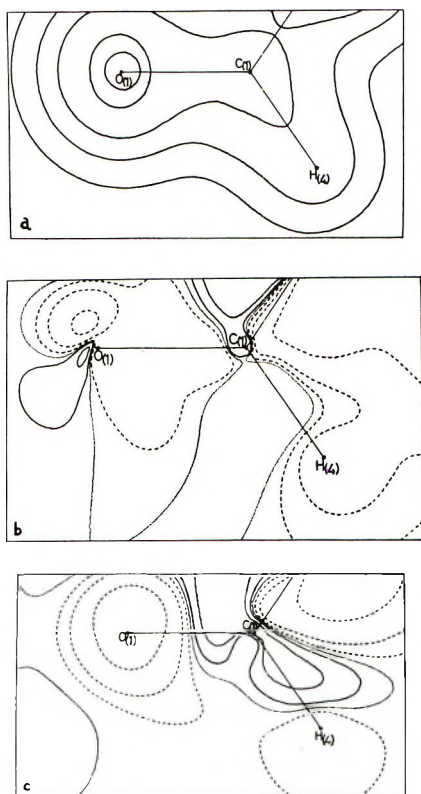


Figure 2: The electron density in the formyl part of methyl formate in a plane through the atoms: (a) total density of the *s*-trans conformation, contours 3.0, 1.0, 0.3, 0.1, and 0.03; (b) difference density between I and III, contours 0.01, 0.003, 0.001 (solid lines), ± 0.0 (dotted lines), -0.001 , -0.003 , and -0.01 (dashed lines); (c) difference density between I and II, contours as in b.

pair repulsion has no direct definition in a Hartree-Fock calculation, it is difficult to say if it is important or not. One would, however, expect the following consequences: (i) a decrease in electron density in the region between the two oxygen atoms, especially in the region close to the carbonyl oxygen, in the *s*-cis conformation (*cf.* Figure 2b); (ii) characteristic changes in overlap populations between the oxygen in some orbitals containing large coefficients at the oxygen; and (iii) characteristic changes of orbital energies of orbitals of the lone-pair type. None of these effects is found however, and it may be said that the calculations in no way support the theory of lone pair-lone pair repulsion. It should be remembered that the oxygen atoms in the present case are separated by two chemical bonds, and the situation can be quite different if the oxygens are directly bonded, as, for example, in hydrogen peroxide. Marsaen and Sutton¹¹ suggest that the energy difference between the *s*-trans and *s*-cis conformations of esters could be partially accounted for by considering the interaction between the $O_{(1)}-C_{(1)}$ and $O_{(2)}-C_{(2)}$ bond dipoles. This picture is supported by the present study. It seems, however, to be both simpler and more elucidating to handle these electro-

static interactions as forces between point charges placed at the nuclei instead of forces between bond dipoles. In the present case of methyl formate, the formal atomic charges can be obtained from the population analysis. Figure 3 shows the relevant gross atomic charges. The electrostatic energy is then simply obtained from $\sum_{i<j} q_i q_j / r_{ij}$. Owing to the uncertainties in the individual charges in the methyl group (*cf.* above), the latter is treated as a single entity. The difference in Coulomb energy between III and I is 7.5 kcal/mol (if the atoms in the methyl group are treated separately, one gets $\Delta E = 10$ kcal/mol), in good agreement with the 9.0 kcal/mol obtained in the *ab initio* calculation, indicating that the electrostatic effects are of major importance in determining the most stable conformation. This conclusion is further supported by the population analysis and by the values of the electrostatic potentials at the nuclei. Table IV shows that the effect of going from I and III is a drift of electrons from $O_{(1)}$ and $C_{(1)}$ toward $H_{(4)}$ to obtain a screening of the $H_{(4)}$ nucleus from the positive methyl group. Table V shows that the methyl group nuclei have a marked higher potential in III than in I, which is expected from an electrostatic model. Against this electrostatic picture it can be argued that it is in a way senseless to talk about formal charges of atoms in molecules. At long distance, however, the Coulomb interactions become increasingly important and the details of the electronic distribution are then of lesser significance. The mere presence of a rotational barrier clearly shows that other factors than the electrostatic ones are important, and this should of course be kept in mind.

A more detailed picture of the difference between the *s*-trans and *s*-cis conformations in what regards the electronic densities is given in Figures 2a and 2b. Figure 2a shows the electron density for I in the symmetry plane. Only the part of the molecule which is not directly affected by the rotation is shown. Figure 2b shows the corresponding difference in electron densities between I and III. Figure 4 illustrates the corresponding results for the π electrons 1 Å above the symmetry plane. The "in-plane" picture, Figure 2b, shows a complicated pattern. In the *s*-trans form the methyl group seems to repel the electrons at the carbonyl oxygen, making them go to the far side of the atom. The other clear feature is that the electron density on the $H_{(4)}$ atom has increased in the *s*-cis form. From the differences between the π -electron densities in Figure 4b, it is evident that there is an increased polarization of the π -carbonyl bond toward the oxygen atom in the *s*-trans form.

(C) *The Rotational Barrier.* It is usually assumed that the conversion between *s*-trans and *s*-cis conformations of esters proceeds *via* a rotation of the methyl group. The possibility that the conversion involves an inversion at the ester oxygen cannot be definitely

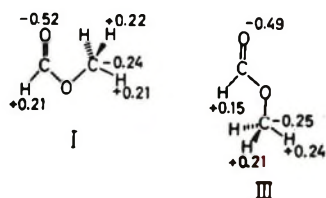


Figure 3. Gross atomic charges of the I and III conformations of methyl formate (only those charges are given which are relevant for the calculation of electrostatic effects).

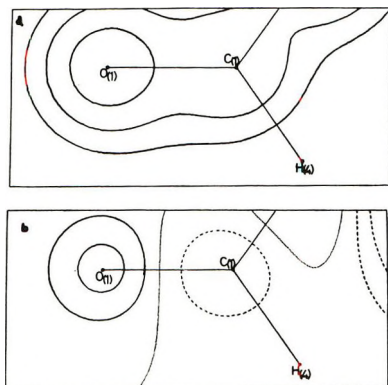


Figure 4. The π -electron density in the formyl part of methyl formate in a plane parallel with and 1 au above the plane through the atoms: (a) total density of I, contours 0.3, 0.1, and 0.03; (b) difference density between I and III, contours as in Figure 2b.

excluded, though both CNDO calculations,¹⁷ *ab initio* minimal basis calculations, and infrared spectroscopic observations¹³ indicate the preference of the rotational pathway. The barrier is generally assumed to arise from the interruption of the conjugation between the carbonyl π bond and the π lone pair of the ester oxygen.

The calculated height of the barrier is affected by mainly two errors. The geometry of the transition state of the rotation is to no extent given by symmetry, and the assumed geometry can only be regarded as a first guess. The present results indicate that a higher energy value should be obtained by rotating the methyl group more toward the s-cis conformation (*cf.* the discussion on formic acid in ref 2). It can be expected that the lack of geometry optimization partly cancels this error. The solvent effects discussed above are of course important if the barrier to internal rotation is considered in the liquid phase. Since II has a dipole moment intermediate between those of I and III, the solvent effect is smaller and can be estimated to lower the barrier 2 ± 1 kcal/mol relative to the energy of the s-trans conformation. The first error mentioned above is more difficult to estimate, but cancellation of errors should occur and an uncertainty of ± 1 kcal/mol is a reasonable value. This gives for the barrier to internal rotation, taking the errors under part A into

account, of $\Delta H^\ddagger = 13 \pm 2$ kcal/mol in the gas phase and $\Delta H^\ddagger = 11 \pm 3$ kcal/mol in the liquid phase. Here again, the experimental values are well within the error bounds. New information on the rotational barrier problem is given in the present work by the electron density plot and the population analysis. Figure 2c shows how the $O_{(1)}$ atom has an electron deficiency in the $O_{(1)}-C_{(1)}-O_{(2)}$ plane in the conformation I. The population analysis (Table IV) shows that this deficiency is compensated by an increased π -electron density.

(D) *One-Electron Properties of the Trans Conformation of Methyl Formate.* The s-trans conformation of methyl formate is the only experimentally observed one, and for this form several one-electron properties have been experimentally determined. These properties have also been obtained from the wave function obtained in the *ab initio* calculations. A comparison between experimental and calculated values is given in Table VI. The excellent agreement in dipole moment in absolute magnitude and direction is remarkable for such a complicated molecule and is probably to a certain degree due to cancellation of errors. The quadrupole moments, on the contrary, show a discrepancy between calculated and experimental values not usually found in calculations with the basis set used. An analysis shows that the error probably arises from an incorrect value of the z component of the second moment of the charge distribution. The calculation is performed with the molecule rigidly in the symmetry plane, but the actual molecule has low-energy torsional vibrations¹³ (325 cm^{-1}), causing an increase in $\langle z^2 \rangle$ for both electrons and nuclei.

The second moment of the electronic distributions agree within the limits of error of the experimental value. The second moments should be correct, since they are but a crude measure of the geometry of the molecule. The small difference between $\langle z^2 \rangle_{\text{exptl}}$ and $\langle z^2 \rangle_{\text{calcd}}$ is sufficient to give the large differences in quadrupole moment, showing the large sensitivity of quadrupole moments to the electronic distribution.

Final Remarks

The main result of the present calculation is that a simple electrostatic picture is able to explain the energy difference between the s-trans and s-cis conformations of methyl formate. The nature of this explanation suggests that electrostatic effects may be a general factor in determining conformations of simple organic molecules and in particular their dihedral angles. It is revealing to compare methyl formate with the analogous molecules formic acid, propionaldehyde, methyl nitrite, and *N*-methylformamide (see Chart I). In formic acid ΔE is great and the calculations in ref 2 give the same interpretation as the present one for

(17) W. Egan, private communication.

Chart I: The Stable Conformations of Formic Acid, Propionaldehyde, Methyl Nitrite, and *N*-Methylformamide and the Experimentally Determined Energy Difference between Them

s-Trans type	s-Cis type	ΔE , kcal/mol	Ref
		> 4 (gas phase)	<i>a</i>
		0.900 (gas phase)	<i>b</i>
		0.800 (liquid phase)	<i>c</i>
		0.275 (gas phase)	<i>d</i>
		- 0.2 (liquid phase)	From <i>e</i>
		+ 1.3 (liquid phase)	<i>f</i>

^a D. R. Lide, Jr., *Annu. Rev. Phys. Chem.*, **15**, 234 (1964).

^b S. S. Butcher and E. B. Wilson, Jr., *J. Chem. Phys.*, **40**, 1671

(1964). ^c G. J. Karabatsos and N. Hsi, *J. Amer. Chem. Soc.*, **87**, 2864 (1965).

^d P. T. Inglefield, E. Krakower, L. W. Reeves, and R. Stewart, *Mol. Phys.*, **15**, 65 (1968).

^e W. D. Gwinn, R. J. Anderson, and D. Stelman as cited in O. Bastiansen, H. M. Seip, and J. E. Boggs in "Perspectives in Structural Chemistry," Vol. IV, J. D. Dunitz and J. A. Ibers, Ed., Wiley, New York, N. Y., 1971, p 122.

^f T. Drakenberg, K.-I. Dahlqvist, and S. Forsén, *J. Phys. Chem.*, in press.

ab initio value 8.1 kcal/mol. Propionaldehyde is different from the other molecules in the series in not having any π conjugation. The charge of carbon atoms in a chain is generally considered to alternate, and this gives a small predicted net charge on the methyl group¹⁸ which in turn should tend to make the trans type conformation the most stable. If the charge of the oxygen atom and the aldehyde proton are taken as -0.5 and $+0.2$, respectively, the experimental energy difference is reproduced with a methyl group charge $+0.07$, which seems a reasonable value. In methyl nitrite the cis type conformation is the most stable in solution, the trans type in the gas phase. The value of ΔE in the gas phase is approximately 2 kcal/mol less than an electrostatic model predicts. This discrepancy could be interpreted as the effect of a steric repulsion between the double-bonded oxygen and the methyl group, which is not compensated by a similar repulsion in the cis type conformation, since no formyl hydrogen is present. A nitrogen lone pair-oxygen lone pair repulsion could also give important contributions. In *N*-methylformamide the methyl group is expected to have a greater formal charge than the amide hydrogen owing to its greater electron donation power. An electrostatic consideration then predicts the most stable conformation correctly (*cf.* ref 19). To conclude, it can be stated that electrostatic interactions between atoms or groups three or more bonds apart are often important in determining the conformation of small organic molecules.

Acknowledgments. Part of this work was supported by grants from the Natural Science Research Council and The Board for Technical Development. Dr. Jan Almlöf is heartedly thanked for his indispensable assistance with the numerical computations. We are indebted to Dr. William Egan for revising the English of the manuscript.

methyl formate. With the use of atomic populations from ref 2, a point-charge calculation of ΔE gives $\Delta E = 11$ kcal/mol, in reasonable agreement with the

(18) See, for example, G. J. Karabatsos and P. J. Fenoglio, *Top. Stereochem.*, **5**, 175 (1970).

(19) T. Drakenberg, K.-I. Dahlqvist, and S. Forsén, *J. Phys. Chem.*, in press.

Determination of the Partial Specific Volume of Macromolecular Solutes from Light Scattering

by Wilfried Heller

Department of Chemistry, Wayne State University, Detroit, Michigan 48202 (Received July 12, 1971)

Publication costs borne completely by The Journal of Physical Chemistry

It is shown that light scattering can be used for determining the partial specific volume, \bar{V} , of a solute provided its molecular weight is known. The only additional quantities needed are (1) dn/dc and (2) the specific refraction of the substance which forms the solute. The latter information is not needed if one merely wants to determine changes in \bar{V} as a function of experimental conditions, rather than absolute values of \bar{V} . The precision of the latter values is defined by the square root of the precision of light scattering data.

I. Introduction

The application of light scattering to the study of macromolecular solutions has, in general, as its objective the determination of the molecular weight of the solute. In addition, or instead, the numerical values of the parameter(s) defining the shape or conformation of a nonspherical scattering body may be determined in favorable cases. Still another application of light scattering which is virtually unknown is its potential use for determining the partial specific volume of a solute, \bar{V} . In view of considerable recent interest in the value of \bar{V} of macromolecular solutes and in its change as an indicator of changes in molecular conformation or of the interaction between polar groups and water¹ in aqueous solution, it appears of interest to survey briefly the respective potential of the light scattering method. The discussion shall be restricted to solutes which dimensionally are small compared to the wavelength used, so that the simple Debye equation of light scattering is applicable.

II. The Basic Equations

Inspection of the Debye equation shows that its use alone cannot provide information on \bar{V} on the basis of a set of sufficiently simple experiments. This, however, becomes possible on taking advantage of an auxiliary equation which correlates \bar{V} with the quantity dn/dc , i.e., with the rate of change, with the concentration c of the solute, in the refractive index of the solution. Such an equation follows readily from the combination of two equations given previously,² viz.

$$\bar{V} = \frac{k}{A} - f(dn/dc) \quad (1)$$

where

$$f = 2n_1 \frac{(1-A)^2}{3A} = \frac{6n_1}{(n_1^2 + 2)(n_1^2 - 1)}$$

$$A = (n_1^2 - 1)/(n_1^2 + 2)$$

n_1 is the refractive index of component 1 (solvent) and k is, as discussed presently, numerically identical with k_0 ,³ the specific refraction of component 2 (solute), prior to mixing with component 1

$$k_0 = [(n_2^2)_0 - 1]/[(n_2^2)_0 + 2]\rho_{2_0} \quad (2)$$

ρ_{2_0} and n_{2_0} being the density and refractive index, respectively, of the pure component 2. These quantities are either known or easily determined.

A simple rearrangement of the Debye light scattering equation leads to

$$\frac{dn}{dc} = \frac{\lambda_0^2}{\pi n_1} \left(\frac{N_A}{2M} \right)^{1/2} \left(\frac{R_{90}}{c} \right)^{1/2} \quad (3)$$

Here, λ_0 is the vacuum wavelength used in the light scattering experiments, N_A is Avogadro's number, M is the molecular weight of the solute, and R_{90}/c is the specific intensity of light scattering at an angle θ of 90° with respect to the direction of the incident beam ($\theta = 90^\circ$ is selected here because this yields the simplest form of the equation). Substituting eq 3 into eq 1 yields, since $k = k_0$

$$\bar{V} = \frac{k_0}{A} - \frac{F}{M^{1/2}} \left(\frac{R_{90}}{c} \right)^{1/2} \quad (4)$$

where

$$F = \frac{\lambda_0^2}{3\pi} \frac{(1-A)^2(2N_A)^{1/2}}{A} = \frac{3\lambda_0^2}{\pi} \frac{(2N_A)^{1/2}}{(n_1^2 + 2)(n_1^2 - 1)}$$

The value of \bar{V} can therefore, in principle, be determined from a simple light scattering experiment if M and k_0 are known. If the former is unknown, it can

(1) J. Rasper and W. Kauzmann, *J. Amer. Chem. Soc.*, **84**, 1774 (1962); W. Kauzmann, *Biochim. Biophys. Acta*, **28**, 87 (1958); A. Ikegami, *Biopolymers*, **6**, 431 (1968); M. J. Hunter, *J. Phys. Chem.*, **70**, 3285 (1966).

(2) Equations 4 and 8a in W. Heller, *J. Polym. Sci., Part A-2*, **4**, 209 (1966).

(3) W. Heller and E. S. E. Schwartz, to be published.

readily be determined by carrying out a measurement of dn/dc using the conventional Debye equation. As regards k_0 , its numerical value and that of the constant k , which pertains to n_2 and ρ_2 of the solute *after* mixing with component 1, are, as stated, in general the same. Thus, the k value derived from eq 1 for five proteins in aqueous solution using densitometric and refractometric literature data³ averages out to 0.2540, the average departure from this value being ± 0.0015 . On the other hand, the k_0 value obtained from refractive index and density data of the literature for a crystal of chemically modified albumin is 0.2547. Thus, k_0 and k are practically the same although the apparent refractive index of the solute, n_2 , and its apparent density, ρ_2 , differ appreciably from n_{2_0} and ρ_{2_0} , respectively. The situation is the same for the simpler case of a solution of a nonpolar solute in a nonpolar solvent. This was tested for polystyrene.⁴ Here, the k_0 value derived from eq 2 from the density and refractive index of solid polystyrene, 0.32519, gives, on assuming that $k = k_0$, an average apparent specific volume of 0.9295 in various solvents which compares well with an average of 0.921 calculated from experimental data given in the literature.⁴

III. Determination of Changes in \bar{V}

If one is not interested in \bar{V} itself, but only in its change, $\Delta\bar{V}$, as a function of experimental conditions, one has, at constant n_1 , for the transition from state 1 to state 2 simply

$$\Delta\bar{V} = \bar{V}_1 - \bar{V}_2 = -F'_1(R_{90}/c)_1^{1/2} + F'_2(R_{90}/c)_2^{1/2} \quad (5)$$

where $F'_n = F/M_n^{1/2}$.

If M is constant also

$$\Delta\bar{V} = -F''\Delta(R_{90}/c)^{1/2} \quad (5a)$$

where

$$F'' = \frac{F'}{M^{1/2}}$$

While the simplicity of eq 5a seems to make the light scattering method extremely attractive for $\Delta\bar{V}$ measurements, at least in principle, the discussion in section IV will show that it will actually be useful for such differential measurements only if $\Delta\bar{V}$ is sufficiently large.

IV. Discussion

The optical method proposed here has several advantages over nonoptical methods. They are (1) measurements are possible without interfering in any way with the system; (2) the size of the sample needed is, except for the diver technique, incomparably smaller than required with conventional densitometric or dilatometric methods; and (3) measurements of fast changes in \bar{V} are possible since no inertia effects exist (such as those caused by viscosity in the densitometric

diver technique). Advantages 1 and 3 are shared with the refractometric method proposed previously.³ The latter, on the other hand, requires a larger sample size.

An important consideration in the choice of a method for determining \bar{V} is the precision attainable. This is defined by the experimental uncertainty in light scattering measurements which, in general, is not in excess of 1–2%. Therefore, for a given n_1 and k_0 , the nonsystematic uncertainty in the \bar{V} values obtained should not be in excess of 2–4%. The precision of the \bar{V} value obtained by light scattering will, therefore, be sufficient for many purposes. On the other hand, the precision of $\Delta\bar{V}$ values will be sufficient only when changes in \bar{V} are reasonably large.

It is important to note that the \bar{V} values obtained by nonoptical methods, by the refractometric method, and by the light scattering method may not be the same but may show analytically very useful differences. While these differences in \bar{V} should, in general be only minor, major differences can be anticipated for the $\Delta\bar{V}$ values obtained by the various methods whenever changes in \bar{V} are due to changes in (a) molecular weight, or (b) molecular shape, or (c) the degree of solvation of the solute. Any of these changes may occur on changing pH or ionic strength in aqueous solution, the nature of the solvent, or the temperature. As regards changes in M , the light scattering method will be exceedingly sensitive to them, while the refractometric method and densitometric method will be completely insensitive to them provided $M > 30,000$.⁵ As regards factor b, the light scattering method will be very sensitive to it, the refractometric method will be relatively insensitive to it, and the nonoptical methods of \bar{V} determinations will rank in sensitivity between the other two.⁶ Thus, the change in specific scattered intensity found by Doty, *et al.*,⁷ in two different solvents for poly-(benzyl-L-glutamate) amounting to 6–7% and explained by the authors as the result of conformational differences is unquestionably due largely to this difference. However, it is now clear that a change in \bar{V} should be considered as an additional factor contributing to the change in light scattering. On the other hand, dilatometric or densitometric data will reflect exclusively changes in \bar{V} during conformational transitions. As regards factor c, changes in the degree of electrostriction, resulting from changes in solvation in the case of aqueous solutions of polar solutes, should affect primarily the densitometric results, but relatively little the

(4) W. Heller, *J. Polym. Sci., Part A-2*, **4**, 209 (1966).

(5) According to M. L. Huggins, who evaluated the M dependence of n_2 and ρ_2 in *J. Amer. Chem. Soc.*, **63**, 116, 916 (1941); **76**, 843 (1954).

(6) O. Wiener evaluated the effect of shape upon the refractive index of solutes in *Leipziger Ber.*, **62**, 256 (1910). The effect is relatively small.

(7) P. Doty, J. K. Bradbury, and A. M. Holzer, *J. Amer. Chem. Soc.*, **78**, 947 (1956); see particularly Table II.

results obtained with either of the two optical methods unless electrostriction is large enough to affect the polarizability of the solute significantly.

It follows from this discussion that one can expect to get valuable additional information on the behavior of a

solute by considering the differences of results on the apparent \bar{V} or on changes in \bar{V} obtained by a nonoptical method, on the one hand, and one or both of the optical methods on the other hand, whenever all yield quantitatively significant results.

Nuances of the $\bar{E}CE$ Mechanism. IV. Theory of Cyclic Voltammetry and Chronoamperometry and the Electrochemical

Reduction of Hexacyanochromate(III)¹

by Stephen W. Feldberg^{*2a} and Ljubomir Jeftic^{2b}

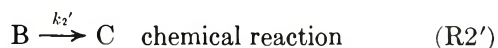
Brookhaven National Laboratory, Upton, New York 11973, and
Rudjer Boskovic Institute, Zagreb, Yugoslavia (Received February 14, 1972)

Publication costs assisted by the U. S. Atomic Energy Commission

The $\bar{E}CE$ mechanism in its simplest form is: $e^- + A \rightleftharpoons B$, electron transfer, R1; $B \rightarrow C$ (k_2), chemical reaction, R2; $C \rightleftharpoons D + e^-$, electron transfer, R3; $A + C \rightleftharpoons B + D$ (k_4 forward, k_{-4} reverse), redox cross reaction, R4. The dependence of the current on time and on the various kinetic parameters is calculated for cyclic voltammetry, chronoamperometry, and chronocoulometry. A preliminary investigation of the reduction of hexacyanochromate(III) in 2 M NaOH is presented as an example of the $\bar{E}CE$ mechanism. Reaction R2 corresponds to water substitution (or cyanide ejection) of the hexacyanochromate(II) species with $k_2 = 11 \text{ sec}^{-1}$. Reaction R4 corresponds to a homogeneous electron transfer between hexacyanochromate(III) and aquohydroxychromate(II) with $k_4 \approx 10^4 \text{ M}^{-1} \text{ sec}^{-1}$.

Introduction

The classical ECE mechanism is usually presented



The mechanism has been the subject of many publications,³⁻⁶ the majority of them considering only those cases where n_3 and n_1 both have the same sign, *i.e.*, reactions R1' and R3' are both reductions or both oxidations. A few workers,^{4,5} however, have considered the case where n_1/n_3 is negative. We shall refer to this modification as the $\bar{E}CE$ mechanism (as distinguished from the classical $\bar{E}CE$), and for the case where $n_1 = -n_3 = 1$, it would be written



In several previous papers in this series³ we have pointed out the modifying effects of reaction R4' on the behavior of the $\bar{E}CE$ mechanism. The analogous effect of R4 on the behavior of the $\bar{E}CE$ is considerably more interesting. In the present paper we shall

(1) This work was performed under the auspices of the United States Atomic Energy Commission.

(2) (a) Brookhaven National Laboratory; (b) Rudjer Boskovic Institute.

(3) (a) S. W. Feldberg, *J. Phys. Chem.*, **75**, 2377 (1971), and references therein; (b) M. D. Hawley and S. W. Feldberg, *ibid.*, **70**, 3459 (1966); (c) R. N. Adams, M. D. Hawley, and S. W. Feldberg, *ibid.*, **71**, 851 (1967).

(4) (a) N. Tanaka and K. Ebata, *J. Electroanal. Chem.*, **8**, 120 (1964); (b) E. Fischerová, O. Dražka, and M. Meloun, *Collect. Czech. Chem. Commun.*, **33**, 473 (1968).

(5) H. B. Herman and P. M. Surana, presented at the 162nd National Meeting of the American Chemical Society, Washington, D. C., 1971; submitted for publication.

(6) G. S. Alberts and I. Shain, *Anal. Chem.*, **35**, 1959 (1963).

discuss the unusual manifestations of this mechanism (reactions R1-R4) in cyclic voltammetry and chronoamperometry.

Calculations were carried out by digital simulation⁷ on a Control Data Corp. 6600. Voltammograms and working curves were generated on the Calcomp CRT.

Theory

The equilibrium constant for reaction R4 of the $\bar{E}CE$ mechanism is

$$K_4 = \frac{[B][D]}{[A][C]} = k_4/k_{-4} \quad (1)$$

where k_4 and k_{-4} are the rate constants for the electron-transfer reaction. The value of K_4 is, of course, directly related to E_1^0 and E_3^0 , the E^0 's for reactions R1 and R3, respectively

$$K_4 = \exp\left[\frac{F}{RT}(E_1^0 - E_3^0)\right] \quad (2)$$

Just as in the case of the classical $\bar{E}CE$, there is an infinity of combinations of rate terms (k_2 , k_{-2} , k_4 , k_{-4}) which effects different mechanistic behavior. It is clearly impossible to consider every possible combination; several cases of interest, however, can be considered, and these will shed light on the more general behavioral characteristics of the $\bar{E}CE$.

To calculate some sample cyclic voltammograms, the kinetic problem will be reduced to two variables: k_2 and K_4 . Three values of K_4 will be considered: (1) $E_3^0 = E_1^0 + 0.3$ V ($K_4 < 10^{-6}$; assume $K_4 = 0$), (2) $E_3^0 = E_1^0$ ($K_4 = 1$), (3) $E_3^0 = E_1^0 - 0.3$ V ($K_4 > 10^{+6}$; assume $K_4 = \infty$). For each of these three cases we shall consider two limiting possibilities: (A) reaction R4 is always in equilibrium, i.e., k_4 and/or k_{-4} is infinitely fast; (B) reaction R4 is nonoperable, i.e., $k_4 = k_{-4} = 0$. In Figures 1-4, the cyclic voltammograms for each of the six possibilities, 1A, 1B, 2A, 2B, 3A, 3B, are shown for several values of k_2^* , where

$$k_2^* = \frac{k_2}{\frac{F}{RT} \frac{dE}{dt}}$$

(The voltammograms for $k_2^* = 0$ are not shown but are identical with those of Figure 1, ref 3a.) In each case two cycles were calculated. In these and subsequent calculations the following assumptions are made: diffusion coefficients of all species are the same, semiinfinite linear diffusion obtains, and the heterogeneous one-electron transfers are infinitely fast.

One observes some rather startling behavior for case 3A voltammograms reflecting the catalytic conversion of species A to D (reaction R4). For larger values of the normalized rate constant k_2^* (Figure 4), the current actually changes sign during the first cathodic sweep. By the time the second cathodic sweep has begun, virtually all of species A has been removed

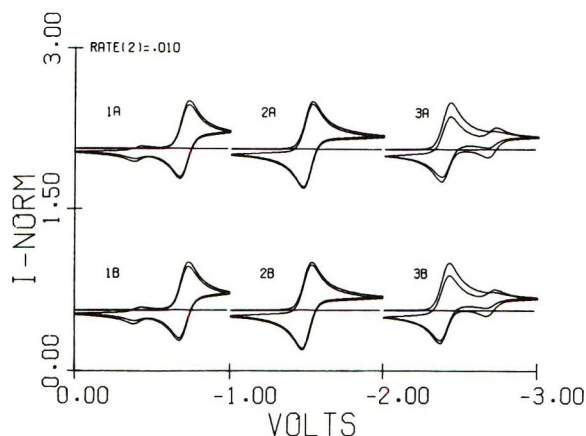


Figure 1. $RATE(2) = (k_2 RT/F)(dE/dt)^{-1} = 0.01$. Abscissa and ordinate indicate scale rather than absolute values:

$I-NORM = i^0 / (nFA_{bulk} \sqrt{D(F/RT)(dE/dt)})$ and $E_{rev} = E_{start} - 1.0$ V. For 1A and 1B $\bar{E}CE$'s, $E_1^0 = E_{start} - 0.7$ V and $E_3^0 = E_{start} - 0.4$ V. For 2A and 2B $\bar{E}CE$'s, $E_1^0 = E_3^0 = E_{start} - 0.5$ V. For 3A and 3B $\bar{E}CE$'s, $E_1^0 = E_{start} - 0.4$ V and $E_3^0 = E_{start} - 0.7$ V. Heterogeneous one-electron transfers are infinitely fast.

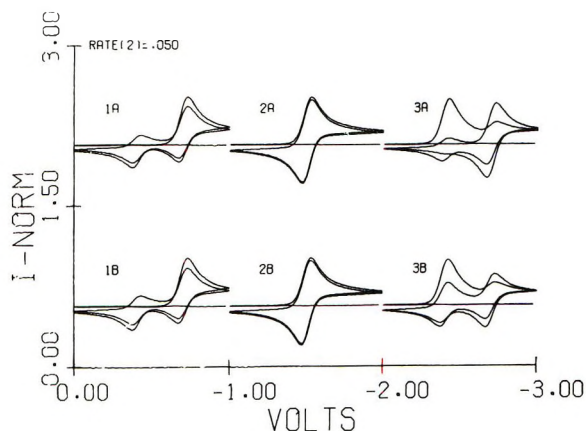


Figure 2. $RATE(2) = 0.05$. See Figure 1 caption for details.

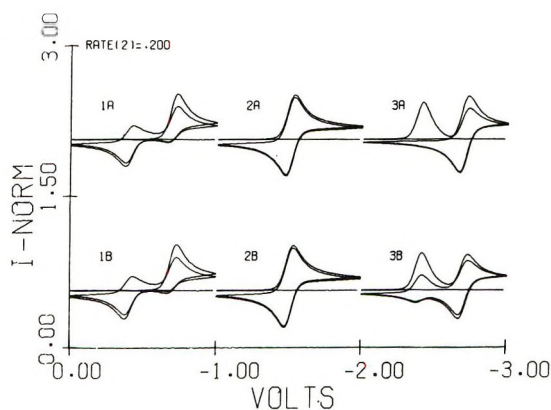


Figure 3. $RATE(2) = 0.20$. See Figure 1 caption for details.

(7) S. W. Feldberg, "Electroanalytical Chemistry," Vol. 3, A. J. Bard, Ed., Marcel Dekker, New York, N. Y., 1969, p 199; S. W. Feldberg, "Computer Applications in Analytical Chemistry," H. B. Mark, Ed., Marcel Dekker, New York, N. Y., 1972, p 185.

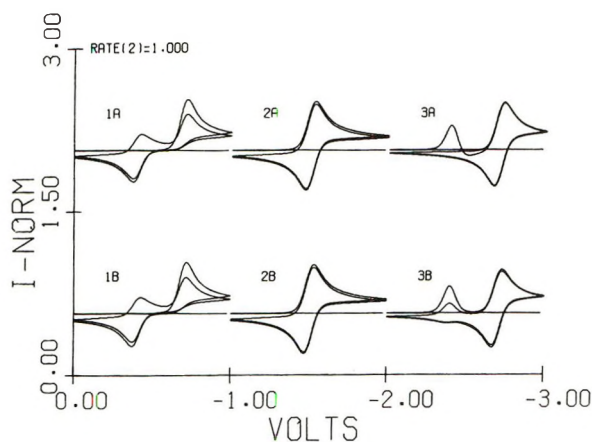


Figure 4. RATE(2) = 1.00. See Figure 1 caption for details.

from the diffusion layer and one sees essentially the reversible cyclic voltammogram for reaction R3. Because the catalytic removal of species A by reactions R4 and R2 cannot occur in the case 3B voltammograms, the effects are less dramatic.

Cases 2A and 2B are quite predictably uninteresting, since both the R1 and R3 couples have the same E^0 .

Cases 1A and 1B cyclics differ only slightly from each other. On the first cathodic sweep they are identical, exhibiting characteristics of an EC^s reaction, since the product of reaction R2, species C, cannot oxidize at the electrode surface and since the equilibrium for reaction R4 is all the way to the left. Small differences between 1A and 1B behavior arise after 0.5 cycle when species D is generated on the first anodic sweep and reaction R4 can proceed to the left. Spectroelectrochemical techniques capable of distinguishing species in the diffusion layer can, of course, make distinctions that electrochemistry alone cannot.⁹ (For case 2A or case 2B, systems where electrochemistry yields no information, auxiliary spectral techniques are essential.) Although there is superficial similarity between case 1 $\vec{E}\vec{C}\vec{E}$ and case 1 $\vec{E}\vec{C}\vec{E}$,^{3a-c,8} one will note that in the latter case the height of the second cathodic peak increases markedly as RATE(2) increases from 0 to 1. The corresponding peak of the case 1 $\vec{E}\vec{C}\vec{E}$ exhibits almost no change in height.

Chronoamperometry is of interest only when the conditions of case 3 exist¹⁰ and only when the potential is stepped from positive of E_1^0 to a potential between E_1^0 and E_3^0 so that the following surface boundary conditions exist before ($t < 0$) and during ($t \geq 0$) electrolysis

$$t < 0: A_{x=0} = A_{\text{bulk}} \quad (3)$$

$$t \geq 0: A_{x=0} = 0; C_{x=0} = 0 \quad (4)$$

The relationship between n_{app} , where

$$n_{\text{app}} = \frac{\pi^{1/2} D^{1/2} t^{1/2}}{F D^{1/2} A_{\text{bulk}}} \quad (5)$$

and the rate parameter $\log k_2 t$ is shown in Figure 5 for

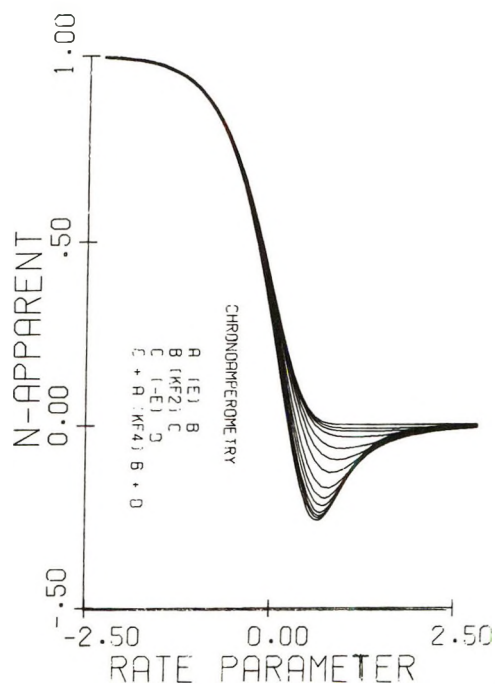


Figure 5. Chronoamperometric working curves for the $\vec{E}\vec{C}\vec{E}$ mechanism. Rate parameter = $\log k_2 t$. Curves (upper to lower) correspond to $k_4 A_{\text{bulk}}/k_2 = 0, 0.05, 0.10, 0.20, 0.50, 1.0, 2.0, 5.0, 10.0, 20.0, 50.0, 100.0, 200.0$, and ∞ .

$k_{-4} = 0$ and various values of the parameter $k_4 A_{\text{bulk}}/k_2$. The curve for case 3B, uppermost curve, Figure 5, as Herman has noted,⁵ represents a simple transformation of the equation derived by Alberts and Shain⁶ for the classical $\vec{E}\vec{C}\vec{E}$

$$n_{\text{app}} = n_1 + n_3(1 - e^{-k_2 t}) \quad (6)$$

In the $\vec{E}\vec{C}\vec{E}$

$$n_1 = -n_3 = 1 \quad (7)$$

and eq 6 reduces to

$$n_{\text{app}} = e^{-k_2 t} \quad (8)$$

The curve describing case 3A behavior, lowest curve, Figure 5, $k_4 A_{\text{bulk}}/k_2 = \infty$, shows the interesting property of actually changing sign. The resulting chronoamperometric curves for $0 < k_4 < \infty$ will obviously describe the intermediate region between case 3A ($k_4 = \infty$) and case 3B ($k_4 = 0$) behavior. These curves are also shown in Figure 5. The corresponding

(8) R. S. Nicholson and I. Shain, *Anal. Chem.*, **36**, 706 (1964).

(9) See, for example, T. Kuwana and J. Strojek, *Discuss. Faraday Soc.*, **45**, 134 (1968); A. Prostak, H. B. Mark, and W. N. Hansen, *J. Phys. Chem.*, **72**, 2576 (1968); D. R. Tallant and D. H. Evans, *Anal. Chem.*, **41**, 835 (1969); P. T. Kissinger and C. N. Reilly, *ibid.*, **42**, 12 (1970).

(10) The prosaic behavior of case 1 and case 2 chronoamperograms is easily explained. In both these cases it is necessary to step to a potential negative to both E_1^0 and E_3^0 , thus establishing the following boundary condition during electrolysis: $t \geq 0$, $A_{x=0} = 0$, $D_{x=0} = 0$. Inspection of reactions R1, R2, R3, and R4 will indicate that regardless of the values of k_2 , k_1 , and k_{-1} , the value of n_{app} will remain unity.

Table I: Chronoamperometric and Chronocoulometric Data for the ECE Mechanism

$\log k_{sf}$	0	0.1	0.2	0.5	1.0	2.0	5.0	10.0	20	100	∞
$-\infty$											
-2.003	0.990 ^a									0.905	0.904
0.999 ^b											
-1.503	0.969										
0.992											
-1.003	0.906										
9.970											
-0.503	0.731										
0.906											
-0.003	0.373	0.372	0.371	0.368	0.364	0.358	0.730	0.728	0.726	0.722	0.717
0.750	0.750	0.750	0.750	0.750	0.749	0.748	0.906	0.906	0.906	0.905	0.903
0.197	0.210	0.208	0.205	0.198	0.188	0.173	0.745	0.742	0.739	0.733	0.727
0.397	0.656	0.655	0.655	0.653	0.651	0.648	0.641	0.635	0.629	0.618	0.610
	0.085	0.079	0.074	0.058	0.383	0.010	-0.035	-0.068	-0.095	-0.135	-0.165
0.597	0.551	0.550	0.548	0.545	0.540	0.533	0.520	0.509	0.499	0.482	0.469
	0.021	0.010	-0.001	-0.026	-0.057	-0.096	-0.148	-0.181	-0.207	-0.242	-0.259
0.697	0.449	0.446	0.443	0.436	0.427	0.414	0.393	0.377	0.364	0.342	0.326
	0.008	-0.006	-0.018	-0.048	-0.082	-0.121	-0.171	-0.200	-0.221	-0.248	-0.256
0.797	0.403	0.399	0.395	0.386	0.374	0.357	0.333	0.316	0.301	0.278	0.263
	0.023	-0.014	-0.028	-0.060	-0.094	-0.131	-0.174	-0.197	-0.212	-0.228	-0.229
0.897	0.361	0.356	0.351	0.339	0.325	0.306	0.279	0.260	0.245	0.223	0.208
	0.005	-0.017	-0.032	-0.064	-0.097	-0.129	-0.163	-0.178	-0.188	-0.195	-0.191
0.997	0.323	0.317	0.311	0.297	0.280	0.260	0.231	0.212	0.197	0.176	0.163
	0.00008	-0.019	-0.034	-0.0648	-0.093	-0.120	-0.143	-0.152	-0.157	-0.158	-0.152
1.097	0.290	0.282	0.275	0.259	0.240	0.219	0.190	0.172	0.158	0.138	0.127
	0.000008	-0.019	-0.034	-0.063	-0.087	-0.107	-0.122	-0.126	-0.126	-0.123	-0.118
1.197	0.260	0.251	0.243	0.225	0.206	0.184	0.156	0.139	0.127	0.108	0.099
	0.234	-0.019	-0.033	-0.059	-0.079	-0.093	-0.101	-0.102	-0.100	-0.096	-0.091
1.297	0.211	0.224	0.215	0.196	0.176	0.154	0.128	0.112	0.100	0.085	0.077
	0.171	-0.019	-0.032	-0.055	-0.070	-0.080	-0.083	-0.082	-0.079	-0.074	-0.070
1.494	0.136	0.122	0.111	0.093	0.077	0.062	0.047	0.039	0.033	0.027	0.023
	0.096	-0.014	-0.020	-0.025	-0.025	-0.023	-0.019	-0.017	-0.015	-0.013	-0.012
1.692	0.054	0.082	0.072	0.057	0.045	0.035	0.026	0.021	0.017	0.013	0.012
	0.038	-0.010	-0.012	-0.012	-0.011	-0.009	-0.007	-0.006	-0.005	-0.004	-0.004
2.790	0.038	0.041	0.034	0.025	0.018	0.014	0.009	0.007	0.006	0.004	0.004
	0.026	-0.008	-0.009	-0.008	-0.007	-0.005	-0.004	-0.003	-0.003	-0.002	-0.002
			0.021	0.014	0.011	0.008	0.005	0.004	0.003	0.002	0.002

^a Top number is n_{app} for chronoamperometry at a given value of k_{sf} and k_4A_{bulk}/k_2 . ^b Bottom number is n_{app} for chronocoulometry at a given value of k_{sf} and k_4A_{bulk}/k_2 .

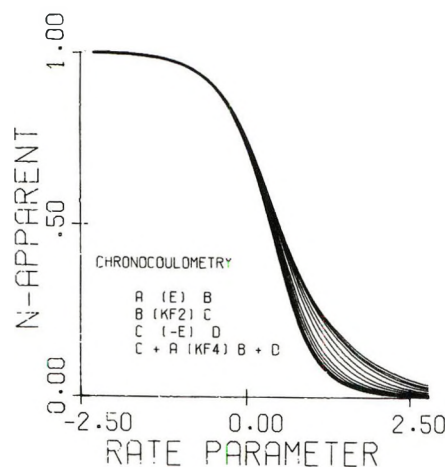


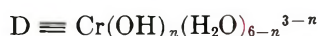
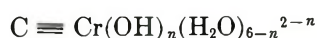
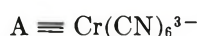
Figure 6. Chronocoulometric working curves for the $\bar{E}CE$ mechanism. Rate parameter = $\log k_2t$. Curves (upper to lower) correspond to $k_4A_{\text{bulk}}/k_2 = 0, 0.05, 0.10, 0.20, 0.50, 1.0, 2.0, 5.0, 10.0, 20.0, 50.0, 100.0, 200.0$, and ∞ .

chronocoulometric curves are shown in Figure 6, and the numerical data for Figures 5 and 6 are given in Table I. In chronocoulometry

$$n_{\text{app}} = \frac{\pi^{1/2} [\int_0^t i^0 dt - q_{\text{dl}}]}{2FD^{1/2}A_{\text{bulk}}t^{1/2}} \quad (9)$$

Experimental Section

The chemical system which prompted our interest in the $\bar{E}CE$ mechanism is the reduction of hexacyanochromate(III) in alkaline medium (ref 11 and references therein). Chromium(II) catalyzed aquation in a basic medium and in the absence of cyanide produced a soluble aquohydroxychromate(III) species and no other intermediates.¹¹ The data we shall present here represent a preliminary study for the purpose of demonstrating some of the phenomena discussed theoretically. On the basis of this study we have established the following correspondence between species A, B, C, and D of the $\bar{E}CE$ mechanism (reactions R1, R2, R3, and R4)



The E_1^0 has been established at -1.39 V,¹² while E_3^0 , though not established, is more negative than -1.8 V. All potentials are vs. the saturated calomel electrode. The temperature is $25^\circ \pm 0.1$.

Tripotassium hexacyanochromate(III) (City Chemical Corp., New York, N. Y.) was purified by heating in 1 M potassium hydroxide, causing hydrolysis of all aquocyano species (the hexacyanochromate(III) is relatively stable) and precipitating the aquohydroxy species. The tripotassium hexacyanochromate(III)

was precipitated from the filtrate with ethanol.¹³ The data presented here reflect the electrochemistry of hexacyanochromate(III) in 2 M sodium hydroxide (prepared from commercially standardized Acculute, Anachemia Chemicals Ltd.). Supporting electrolytes containing various combinations of NaOH, NaCN, and NaClO₄ ($\mu = 2.0$ M) were also used in the preliminary study. The electrode assembly consisted of a Metrohm hanging mercury drop electrode, a Beckman ceramic tip calomel, and a platinum auxiliary. A potential step and potential sweep generator drove a solid-state potentiostat, digital data acquisition system,^{14,15} and a Tektronix 564 oscilloscope. The hanging mercury drop assembly was modified by sealing a 10-mil platinum lead into the capillary about 1 cm from the tip to reduce iR drop. Polyethylene shrink tubing (Pennsylvania Fluorocarbon Co., Inc.) insulated the wire from the solution.

Cyclic Voltammetry. Two sample cyclic voltammograms are shown in Figure 7. The left cyclic is on a solution of 0.0050 M $\text{K}_3\text{Cr}(\text{CN})_6$ at a sweep rate of 41 V sec⁻¹. It is virtually reversible. The right cyclic was carried out on a 0.021 M solution at a sweep rate of 0.057 V sec⁻¹. This voltammogram clearly exhibits a current reversal phenomenon similar to that predicted by the theoretical type 3A cyclic in Figure 4.

Chronoamperometry. In order to verify $\bar{E}CE$ behavior and evaluate the rate parameters for the chromium system under these conditions, a chronoamperometric experiment was carried out on a 0.005 M $\text{K}_3\text{Cr}(\text{CN})_6$ solution. The potential was stepped from -0.8 to 1.6 V. At 0.044 sec the potential was adjusted to -1.5 V in order to minimize the effect of background current. This background increases in the presence of the aquohydroxychromate(III) species, probably due to its reduction. The resulting data are shown in Figure 8 as a plot of n_{app} vs. $\log t$. (A correction for sphericity¹⁶ was introduced by dividing the right-hand side of eq 6 by $[1 + (\pi^{1/2}D^{1/2}t^{1/2}/r)]$.) The solid line superimposed on the data points corresponds to the theoretical curve (Figure 5) for $k_4A_{\text{bulk}}/k_2 = 5$. From the value of the parameter $\log k_2t$ and the corresponding value of $\log t$, we estimate $k_2 = 11$ sec⁻¹ and thus $k_4 \approx 10^4$ M sec⁻¹. The discrepancy between the theoretical curve and experimental data at short times can be explained by an intermediate rate step interposed in reaction R2, *i.e.*



(11) L. Jeftić and S. Feldberg, *J. Phys. Chem.*, **75**, 2381 (1971).

(12) D. N. Hume and I. M. Kolthoff, *J. Amer. Chem. Soc.*, **65**, 1897 (1943).

(13) Ethanol, not methanol, as erroneously reported in ref 11.

(14) G. L. Booman, *Anal. Chem.*, **38**, 1141 (1966).

(15) G. Kissel and S. Feldberg, *J. Phys. Chem.*, **73**, 3082 (1969).

(16) P. Delahay, "New Instrumental Methods in Electrochemistry," Interscience, New York, N. Y., p 61.

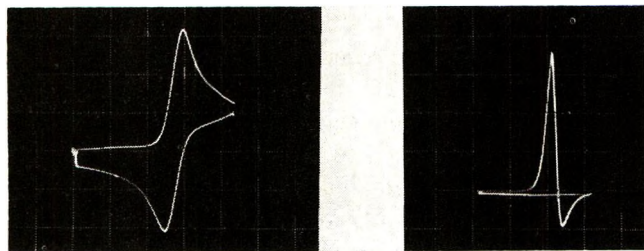


Figure 7. Experimental cyclic voltammograms in 2 M NaOH, horizontal scale = 0.21 V cm⁻¹. Left: 0.005 M K₃Cr(CN)₆, area = 0.029 cm², $v = 41$ V sec⁻¹, vertical scale = 2.1×10^{-4} A cm⁻¹, and $E_{\text{start}} = -0.84$. Right: 0.021 M K₃Cr(CN)₆, area = 0.046 cm², $v = 0.057$ V sec⁻¹, vertical scale = 1.05×10^{-5} A cm⁻¹, and $E_{\text{start}} = -1.05$.

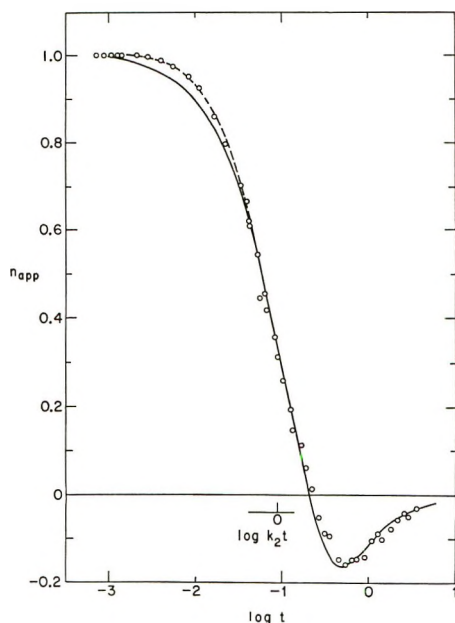


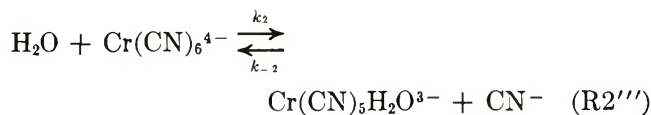
Figure 8. Experimental chronoamperogram for 0.005 M K₃Cr(CN)₆ in 2 M NaOH. Solid line corresponds to theoretical curve (Figure 9) for $k_4A_{\text{bulk}}/k_2 = 5$. Dotted line corresponds to modification indicated by reaction R2'' with $k_2'' = 200$ sec⁻¹. $D = 4.7 \times 10^{-6}$ cm² sec⁻¹.

Assuming a value of $k_2'' \approx 200$ sec⁻¹ gives the dotted theoretical curve (Figure 8).

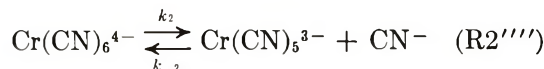
The observed facts in this preliminary study may be synopsized. The E_1^0 during fast sweeps is about -1.40 V *vs.* sce compared to the reported value of -1.39 V;¹² the rate k_2 appears to be independent of the hydroxide ion concentration as long as it is greater than 1 M and also independent of the concentration of K₃Cr(CN)₆; cyanide ion effects an apparent decrease in k_2 and removes the current reversal phenomenon.

Discussion

A mechanistic interpretation of these preliminary data is at best tenuous. Nevertheless, we suggest that a mechanism consistent with the observed facts must denote the rate step as either a water substitution reaction

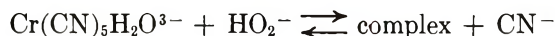


or alternatively as a cyanide ejection



In a high base, low cyanide medium, follow-up acid-base equilibria and aquation are fast and thus k_2 becomes the controlling factor.

Davies, Sutin, and Watkins¹⁷ have studied the kinetics and mechanism of the reaction of chromium(II) cyanide complexes with hydrogen peroxide in alkaline aqueous media. The mechanism they propose is considerably more detailed than anything we might say at this preliminary stage. There are, however, some correlations worth noting. Davies, *et al.*, showed that with increasing hydroxide/cyanide ratio and increasing H₂O₂ concentration a limiting reaction rate is attained that is dependent only on the concentration of the chromium(II)—the rate constant they deduce is 21 sec⁻¹, notably close to our value for k_2 . The limiting rate step they propose, however, is the decomposition of the inner-sphere complex formed by



They do, however, also propose an initial infinitely fast aquation equilibrium which is virtually identical with reaction R2''' but inconsistent with our observed invariance of E_1^0 . We hope that further work will elucidate a mechanism compatible with our electrochemical data and their kinetic data.

Marcus¹⁸ has developed the correlation between heterogeneous and homogeneous electron-transfer rates, and the implications of the theory in $\bar{\text{E}}\bar{\text{C}}\bar{\text{E}}$ mechanisms have been discussed.^{3,19} One can estimate a theoretical limit

$$k_4 \approx 10^3 k_{\text{hs1}} k_{\text{hs3}} \exp \frac{F}{2RT} |E_1^0 - E_3^0| \quad (10)$$

Since k_{hs1} for reaction R1 has been measured²⁰ at 0.25 cm sec⁻¹, if one assumes a similar value for k_{hs3} and $E_3^0 \approx -1.8$ V, then

$$k_4 \approx 10^5 \text{ M}^{-1} \text{ sec}^{-1} \quad (11)$$

Admittedly, this a rough guess, but it does come out surprisingly close to the experimentally estimated value of $10^4 \text{ M}^{-1} \text{ sec}^{-1}$.

Although the current reversal phenomenon has not

(17) G. Davies, N. Sutin, and K. O. Watkins, *J. Amer. Chem. Soc.*, **92**, 1892 (1970).

(18) R. A. Marcus, *J. Phys. Chem.*, **67**, 853 (1963).

(19) A. E. J. Forno, M. E. Peover, and R. Wilson, *Trans. Faraday Soc.*, **66**, 1322 (1970).

(20) J. E. B. Randles and K. W. Somerton, *ibid.*, **48**, 957 (1952).

previously been reported in the literature, Gulens²¹ has observed the phenomenon during reduction of monochloropentaamineosmium(III) complexes. The fact that one might be tempted to interpret such a phenomenon as a manifestation of adsorption or instrumental artifacts suggests that the $\vec{E}\vec{C}\vec{E}$ mechanism may well occur more often than its absence from the literature indicates.

Nomenclature

E_1^0, E_3^0	E^0 's for reactions R1 and R3
k_2^*	Normalized rate constant for cyclic voltammetry

$$k_2^* = \frac{k_2}{\left(\frac{F}{RT}\right)^v}$$

Scan rate for cyclic voltammetry

$$v = \frac{dE}{dt} \text{ V sec}^{-1}$$

F	Faraday, 96,500 C
R	Gas constant, 8.314 J deg ⁻¹ equiv ⁻¹
T	Absolute temperature, Kelvin
A_{bulk}	Bulk concentration of species A in solution
$A_{x=0}, B_{x=0}, C_{x=0}, D_{x=0}$	Concentrations of species A, B, C, or D at the electrode surface, moles per cubic centimeter
D	Diffusion coefficient of all species, (centimeters) ² per second
i^0	Current density, amperes per (centimeter) ²
q_{dl}	Coulombs per (centimeter) ² required to charge the double layer during a chronocoulometric experiment
k_{hs1}, k_{hs3}	Standard rate constant for a heterogeneous electron transfer, centimeters per second

Appendix

Although we have discussed the prerequisite conditions for $\vec{E}\vec{C}\vec{E}$ behavior in terms of E_1^0 and E_3^0 , it should be clear from inspection of reactions R1–R4 that the critical prerequisites for type 3A or type 3B behavior are that for the reaction



$$K_5 > 1 \quad (12)$$

and that the kinetics of (R5) be infinitely slow. (In light of this it is not surprising that reported $\vec{E}\vec{C}\vec{E}$ studies deal with chromium(III) complexes.) Defining an equilibrium constant for reaction R2

$$K_2 = [C]/[B] \quad (13)$$

it is straightforward to derive

$$K_5 = K_2 K_4 \quad (14)$$

Under the conditions we defined for type 3A or type 3B behavior, *i.e.*

$$K_4 \gg 1 \quad (15)$$

$$K_2 > 1 \quad (16)$$

it must follow from eq 13 that

$$K_5 \gg 1 \quad (17)$$

It is obvious, however, from eq 14 that there is a variety of possible combinations of values of K_2 and K_4 which produce large values of K_5 and that we have only developed theory for the conditions defined by eq 15 and 16. The possibility that reaction R2 is quasireversible, with $K_2 < 1$, presents another dimension of complications. A limiting condition can be described where K_2 is very small—so small that oxidation of species C at the electrode surface (reaction R3) is effectively vitiated. The rate equations for the homogeneous kinetics are

$$\frac{d[C]}{dt} = 0 = k_2[B] - k_{-2}[C] - k_4[A][C] \quad (18)$$

and thus

$$\frac{d[A]}{dt} = \frac{-k_4 k_2 [A][B]}{k_{-2} + k_4 [A]} \quad (19)$$

For simplicity we shall present here only two possibilities

$$k_4 [A] / k_{-2} \ll 1 \quad (20)$$

and

$$k_4 [A] / k_{-2} = \infty \quad (21)$$

Under the conditions of eq 20, reaction R2 is always in equilibrium, reaction R4 becomes the rate step, and the decrease in n_{app} is a function of the second-order rate parameter $\log K_2 k_4 A_{\text{bulk}}$ (Figures 9 and 10), while

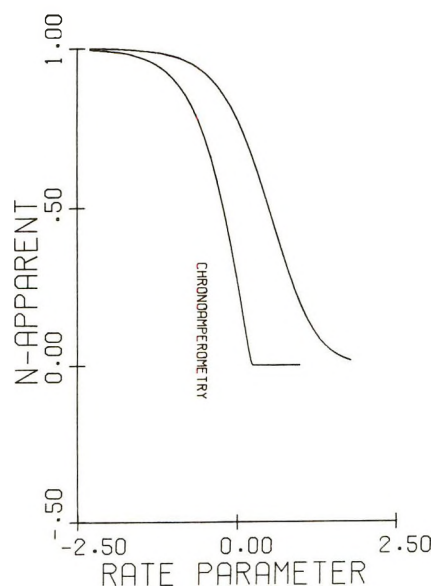


Figure 9. Chronoamperometric working curves for the $\vec{E}\vec{C}\vec{E}$ mechanism with $K_2 \ll 1$. Left curve: $k_4 A_{\text{bulk}} / k_{-2} = \infty$, rate parameter = $\log k_2 t$. Right curve: $k_4 A_{\text{bulk}} / k_{-2} \ll 1$, rate parameter = $\log K_2 k_4 t$.

(21) J. Gulens, private communication, and Ph.D. Thesis, Queens University, Kingston, Ontario, Canada, Sept 1971.

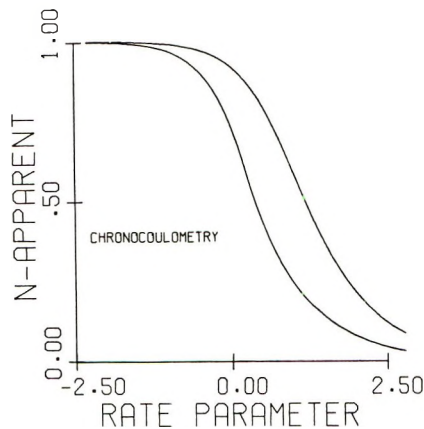


Figure 10. Chronocoulometric working curves for the $\overline{\text{ECE}}$ mechanism with $K_2 \ll 1$. Left curve: $k_4A_{\text{bulk}}/k_{-2} = \infty$, rate parameter = $\log k_2t$. Right curve: $k_4A_{\text{bulk}}/k_{-2} \ll 1$, rate parameter = $\log K_2k_4t$.

under the conditions of eq 21 reaction R4 is infinitely fast and n_{app} is a function of the first-order rate parameter $\log k_2t$ (Figures 9 and 10). Note that there is no current reversal. In all probability there would be mixed first-order and second-order control with second-order effects increasing at low n_{app} and lower concentrations. Numerical data for Figures 9 and 10 appear in Table II. Note that the chronoamperometric behavior for the case where $k_4A_{\text{bulk}}/k_{-2} \gg 1$ (Table II) is the same as for the case where $k_4A_{\text{bulk}}/k_2 = \infty$ (Table I) as long as $n_{\text{app}} \geq 0$.

The possibility that n_1/n_3 is negative and that $n_1 \neq -n_3$ is also worth mentioning. Characteristics will be approximately described by eq 6, but a generalized presentation of the effects of the multifarious redox reactions that could occur would be rather unwieldy. Interestingly, if $-n_3 > n_1$ it is possible to observe current reversal phenomena even in the absence of a redox cross-reaction corresponding to R_4 . Bond and co-workers²² have observed a current reversal phenomenon

Table II: Chronoamperometric and Chronocoulometric Data for the $\overline{\text{ECE}}$ Mechanism, where $K_2 \ll 1$

Rate parameter	Log rate parameter	n_{app}^a	n_{app}^b
0	$-\infty$	1.000	1.000
		1.000	1.000
0.00993	-2.003	0.990	0.998
		0.999	1.000
0.0314	-1.503	0.969	0.992
		0.992	0.999
0.0993	-1.003	0.904	0.974
		0.970	0.993
0.314	-0.503	0.717	0.920
		0.903	0.974
0.993	-0.003	0.279	0.777
		0.727	0.921
1.574	0.197	0.042	0.681
		0.610	0.881
1.667	0.222	0.012	
		0.593	
3.14	0.497	0	0.498
		0.432	0.794
9.93	0.997	0	0.194
		0.244	0.584
31.2	1.494	0	0.044
		0.141	0.367
98.2	1.992	0	0.006
		0.079	0.214
309.7	2.491	0	0.0004
		0.045	0.122
616.6	2.790	0	0.00005
		0.032	0.086

^a $k_4A_{\text{bulk}}/k_{-2} \gg 1$, and rate parameter is k_2t . ^b $k_4A_{\text{bulk}}/k_{-2} \ll 1$, and rate parameter is $K_2k_4A_{\text{bulk}}t$.

in reduction of a variety of vanadium(IV) complexes, which may well be an example of this $\overline{\text{ECE}}$ variation.

(22) A. M. Bond, A. T. Casey, and J. Thackeray, private communication, University of Melbourne, 1971.

Effective Fixed Charge Density Governing Membrane Phenomena. IV.

Further Study of Activity Coefficients and Mobilities of Small Ions in Charged Membranes

by Tetuo Ueda,* Naoki Kamo, Naobumi Ishida, and Yonosuke Kobatake

*Faculty of Pharmaceutical Sciences, Hokkaido University, Sapporo, 060, Japan (Received January 17, 1972)**Publication costs borne completely by The Journal of Physical Chemistry*

The mobilities of counter- and coions in charged membranes were determined experimentally by use of the flux measurements of radioisotope in a wide range of salt concentrations. The mobility of coions was identical with that in the bulk solution in the whole range of concentration studied, while that of counterions decreased very much with decrease of the external salt concentration. The concentration dependencies of both mobilities and activity coefficients of mobile ions were found to be the same, and they agreed with the "additivity rule" found empirically in the field of polyelectrolyte studies. The amount of counterions bounded in the vicinity of membrane skeleton, however, depended on the salt concentration, which was different from that observed in the polyelectrolyte solutions. The identity between the concentration dependencies of the mobility and the activity coefficient of counterions leads to a great simplification of the theoretical analysis of various membrane phenomena and enables us to evaluate the fixed charge density effective to the membrane phenomena from a simple measurement of the membrane potential at an arbitrary salt concentration. Theoretical values of various membrane phenomena other than the membrane potential were evaluated by use of the effective fixed charge density determined from the membrane potential data and were compared with the corresponding experimental data. The agreement between theory and experiment was satisfactory.

Introduction

In a different series of papers¹ concerned with the physicochemical studies of membrane phenomena, we stressed repeatedly that the nonideal behaviors of small ions in a charged membrane should be properly taken into consideration for quantitative description of the transport processes in the charged membrane. The nonideality of small ions in the membrane phase stems from the strong ionic interaction between movable ions and the charges fixed on the membrane skeletons. This situation is essentially the same as that in a polyelectrolyte solution. In part I of this series,² the activity coefficients of movable ions in a charged membrane with known fixed charge density were determined experimentally, and they were found to be expressed by the equation

$$\gamma_{\pm} = \gamma_{\pm}^{\circ} \frac{C_{-} + \phi X}{C_{-} + X}, \quad \gamma_{-} = \gamma_{\pm}^{\circ} \quad (1)$$

where γ_{\pm}° , C_{-} , X , and ϕ stand for the mean activity coefficient of an electrolyte component in the bulk solution, the concentration of the anion in the membrane, the stoichiometric fixed charge density, and a numerical constant less than unity, respectively. Equation 1 has the same functional form as the "additivity rule" found empirically in the field of polyelectrolyte solution studies.³ ϕX is generally referred to as the thermodynamically effective charge density

of the membrane or of the polyelectrolyte component, and ϕ represents the fraction of free counterions which is not bounded in the vicinity of the polymer chains. Although the fraction of free counterions was considered to be constant irrespective of the external salt concentration in a polyelectrolyte solution, ϕ in the charged membrane was shown to be dependent on the salt concentration. Furthermore, in part I, the mobilities of movable ions in the membrane were determined experimentally by combining the data of the membrane potential and the salt flux together with the analytical amount of cation and anion species adsorbed into the membrane phase. The results were represented as

$$u_{+} = u_{+}^{\circ} \frac{C_{-} + \phi' X}{C_{-} + X}, \quad u_{-} = u_{-}^{\circ} \quad (2)$$

where u_i° stands for the mobility of ion species i in the bulk solution, and $\phi' X$ is the charge density of the membrane effective to the mobilities. Of special interest is the identity of the concentration dependencies of mobilities and activity coefficients of small ions in the membrane phase, i.e., ϕ and ϕ' in eq 1 and 2 are

(1) Y. Toyoshima, M. Yuasa, Y. Kobatake, and H. Fujita, *Trans. Faraday Soc.*, **63**, 2803, 2814, 2828 (1967).

(2) N. Kamo, Y. Toyoshima, Y. Kobatake, and H. Nozaki, *Kolloid-Z. Z. Polym.*, **284**, 914 (1971).

(3) A. Katchalsky, Z. Alexandrowics, and O. Kedem, "Chemical Physics of Ionic Solutions," Wiley, New York, N. Y., 1966, p 296.

identical in the whole range of the salt concentration studied. In part I, however, we determined γ_i and u_i ($i = +, -$) only for the case of KCl as the external electrolyte component. To generalize the conclusion described above, it is necessary to survey various combinations of membrane and electrolyte pair other than that employed in part I.

This paper purports to confirm eq 1 and 2 for different electrolyte species with the same membranes studied in part I. When the concentration dependencies of the mobilities and activity coefficients of small ions in the charged membrane always follow eq 1 and 2 with $\phi = \phi'$, great simplification is obtained in the derivation of the theoretical equations for various membrane phenomena, and also the parameter ϕX characteristic to a given pair of membrane and electrolyte can be determined only from a measurement of the membrane potential. The other transport phenomena for the same pair of membrane and electrolyte can be described theoretically by using the value of ϕX . The comparison between theory and experiment provides further confirmation of the applicability of eq 1 and 2.

Experimental Section

Materials. The membranes used were the same as those used in the previous papers, which were collodion-based polystyrenesulfonic acid membranes.² It was noted that both stoichiometric charge density, X , and the water content of each of these sample membranes stayed constant irrespective of the species and concentration of the electrolyte component in the external aqueous solution.⁶ The relevant characteristics are listed in Table I.

Table I: Some Characteristics of Membrane Used

Membrane	X , equiv./l.	Water content, wt %	L_0 , cm
PS-1	0.224	0.78	0.053
PS-2	0.116	0.86	0.101
PS-3	0.0438	0.85	0.090

The salts used were LiCl, KCl, NaCl, and RbCl. Potassium chloride of analytical grade was purified by recrystallization. Sodium chloride of standard reagent and lithium chloride and rubidium chloride of analytical grade were used as delivered.

Radioactive isotopes used as tracers were sodium-22 and chlorine-36 in NaCl aqueous solution, and they were purchased from the Radiochemical Center.

The water used as solvent was obtained by passing distilled water through both cation and anion exchangers.

Activity Coefficients of Small Ions in the Membrane. The system considered here is a negatively charged

membrane immersed in an aqueous solution of a 1:1 type electrolyte. The spatial distribution of the fixed charges in the membrane is assumed to be uniform. The condition of the equilibrium between the membrane and the solution phases leads to

$$a_+a_- = a^2 = (\gamma_{\pm}^{\circ})^2 C^2 \quad (3)$$

Here, a_i denotes the activity of ion species i in the membrane, and a and C are the activity and the concentration of the electrolyte component in the bulk solution, respectively. As shown in part I, the contribution of the difference in the osmotic pressures in two phases to eq 3 was less than 0.6% in the whole range of concentration studied. The activity coefficients of small ions in the membrane, γ_+ and γ_- , are defined by $a_+ = \gamma_+C_+$, $a_- = \gamma_-C_-$. Thus, eq 3 is rearranged to give

$$\gamma_+\gamma_-/(\gamma_{\pm}^{\circ})^2 = C^2/(C_+C_-) \quad (4)$$

Equation 4 reads that the activity coefficient of the electrolyte component in the membrane, $\gamma_+\gamma_-$, can be determined from the analysis of C_- and C_+ .

The concentration of anion in the membrane, C_- (Cl^- ion for the present case), was determined by titration against AgNO_3 by the usual way or by the potentiometric titration as described in part I. The value of C_+ was calculated from the electroneutrality condition, i.e., $C_+ = C_- + X$.

Mobilities of Small Ions in the Membrane. The mobilities of movable ions can be determined by measuring the isotope fluxes. The tracer method for the determination of mobility in the membrane has the following two advantages over the method proposed in part I. (a) The experiments can be performed with no gradient in the concentration of the electrolyte component, and (b) the movement of the local center of mass does not occur in the system in problem, and hence the ambiguity which stems from the mass movement is not included in the observed mobility. The slight inaccuracy due to isotope effect in electrolyte solutions may be neglected in the membrane systems encountered here. In the measurement of the isotope flux, the effect of the unstirred liquid film adjacent to the membrane surface on the observed flux must be taken into account. However, Lakshminarayanaiah⁴ showed that the contribution of this layer to the isotope flux is negligibly small in an ordinary membrane-electrolyte system. Then the following equation is obtained for the flux of the isotope, J^*

$$J^* = \left(\frac{RT}{F} \right) u_i C_i \frac{\Delta C^*}{LC} \quad (5)$$

where C_i stands for the concentration of the cold ion species i in the membrane, L the effective thickness

(4) N. Lakshminarayanaiah, "Transport Phenomena in Membranes," Academic Press, New York, N. Y., 1969, p 131.

of the membrane, C the concentration of the external solution, and ΔC^* the difference of tracer concentration in two compartments. Equation 5 tells that the measurements of the tracer flux enable us to evaluate the mobility of species i in the membrane provided that the concentration C_i of the cold ion species i in the membrane is known.

Two solutions of identical concentration were separated by the membrane. The geometrical area of the membrane was 1.04 cm². Each compartment contained 40.0 ml in volume of the salt solution. The solutions were stirred vigorously and were changed several times every 2 or 3 hr before introducing the radioisotope. This procedure permits the membrane and bulk solution to be in equilibrium. Then, the solution of radioactive isotope (0.1 ml) was added to one compartment. With a determined time interval the solutions were picked up by a micropipet (0.20 ml) from each compartment. The radioactivity of the solutions containing ²²Na or ³⁶Cl was counted by a scintillation spectrometer (Aloka model LSC 501). The radioactivity in the hot compartment, (CPM)₂, stayed constant within the experimental error, and that in the cold compartment, (CPM)₁, increased linearly with time after a short period of time from the onset. When the slope of this linear portion is denoted by S , the mobility u_i can be evaluated by the equation

$$u_i = \left(\frac{F}{RT} \right) J^* \frac{C}{C_i} \frac{L}{\Delta C^*} = f \cdot V \left(\frac{F}{RT} \right) \left(\frac{L_0}{A_0} \right) \left(\frac{C}{C_i} \right) \frac{S}{(\text{CPM})_2} \quad (6)$$

where V is the volume of electrolyte solution in each compartment, A_0 and L_0 are the geometrical area and thickness of the membrane, respectively, and f is the tortuosity factor. In general, the effective area, A , is smaller than A_0 , and the effective thickness of the membrane, L , is larger than L_0 . Then f is defined by the equation⁵

$$f = (A_0/L_0)/K \quad (7)$$

Here K stands for A/L . The value of f may be constant irrespective of the species and concentration of ions when the degree of swelling of the membrane is not changed by the salt concentration as encountered in the present study. Since the effects of the fixed charges in the membrane on the activities and mobilities are diminished when the concentration of the external solution is high enough in comparison with the fixed charge density, X , the value of f is able to be determined from the limiting value of the concentration of the external solution. Then we have

$$f = \left(\frac{RT}{F} \right) \left(\frac{A_0}{L_0} \right) \frac{(\text{CPM})_2}{S \cdot V} u_i^\circ \quad (8)$$

Here, u_i° stands for the mobility of ion species i in the bulk solution at a concentration C . Once the value of f is determined, the absolute value of the mobility of i ion in the membrane can be evaluated from eq 6 with use of data on C_i in the membrane at a given concentration of the external salt solution.

Measurements of Membrane Potential and Dc Resistance. The cells and procedures adopted for the measurements of the membrane potential and dc resistance were the same as those used in the previous study.^{2,6}

All experiments were performed in an air oven regulated at $25 \pm 0.2^\circ$.

Results and Discussion

Activity Coefficients in the Membrane. Introducing the results of the analysis of C_+ and C_- in the membrane into eq 4, we obtain the value of $\gamma_+\gamma_-/(\gamma_\pm^\circ)^2$. Figure 1 shows the data for $\gamma_+\gamma_-/(\gamma_\pm^\circ)^2$ as a function of C_-/X in various pairs of NaCl and LiCl and three membranes with different X . In Figure 2, the data of $\gamma_+\gamma_-/(\gamma_\pm^\circ)^2$ for KCl in the same membrane as in Figure 1 are plotted against C/X , which are taken from part I. It is seen that the data points for different pairs of X and C follow a single sigmoid-shaped curve when plotted against C_-/X for each electrolyte species studied.

In part I, we showed that the value of ϕ in eq 1 for a pair of KCl and the membrane is varied from 0.4 ± 0.05 in a concentrated solution to 0.1 in a dilute KCl solution. In Figures 1 and 2, two dashed lines represent the values calculated from eq 1 with ϕ being 0.4 and 0.1, respectively. From these two figures, it is considered that the value of ϕ for NaCl and LiCl varies with the concentration of external solution as in the

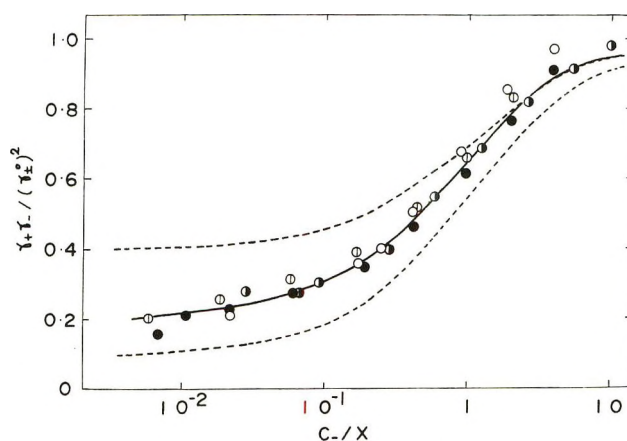


Figure 1. Plots of $\gamma_+\gamma_-/(\gamma_\pm^\circ)^2$ against $\log(C_-/X)$ for systems of three kinds of membrane and NaCl and LiCl solution: \odot , PS-1; \bullet , PS-2; \ominus , PS-3 for NaCl, and \circ , PS-2 for LiCl.

(5) J. S. Mackie and P. Mears, *Proc. Roy. Soc., Ser. A*, **232**, 498 (1955).

(6) N. Kamo, Y. Toyoshima, and Y. Kobatake, *Kolloid-Z. Z. Polym.*, **249**, 1061 (1971).

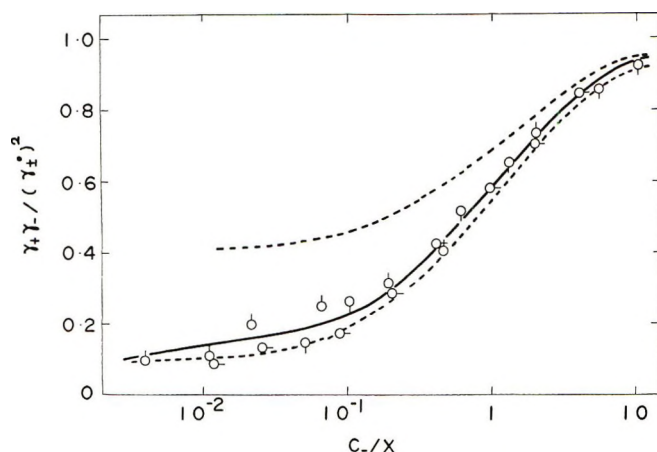


Figure 2. Plots of $\gamma_+ \gamma_- / (\gamma_{\pm}^\circ)^2$ against $\log(C_-/X)$ for three kinds of membranes: \circ , PS-1; \ominus , PS-2; \odot , PS-3 for KCl.

KCl solution. This fact is slightly different from the "additivity rule" found in polyelectrolyte solutions, where ϕ is believed to be constant irrespective of the concentration of added salt.³ Precise comparison of the data shown in Figures 1 and 2 reveals that the value of ϕ for NaCl and LiCl is slightly different from that for KCl when the concentration is low enough, i.e., $C/X \ll 1$. This means that a selectivity of counterion species exists for the membrane in a dilute solution. Strictly speaking, the data shown in Figure 2 for KCl were obtained at 30°, while those in Figure 1 for NaCl and LiCl were determined at 25°. As pointed out in part III of this series,⁷ however, the Donnan uptake of small ions in the present membranes did not change between 25 and 30° within experimental error. Thus the comparison between Figures 1 and 2 is allowed.

u_+ and u_- in the Membrane. The radioactivity of the cold compartment increased proportionally with time after about 20 min from the onset of each run. The linear portion of this plot is used for the determination of the flux of the isotope. The experimental error in determination of the slope was less than $\pm 5\%$.

Figure 3 illustrates the determination of the tortuosity factor f in accordance with eq 8. The ordinate of the figure represents

$$\frac{F(L_0)}{RT(A_0)(\text{CPM})_2 u_i^\circ} \frac{S \cdot V}{u_i^\circ}$$

and the abscissa is $1/C$. The ordinate intercept of this plot gives the value of $1/f$. As seen in the figure, f is a constant irrespective of ion species i for a given pair of membrane and electrolyte.

Figure 4 shows the values of u_+ and u_- determined from eq 6 for pairs of NaCl and three kinds of membrane, where u_+/u_+° and u_-/u_-° are plotted against $\log(C_-/X)$. It is noted that u_- (coions in the present case) in the membrane stays constant and equal to the value in a bulk solution u_i° in the whole range of concentration investigated here. This behavior

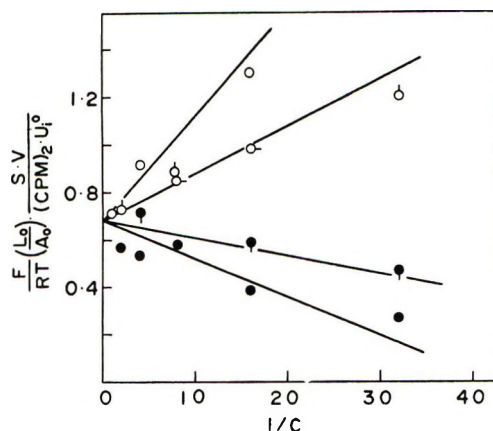


Figure 3. Determination of the tortuosity factor, f , for systems of two kinds of membrane and ^{22}Na and ^{36}Cl . Results of ^{22}Na : \circ , PS-1; \odot , PS-2; \ominus , PS-3 results of ^{36}Cl : \bullet , PS-1; \bullet , PS-2.

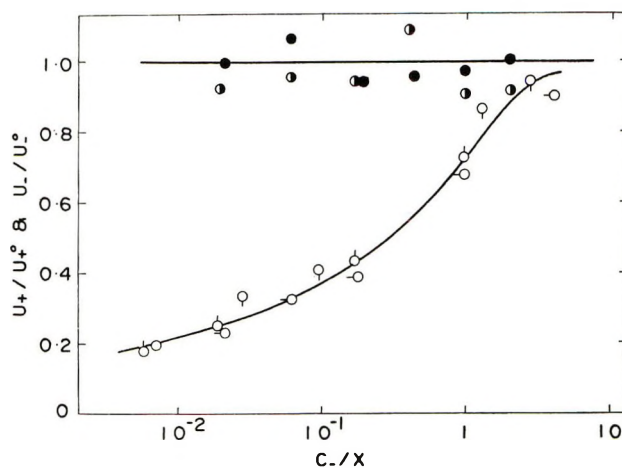


Figure 4. Plots of u_+/u_+° and u_-/u_-° against $\log(C_-/X)$ for systems of three kinds of membrane and NaCl solutions at a fixed concentration. Results of cation (counterion): \ominus , PS-1; \odot , PS-2; \odot , PS-3; results of anion (coion): \bullet , PS-1; \bullet , PS-2.

of coions was also found in part I for KCl external solution. On the contrary, u_+/u_+° decreases with decrease of C_-/X and approaches about 0.2 when the concentration becomes dilute. The depression of u_+/u_+° in a dilute solution can be represented by eq 2. Note that both the activity coefficient and the mobility of the counterions are reduced to a single curve when these values are plotted against C_-/X irrespective of the magnitude of X . This implies that the depressions of u_+ and γ_+ mainly stem from the interactions between the movable ions and the charges fixed in the membrane. As noted above, ϕX in eq 1 and $\phi'X$ in eq 2 were equal to each other within the experimental errors in the case of KCl. Figure 5 illustrates that the same thing holds also for NaCl, where both u_+/u_+° and $\gamma_+ \gamma_- / (\gamma_{\pm}^\circ)^2$ are plotted against $\log(C_-/X)$. Therefore, it is concluded that both mobility and activity

(7) M. Kamo and Y. Kobatake, *Kolloid-Z. Z. Polym.*, **249**, 1069 (1971).

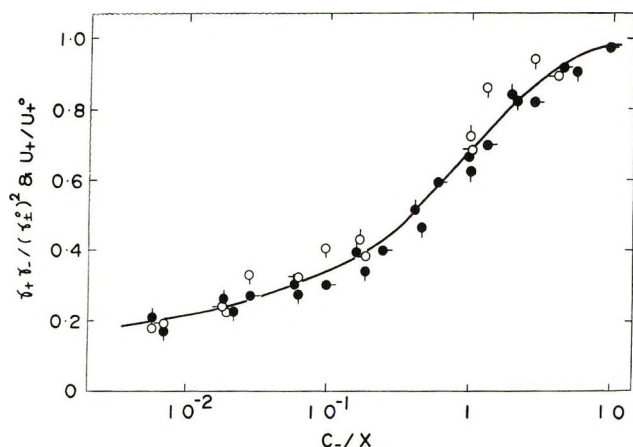


Figure 5. Comparison of the concentration dependencies of $\gamma_+ \gamma_- / (\gamma_+^0 \gamma_-^0)$ and u_+^0 / u_+^0 for a pair of NaCl and three kinds of membrane: \circ , PS-1; \circ , PS-2; \circ , PS-3 for mobility; and \bullet , PS-1; \bullet , PS-2; \bullet , PS-3 for activity coefficient.

coefficient of small ions in charged membranes have the same concentration dependence in the wide range of concentrations for both KCl and NaCl solutions. Hence we have the equality $\phi = \phi'$ irrespective of ion species and of its concentration, although the value of ϕ depends on the concentration of the external solution as pointed out above.

Interrelation of Membrane Phenomena. The above conclusion for mobilities and activity coefficients of mobile ions in the membrane leads to a great simplification of the further analysis of the transport processes in a system of a charged membrane and a 1:1 type electrolyte. As shown in the previous series of papers,¹ the theoretical equations for various membrane phenomena are easily derived by using eq 1 and 2 for γ_i and u_i , provided that the effective charge density of the membrane, ϕX , is known as a function of the external salt concentration. In other words, if we are able to evaluate the value of ϕX from the data of any one of the membrane phenomena, *e.g.*, membrane potential, it is possible to predict the value of the other phenomenon at an arbitrary external concentration. Comparison between the theory and experiments for an arbitrary electrolyte species enables us to check the correctness of the theory and also the applicability of the basic assumptions for the mobilities and activity coefficients of small ions given by eq 1 and 2 with $\phi = \phi'$.

A simple method for evaluation of ϕX of a given pair of membrane and electrolyte at an arbitrary salt concentration was proposed in part II of this series,⁶ and hence only a brief account of the method is illustrated here. Let us define the apparent transference number of coions in the membrane by the Nernst equation

$$\Delta\phi = -(RT/F)(1 - 2\tau_{\text{app}}^-) \ln (C_2/C_1) \quad (9)$$

where $\Delta\phi$ stands for the membrane potential arisen between two aqueous solutions of different concentrations C_1 and C_2 ($C_1 < C_2$). On the other hand, the mass

fixed transference number of coions τ^- in the membrane immersed in an electrolyte solution of concentration C is given by

$$\tau^- = u_- C_- / (u_+ C_+ + u_- C_-) \quad (10)$$

τ_{app}^- defined by eq 9 was found to agree with τ^- within 2% of a wide range of concentrations, when C is replaced by $(C_1 + C_2)/2$, provided that C_2/C_1 is not too large. Thus τ_{app}^- determined from the membrane potential data may be considered to be approximately equal to τ^- at the averaged salt concentration $C = (C_1 + C_2)/2$. Introducing eq 1 and 2 into eq 10 and rearranging, we obtain

$$\phi X = C \frac{\left(\frac{1 - \tau^-}{\alpha}\right) - 1}{\sqrt{\tau^- \left(\frac{1 - \tau^-}{\alpha} - 1 + \tau^-\right)}} \quad (11)$$

where α stands for the cation transference number in the bulk solution given by $\alpha = u_+^0 / (u_+^0 + u_-^0)$ at the concentration C . Equation 11 illustrates that the observation of the membrane potential permits us the determination of the effective charge density ϕX of the membrane at a given averaged salt concentration. ϕX thus determined for various pairs of membranes and electrolytes agreed with that obtained from the Donnan uptake experiments as will be reported elsewhere.

Once ϕX is determined from the membrane potential data at an arbitrary concentration, C , any other transport phenomenon in the membrane can be calculated theoretically, and compared with the experimental value. As a typical example, we shall discuss the dc resistance of the membrane. The electrical resistance, R , is represented by

$$R = \frac{1}{KF(u_+ C_+ + u_- C_-)} \quad (12)$$

Here the effect of the mass movement was ignored since this term was evaluated to be less than a few per cent of $(u_+ C_+ + u_- C_-)$.⁶ Introducing eq 1 and 2 with $\phi = \phi'$ into eq 12 and rearranging, we obtain

$$R = \frac{2}{KF\Lambda^0} \cdot \frac{1}{\sqrt{4C^2 + \phi^2 X^2 + (2\alpha - 1)\phi X}} \quad (13)$$

where Λ^0 stands for $(u_+^0 + u_-^0)$, whose value can be taken from an appropriate table,⁸ and K is the geometrical constant of the membrane as encountered in eq 7. Comparison between the calculated and the observed values of R is shown in Figure 6, where the systems are composed of membrane SP-1 or SP-2 in

(8) "Landolt-Börnstein Tabellen," II-7, 6th ed, Springer-Verlag, West Berlin, 1960.

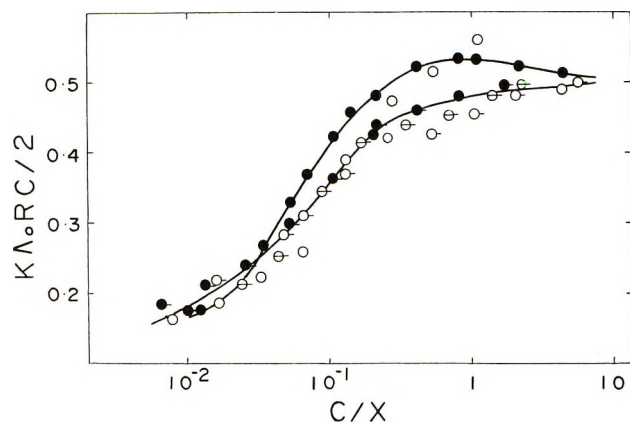


Figure 6. Comparison of the observed electrical resistance with the value calculated from eq 13 for LiCl and RbCl. The effective charge density, ϕX was determined from membrane potential data as described in the text: ●, LiCl; ●, RbCl for the calculated value; and ○, PS-2, LiCl; ○, PS-3, RbCl; ○, PS-2, RbCl.

various concentrations of RbCl and LiCl solutions. The ordinate of this figure represents $KA^{\circ}RC/2$ and the abscissa is $\log (C/X)$. The agreement between cal-

culated and observed values is satisfactory within the experimental error.

Concluding Remarks. Various experiments described in this article and in the previous papers^{1,2} show that the mobilities and the activity coefficients of small ions in a charged membrane are represented by eq 1 and 2, and the concentration dependencies of them are the same for all systems studied. That is, ϕ in eq 1 is identical with ϕ' in eq 2 in the whole range of the external salt concentrations for various pairs of membranes and electrolyte species. Using this result the fixed charge density effective to the membrane phenomena, ϕX , in an arbitrary salt concentration can be determined from an experimental value of the membrane potential. The value of ϕX thus obtained depended on the concentration of the external solution and on the species of the electrolyte component. For example, NaCl and LiCl give a larger value of ϕ in comparison with that for KCl and RbCl in the membranes used. In other words, the collodion-based polystyrenesulfonic acid membrane shows a slight selectivity for cation species in a dilute salt solution. Detailed discussion for the selectivity of ion species in the membrane is left for a subsequent paper of this series.

Conductance of an Intermolecular Charge-Transfer Complex within an Ion Pair

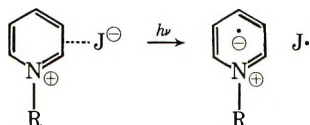
by Hans Güsten* and Leo Klasinc¹

Institut für Strahlenchemie, Kernforschungszentrum Karlsruhe, Karlsruhe, Germany (Received July 1, 1971)

Publication costs assisted by Kernforschungszentrum Karlsruhe

A linear dependence of the ion-pair concentration of a quaternary stilbazolium iodide in chloroform at 25° with its charge-transfer absorption is shown. Extensive ion pairing still occurs at unusually low concentrations ($\sim 10^{-6} M$). The electrochemically measured degree of dissociation and the independently measured extinction represent a method for the observation of solvent-separated and contact ion pairs in a CT complex.

The electronic spectra of pyridinium and quinolinium salts, particularly in the case of the iodides, show new absorption bands beyond the long wavelength absorption limit of the heteroaromatic cation.² The strong dependence of these new absorption bands on the polarity of the solvent and on the temperature³ and the fact that they do not obey Beer's law are explained by Kosower,⁴ Mason,⁵ and Briegleb⁶ as a transition of an electron from the anion to the lowest unoccupied π orbital of the cation within an ion pair.



During the course of our work on the thermal cis-trans isomerization of stilbazolium salts^{7,8} we have found a new absorption band at 462 m μ in the elec-

(1) Guest from the Institute "Ruder Bošković," Zagreb, Croatia, Yugoslavia.

(2) F. Kröhnke, *J. Prakt. Chem.*, (4) 6, 235 (1958).

(3) A. Hantzsch, *Ber. Deut. Chem. Ges.*, 52, 1535, 1544 (1919).

(4) (a) E. M. Kosower and P. E. Klinedinst, Jr., *J. Amer. Chem. Soc.*, 78, 3493, 5700 (1956); (b) E. M. Kosower, *ibid.*, 80, 3253 (1958).

(5) S. F. Mason, *J. Chem. Soc.*, 2437 (1960).

(6) G. Briegleb, W. Jung, and W. Herre, *Z. Phys. Chem. (Frankfurt am Main)*, 38, 253 (1962).

(7) H. Güsten and D. Schulte-Frohlinde, *Tetrahedron Lett.*, 3567 (1970).

(8) D. Schulte-Frohlinde and H. Güsten, *Justus Liebigs Ann. Chem.*, 749, 49 (1971).

tronic spectrum of 4-(4-nitrostyryl)-*N*-ethylquinolinium iodide (λ_{\max} 375 m μ , ϵ 2.51×10^4) in chloroform and *cis*-1,2-dichloroethylene beyond the long wavelength absorption limit of the stilbazolium salt. We interpret this new absorption band as an intermolecular charge-transfer absorption between the iodide anion and the stilbazolium cation within an ion pair. Replacement of the iodide anion by the perchlorate anion causes loss of the charge-transfer absorption. In stilbazolium iodides having H-, Cl-, HO-, H₃CO-, or N(CH₃)₂- groups in the 4 position of the styryl group, the charge-transfer absorption is hidden by the absorption of the cation. In the concentration range of 2.5×10^{-6} to 10^{-4} *M* the CT absorption of 4-(4-nitrostyryl)-*N*-ethylquinolinium iodide in CHCl₃ does not obey Beer's law. Extrapolation to high concentrations results in a limiting value of 1650 for the molar extinction coefficient of the CT band at 462 m μ .

To find a relationship between the ion-pair concentration and the extinction of the CT absorption we have measured the electric conductivity of 4-(4-nitrostyryl)-*N*-ethylquinolinium iodide in CHCl₃⁹ at 25° in the concentration range of 1.0×10^{-6} to 10^{-4} *M*. The conductance curve Λ vs. \sqrt{c} (Table I) shows an inflection concave-up at $\sim 10^{-5}$ *M* belonging to type IV of Fuoss's classification,¹⁰ and the Fuoss-Kraus equation or the semiempirical Shedlovsky method serves to reproduce our data.¹⁰ The equivalent conductivity at infinite dilution, Λ_0 , and the dissociation constant for the ion pair, K_D , were derived according to the method of Shedlovsky¹⁰ from the concentration dependence of the equivalent conductivity. From the calculated Shedlovsky plot (the computations were programmed for the IBM 7074) we obtained the following values: $\Lambda_0 = 1.44$ cm² equiv⁻¹ ohm⁻¹, $K_D = 5.11 \times 10^{-5}$. In spite of the low dielectric constant of CHCl₃ (5.14 at 25°) we can assume that in our concentration range no aggregation to triple ions or higher associates occurs. The critical concentration¹⁰ c_0 for the ion-ion pair equilibrium in CHCl₃ at 25° is $c_0 = 4.3 \times 10^{-5}$. The log $\Lambda_c/\log c$ diagram gives a straight line with a slope of -0.50 which, according to Fuoss,^{10,11} indicates only association to ion pairs.

The electrochemical data show that at a concentration of 1.0×10^{-6} *M* extensive ion pairing still occurs.

The very low limiting equivalent conductance for a 1:1 electrolyte is unusual. Similar low conductance data in high dilution have been measured by Walden¹² for tetraalkylammonium salts in solvents of low dielectric constants, *i.e.*, CHCl₃. Evaluation of his conductance data with classical methods (Walden's¹⁰ rule with accepting Λ_{07} values from aqueous solution) results in limiting equivalent conductance in the order of 100–150 and α values of 10^{-2} to 10^{-3} . However his actually measured conductances (Λ) in extremely high dilution are more than a hundredfold less than Λ_0 .

Since to our knowledge this is the first determination

Table I: Concentration Dependence of the Degree of Dissociation α and the Extinction E/cm of the Intermolecular Charge-Transfer Absorption at 462 m μ of 4-(4-Nitrostyryl)-*N*-ethylquinolinium Iodide in CHCl₃ at 25°

c , mol/l. ^a	Λ , equiv ⁻¹ ohm ⁻¹ cm ²	α^b	E/cm	$c' =$ $c(1 - \alpha)$
1.0×10^{-6}	1.15	0.602
2.50×10^{-6}	1.04	0.485	0.0022	1.29×10^{-6}
5.37×10^{-6}	0.8	0.388	0.0055	3.29×10^{-6}
1.07×10^{-5}	0.69	0.269	0.0134	7.82×10^{-6}
2.68×10^{-5}	0.41	0.148	0.0390	2.28×10^{-5}
5.17×10^{-5}	0.36	0.099	0.0792	4.66×10^{-5}
1.02×10^{-4}	0.26	0.059	0.1617	9.60×10^{-5}

^a The concentration was used in the conductivity and the extinction measurements. ^b $\alpha = \Lambda/\Lambda_0 F_{(z)}$ was taken from the final iteration of the Shedlovsky calculation. For the meaning of $F_{(z)}$, see ref 10.

of limiting conductance for an aromatic quinolinium salt, no independent check for our data is available. In connection with kinetic measurements on stilbazolium salts¹³ we obtained limiting equivalent conductance data for 4-(4-methoxystyryl)-*N*-ethylquinolinium iodide at 25° in different solvents ranging from $\Lambda_0 = 2.52$ in chloroform to $\Lambda_0 = 190$ in acetone. Walden's rule¹⁰ holds only in those solvents where complete dissociation occurs. The usual 1:1 electrolytes studied in nonpolar and aprotic solvents have bulky organic cations such as tetraalkylammonium,^{10,12} where the positively charged atoms are buried in the center of a tetrahedron and the cation is considered as a charged sphere. The *trans*-stilbazolium cations, however, are long flat polarizable aromatic cations.⁷ If coulombic stabilized cation-anion pairing is an important factor, shorter contact distance might be possible as normally is accepted in the continuum theory. In addition ion-pair stabilization by dispersion forces depending on the polarizability may account also for the extensive ion pairing at such unusual low concentrations.

Molar extinction coefficients of intermolecular charge-transfer absorptions of quinolinium iodides in CHCl₃ are in the range of 1600–1700.⁵ From the slope of Figure 1 we obtain a value of $\epsilon_{CT} \sim 1700$ for 4-(4-nitrostyryl)-*N*-ethylquinolinium iodide.

The ion-pair concept demands that the extinction of the CT band increases linearly with the increasing ion-

(9) Chloroform p.a. (Merck) was prepared for conductivity measurements by washing five times with half its volume of water, drying with MgSO₄, and fractionally distilling under nitrogen in a dark flask. Solvent conductance, 6.5×10^{-11} ohm⁻¹ cm⁻¹.

(10) R. M. Fuoss and F. Accascina, "Electrolytic Conductance," Interscience, New York, N. Y., 1959.

(11) R. M. Fuoss, *J. Amer. Chem. Soc.*, **81**, 2659 (1959).

(12) P. Walden, *Z. Phys. Chem. (Leipzig)*, **147**, 1 (1930).

(13) H. Güsten and D. Schulte-Frohlinde, to be published.

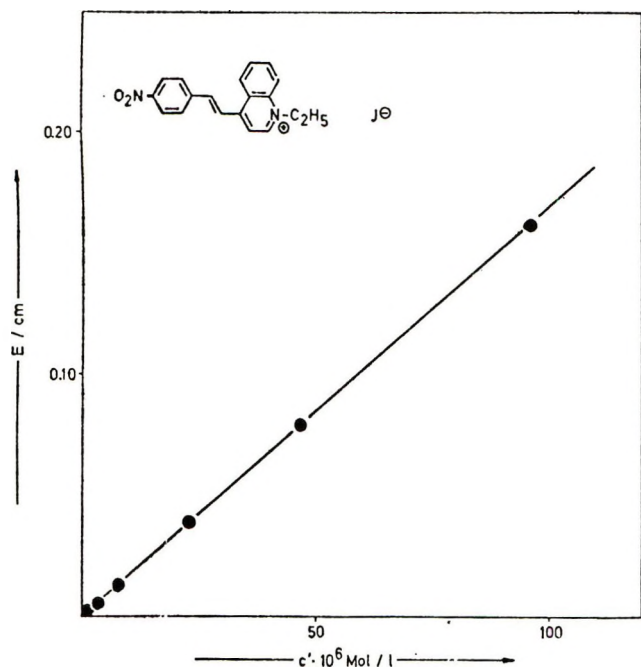
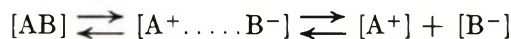


Figure 1. Correlation of the extinction E/cm of the intermolecular charge-transfer absorption of 4-(4-nitrostyryl)-*N*-ethylquinolinium iodide at $462 \text{ m}\mu$ in CHCl_3 at 25° with the sum of the ion-pair concentration $c' = c(1 - \alpha)$.

pair concentration. The degree of dissociation α , however, is not necessarily a direct measure of the ion-pair concentration since solvent-separated ion pairs might exist in the equilibrium.¹⁴



The visible CT band should arise only from the contact ion pair.^{4b} Since contact and solvent-separated ion pairs will be counted together as $c' = c(1 - \alpha)$ (Table I) via the electrochemically obtained α , deviation from the straight line in the plot E vs. c' may be ascribed to the presence of solvent-separated ion pairs. In the present case (Figure 1) we do not find such a deviation and the equilibrium constant for the ion pair-free ion equilibrium can be derived from absorption measurements alone.¹⁵ In CHCl_3 with its low dipole moment charge-charge interaction is expected to be much larger than ion-solvent contact. Nevertheless, the procedure of the independently measured extinction and degree of dissociation could be a useful one for the observation of the often proposed solvent-separated ion pairs in solvents with higher dielectric constants.

(14) S. Winstein, *Experientia, Suppl.*, **2**, 137 (1955).

(15) E. M. Kosower and J. C. Burbach, *J. Amer. Chem. Soc.*, **78**, 5838 (1956).

Hydration of Perchlorate, Tetraphenylboride, and Nitrate Ions in Some Organic Solvents¹

by T. Kenjo and R. M. Diamond*

Lawrence Berkeley Laboratory, University of California, Berkeley, California 94720 (Received February 23, 1972)

Publication costs assisted by the Lawrence Berkeley Laboratory

The hydration of ClO_4^- , $\text{B}(\text{C}_6\text{H}_5)_4^-$, and NO_3^- in various organic solvents has been studied by means of the extraction of the tetraalkylammonium salts. The dependence of the extraction on the aqueous salt concentration indicates that tetrapropylammonium perchlorate and tetrabutylammonium nitrate in nitrobenzene are essentially dissociated up to 10^{-2} M . But in solvents of lower dielectric constant, such as dichloroethane or 80% benzene-20% nitrobenzene, the salts associate to ion pairs and still larger ion aggregates. In all these solvents about 0.3-0.4 mol of water is coextracted with the tetraalkylammonium perchlorate. No water coextracts with tetraalkylammonium tetraphenylboride in nitrobenzene. With the nitrate salt, ~ 1.4 mol of water is involved per NO_3^- .

Introduction

The distribution of salts between water and an immiscible organic phase can be made relatively high if either the cation or anion is large and hydrophobic enough. In particular, the extraction of anions can be studied by using large tetraalkylammonium cations.

Earlier reports² describe the organic phase complexing of F^- and Cl^- in such salts by water-immiscible phenols

(1) Work performed under the auspices of the U. S. Atomic Energy Commission.

(2) (a) D. J. Turner, A. Beck, and R. M. Diamond, *J. Phys. Chem.*, **72**, 2831 (1968); (b) T. Kenjo, S. Brown, E. Held, and R. M. Diamond, *ibid.*, **76**, 1775 (1972).

and alcohols. From the fact that definite complexes were indicated, we wondered if distribution of the salts alone and determination of the water coextracted would not yield information on the first-shell hydration of the anions.

It would be advantageous in such a study if the extracted salts were dissociated into independent ions, for then if one ion could be shown to be anhydrous or to have a definite amount of water associated with it in a particular solvent, the determination of the total water extracted by a salt containing that ion yields the water bound to the coion. For this purpose a solvent of high dielectric constant was first chosen, namely nitrobenzene ($\epsilon = 34.8$ at 25°).³ Then, to see if ion association changes the hydration numbers found, lower-dielectric-constant solvents were also investigated.

A number of recent studies have described the interactions of anions with protic solvents such as water, alcohol, and amines.^{2,4-10} Spectroscopic evidence for nitrate-solvent interactions have been found for tetrabutylammonium nitrate-methanol in benzene,⁴ for alkali metal nitrate-water in aqueous solutions,⁵ with alkylammonium nitrate salts in alcohol-methylene chloride or water-methylene chloride systems,⁶ and for aqueous and chloroform solutions of alkali metal and tetraphenylarsonium nitrates.⁷ Transient perhenate-water interactions have been suggested as the origin of the inhomogeneous electric-field gradient causing the quadrupole relaxation in aqueous solutions of NaReO_4 as observed in broad-line nmr spectroscopy.⁸ Perhenate-alkylammonium interactions are thought to be responsible for the appearance in the infrared spectrum of the perhenate ion, in alkylammonium perhenate salts, of splittings of the Re-O stretching vibrations at $850\text{--}1000\text{ cm}^{-1}$.⁹ However, nmr¹⁰ and ir⁶ studies show that this interaction is one of the weakest between anions and the alkylammonium cations.

Experimental Section

Reagents. The desired form of tetraalkylammonium salt was obtained in the manner described in the previous paper.^{2b} Tetraalkylammonium iodide (Eastman Organic Chemicals, White Label) was converted into the hydroxide form by shaking a suspension of the iodide in water with silver oxide (Baker and Adamson, reagent grade). The hydroxide obtained was neutralized with nitric or perchloric acid to the nitrate or perchlorate salt, respectively. Tetrabutylammonium tetraphenylboride was obtained as a precipitate by adding sodium tetraphenylboride to a tetrabutylammonium solution. The precipitate was washed with water until no bromide was observed in the filtrate and then dried at 60° . The benzene and dichloroethane used were J. T. Baker reagent grade. The nitrobenzene was Eastman Organic Chem-

icals, White Label. The sodium tetraphenylboride used was Mallinckrodt Chemical Works, reagent grade.

Procedure. Various aqueous solutions of tetrabutylammonium nitrate were shaken with nitrobenzene for 2 hr. For the perchlorate salt, because of its low solubility in water, we started with the salt in the organic phase and shook with water for the same time. The volume ratio of organic to aqueous phase used was 1:1. After shaking, the phases were centrifuged and separated. For dilute solutions the tetraalkylammonium cation concentration in the aqueous phase, and for more concentrated solutions the cation concentration in both phases, were determined spectrophotometrically using picrate;¹¹ the procedure was essentially the same as in the previous work.^{2b} After dilution of the sample of aqueous solution to the range 10^{-5} to 10^{-4} M , a 5-ml aliquot was shaken with 5 ml of 0.010 M sodium picrate, 5 ml of saturated MgSO_4 , and 5 ml of chloroform. For the organic phase determination, the solution was diluted to the same range of concentration with the organic solvent, and then an aliquot was shaken with the aqueous solution of picrate and MgSO_4 . Calibration curves for each solvent were prepared. The wavelengths used for nitrobenzene, dichloroethane, and 20% nitrobenzene-80% benzene mixture were 434, 383, and $426\text{ m}\mu$, respectively.

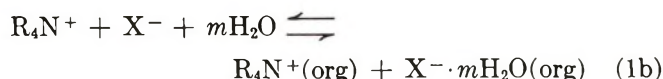
Water determinations in the organic phase were made by the Karl Fischer method using an electrometric end point. All experiments were done at $25 \pm 2^\circ$.

Results and Discussion

As described in earlier papers,² slope analysis is useful to determine the molecularity of the species in the organic phase. The equation for the distribution of a tetraalkylammonium salt into a solvent can be written



or



(3) A. A. Maryott and E. R. Smith, *Nat. Bur. Stand. U. S., Circ.*, No. 14, 18 (1951).

(4) J. Bufalini and K. H. Stern, *J. Amer. Chem. Soc.*, **83**, 4362 (1961).

(5) D. E. Irish and A. R. Davis, *Can. J. Chem.*, **46**, 943 (1968).

(6) Yu. G. Frolov, V. V. Sergievskii, and A. I. Sergievskaya, *Zh. Neorg. Khim.*, **13**, 1909 (1968) [*Russ. J. Inorg. Chem.*, **13**, 994 (1968)].

(7) A. R. Davis, J. W. Macklin, and R. A. Plane, *J. Chem. Phys.*, **50**, 1478 (1969).

(8) R. A. Dwek, Z. Luz, and M. Shporer, *J. Phys. Chem.*, **74**, 2232 (1970).

(9) K. A. Bol'shakov, N. M. Sinitsyn, K. I. Petrov, V. F. Travkin, and M. V. Rubtsov, *Zh. Neorg. Khim.*, **13**, 3082 (1968) [*Russ. J. Inorg. Chem.*, **13**, 1589 (1968)].

(10) W. E. Keder and A. S. Wilson, *Nucl. Sci. Eng.*, **17**, 287 (1963).

(11) R. R. Grinstead and J. C. Davis, Annual Summary Progress Report, 1966-67, from the Dow Chemical Co. to the Office of Saline Water, p 65; modified from K. Gustavii and G. Schill, *Acta Pharm. Suecica*, **3**, 241 (1966); *ibid.*, **3**, 259 (1966); *ibid.*, **4**, 233 (1967).

depending on whether the species in the organic phase is associated to an ion pair or is dissociated. The corresponding equilibrium constants are

$$\mathcal{K}^a = \frac{(R_4N^+ \cdots X^- \cdot mH_2O)_0}{(R_4N^+)(X^-)(H_2O)^m} = \frac{[R_4N^+ \cdots X^- \cdot mH_2O]_0 y_0}{(R_4N^+)(X^-)(H_2O)^m} = K^a y_0 \quad (2a)$$

$$\mathcal{K}^d = \frac{(R_4N^+)_0 (X^- \cdot mH_2O)_0}{(R_4N^+)(X^-)(H_2O)^m} = \frac{[R_4N^+]_0 [X^- \cdot mH_2O]_0 y_{\pm}^2}{(R_4N^+)(X^-)(H_2O)^m} = K^d y_{\pm}^2 \quad (2b)$$

where parentheses denote activities, brackets indicate concentrations, and y is an activity coefficient. A log-log plot of the (organic phase activity)^{1/2} vs. the aqueous concentration should be a straight line whose slope is 2 or 1, depending on whether case a or b is involved.

It has been shown in a different type of study¹² that ClO_4^- in nitrobenzene is essentially anhydrous, so tetrapropylammonium perchlorate was the first salt studied. Figure 1 shows a log-log plot of the organic phase salt concentration in nitrobenzene vs. the equilibrium aqueous concentration for tetrapropylammonium perchlorate. But even with a dielectric constant of 35, the decrease in the activity coefficients from unity at the higher organic phase salt concentrations becomes significant. So they were calculated by a Debye-Hückel type expression¹³ (using a distance of closest approach, a , of 6 Å). Activity coefficients in the aqueous phase were estimated by means of Poirier's expressions,¹⁴ and, as can be seen in Figure 1, the corrected points (filled triangles) up to $10^{-2} M$ fall on the same straight line of unit slope extended from the more dilute solutions where the corrections are negligible. Since the salt is surely dissociated in the dilute aqueous phase, the observed slope of unity shows that it is also dissociated in the organic phase over that range of concentration.

Table I shows the results of determining, by Karl Fischer titrations, the water coextracted by three concentrations of tetrapropylammonium perchlorate in nitrobenzene. Approximately 0.3–0.4 mol of water appears per mole of extracted salt. This value is obtained by subtracting the water distributing into the nitrobenzene alone (calculated as the volume fraction of nitrobenzene times the solubility of water in nitrobenzene, 0.16–0.18 M , depending on the temperature) from the total amount of water determined for the organic phase. It is not clear whether the ~ 0.4 mol of water found is (a) associated with the cation, (b) associated with the anion, or (c) just an increase in water dissolved in the nitrobenzene solvent because the presence of the dissolved salt changes the properties of the solvent. To help understand this, a still larger cation,

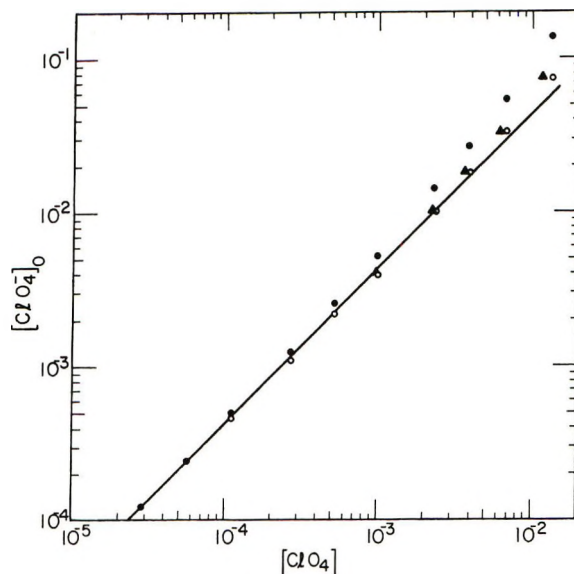


Figure 1. The tetrapropylammonium perchlorate concentration in nitrobenzene vs. the aqueous tetrapropylammonium perchlorate concentration, ●; organic phase concentration corrected by Debye-Hückel type activity coefficient with a distance of closest approach of 6 Å, ○; corrected to aqueous phase activity, calculated from Poirier's expressions with $a = 2.5$ Å, ▲.

Table I: Water Coextracted with Tetraalkylammonium Salts in Nitrobenzene

Salt	Molarity of salt(org) $\times 10^2$	Molarity of water(org) ^a $\times 10^2$	Ratio of water to salt molarity
Tetrapropylammonium perchlorate	13.9	5.2	0.37
	2.66	1.0	0.38
	1.41	0.5	0.4
Tetrahexylammonium perchlorate	20.3	7.9	0.39
	8.13	2.7	0.33
	4.07	1.5	0.37
Tetrabutylammonium tetraphenylboride	1.63	0.6	0.4
	10.0	0.8	0.08
	3.98	0.2	0.05
Tetrabutylammonium nitrate	1.99	0.1	0.05
	20.4	29.6	1.45
	9.11	12.8	1.41
	4.12	5.8	1.41
	1.52	1.9	1.3

^a The water extracted by the diluent alone (diluent volume fraction \times water solubility in diluent) has been subtracted.

the tetrahexylammonium ion, was used, and the results are also shown in Table I. They are the same, ~ 0.4 mol of water/mole of salt. Since we might expect that doubling the size of the cation would change (re-

(12) J. J. Bucher and R. M. Diamond, to be published.

(13) R. A. Robinson and R. H. Stokes, "Electrolyte Solutions," Butterworths, London, 1959, 2nd ed, Chapter 9.

(14) J. C. Poirier, *J. Chem. Phys.*, 21, 965 (1953).

duce) the amount of water associated with it, this result suggests that possibility a is not likely. Indeed, the use of a larger anion, the tetraphenylboride ion, which coextracts essentially zero water under these conditions (Table I), indicates that possibility b is the correct one. That is, essentially an independent and anhydrous tetraalkylammonium cation is present in these (dilute) nitrobenzene salt solutions, and the ~ 0.4 mol of water with the perchlorate salt is probably bound to ClO_4^- .

For such large, poorly solvated anions, we might expect that the process of associating to ion pairs or to ion quadrupoles or to still higher aggregates would not change the water uptake much, possibly reducing it still further. We can test this by employing lower-dielectric-constant solvents where the extracted species is indeed aggregated. So the water uptake for tetraalkylammonium perchlorate in 20 vol % nitrobenzene–80 vol % benzene and in dichloroethane was studied. The extraction curves, Figures 2 and 3, show that in these solvents, particularly the former, at concentrations above $10^{-3} M$ the salt has aggregated to ion pairs and then to ion quadrupoles and beyond. But the water coextracted is still 0.3–0.4 mol/mol of salt, as listed in Table II, and again changing the size of the cation had little effect. In fact, even going to pure benzene as solvent, where the solution properties would surely be most changed by the addition of the salt, made little difference in the water uptake per mole of salt; the slight decrease observed may be related to the much lower water solubility in benzene compared to nitrobenzene or dichloroethane.

The results indicate that only one out of three to

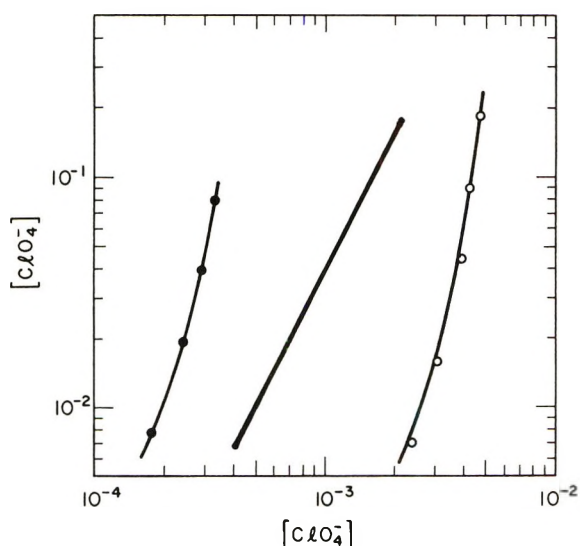


Figure 2. The tetraalkylammonium perchlorate concentration in 20% nitrobenzene–80% benzene vs. the aqueous tetraalkylammonium perchlorate concentration: tetrabutylammonium perchlorate, \circ ; tetrapentylammonium perchlorate, \bullet . The straight line segment is drawn with a slope of 2, indicating association to ion pairs.

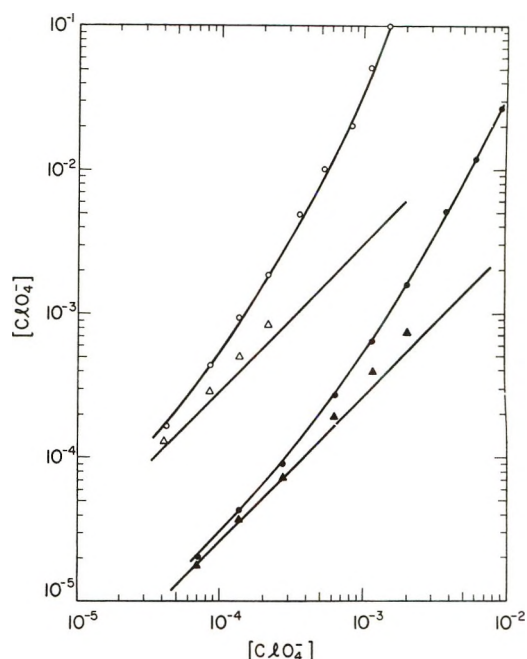


Figure 3. The tetraalkylammonium perchlorate concentration in dichloroethane vs. the aqueous tetraalkylammonium perchlorate concentration: tetrabutylammonium perchlorate, \circ ; corrected by Debye–Hückel activity coefficient, Δ ; tetrapropylammonium perchlorate, \bullet ; corrected by Debye–Hückel activity coefficient, \blacktriangle . The straight line segments are drawn with unit slope, indicating a dissociated species.

Table II: Water Coextracted with Tetraalkylammonium Perchlorate in Organic Solvents

Solvent	Cation	Molarity of salt- (org) $\times 10^3$	Molarity of water- (org) ^a $\times 10^3$	Ratio of water to salt molarity
Dichloroethane	Tetrapropyl- ammonium	5.30	2.2	0.42
		2.06	0.9	0.4
		1.00	0.4	0.4
		0.47	0.2	0.4
	Tetrabutyl- ammonium	20.6	6.7	0.33
		10.3	3.3	0.32
	Tetrahexyl- ammonium	5.09	1.7	0.33
		7.57	2.7	0.36
20% Nitroben- zene–80% benzene	Tetrapentyl- ammonium	3.78	1.3	0.34
		1.89	0.7	0.4
		0.76	0.4	0.5
		18.3	5.1	0.28
	Tetrabutyl- ammonium	8.98	2.9	0.32
		4.31	1.5	0.35
		1.58	0.5	0.3
		7.89	2.4	0.30
Benzene	Tetrapentyl- ammonium	3.93	1.3	0.33
		1.96	0.6	0.3
	Tetrahexyl- ammonium	9.44	1.85	0.20
		3.78	0.79	0.21
		1.89	0.40	0.21
		0.76	0.17	0.22

^a The water dissolved by the volume fraction of solvent alone has been subtracted.

five ClO_4^- ions carry a water molecule in these organic solvents. What can be said about their first-shell hydration number in an aqueous solution? For such poorly hydrated ions as ClO_4^- , it may not be meaningful to even speak of such a quantity in the aqueous phase, as the water molecules may switch rapidly between orientation towards the ion and towards the surrounding water structure, with no fixed coordination number around the ion. This would correspond to the "thawed" region of Frank and Wen,¹⁵ or to the range of zero (negative) hydration of Samoilov,¹⁶ or to the "structure-breaking" of Gurney.¹⁷

However, it does seem clear that there is no water associated with the tetraalkylammonium cations. So it should be possible to study the water carried into nitrobenzene by the distribution of other dissociated tetraalkylammonium salts and ascribe all the water found to the anions. Figure 4 shows a log-log plot of the organic phase concentration of tetrabutylammonium nitrate *vs.* the aqueous phase value. Activity coefficient corrections are made for the most concentrated organic solutions, again using the same Debye-Hückel expression, and for the concentrated aqueous phase by use of Poirier's expressions (calculated with a distance of closest approach of 2.5 Å so as to approximate the experimental values for tetrabutylammonium bromide¹⁸ for molalities between 0.1 and 1.0). A straight line of unit slope results up to $10^{-2} M$, indicating dissociation of the salt in nitrobenzene for that range of concentration, and a considerable proportion still dissociated even at $10^{-1} M$. Table I lists values for the water coextracted with the NO_3^- ; of the order of 1.4 mol of water is involved per NO_3^- .

Since we only determine the stoichiometric water uptake, the average value for the anion, we cannot translate this result uniquely into a description of the anion hydrates involved. For example, there may be a mixture of $\text{NO}_3^- \cdot \text{H}_2\text{O}$ and $\text{NO}_3^- \cdot 2\text{H}_2\text{O}$ extracting, or all possible mixtures of these two plus anhydrous NO_3^- and the species $\text{NO}_3^- \cdot 3\text{H}_2\text{O}$ with a completely hydrated first shell, so as to yield the observed hydration number, ~ 1.4 . Even if only the two species, $\text{NO}_3^- \cdot \text{H}_2\text{O}$ and $\text{NO}_3^- \cdot 2\text{H}_2\text{O}$ exist, we do not know whether the dihydrate has two water molecules hydrogen-bonded to two oxygens of the nitrate anion, giving it a coordination number of 2, or whether the second water is hydrogen-bonded to the first leaving the nitrate anion with a coordination number of 1.

The observed hydration of NO_3^- can be compared with the alcoholation number found in an extraction study of tetrabutylammonium nitrate into 1,2-dichloroethane with decanol;¹⁹ only one alcohol complexed the NO_3^- for alcohol concentrations from 0.08 to 0.5 M . But in that study it was not possible to determine the water uptake to better than 1 ± 1 water molecule, and if there is a water molecule involved, again we do not know whether the water and alcohol molecules are

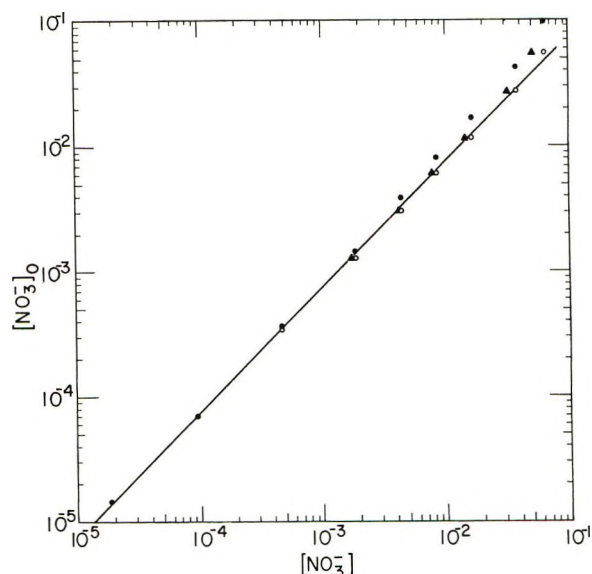


Figure 4. The tetrabutylammonium nitrate concentration in nitrobenzene *vs.* the aqueous ammonium nitrate concentration, ●; corrected to organic phase activity using a Debye-Hückel activity coefficient with $a = 6 \text{ \AA}$, ○; corrected to an aqueous phase activity reproducing the experimental activity coefficients of tetrabutylammonium bromide, ▲.

hydrogen-bonded to two nitrate oxygens, or whether the water is a bridge between the alcohol and the anion, leaving the latter monocoordinated. In that study, it was also necessary to determine the amount of water extracted with uncomplexed NO_3^- into the 1,2-dichloroethane diluent alone. The ratio of water/nitrate found there in two determinations was 1.25, in agreement with the present results in nitrobenzene.

For such anions that carry into the organic phase more than 1 mol of water per ion, we believe that the hydration number observed in the organic phase may be only a lower limit to the first-shell hydration number in water. For in the aqueous phase, the first-shell waters receive additional solvation from the water molecules farther out; but in the organic phase, they exchange this (hydrogen-bonded) solvation for the (usually) poorer solvation of the surrounding organic diluent. The poorer environment there would thus tend to reduce the first-shell hydration number over that in water itself.

The procedure described in this paper for determining the water carried by an anion is certainly simpler than the use of trioctylphosphine oxide in nitrobenzene or in 1,2-dichloroethane to extract the corresponding

(15) H. S. Frank and W.-Y. Wen, *Discuss. Faraday Soc.*, **24**, 133 (1957).

(16) O. Ya. Samoilov, *ibid.*, **24**, 141 (1957).

(17) R. W. Gurney, "Ionic Processes in Solution," McGraw-Hill, New York, N. Y., 1953, Chapter 16.

(18) S. Lindenbaum and G. E. Boyd, *J. Phys. Chem.*, **68**, 911 (1964).

(19) D. J. Turner and R. M. Diamond, *J. Inorg. Nucl. Chem.*, **30**, 3039 (1968).

acid.¹² By the latter method a value for the hydration number of NO_3^- in nitrobenzene of ~ 2 was obtained, but there was uncertainty introduced by the presence of binitrate ion produced from the aqueous nitric acid solution. This problem of binitrate ion formation cannot arise in the present study of neutral salt solutions, so that the value of 1.3–1.4 mol of water per

NO_3^- is the better one. The distribution of other alkylammonium salts, particularly the halides, into nitrobenzene and into 1,2-dichloroethane will be similarly studied to see what regularities do occur in the hydration of these anions in the organic solvents.

Acknowledgment. The authors would like to thank Mr. J. Bucher for helpful discussions.

Selectivity in Heterovalent Anion Exchange. Ion Pairing vs. Ion Hydration¹

by J. Bucher, R. M. Diamond,*

Lawrence Berkeley Laboratory, University of California, Berkeley, California 94720

and B. Chu

Department of Chemistry, State University of New York, Stony Brook, New York (Received February 23, 1972)

Publication costs assisted by the Lawrence Berkeley Laboratory

The values of the selectivity coefficients, $K_{B/A}$, for heterovalent exchange with a strong-base resin and radio-tracer ReO_4^- , CrO_4^{2-} , and WO_4^{2-} vs. macro Cl^- , and radiotracer $\text{Cr}(\text{CN})_6^{3-}$, $\text{Co}(\text{CN})_6^{3-}$, and $\text{Fe}(\text{CN})_6^{4-}$ vs. macro CN^- , have been determined. These results show that in such systems, contrary to early ideas on the nature of resin selectivity, the direction of the exchange is determined by the superior hydration of the ions in the dilute external aqueous phase over that in the resin phase, and not by ion pairing in the latter phase.

Introduction

For the ion-exchange reaction



where the superscript bar indicates the resin phase, it has become customary to write the equilibrium constant

$$\mathcal{K}_{B/A} = \frac{(\bar{B})(A)}{(\bar{A})(B)} = \frac{[\bar{B}][A]\tilde{\gamma}_B\gamma_A}{[\bar{A}][B]\tilde{\gamma}_A\gamma_B} = K_{B/A} \frac{\tilde{\gamma}_B\gamma_A}{\tilde{\gamma}_A\gamma_B} \quad (2)$$

and to assume the same standard state for both phases.^{2,3} Then

$$\mathcal{K}_{B/A} = 1 = K_{B/A} \frac{\tilde{\gamma}_B\gamma_A}{\tilde{\gamma}_A\gamma_B} \quad (3)$$

If, as is usually the case, the standard state chosen is the hypothetical state of unit activity with the properties of the infinitely dilute solution, the ratio γ_A/γ_B of the external-phase activity coefficients can be made as close to unity as is desired by decreasing the concentration of that phase. Thus eq 3 becomes

$$\mathcal{K}_{B/A} = 1 = K_{B/A} \frac{\tilde{\gamma}_B}{\tilde{\gamma}_A} \quad (4)$$

or

$$K_{B/A} = \frac{\tilde{\gamma}_A}{\tilde{\gamma}_B}$$

The equilibrium quotient or selectivity constant, $K_{B/A}$, depends only on the resin phase activity coefficients. Partly as a result of this type of derivation, early researchers often formulated ion-exchange resin selectivity as a function mainly of resin properties.^{4–10}

(1) Work performed under the auspices of the U. S. Atomic Energy Commission.

(2) (a) K. A. Kraus and F. Nelson in "The Structure of Electrolyte Solutions," W. J. Hamer, Ed., Wiley, New York, N. Y., 1959, p 340; (b) B. Chu, Thesis, Cornell University, Ithaca, N. Y., 1959.

(3) Y. Marcus and A. S. Kertes, "Ion Exchange and Solvent Extraction of Metal Complexes," Wiley-Interscience, New York, N. Y., 1969, p 278.

(4) G. E. Boyd, J. Schubert, and A. W. Adamson, *J. Amer. Chem. Soc.*, **69**, 2818 (1947).

(5) H. P. Gregor, *ibid.*, **73**, 642 (1951).

(6) T. R. E. Kressman and J. A. Kitchener, *J. Chem. Soc.*, 1190 (1949).

(7) K. W. Pepper and D. Reichenberg, *Z. Elektrochem.*, **57**, 183 (1953).

(8) J. L. Pauley, *J. Amer. Chem. Soc.*, **76**, 1422 (1954).

(9) H. P. Gregor, J. Belle, and R. A. Marcus, *ibid.*, **77**, 2713 (1955).

(10) F. E. Harris and S. A. Rice, *J. Chem. Phys.*, **24**, 1258 (1956).

But we are free to choose the standard states in whatever manner we desire. If we choose the standard state to be the pure salt resinate, then, although the ratio $\bar{\gamma}_B/\bar{\gamma}_A$ is not unity, the greatest part of the variation in $K_{B/A}$ comes from γ_A/γ_B , the aqueous phase ratio. Now the source of resin selectivity would appear to come mainly from the external solution phase.

In fact, of course, the origin of resin selectivity comes from a difference of differences; the differences in the interactions of the two ions in the two different phases. However, the properties and characteristics of one phase may actually dominate the exchange. A number of types of studies can indicate the relative importance of the various interactions. One such type is a study of heterovalent exchange, in particular the direction of selectivity for ions of different charge. Several ion-exchange models⁸⁻¹⁰ postulate the dominant importance of Coulomb forces in the resin phase, that is, of ion pairing between the counterion and the resin-fixed ion. As a natural consequence of such models, ion selectivity can be predicted to go up, the higher the charge on the ion, and indeed such a general rule has been given by a number of authors.

But the opposite behavior, a decrease in resin affinity with increasing ionic charge, would be the rule if, as has also been proposed,^{2b,11,12} ion-water interactions (hydration) in the dilute external solution, rather than ion-resin ion contacts (ion pairing), were the most important factors in exchanges involving strong-base or strong-acid resins and nonhydrophobic ions. The higher-charged ion has a greater need for hydration, a larger hydration energy, than the lower-charged one. And since the best hydration is obtained in the dilute external phase rather than in the concentrated resin phase, the higher-charged ion goes into the aqueous solution preferentially, forcing the other ion into the less desirable resin phase.

The present paper presents some experimental evidence for choosing between these points of view; the data come from the heterovalent ion exchange of some large complex ions. Obviously it would be best to compare ions of similar size and structure, though differing in charge, so as to minimize all effects other than that of the charge on the selectivity. For this reason, tracer ReO_4^- , WO_4^{2-} , and CrO_4^{2-} were measured *vs.* Cl^- as the macro anion, and tracer $\text{Cr}(\text{CN})_6^{3-}$, $\text{Co}(\text{CN})_6^{3-}$, and $\text{Fe}(\text{CN})_6^{4-}$ were determined *vs.* macro concentrations of CN^- .

Experimental Section

Reagents. The resins used in the present experiments were two batches of Dowex 1, a strong-base resin, one of 10% and the other of 8% DVB cross linking. They had capacities of 3.04 and 3.46 mequiv/g of dry Cl-form resin, respectively.

The chloride solutions employed were made from reagent grade salts and used without further purifica-

tion. The concentrations of these solutions were determined by the Volhard method.¹³ The cyanide solutions were made from Baker and Adamson KCN, reagent grade, and the stock solution was determined by the Denigès-Liebig method,¹³ using a visual end point.

The 3.87-day $^{186}\text{ReO}_4^-$ tracer was obtained from Oak Ridge, as was the 27.8-day $^{51}\text{CrCl}_3$. The latter was diluted with $10^{-3} M$ stable CrCl_3 , oxidized with Na_2O_2 , and then boiled to destroy the peroxide. The oxidation to CrO_4^{2-} could be followed by the change in color to the yellow of CrO_4^{2-} . The batch experiments with this ion were done at pH 8-10. Below pH 8, HCrO_4^- forms and dimerizes. The 73.2-day $^{185}\text{WO}_4^{2-}$ came from Oak Ridge in dilute KOH; the experiments with it were performed in slightly basic solution.

The three tracer cyano complexes were prepared from radioactive ^{59}Fe , ^{60}Co , and ^{51}Cr , supplied by Oak Ridge as the chlorides in HCl. A small amount of each tracer was added to water and taken to near dryness several times to remove the HCl. About 1 g of KCN was then added, and the mixture was heated until the KCN fused. After cooling, the solid was dissolved in 0.01 M KOH. The concentrations of the cyano complexes were less than $10^{-6} M$ in the batch experiments performed, and the pH was 11-12.

Procedure. In the batch experiments, 5, 10, or 20 ml of a chloride or cyanide solution of known concentration, to which 50 μl of tracer had been added, was shaken overnight with small amounts (10-150 mg) of resin in 25-ml glass-stoppered flasks or 60-ml glass-stoppered bottles. Duplicate 2- or 3-ml aliquots of the equilibrium solution were withdrawn through glass-wool filters into screw-cap vials, and were then γ -counted in a 2 in. \times 2 in. NaI(Tl) well-type scintillation counter, using a single-channel analyzer. A standard solution was treated in the same way, but without any resin being added. After correcting the counting rates for background, the value of D , the distribution ratio for the tracer species, could be obtained

$$D = \frac{(\text{counts/min/ml of standard soln}) - (\text{counts/min/ml of equil soln})}{(\text{counts/min/ml of equil soln})(\text{g of dry resin})} \quad (5)$$

Results

The results of the distribution experiments with alkali chloride solutions (mainly NaCl) from 0.02 to 0.5 *m* and tracer ReO_4^- , CrO_4^{2-} , and WO_4^{2-} are shown in Figure 1. Similarly, Figure 2 gives the plots of $\log D$ *vs.* KCN solutions from 0.1 to 1 *m*. Since for the tracer ion, $D' = [\bar{B}]/[B] = D/\text{swc}$, where *swc* stands for specific water content (g of water/g of dry

(11) B. Chu, D. C. Whitney, and R. M. Diamond, *J. Inorg. Nucl. Chem.*, **24**, 1405 (1962).

(12) G. Eisenman, *Biophys. J. Suppl.*, **2**, 259 (1962).

(13) H. A. Laitinen, "Chemical Analysis," McGraw-Hill, New York, N. Y., 1960.

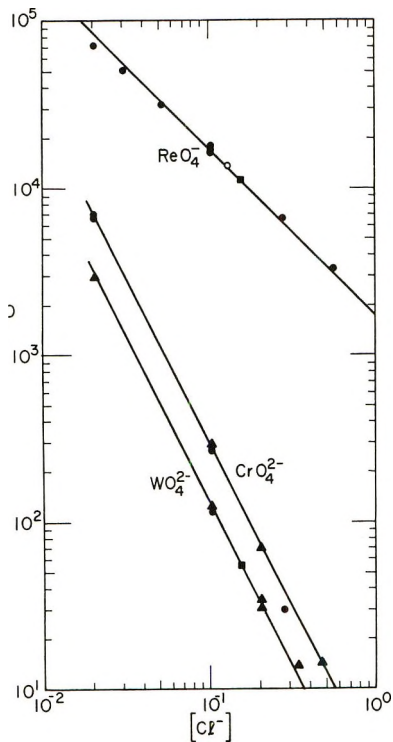


Figure 1. Plot of D for tracer ReO_4^- , CrO_4^{2-} , and WO_4^{2-} vs. Cl^- molality; lines are drawn with slopes of -1 , -2 , and -2 , respectively. Data are for X10 resin, and for NaCl solutions except for symbols indicating LiCl, \circ ; CsCl, \blacksquare ; $(\text{CH}_3)_4\text{NCl}$, \blacktriangle .

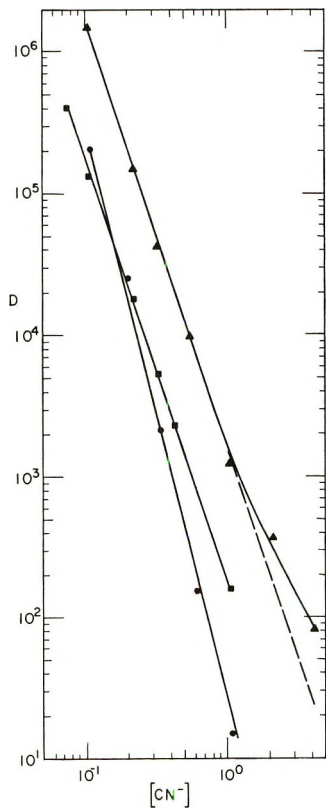


Figure 2. Plot of D for tracer $\text{Co}(\text{CN})_6^{3-}$ (\blacktriangle), $\text{Cr}(\text{CN})_6^{3-}$ (\blacksquare), and $\text{Fe}(\text{CN})_6^{4-}$ (\bullet) vs. KCN molality for X8 resin; lines are drawn with slopes of -3 , -3 , and -4 , respectively.

resin), substitution into the appropriate form of eq 2 for heterovalent exchange yields

$$D' = \mathcal{K}_{B/A} \frac{[\bar{A}]^n \bar{\gamma}_A^n \gamma_B}{[A]^n \bar{\gamma}_B \gamma_A^n} = K_{B/A} \frac{[\bar{A}]^n}{[A]^n} \tag{6}$$

In dilute solutions where resin invasion is negligible, $[\bar{A}] = \bar{C}/swc$, where \bar{C} is the capacity of the resin (mequiv/g of dry resin), $\gamma_B/\gamma_A^n = \text{constant}$ ($\rightarrow 1$ as solution becomes more dilute), and for tracer concentrations of B, $\bar{\gamma}_A/\bar{\gamma}_B = \text{constant}$. Then

$$D' = \left(\mathcal{K}_{B/A} [\bar{A}]^n \frac{\bar{\gamma}_A^n}{\bar{\gamma}_B} \right) [A]^{-n} \tag{7}$$

and the terms inside the parentheses are a constant. So D' and D depend inversely on the n th power of the aqueous phase macroion concentration, $[A]$.

Since the log-log plots of D vs. molality in Figures 1 and 2 are straight lines with the proper slope n , the conditions described in the previous paragraph must hold, and $K_{B/A}$ can be evaluated from the plots by means of eq 6 with the additional knowledge of the resin capacity, \bar{C} , and the specific water content, swc . These values of $K_{B/A}$ are given in Table I; note that the first three are for Cl^- -form X10 resin, and that the second group is for CN^- -form X8 resin.

Table I: Selectivity Coefficients for Tracer Anions on Dowex 1

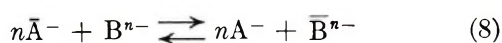
Tracer anion of charge n	Macro-anion	$K_{B/A}$	$K_{B/A}^{1/n}$
X10 Resin			
ReO_4^-	Cl^-	570	570
WO_4^{2-}	Cl^-	0.10	0.32
CrO_4^{2-}	Cl^-	0.23	0.48
X8 Resin			
$\text{Cr}(\text{CN})_6^{3-}$	CN^-	2.0	1.3
$\text{Co}(\text{CN})_6^{3-}$	CN^-	22	2.8
$\text{Fe}(\text{CN})_6^{4-}$	CN^-	0.073	0.52

Discussion

Before discussing what the results indicate about the choice between models stressing ion pairing in the resin phase and models stressing the differential hydration of the ions, one should note the effect of “electroselectivity” in heterovalent exchange. That is, as discussed in ref 14, the Donnan potential of the ion-exchange resin acts on the counterions with a force proportional to their charge. Thus the counterion of higher charge is more strongly attracted by the ion exchanger. And because the Donnan potential increases with dilution of the external solution and with increasing concentration of the resin-fixed ions, the attraction for the higher-

(14) F. Helfferich, “Ion Exchange,” McGraw-Hill, New York, N. Y., 1962, p 156.

charged ions follows the same pattern. Since in most ion-exchange operations the external solution is dilute compared to the resin phase, this leads to the empirical observation that resins prefer the ion of higher charge. But, in fact, if the external solution is made quite concentrated, this order can be reversed. This type of selectivity, called electroselectivity,¹¹ is not intrinsic to the exchanger, but follows merely from the difference in ionic charge of the two ions and the difference in concentration of the two phases. It can be seen more simply, perhaps, as an example of Le Chatelier's principle in the equilibrium



where ion type A is univalent (for simplicity) and ion type B is n -valent. If the external solution is made much more dilute than the resin phase, the equilibrium reacts so as to try to put more ions into the external phase and decrease the number of ions in the exchanger. This means a shift to the right, favoring ion B in the exchanger and ion A in the external solution.

However, the value of the equilibrium quotient, or selectivity coefficient, for eq 8

$$K_{B/A} = \frac{[\bar{B}][A]^n}{[\bar{A}]^n[B]} \quad (9)$$

does give a direct measure of the intrinsic selectivity even for heterovalent exchanges. A complication is that the value $K_{B/A}$ may vary with resin composition. To circumvent this, the ions to be compared can be in tracer quantities in the presence of macro amounts of a third ion which thus dominates the composition in both phases. Experimentally it is more convenient to measure $K_{B/A}$ for one tracer ion at a time in the presence of the same macro species, and this is what has been done in the present study.

Table I lists the values of the equilibrium quotients

found. Actually, there is some uncertainty as to the most appropriate way to compare heterovalent exchanges. A fairer comparison than the values of K directly might be $K^{1/ab}$, or $K_{B/A}^{1/n}$ in the present case, so that the equilibrium is normalized to 1 equiv of exchange; these values are also listed. It can be seen from either set of values that there is a marked decrease in resin selectivity with an increase in the charge on the anion.

So at least with a strong-base resin, electrostatic ion pairing in the resin phase does not determine the order of selectivity. On the contrary, resin selectivity appears to go with the inverse order of the hydration energies of the ions, if one makes the reasonable assumption that hydration increases with increasing charge on the ion (radius held constant). This is, in fact, what would generally be expected from a model for ion-exchange selectivity based on the difference in hydration energies of an ion between the two phases,^{2b,11} as this difference should be roughly proportional to the hydration energy in the better phase, in pure water itself, at least for lowly and moderately cross-linked resins. Thus we believe it is more correct in the present systems to speak of selective binding of the ions into the external aqueous phase, rather than of ion pairing in the resin phase.

Finally, carrying this hydration argument to an extreme provides a possible explanation for the difference in $K_{B/A}$ for CrO_4^{2-} and WO_4^{2-} and for $\text{Co}(\text{CN})_6^{3-}$ and $\text{Cr}(\text{CN})_6^{3-}$. The tungsten(VI) and chromium(III) are more electropositive than the chromium(VI) and cobalt(III), respectively; as a result, the electron densities on the surfaces of WO_4^{2-} and $\text{Cr}(\text{CN})_6^{2-}$ are a little higher than those on CrO_4^{2-} and $\text{Co}(\text{CN})_6^{3-}$. This means slightly greater hydration by water, and so somewhat greater binding of WO_4^{2-} and $\text{Cr}(\text{CN})_6^{3-}$ into the dilute external aqueous phase and somewhat smaller values of $K_{B/A}$, as observed.

Diffusion of Acetic Acid Dimers and Their Homomorphs

by F. A. L. Dullien*^{1a} and G. H. Shroff*^{1b}

Department of Chemical Engineering, University of Waterloo, Waterloo, Ontario, Canada (Received November 18, 1971)

Publication costs assisted by the National Research Council of Canada

The interdiffusion coefficient attributed to the acetic acid dimer in infinitely dilute CCl_4 solutions is significantly greater than the interdiffusion coefficients found in the case of various homomorphs of the dimer. Homomorphs of the cyclic dimer investigated were *N,N'*-dimethylpiperazine, 2,5-dimethylpiperazine (cis), 5-ethyl-2-methylpyridine, and 1,4-dimethylcyclohexane (trans). Homomorphs of the open dimer investigated were 2,5-dimethylhexane, isobutyl acetate, and acetylacetone. Explanation for the observed behavior is offered in terms of the greater flexibility of the dimer as compared with the homomorphs. The two monomers are presumed to swing about the axis formed by the two hydrogen bonds with relative freedom. The resulting segmental type of motion of the dimer may be expected to meet with less resistance.

Introduction

The question of the nature of kinetic units in liquid diffusion is an intriguing one. It has been customary²⁻⁴ to explain the often anomalous values of diffusion coefficients found in associating solutions by assuming that in such systems the kinetic units are the associating complexes rather than the monomers. The existence of associating complexes in some pure liquids and solutions has been firmly established from the study of a variety of equilibrium properties.^{2a,5-7}

In association, generally there is dynamic equilibrium between the monomers and the complexes, characterized by frequent exchange of monomers. In the course of each exchange process, there is a brief transition stage in which the bonds holding the complex together are greatly weakened. It is quite plausible to assume that higher energy conformations occur quite frequently in the life of a complex, regardless of whether an exchange process is involved or not. From a high energy state the complex may either dissociate into monomers or return to its stable state, depending on the conditions.

A complex in a high energy conformation can be expected to have increased mobility because under such conditions the constituent monomers may be able to move more as independent segments than in a stable molecule. The time any complex spends in high energy states may be presumed to be only a small fraction of its life. Nevertheless, it is possible that by frequent passages through such states the net diffusion rate of the complex may be significantly increased, because the occurrence of high energy states may be presumed to be strongly correlated with the diffusional moves made by individual monomers. Under the impact of a high energy collision with a neighbor molecule, some of the hydrogen bonds in the complex may be loosened up, and simultaneously some monomers may be pushed by the force of the same impact into new positions. It is not implied that the monomers in the complex move any significant distance from each

other, but rather that the complex diffuses as a highly flexible unit, by a type of segmental diffusion with the monomers acting as segments. This diffusion mechanism, widely accepted in the case of chain molecules, results in greater mobility of the diffusing entity. The same mechanism may also be significant in the diffusion of associating complexes in which the monomers are held together by relatively weak forces. As a result, the diffusion coefficient involving an associating complex may turn out to be bigger than the value which would be observed if the constituent monomers of the complex were rigidly bonded to each other all the time. Since there is no known theoretical method to estimate the magnitude of this effect, an experimental approach has been chosen in the present work.

Dilute solutions of acetic acid in carbon tetrachloride have been selected for study because acetic acid dimers are among the most strongly hydrogen-bonding substances, and the acetic acid dimers in dilute solutions are relatively well-defined entities. Acetic acid in carbon tetrachloride is known to form complexes^{2a,8-10} which are believed to consist mainly of cyclic dimers with the possible existence of smaller quantities of noncyclic or "open" dimers. The interdiffusion

(1) (a) Visiting Professor in School of Chemical Engineering, Purdue University, on leave from University of Waterloo. (b) Control Systems Research, Inc., Arlington, Va.

(2) (a) I. Prigogine and R. Defay (transl. D. H. Everett), "Chemical Thermodynamics," Longmans, Green and Co., New York, N. Y., 1954; (b) R. H. Stokes, *J. Phys. Chem.*, **69**, 4012 (1965).

(3) H. Eyring and M. S. Jhon, "Significant Liquid Structures," Wiley, New York, N. Y., 1969.

(4) D. K. Anderson and A. L. Babb, *J. Phys. Chem.*, **66**, 899 (1962).

(5) H. A. Stuart, "Molekulstruktur," Springer-Verlag, Berlin, 1967.

(6) M. Davies, P. Jones, D. Patraik, and E. A. Moelwyn-Hughes, *J. Chem. Soc.*, 1249 (1951).

(7) L. W. Reeves and W. G. Schneider, *Trans. Faraday Soc.*, **54**, 314 (1958).

(8) K. Venkateswarlu and S. Sriraman, *ibid.*, **53**, 433 (1957).

(9) H. A. Pohl, M. E. Hobbs, and P. M. Gross, *J. Chem. Phys.*, **9**, 408 (1941).

(10) S. Fénéant, *C. R. Acad. Sci.*, **235**, 240 (1952).

coefficients in this system have been determined at various dilutions by several authors.^{4,11}

The approach used in the present study consisted of measuring the interdiffusion coefficients of various homomorphs of the acetic acid dimers in carbon tetrachloride solutions at increasing dilutions and comparing the measured values with the known interdiffusion coefficients of dilute solutions of acetic acid in carbon tetrachloride. (Molecules of two different compounds are said to be homomorphs if their molecular structures are geometrically similar.) The method of using non-polar homomorphs of polar organic compounds to predict thermodynamic properties of the latter have been used for quite some time.¹² The method has been used also in liquid diffusion work.¹³ In the present study it has been assumed that the diffusion coefficient at infinite dilution of a homomorph of an acetic acid dimer has the same value as the dimer would have, if it behaved as a stable molecule. If the value of the observed diffusion coefficient of the acetic acid dimer were greater than those of its various homomorphs, this may be interpreted as evidence that hydrogen-bonding complexes tend to diffuse by a different mechanism than stable molecules of similar size and shape.

Experimental Section

The following homomorphs of the cyclic dimer of acetic acid have been investigated: 2,5-dimethylpiperazine (cis), *N,N'*-dimethylpiperazine, 1,4-dimethylcyclohexane (trans), 5-ethyl-2-methylpyridine.

The following homomorphs of the "open" dimer of acetic acid have been investigated: acetylacetone, isobutyl acetate, 2,5-dimethylhexane.

The interdiffusion coefficients of the above compounds and of acetic acid have been measured at 25° in the 0.5–10 g/100 ml concentration range.

All homomorphous compounds used were of research grade purity (Aldrich Chemical Co). Glacial acetic acid of 99.8% purity was used without further purification. Due care was exercised in handling the chemicals so as not to expose them to light or humid air. Spectroscopic grade carbon tetrachloride (99.9% purity) was used directly. The potassium chloride used in the calibration of the diffusion cells was Baker Analyzed reagent (J. T. Baker Chemical Co.) and had a stated purity of 99.9%. Water used in the calibration runs was demonized and distilled.

Magnetically stirred diaphragm-cell technique¹⁴ was employed. To minimize loss of solution by evaporation, all connections between the compartments of the cell and the surroundings were made by four glass capillary legs (i.d. = 0.4 mm), two to each compartment. The legs were fitted with Teflon needle valves (Manostat Corp.). A compact stirring and support apparatus housed a battery of six diaphragm cells. Constructional details of the apparatus are given in ref 15.

The KCl solutions used in the calibration runs were analyzed gravimetrically by evaporating them to dryness,¹⁵ and the organic solutions were analyzed by density measurements, using modified Sprengel pycnometers.¹⁵

Results and Discussion

The results of the diffusion measurements have been plotted in Figures 1 and 2, for the cyclic and the "open" homomorphs, respectively. In each case, the interdiffusion coefficients of the acetic acid-carbon tetrachloride system, as determined by Longworth,¹¹ Anderson and Babb,⁴ and by us, have been also plotted in the diagrams.

It is apparent from Figure 1 that all four cyclic homomorphs extrapolated to $D^\circ \approx 1.1 \times 10^{-5}$ cm²/sec at infinite dilution, whereas the acetic acid extrapolated to $D^\circ = 1.42 \times 10^{-5}$ cm²/sec. The latter value has already been corrected for the existence of monomers in the solutions and, therefore, it may be attributed to the dimer.¹¹ As is apparent from Figure 2, 2,5-dimethylhexane and isobutyl acetate extrapolated to $D^\circ \simeq 1.25 \times 10^{-5}$ cm²/sec, whereas acetylacetone extrapolated to $D^\circ \simeq 1.0 \times 10^{-5}$ cm²/sec, at infinite dilution.

The values of D° , obtained by linear extrapolation to infinite dilution, have been listed in Table I, along with the apparent molal volumes ϕ of the solutes at infinite dilution, calculated from our density measurements on the solutions. The close agreement of the four diffusion coefficients obtained in the case of the cyclic homomorphs is quite remarkable. It is apparent from the data in Table I that the four diffusion coefficients do not correlate with the molar volumes of the respective compounds. Lack of correlation of the diffusion data with the molar volumes becomes even more conspicuous when the "open" homomorphs are also included in the comparison. Both 2,5-dimethylhexane and isobutyl acetate have significantly greater diffusion coefficients, at infinite dilution, than the four cyclic compounds, although the molar volume of the former is the biggest of all the compounds studied, and the molar volume of the latter occupies an intermediate position with respect to those of the four cyclic compounds. Most striking, however, is the case of acetylacetone, as this substance has the smallest diffusion coefficient and also the least molar volume of all the eight substances investigated in this study. The behavior of this substance is probably best explained by assuming that it was not free from association under

(11) L. G. Longworth, *J. Colloid Interface Sci.*, **22**, 3 (1966).

(12) R. C. Reid and T. K. Sherwood, "The Properties of Gases and Liquids," McGraw-Hill, New York, N. Y., 1966.

(13) R. L. Robinson, Jr., W. C. Edmister, and F. A. L. Dullien, *Ind. Eng. Chem., Fundam.*, **5**, 74 (1966).

(14) F. A. L. Dullien and L. W. Shemilt, *Can. J. Chem. Eng.*, **39**, 242 (1961).

(15) F. A. L. Dullien, Ph.D. Dissertation, University of British Columbia, 1960.

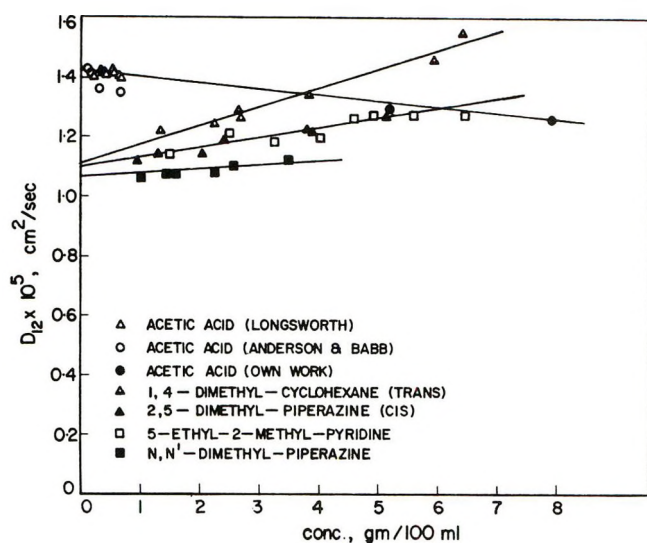


Figure 1. Cyclic homomorphs.

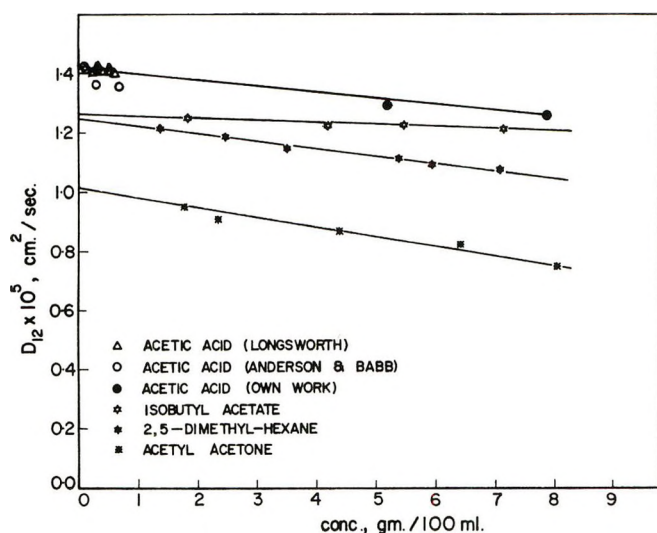


Figure 2. Noncyclic homomorphs.

the conditions used in the diffusion experiments. For this reason acetylacetone will be excluded from further comparisons.

Table I: Diffusion Coefficients at Infinite Dilution (Solvent: CCl_4 ; $t = 25^\circ$)

Solute	$D^\circ \times 10^5$, cm^2/sec	ϕ , ml/mol	D_{cor}° $\times 10^5$, cm^2/sec
Acetic acid (dimer)	1.42	120	1.42
2,5-Dimethylhexane	1.245	164	1.52
Isobutyl acetate	1.26	133	1.33
Acetylacetone	1.015	109	0.955
1,4-Dimethylcyclohexane	1.11	148	1.26
5-Ethyl-2-methylpyridine	1.096	131	1.15
2,5-Dimethylpiperazine (cis)	1.096	125	1.12
N,N'-Dimethylpiperazine	1.065	130	1.12

From the above comparison of diffusion coefficients and molar volumes it seems safe to conclude that, within this group of substances, the molar volume by itself is an extremely poor correlating parameter for diffusion coefficients. Nevertheless, because the apparent molar volume of the acetic acid dimer is somewhat less than the apparent molar volumes of the remaining six homomorphs, the possible effect of the larger molar volumes of the homomorphs (as compared with the molar volume of acetic acid) has been taken into account by calculating corrected diffusion coefficients $D_{\text{cor}}^\circ = D^\circ(\phi_{\text{homomorph}}/\phi_{\text{acetic acid dimer}})^{0.6}$. D_{cor}° has been listed in Table I along with the other data. All but one (2,5-dimethylhexane) of the corrected diffusion coefficients have been found to be significantly less than $1.42 \times 10^{-5} \text{ cm}^2/\text{sec}$, the value attributed to the diffusion coefficient of acetic acid dimer. It is apparent that the corrected diffusion coefficients of all the cyclic homomorphs remained smaller than those of the noncyclic ones (acetylacetone excluded).

The pattern emerging from this comparison suggests a qualitative explanation based on existing differences between the *shapes* and *structural flexibilities* of the various molecules. 2,5-Dimethylhexane can be expected to owe its relatively great mobility both to its chainlike shape and to a high degree of structural flexibility, enabling the molecules of this substance to advance by segmental diffusion, in a snakelike manner. Isobutyl acetate can be expected to be a somewhat less flexible chain, owing to the presence of the carboxyl group. The fact that the four cyclic homomorphs are bulkier than the chain types may be the main reason for their lower diffusion coefficients. Chain molecules tend to have higher diffusion coefficients than bulkier molecules of similar molar volume.¹² It is interesting to note that in this group 1,4-dimethylcyclohexane has the greatest diffusion coefficient. Considering the structural isomerization of cyclohexane, it is possible that the relative lack of rigidity of the cyclohexane ring, as compared with the three heterocyclic rings, is responsible for the somewhat greater mobility of the cyclohexane derivative.

The value of D° for acetic acid is the second highest of all the homomorphs (after correcting for molar volume differences), which is inconsistent with the existence of kinetic units consisting of rigid acetic acid dimers. From the results obtained with the cyclic homomorphs, the diffusion coefficient of the stable cyclic dimer is estimated at $1.1\text{--}1.2 \times 10^{-5} \text{ cm}^2/\text{sec}$. The diffusion coefficient of the acetic acid monomer has been estimated at $\sim 2 \times 10^{-5} \text{ cm}^2/\text{sec}$.¹¹ The experimental value of $1.42 \times 10^{-5} \text{ cm}^2/\text{sec}$, attributed to the acetic acid dimer,¹¹ lies between these two values, and it differs significantly from both of them. Naturally, the most obvious explanation for this behavior of the acetic acid dimer would be that it dissociates

significantly at high dilution. The fact of the matter is, however, that according to measurements of the dissociation constant by several independent investigators,^{6,7,16} acetic acid dissociates only slightly at the highest dilutions at which diffusion measurements have been performed (about 10^{-2} *m*). The value $D^\circ = 1.42 \times 10^{-5}$ cm²/sec has already been corrected for the presence of monomers by Longworth,¹¹ who reported it as the diffusion coefficient of the dimer extrapolated to infinite dilution. Hence, a different explanation must be sought to explain the anomalously high value of this quantity.

A possible explanation can be offered within the same framework of ideas as used to explain the different values found in the case of the various homomorphs. It is postulated, therefore, that the two acetic acid molecules in the dimer form an entity with a significantly lower degree of structural rigidity than that of any of the homomorphs. This assumption is in harmony with the fact that the energy of the hydrogen bond in the dimers is also less than that of the covalent bonds in the homomorphs. The associating acetic acid molecules may be presumed to be forced by the constant bombardment of neighboring solvent molecules to swing about the axis formed by the two hydrogen bonds. Measurements indicating a sizable dipole moment in carbon tetrachloride solutions of acetic acid^{9,17} have been explained by Buckingham and Raab¹⁷ by suggesting the presence of "atomic polarization from slow bending vibrations" of the dimer. Under the impact of a neighboring molecule, one acetic acid molecule at a time may swing into a new position, relatively unhindered by the presence of the other associating molecule. The resulting process is a segmental diffusion, where the segments are the individual acetic acid molecules in the dimer.¹⁸ It may be expected that this mechanism of diffusion encounters less resistance than if the dimers were moving as rigid entities.

Conclusions

Comparison of interdiffusion coefficients, extrapolated to infinite dilution, of acetic acid and six homomorphs of acetic acid dimers in carbon tetrachloride has indicated that the homomorphs tend to have lower diffusion coefficients than the dimers. Interpretation

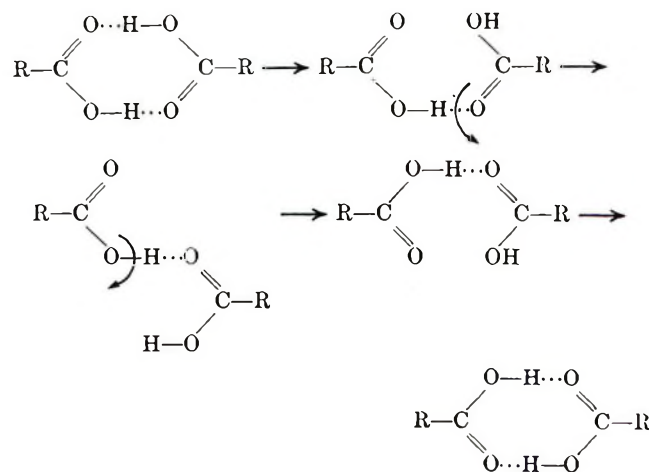
of these results has been offered, utilizing the fact that the hydrogen bonds in the dimer are weaker than the covalent bonds in the homomorphs. Consequently, the force of impact received on collision with neighboring solvent molecules may be sufficient to bend the dimer about the line formed by the two hydrogen bonds. Thus, the constituent acetic acid molecules of a dimer may be able to swing into new position relatively independently of each other. The resulting segmental type of diffusion may be expected to meet with less resistance than if the dimer were to diffuse as a rigid entity. Similar effects may be expected to affect the diffusion rates of other, less strongly hydrogen-bonded complexes, to an even greater degree.

Acknowledgments. Grants-in-aid by the National Research Council of Canada and by the University of Waterloo Research Fund are gratefully acknowledged by the authors. One of the authors (G. H. S.) is indebted to the Faculty of Engineering of the University of Waterloo for the award of a Postdoctoral Fellowship. One of the authors (F. A. L. D.) wishes to express his thanks to T. G. Theofanous for stimulating discussions.

(16) J. Wenograd and R. A. Spurr, *J. Amer. Chem. Soc.*, **79**, 5844 (1957).

(17) A. D. Buckingham and R. E. Raab, *Trans. Faraday Soc.*, **55**, 377 (1959).

(18) The authors are indebted to Sister Mary Andrew Matesich of Ohio Dominican College, for suggesting the following possible mechanism for segmental diffusion of the dimer



Ion-Molecule Reactions of Diborane and Oxygen-Containing Compounds

by Robert C. Dunbar

Department of Chemistry, Case Western Reserve University, Cleveland, Ohio 44106 (Received January 7, 1972)

Publication costs assisted by the Petroleum Research Fund and the National Science Foundation

Ion-molecule reaction involving cations in mixtures of diborane with several alcohols and dimethyl ether were investigated by ion cyclotron resonance techniques. $B_2H_5^+$ was found to react very rapidly with methanol, and the reaction $B_2H_5^+ + CH_3OH \rightleftharpoons CH_3OHBH_2^+ + BH_3$ was found to have a rate constant of about 1×10^{-9} cm³/molecule-sec. The analogous reactions with ethanol, *n*-propyl alcohol, and dimethyl ether also proceeded at a lower rate. The products of these reactions were conjectured to be isoelectronic with corresponding aminoboranes. Reaction sequences initiating with $B_2H_4^+$ and $B_2H_2^+$ yielded a variety of ions containing two boron atoms in unsaturated or cyclic structures.

Cation-molecule reactions have been studied in diborane,¹ in higher boron hydrides,² and in mixtures of boron hydrides with methane and other proton donors and acceptors.³ The condensation reaction products observed in such highly electron-deficient reaction systems are difficult to understand without detailed structural information, and it seemed of interest to examine reactive systems in which the electron deficiency of the boron hydride is compensated by the presence of an electron-rich atom such as oxygen. It was hoped that the reaction products would be more amenable to interpretation in terms of normal valence states of the atoms. Reaction with several oxygen bases proceeded readily, and the reaction products could be understood as containing a trivalent oxygen (+1) atom, isoelectronic with a neutral nitrogen atom. These systems show the first rapid cationic condensation reactions reported involving diborane.

Experimental Section

These experiments were carried out using a standard Varian Associates ICR-9 ion cyclotron resonance spectrometer. The use of the icr technique to determine the ions formed in gaseous systems where extensive ion-molecule reaction processes are possible has been described,⁴ as has the use of the ion cyclotron double resonance technique to determine the nature of the ion-molecule reaction pathways occurring in the system.^{4,5} In examining some of the cationic products of very slow reactions it was necessary to use high sample pressures (near 10^{-4} Torr) and low drift voltages, leading to very extensive reactions and numerous impurity peaks whose identity and peak intensity varied with the history of the sample and the spectrometer. The criterion was used that only ions which were shown by good double resonance signals to originate from reactions of the desired species were considered as significant ions.

At the ionizing voltages of 15–16 eV, reactions of boron hydride ions with diborane¹ were not observable.

The reactions of the oxygen-containing ions with their parent compounds were readily identified from the literature⁶ and disregarded, and only those ions containing boron will be discussed.

Diborane was prepared by a standard procedure⁷ and purified by several distillations through a carbon disulfide slush bath. Diborane ¹⁰B (96%) was prepared by standard techniques⁸ from calcium fluoroborate.

Results

Assignment of the Peaks. Because of the extreme novelty of the ions observed in this work and the lack of data on any comparable system to use for comparison, it was in many cases difficult to determine the composition of the ion giving a mass peak at a given mass-to-charge ratio. In making such assignments, one is aided by the existence of the two boron isotopes, ¹⁰B and ¹¹B, which permits one to give in all cases an upper bound to the boron content of an observed ion, and usually suggests a specific boron content. In cases where ambiguities in composition remained, it was necessary to make comparisons with spectra obtained with ¹⁰B-enriched diborane and deuterium-substituted methanol.

Cationic reaction products were examined in mixtures of diborane with four compounds: methanol, ethanol, *n*-propyl alcohol, and dimethyl ether.

- (1) R. C. Dunbar, *J. Amer. Chem. Soc.*, **90**, 5676 (1968).
- (2) R. C. Dunbar, *ibid.*, **93**, 4167 (1971).
- (3) J. J. Solomon and R. F. Porter, *ibid.*, **94**, 1443 (1972).
- (4) J. D. Baldeschwieler and S. D. Woodgate, *Accounts Chem. Res.*, **4**, 114 (1971).
- (5) G. C. Goode, A. J. Ferrer-Correia, and K. R. Jennings, *Int. J. Mass Spectrom. Ion Phys.*, **5**, 229 (1970).
- (6) J. L. Beauchamp and R. C. Dunbar, *J. Amer. Chem. Soc.*, **92**, 1477 (1970); J. M. S. Henis, *ibid.*, **90**, 844 (1968); J. L. Beauchamp, Ph.D. Thesis, Harvard University, 1968.
- (7) W. L. Jolly, "The Synthesis and Characterization of Inorganic Compounds," Prentice-Hall, Englewood Cliffs, N. J., 1970, p 492.
- (8) A. D. Norman, R. Schaeffer, A. B. Bayliss, G. A. Pressley, Jr., and F. E. Stafford, *J. Amer. Chem. Soc.*, **88**, 2151 (1966).

Methanol. With a mixture of diborane and methanol, a very large peak was found at m/e 45 (\leq one boron) which shifted to m/e 46 using CH_3OD and to m/e 44 using $^{10}\text{B}_2\text{H}_6$, showed very strong double resonance for the B_2H_5^+ precursor and was assigned as BCH_6O^+ . A smaller peak was found at m/e 43, shifting to m/e 42 with $^{10}\text{B}_2\text{H}_6$ and remaining at m/e 43 with CH_3OD , showed a B_2H_5^+ precursor, and was assigned as BCH_4O^+ . Also in this mixture a small peak was observed at m/e 41 (\leq two borons) which shifted to m/e 42 (\leq two borons) with CH_3OD and to m/e 39 with $^{10}\text{B}_2\text{H}_6$. This ion gave a strong negative double resonance signal for B_2H_4^+ and a smaller signal for B_2H_2^+ . While a composition B_2CH_7^+ is possible, it seems highly unlikely that oxygen would be lost while the hydroxylic hydrogen was retained; moreover, this would mean that the product from B_2H_2^+ (which cannot contain seven hydrogen atoms) had different composition from that from B_2H_4^+ . This ion is therefore taken to be $\text{B}_2\text{H}_3\text{O}^+$. A peak at m/e 55 (\leq two borons) with precursors 41 and (less strongly) 26 and a peak at 69 (\leq two borons) with precursors 55 and (less strongly) 41 were observed, and taken to be $\text{B}_2\text{CH}_5\text{O}^+$ and BC_2H_7^+ , respectively. A peak at 85 (\leq two borons) had 55 as its precursor and was taken to be $\text{B}_2\text{C}_2\text{H}_7\text{O}_2^+$. These latter three were all confirmed as two boron ions from the $^{10}\text{B}_2\text{H}_6$ spectra.

Ethanol. A mixture of diborane and ethanol was examined and a major peak was found at m/e 59 (\leq one boron). It gave a strong negative double resonance signal for the B_2H_5^+ precursor and was assigned as $\text{BC}_2\text{H}_8\text{O}^+$.

***n*-Propyl Alcohol.** In the mixture of diborane with *n*-propyl alcohol, the only peak which could reasonably be identified as resulting from a reaction involving diborane and propyl alcohol was a very small peak at m/e 73 (\leq one boron) which may be assigned as $\text{BC}_3\text{H}_{10}\text{O}^+$.

Dimethyl Ether. The mixture of diborane with dimethyl ether showed a very large peak at m/e 59 (\leq one boron) with a strong double resonance signal for a B_2H_5^+ precursor which was taken to be $\text{BC}_2\text{H}_8\text{O}^+$ based on the evident analogy to the BCH_6O^+ peak found in methanol.

This mixture also showed a small peak at m/e 55 (\leq two borons) with a B_2H_4^+ precursor, which was assigned as $\text{B}_2\text{CH}_5\text{O}^+$, and a small peak at m/e 69 (\leq two borons) showing $\text{B}_2\text{CH}_5\text{O}^+$ as its precursor, which was assigned as $\text{B}_2\text{C}_2\text{H}_7\text{O}^+$.

Discussion

There is no rigorous justification for assigning structures to any of the ions observed, but such a procedure may be justified, if the structures are chemically reasonable, as providing a useful working hypothesis. For all of the ions observed in this study, one or more reasonable structures may be written, and in several

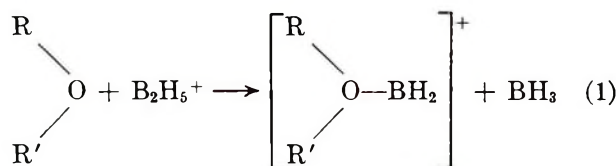
cases one possible structure is isoelectronic with a known nitrogen-containing class of compounds.⁹ Possible structures are indicated in Table I.

Table I: Some Possible Structures of Observed Ions and Correspondence with Isoelectronic Neutral Molecules

Ion	Neutral
1. $\begin{array}{c} \text{R} \\ \diagdown \\ \text{O}^+-\text{BH}_2 \\ \diagup \\ \text{R}' \end{array}$ $\text{R} = \text{H}, \text{CH}_3$ $\text{R}' = \text{CH}_3, \text{C}_2\text{H}_5, n\text{-C}_3\text{H}_7$	$\begin{array}{c} \text{R} \\ \diagdown \\ \text{N}-\text{BH}_2 \\ \diagup \\ \text{R}' \end{array}$ (aminoborane ^a)
2a. $\text{CH}_3-\text{O}^+=\text{BH}$	$\text{CH}_3-\text{N}=\text{BH}$ (boron imide ^b)
b. $\text{CH}_2=\text{O}^+-\text{BH}_2$	c
c. $\begin{array}{c} \text{H} \\ \\ \text{O} \\ / \quad \backslash \\ \text{H}_2\text{C} \quad \text{BH} \end{array}$	c
3a. $\begin{array}{c} \text{R} \\ \\ \text{O} \\ / \quad \backslash \\ \text{B} \quad \text{B} \\ \diagup \quad \diagdown \\ \text{R}' \quad \text{R}'' \end{array}$	c
b. $\begin{array}{c} \text{R}' \\ \\ \text{R}-\text{O}^+=\text{B}-\text{B} \\ \diagup \quad \diagdown \\ \text{R}'' \end{array}$	c
$\text{R}, \text{R}' = \text{H}, \text{CH}_3$ $\text{R}'' = \text{H}, \text{CH}_3, \text{OCH}_3$	

^a Reference 10. ^b Reference 13. ^c While the corresponding neutral nitrogen-containing molecule may reasonably be written, it does not belong to a known series of stable compounds.

The most readily formed cations are those of the type $\text{RR}'\text{O}^+\text{BH}_2$, corresponding to the aminoboranes.¹⁰ These species are formed by the borane elimination reaction



This reaction is rather slow for ethanol and even slower for propyl alcohol, but in methanol and dimethyl ether this is by far the fastest of the reactions studied. Re-

(9) The nitrogen compounds indicated in Table I are not known except in highly substituted form, reflecting the necessity in condensed phase for stabilizing most monomeric boron-nitrogen compounds with stabilizing substituents.

(10) K. Niedenzu and J. W. Dawson in "The Chemistry of Boron and Its Compounds," E. L. Muetterties, Ed., Wiley, New York, N. Y., 1967, Chapter 8.

action 1 for methanol was estimated to have a rate constant of 1×10^{-9} cm³/molecule sec by comparing it directly with the concurrent reactions of methanol protonation (rate constant¹¹ 1.2×10^{-9} cm³/molecule-sec) and methyl transfer to methanol (rate constant¹² 7×10^{-11} cm³/molecule-sec). Reaction 1 for dimethyl ether was also very fast, but no rate constant was determined. These reactions are notable in being the first known rapid reactions of B₂H₅⁺ (which is quite unreactive toward boron hydrides¹), apparently reflecting the effect of the nucleophilicity of the oxygen atom. The other reactions observed in this study had rate constants below 10^{-10} cm³/molecule sec.

The products of reaction 1 do not appear to react further in any instance, in direct analogy with the non-reactivity of the aminoboranes.¹³ The exceptionally rapid and general formation of the ions of this type suggests that the unusual stability of the >N-B< bond, which has been attributed to some degree of π bonding involving the nitrogen lone-pair electrons in the aminoboranes,^{10,13} is also present in the >O⁺-B< bond postulated for the ions observed here.

A peak of composition CH₃OBH⁺ is also formed with methanol apparently by elimination of R'H from the product of reaction 1. Among several possible structures for this ion (Table I, 2a,b,c and others) is one which is isoelectronic with the well-known boron imide structure.¹³

A number of species are formed by reaction with methanol and dimethyl ether containing two borons and one oxygen, with compositions demanding unsaturated or cyclic structures. Several possibilities are noted in Table I, including a cyclic structure isoelectronic with the aromatic cyclopropenyl cation ring.

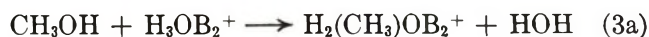
Reactions producing these ions are



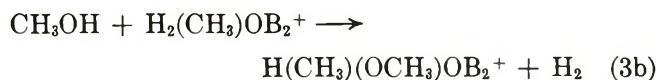
(R = H, CH₃) and



where R' may be H or CH₃. The ions are reactive, and double resonance shows that they may add methyl or methoxy in reactions such as



or



It is interesting to note that the two classes of simple boron-nitrogen compounds showing the highest degree of saturation, the amine-boranes and the diborylamines, have no counterparts among the cationic species observed in this work, but the observed ions appear to correspond to dehydrogenation products of these molecules. This is entirely consistent with earlier observations that boron-containing cations tend to show substantially lower hydrogen contents than related neutral species.^{1,2}

Acknowledgment. Acknowledgment is made to the donors of the Petroleum Research Fund, administered by the American Chemical Society, to the Research Corporation, and to the National Science Foundation for support of this research.

(11) A. G. Harrison, J. J. Myher, and J. C. J. Thynne, *Advan. Chem. Ser.*, **No. 58**, 150 (1966).

(12) This rate may be calculated from data in J. M. S. Henis, *J. Amer. Chem. Soc.*, **90**, 844 (1968).

(13) H. Nöth in "Progress in Boron Chemistry," Vol. 3, R. J. Brotherton and H. Steinberg, Ed., Pergamon, New York, N. Y., 1970, Chapter 4.

Diffusion in Mixed Solvents. III. Iodine in Nonpolar Solutions.

Evidence for Charge-Transfer Interaction

by Koichiro Nakanishi* and Sonoko Kitajima

Department of Industrial Chemistry, Kyoto University, Kyoto, Japan (Received December 21, 1971)

Publication costs borne completely by The Journal of Physical Chemistry

Diffusion coefficients of iodine diluted with six binary solutions composed of nonpolar compounds have been determined at 25.0° by the capillary cell method. It was found that, while the isoviscous diffusion coefficients ($D\eta/T$) of iodine change almost linearly with molar composition (x) of binary solvent for the combinations of noncomplexing solvents (*e.g.*, $n\text{-C}_6\text{H}_{14} + c\text{-C}_6\text{H}_{12}$) and of complexing solvents (*e.g.*, $\text{C}_6\text{H}_6 + \text{C}_6\text{H}_5\text{CH}_3$), there are always relative decreases in $D\eta/T$ for solutions composed of noncomplexing (N) and complexing (C) solvents. Comparison with the results available in the literature has indicated that, in the (N) + (C) type mixed solvents, the $D\eta/T$ vs. x relation for iodine differs from those for other diffusants (*e.g.*, hydrocarbons, acetone, or CO_2). Thus, the diffusivity of iodine is measurably affected by the charge-transfer type interaction between iodine and solvents.

In our previous two papers (referred to hereafter as P-I¹ and P-II²), we reported the molecular diffusion coefficient of iodine in such associated solutions as aqueous alcohol solutions and the solutions of ethanol with nonpolar liquids. In interpreting the relative decrease (in comparison with those in pure solvents) of the diffusivity of I_2 in the latter type of mixed solvents, we have emphasized that the difference in the interactions of solute with two kinds of solvent molecule is of major importance.² If this interpretation is valid, the relative decrease, as measured by a negative deviation of the $D_{11}^0\eta_{23}/T$ vs. x_2 relation³ from the additivity with respect to x_2 , may occur whenever two solvents have different influences on the diffusing solute, irrespective of whether or not these solvents are associated. For the purpose of verifying this prediction, it is interesting to work with nonpolar and/or polar nonassociated solvent systems.

It is well known that iodine forms charge-transfer complexes with aromatic hydrocarbons and many other polar organic molecules.⁴ The thermodynamic properties of dilute iodine solutions have been studied extensively by Hildebrand and his collaborators.⁵ The equilibrium constant, heat of formation, and other thermodynamic quantities of the molecular complexes involving iodine have also been measured by spectroscopic and calorimetric methods.⁶ Such thermodynamic information is a useful guide in selecting appropriate solvent pairs where two components represent possible combinations of complexing and/or noncomplexing solvents for iodine.

In the present study, we will examine the effect of charge-transfer-type interactions on the diffusivity of iodine in nonpolar solvent systems. The following six binary solvent systems are used: n -hexane + cyclo-

hexane, n -hexane + benzene, cyclohexane + benzene, benzene + carbon tetrachloride, benzene + toluene, and cyclohexane + m -xylene. Based on the present results and diffusion data available for other diffusants than I_2 , we will show that the above-mentioned effects are of measurable magnitude, though they are smaller than those in ethanol solutions.

Experimental Section

Solvents and Iodine. All the solvents were of GR grade (JIS (Japan Industrial Standards) guaranteed reagent) and were used without further purification. Iodine was a Merck doubly sublimated reagent.

Diffusion and Viscosity Measurements. The diffusion coefficients D_{11}^0 of iodine diluted in pure and mixed solvents were measured by the capillary cell method. The apparatus and procedures were described in detail in P-I. The initial concentration of I_2 was less than 0.03 M .

For the analysis of iodine, we have again used titration with sodium thiosulfate aqueous solution. We found some difficulties in determining the end point of the titration in several water-insoluble solvents, espe-

(1) K. Nakanishi and T. Ozasa, *J. Phys. Chem.*, **74**, 2956 (1970).

(2) K. Nakanishi, T. Ozasa, and K. Ashtani, *ibid.*, **75**, 963 (1971).

(3) D_{11}^0 = the main diffusion coefficient of I_2 at infinite dilution, η_{23} = the viscosity coefficient of the solvent, T = temperature in °K, and x_2 = the mole fraction of solvent 2 in the binary solution 2 + 3.

(4) See, for a review, R. S. Mulliken and W. B. Person, "Molecular Complexes," Wiley-Interscience, New York, N. Y., 1969, and references cited therein.

(5) J. H. Hildebrand, J. M. Prausnitz, and R. L. Scott, "Regular and Related Solutions," Van Nostrand-Reinhold, Princeton, N. J., 1970.

(6) L. J. Andrews and R. M. Keefer, "Molecular Complexes in Organic Chemistry," Holden-Day, San Francisco, Calif., 1964.

cially in solutions containing toluene or *m*-xylene, which might be due to an incomplete transfer of I_2 into the aqueous phase. This was overcome by adding a small amount of ethanol to the solutions to be titrated.

Pycnometry. The density of $c\text{-C}_6\text{H}_{12}$ + *m*-xylene solutions at 25.0° was measured by a bicapillary-type pycnometer.⁷ The densities of $c\text{-C}_6\text{H}_{12}$ and *m*-xylene were found to be 0.77369 and 0.85953, respectively. They are to be compared with 0.77375 and 0.85990 given in the literature.^{8,9} The data were used to calculate η_{23} from flow time data and to evaluate the excess volumes.

Results and Discussion

Viscosity Coefficient. Our literature survey has indicated that the viscosity coefficients η_{23} are available for all binary solutions except $c\text{-C}_6\text{H}_{12}$ + *m*-xylene. However, there are much scatter and inconsistency among the viscosity data reported for benzene + toluene solutions.¹⁰ Therefore, we have measured the viscosity and density when they are not available for the above two binary solutions at 25.0° . The results, together with the value for the excess volume calculated from the density data, are shown in Table I.¹¹

Diffusion Coefficient. The diffusion coefficients of iodine diluted in six mixed solvent systems used in this work are given in Table II.¹¹ At the end of the table, we have also included a datum for D_{11}^0 of I_2 in a toluene + EtOH solution (molar ratio 9 to 1). Our intention to include this datum will be explained later. Table II also contains the temperature reduced isoviscous diffusion coefficient, $D_{11}^0\eta_{23}/T$.

These results are plotted against x_2 in Figure 1. In order to compare the composition dependence of iodine diffusion with those for noncomplexing diffusants, several diffusion data available in the literature¹²⁻¹⁴ are also included in the same figure. We will first summarize principal experimental evidence, which we believe to be established in the present measurements, with brief explanation of the reason for choosing those particular solvent systems.

(1) In the $n\text{-C}_6\text{H}_{14}$ + $c\text{-C}_6\text{H}_{12}$ system (Figure 1a), where both components are noncomplexing solvents for iodine, the diffusion coefficient *vs.* solvent composition relation for I_2 is essentially the same as those for toluene¹² and benzene.¹⁴ Moreover, $D_{11}^0\eta_{23}/T$ for all three diffusants are nearly linear with respect to x_2 , though a small negative deviation is evident for I_2 .

(2) In the solvent systems $n\text{-C}_6\text{H}_{14}$ + C_6H_6 (Figure 1b) and $c\text{-C}_6\text{H}_{12}$ + C_6H_6 (Figure 1c), where one of components, benzene, is a complexing solvent for I_2 , the profile of the D_{11}^0 *vs.* x_2 curve for I_2 is quite different from those for such diffusants as cyclohexane, *n*-hexane, or acetone.¹⁴ This difference makes the $D_{11}^0\eta_{23}/T$ *vs.* x_2 relation for I_2 definitely negative from the additivity with respect to x_2 . The $D_{11}^0\eta_{23}/T$ *vs.* x_2 relations for

other diffusants may essentially be approximated by a straight line representing the additivity.

(3) In the same figures as cited just above, we see that the diffusion coefficient of I_2 in benzene is relatively smaller than that expected from the values in hexanes. We can verify this quantitatively from the following figures for diffusion coefficient ratios among various diffusants.^{13,15}

	I_2	CCl_4	$c\text{-C}_6\text{H}_{12}$	
$\frac{D_{11}^0 \text{ in } \text{C}_6\text{H}_6}{D_{11}^0 \text{ in } n\text{-C}_6\text{H}_{14}}$	0.472	0.541	0.524	
	I_2	$(\text{CH}_3)_2\text{CO}$	CCl_4	$n\text{-C}_6\text{H}_{14}$
$\frac{D_{11}^0 \text{ in } \text{C}_6\text{H}_6}{D_{11}^0 \text{ in } c\text{-C}_6\text{H}_{12}}$	1.20	1.34	1.34	1.41

It is obvious that the ratios for I_2 are always smaller than those for CCl_4 and other noncomplexing solutes. This may be strong evidence for the effect of charge-transfer-type interactions on the diffusivity of I_2 .

(4) In the benzene + toluene system (Figure 1e), where both components are complexing solvents for iodine, the D_{11}^0 *vs.* x_2 relation for I_2 resembles quite closely that for CO_2 .¹² However, the diffusion coefficient of I_2 in toluene is relatively smaller than that expected from the value for CO_2 in the same solvent and the D_{11}^0 ratio in benzene. This might be ascribed to the stronger complex formation of I_2 with toluene than with benzene. The $D_{11}^0\eta_{23}/T$ *vs.* x_2 relation is almost linear, but there is small but significant positive deviation from additivity with respect to x_2 .

(5) In the CCl_4 + benzene system (Figure 1d), both D_{11}^0 and $D_{11}^0\eta_{23}/T$ change almost linearly with x_2 . Such behavior may be inconsistent with that explained above, since CCl_4 is believed to be a noncomplexing solvent. However, there is a small but significant difference between the $D_{11}^0\eta_{23}/T$ *vs.* x_2 relation for I_2 and those for acetone¹⁶ and carbon dioxide.¹³ These latter

(7) K. Nakanishi, *Bull. Chem. Soc. Jap.*, **33**, 793 (1960).

(8) D. S. Adcock and M. L. McGlashan, *Proc. Roy. Soc., Ser. A*, **226**, 266 (1954).

(9) R. R. Dreisbach, *Advan. Chem. Ser.*, **No. 15**, 15 (1955).

(10) J. Timmermans, "Physicochemical Constants of Binary Systems in Concentrated Solutions," Vol. I, Interscience, New York, N. Y., 1959.

(11) Tables I and II will appear immediately following these pages in the microfilm edition of this volume of the journal. Single copies may be obtained from the Business Operations Office, Books and Journals Division, American Chemical Society, 1155 Sixteenth St., N.W., Washington, D. C. 20036, by referring to code number JPC-72-2470. Remit check or money order for \$3.00 for photocopy or \$2.00 for microfiche.

(12) J. T. Holmes, C. R. Wilke, and D. R. Olander, *AIChE J.*, **8**, 646 (1962).

(13) Y. P. Tang and D. M. Himmelblau, *ibid.*, **11**, 54 (1965).

(14) J. Leffler and H. T. Cullinan, Jr., *Ind. Eng. Chem., Fundam.*, **9**, 88 (1970).

(15) B. R. Hammond and R. H. Stokes, *Trans. Faraday Soc.*, **51**, 1641 (1955).

(16) H. T. Cullinan, Jr., and H. L. Toor, *J. Phys. Chem.*, **69**, 3941 (1965).

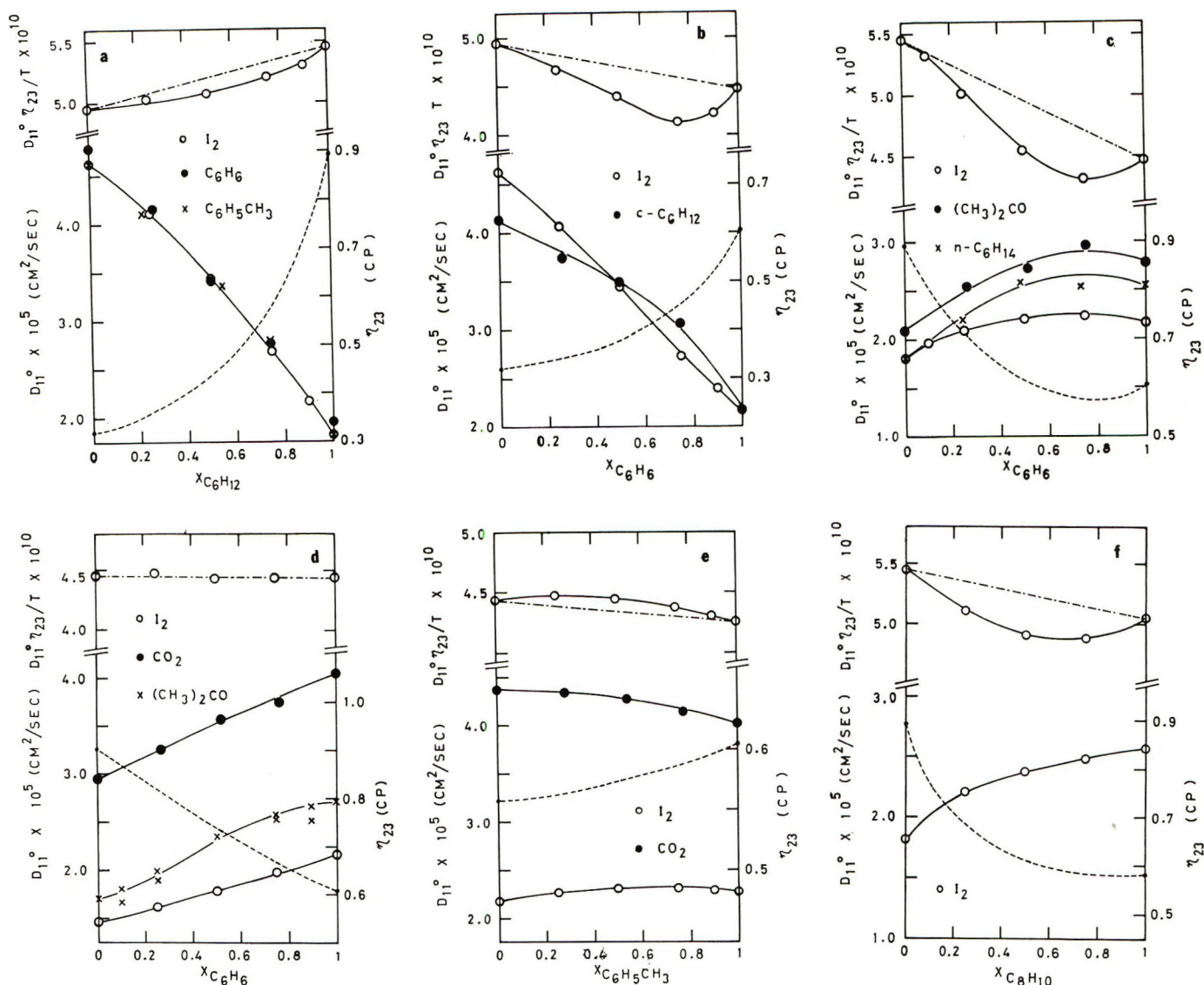


Figure 1. Diffusion coefficient, viscosity coefficient, and isoviscous diffusion coefficient in binary nonpolar solvent systems at 25.0°: (—) D_{11}^0 or $D_{11}^0 \eta_{23}/T$, (---) η_{23} : a, *n*-hexane(2) + cyclohexane(3); b, *n*-hexane(2) + benzene(3); c, cyclohexane(2) + benzene(3); d, carbon tetrachloride(2) + benzene(3); e, benzene(2) + toluene(3); f, cyclohexane(2) + *m*-xylene(3). The D_{11}^0 data for solutes other than I_2 are taken from ref 12, 13, 14, and 16.

diffusants show a small positive deviation from additivity, while nearly perfect additivity is seen for I_2 .

(6) The system $c\text{-C}_6\text{H}_{12} + m\text{-xylene}$ (Figure 1f) may represent another example of the combination of non-complexing and complexing solvents. The deviation of the $D_{11}^0 \eta_{23}/T$ vs. x_2 relation from additivity is again negative. In view of increasing interaction of I_2 with *m*-xylene,⁶ however, the magnitude of this deviation seems to be rather small as compared with that in $c\text{-C}_6\text{H}_{12} + \text{C}_6\text{H}_6$.

(7) It should be remarked that, although the negative deviation in the $D_{11}^0 \eta_{23}/T$ value from the additivity evidenced above is generally asymmetric with respect to x_2 as in the cases of binary ethanol solutions studied in P-II, the minimum point shifts to the complexing solvent side. This is in contrast with the results for ethanol-containing systems.

Evidence for Solute-Solvent Interactions. As mentioned earlier in this paper, the main purpose of the present study was to examine possible influence of weak charge-transfer-type solute-solvent interactions on the diffusivity of I_2 in nonassociated solvent systems. The results given in the above section indicate the presence of this effect, though it is much smaller than in the case of binary solutions of ethanol. Let us now summarize how the solute-solvent interactions in diffusivity both in pure and mixed solvents could have been detected. In an arbitrary order, they were as follows: (1) comparison of the ratio of D_{11}^0 values for each diffusant in two pure solvents, (2) comparison of the $D_{11}^0 \eta_{23}/T$ vs. x_2 relation for each diffusant in mixed solvent system, (3) comparison of the ratio of the $D_{11}^0 \eta_{23}$ value of a diffusant to that of another diffusant in a number of pure solvents,¹⁷ and (4) plot of $D_{11}^0 \eta_{23}/T$ or simply $D_{11}^0 \eta_{23}$

against the molar volume of pure solvents.¹⁵

We have already used the first method in the above section and confirmed that the D_{11}^0 values for I_2 in C_6H_6 or $C_6H_5CH_3$ are relatively smaller than those for a noncomplexing solute in the same solvents. Also, the result of the second method was illustrated in Figure 1, which reveals a relative decrease of diffusivity of I_2 for the combination of a complexing solvent with a non-complexing one. However, comparisons among various solvent systems may be done more clearly by defining the excess isoviscous diffusion coefficient $(D_{11}^0\eta_{23}/T)^E$, which gives the deviation of the $D_{11}^0\eta_{23}/T$ value from the additivity with respect to the mole fraction in mixed solvents, and by plotting these values for each solvent system against x_2 . This plot for I_2 diffusion in representative solvent systems studied by us is shown in Figure 2.

In Figure 2, we see that, while the negative deviation in EtOH + saturated hydrocarbon systems is exceedingly large in comparison with those for nonpolar systems, the positive and highly asymmetrical deviation observed in the EtOH + H_2O system is still larger in magnitude. We may say that unique and anomalous properties of associated or aqueous solutions are evidently reflected by these results. On the other hand, there is only a small deviation in nonpolar solvent systems. As was pointed out in the foregoing section, there is always a small negative deviation for the combination of complexing (C) and noncomplexing (NC) solvents, *e.g.*, $c\text{-}C_6H_{12}$ + $m\text{-}xylene$. For the combination of two complexing solvents and of two non-complexing solvents, the deviation is, in accordance with our prediction, reasonably small. However, if our simple picture of the diffusion in mixed media² is completely valid, there should be no deviation at all for NC + NC and C + C systems, provided that the interactions are the same for two-component solvents. The fact that the deviation is either slightly positive or negative for benzene + toluene or n -hexane + cyclohexane solutions suggests the presence of other factors than the solute-solvent interaction, which are to be superimposed to determine the dependence of $D_{11}^0\eta_{23}/T$ upon x_2 . As one such factor, let us examine possible correlation with thermodynamic excess functions. Table III shows the values of H^M and V^E at an equimolar composition for all the solvent systems used. Positive V^E and H^M may be favorable for the diffusional process from the standpoint of both steric and energetic considerations. In the case of $n\text{-}C_6H_{14}$ + $c\text{-}C_6H_{12}$ solutions, however, both V^E and H^M are positive in sign and not too small in magnitude. This is in conflict with a small negative deviation in $(D_{11}^0\eta_{23}/T)^E$ for this solvent system. Thus, it is not clear whether positive $(D_{11}^0\eta_{23}/T)^E$ for benzene + toluene solutions could be ascribed to these thermodynamical effects.

The third method mentioned above has been used by Stokes, *et al.*,¹⁷ in comparing the diffusion coefficients

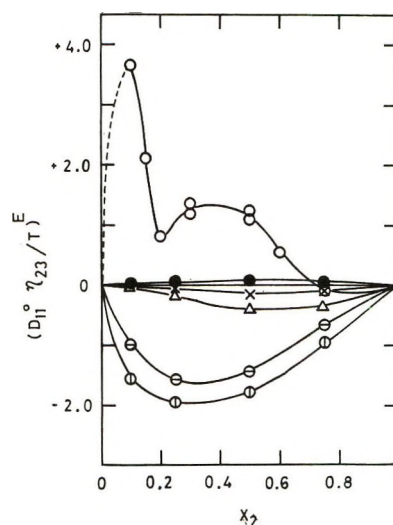


Figure 2. Excess isoviscous diffusion coefficient of iodine in various kinds of binary solvent systems at 25.0°: O, ethanol(2) + water(3); ●, benzene(2) + toluene(3); ×, n -hexane(2) + cyclohexane(3); Δ, cyclohexane(2) + benzene(3); ⊙, ethanol(2) + cyclohexane(3); ⊕, ethanol(2) + n -hexane(3).

Table III: Excess Enthalpy and Volume for Equimolar Mixture of Solvent Systems Used

Solvent system	H^M , J/mol	V^E , ^a ml/mol
$n\text{-}C_6H_{14}$ + $c\text{-}C_6H_{12}$	216 ^{b-d}	0.150 ^a
$n\text{-}C_6H_{14}$ + C_6H_6	870 ^e	0.396 ⁱ
$c\text{-}C_6H_{12}$ + C_6H_6	800 ^{c,e,f}	0.650 ⁱ
CCl_4 + C_6H_6	116 ^{c,e,f}	0.0043 ^k
C_6H_6 + $C_6H_5CH_3$	68.1 ^g	0.088 ^e
$c\text{-}C_6H_{12}$ + $m\text{-}C_6H_4(CH_3)_2$		0.66 ^l

^a Excess volume data published before 1969 are accumulated by R. Battino, *Chem. Rev.*, **71**, 3 (1971). ^b K. N. Marsh and R. H. Stokes, *J. Chem. Thermodyn.*, **1**, 223 (1969). ^c S. Murakami and G. C. Benson, *ibid.*, **1**, 559 (1969). ^d M. L. McGlashan and H. F. Stoeckli, *ibid.*, **1**, 589 (1969). ^e R. S. Rowlinson, "Liquids and Liquid Mixtures," 2nd ed, Butterworths, London, 1969, Chapter 4. ^f R. H. Stokes, K. N. Marsh, and R. P. Tomlins, *J. Chem. Thermodyn.*, **1**, 211 (1969). ^g S. Murakami, V. T. Lam, and G. C. Benson, *ibid.*, **1**, 397 (1969). ^h J. Gomez-Ibanez and C.-T. Lin, *J. Phys. Chem.*, **65**, 2148 (1961). ⁱ K. R. Harris and P. J. Dunlop, *J. Chem. Thermodyn.*, **2**, 813 (1970). ^j R. H. Stokes, B. J. Levien, and K. N. Marsh, *ibid.*, **2**, 43 (1970). ^k B. J. Levien and K. N. Marsh, *ibid.*, **2**, 227 (1970). ^l This work.

of iodine with those of CCl_4 in several solvents. They have shown that the ratio $(D_{11}^0\eta)_{CCl_4}/(D_{11}^0\eta)_{I_2}$ is independent of the solvent, except in the case of toluene.^{17,18} The observed deviation for toluene was ascribed to the abnormally small diffusion coefficient of iodine in this solvent, and no acceptable explanation was given as to why benzene and p -dioxane behave similarly with hydrocarbons and CCl_4 . If the D_{11}^0 of iodine in toluene is 2.28 (this work) instead of 2.13,¹⁷

(17) R. H. Stokes, P. J. Dunlop, and J. R. Hall, *Trans. Faraday Soc.*, **49**, 886 (1953).

(18) H. J. V. Tyrrell, "Diffusion and Heat Flow in Liquids," Butterworths, London, 1961, Chapter 7.

the above ratio then becomes 1.04, a value which is not significantly smaller than the average value for such solvents as n -C₆H₁₄, CCl₄, and C₆H₆. Therefore, we suspect that the D_{11}^0 value reported by Stokes, *et al.*,¹⁷ may be slightly smaller for some reason. It seems that this kind of comparison may not be too sensitive to detect possible solute-solvent interactions. In P-II, we have used ethanol + toluene solutions as a mixed solvent. Since D_{11}^0 for toluene is slightly larger than we assumed, we have added a new datum in this solvent system. This datum, together with new D_{11}^0 value for pure toluene, has established more firmly the $D_{11}^0\eta_{23}/T$ vs. x_2 relation, which is now very similar to that for ethanol + benzene solution. However, the general conclusion given in P-II needs no alteration. There exist

still larger discrepancies between our values and the available data (*e.g.*, the D_{11}^0 values in n -C₆H₁₄ and m -xylene). The validity of our data will be checked further in our future studies on diffusion both in pure and mixed solvents.

In conclusion, the present study has convinced us to conclude that a relative decrease in $D_{11}^0\eta_{23}/T$ values will be observed whenever the interactions of dilute solute with one solvent differ nonnegligibly from those with another solvent.

Acknowledgments. The authors are grateful to Mrs. T. Ozasa-Nakajima for her cooperation in some of the experiments (CCl₄ + C₆H₆ solution) and to Professor N. Watanabe and Mr. H. Touhara for their interest and discussion.

Solvent Effects in Organic Chemistry. XIV. Solvation of Sodium

Salts in Glycerol Acetate Binaries by ²³Na Nuclear Magnetic

Resonance Spectroscopy and Thermodynamics¹

by Edward M. Arnett,* H. C. Ko, and R. J. Minasz

Department of Chemistry, University of Pittsburgh, and Mellon Institute, Pittsburgh, Pennsylvania 15213
(Received February 16, 1972)

Publication costs assisted by the Office of Saline Water, Department of the Interior

Heats of solution are reported for sodium chloride, sodium tetraphenylboron, and tetraphenylarsonium chloride in a series of water-diacetin (glycerol diacetate) mixtures. The results for NaCl are combined with literature values of free energy of transfer to give entropies of transfer for this salt from water to each mixture. Nmr studies of ²³Na⁺ ion from sodium tetraphenylboron are also reported in water-diacetin binaries, and the results are contrasted with those estimated for the single ion behavior of Na⁺ using the (invalid) assumption that (C₆H₅)₄As⁺ is equivalent to B(C₆H₅)₄⁻. The enthalpy results for the water-diacetin system are compared to those for heats of transfer of NaB(C₆H₅)₄ in acetone-diacetin, ethyl acetate-diacetin, and acetone-triacetin (glycerol triacetate) binaries. Exothermic interactions are found for NaB(C₆H₅)₄ and Mg(ClO₄)₂ with cellulose acetate and glucose pentaacetate in acetone solution.

Introduction

Cellulose acetate membranes are unusually effective for desalinating sea water by reverse osmosis.^{2,3} Kraus and his colleagues attempted to elucidate the reasons why cellulose acetate should reject salts under conditions of high water flux by studying the solubility of a number of common electrolytes in binary solvent mixtures composed of water and the mono-, di-, and triacetates of glycerol.⁴

In the interest of gaining a further insight into this system we have measured heats of solution for sodium

chloride (the principal salt in sea water) in a number of water-diacetin mixtures. When our measurements

(1) Supported by grants from the Office of Saline Water and National Science Foundation (GP-6550-X). The ²³Na work described here was made possible through NIH Grant RR-00292 supporting the Mellon Institute nmr laboratory.

(2) U. Merten, Ed., "Desalination by Reverse Osmosis," The MIT Press, Cambridge, Mass., 1966.

(3) S. Sourirajan, "Reverse Osmosis," Academic Press, New York, N. Y., 1970.

(4) K. A. Kraus, R. J. Raridon, and W. H. Baldwin, *J. Amer. Chem. Soc.*, **86**, 2571 (1964).

are combined with those of Kraus, a complete thermodynamic analysis for the transfer of this salt from pure water to 50 mol % diacetin is achieved. To compare the gross thermodynamic changes with the varying solvation of the sodium ion itself, we have also obtained ^{23}Na magnetic resonance data over the same range and have attempted to estimate single ion heats of transfer for sodium ion for comparison. We hope that by the combined use of thermodynamic and spectral techniques it will be possible to broaden our understanding of the interaction of alkali and alkaline earth metals and various types of membrane materials. Such knowledge might serve as a predictive basis for the development of new membranes with considerably enhanced effectiveness.

Experimental Section

Apparatus. The calorimetric equipment and procedures used for this study were essentially the same as described previously⁵ except that two 250-ml calorimeters were used, and they were immersed in a water bath controlled at $25 \pm 0.2^\circ$.⁶ The two thermistors, one in each calorimeter, were connected to the Wheatstone bridge, and the difference in temperatures between the calorimeters was registered on the recorder. Thus, runs could be made alternately on both calorimeters.

All experiments were made at $25 \pm 0.5^\circ$. Accuracy of the calorimeters was checked against accepted values for the heat of solution of potassium chloride⁷ or ethanol⁸ in water once every 2 months.

Materials. Acetone was of reagent grade, stored over molecular sieve Type 4A and used without further purification. Ethyl acetate, diacetin, and triacetin (Fisher Scientific Co.) were distilled at appropriate pressures and stored over molecular sieves. Refractive indices agreed well with literature values. Diacetin was apparently a mixture of 1,2- and 1,3-glycerol diacetates. Different batches of distilled diacetin all showed boiling points ($132\text{--}133^\circ$ (6 mm)) and refractive indices which were not only consistent with each other, but also with those reported by Kraus, *et al.*⁴ Calorimetric measurements using different batches of diacetin gave consistent results.

Sodium tetraphenylboron (Fisher Scientific Co. reagent grade, 99.5%) was vacuum dried at 80° for 24 hr. Tetraphenylarsonium chloride was obtained by heating the dihydrate (Aldrich Chemical Co.) to consistent weight at 150° under vacuum and then analyzed for chloride content. Both gravimetric and volumetric methods agreed well (8.41 and 8.48 wt % Cl, respectively) within experimental error of the theoretical value, 8.47%. Sodium chloride was dried at 150° . Glucose pentaacetate (Eastman Organic Chemicals) and cellulose acetate (Eastman Organic Chemicals) were used without further purification after drying in a vacuum oven. Reagent grade magnesium perchlo-

rate (Fisher Scientific Co.) was analyzed for Mg content by the EDTA titration method and found to be 99.25% pure.

^{23}Na Magnetic Resonance Measurements. The ^{23}Na nmr spectra were obtained with a modified Varian DP-60 spectrometer operating at a frequency of 15.871 MHz. The magnetic field was held constant by an external lock on the proton resonance of water at 60.000000 MHz. The spectra were taken in the absorption mode under frequency sweep conditions. The radiofrequency was generated by a General Radio Co. frequency synthesizer Model GR-1164A. The signal was phase-detected using a Princeton Applied Research lock-in amplifier with a 1-kHz modulation for base line stabilization. The locking and observing frequencies were phase-locked to prevent any drift between them. The frequency of the signal was read directly from an Anadex Model CF-200R electronic counter.

The sample tube had an outside diameter of 15 mm. Corrections due to differences in bulk susceptibilities between samples were expected to be small and thus not applied to the chemical shifts. A sweep rate of about 1 Hz/sec was used, and each sample was swept at least twice in both increasing and decreasing field directions. A shift to lower frequency corresponds to an upfield chemical shift and represents increased screening of the ^{23}Na nucleus. Spinning the sample tube caused extreme sharpening of the ^{23}Na resonance signals.

Results

Heats of solution of NaCl in the H_2O -diacetin binary mixtures are listed in Table I together with the derived thermodynamic values of transfer from H_2O to each H_2O -diacetin mixture. Tables II and III contain the heats of solution of $\text{NaB}(\text{C}_6\text{H}_5)_4$ and $(\text{C}_6\text{H}_5)_4\text{AsCl}$ in the H_2O -diacetin binary mixtures and the derived heats of transfer of each salt from H_2O to each binary.

Owing to low solubilities of NaCl, $\text{NaB}(\text{C}_6\text{H}_5)_4$, and $(\text{C}_6\text{H}_5)_4\text{AsCl}$ in pure diacetin, the values for the heats of solution of each of these salts in that solvent were extrapolated. Assuming that $\text{B}(\text{C}_6\text{H}_5)_4^-$ and $(\text{C}_6\text{H}_5)_4\text{As}^+$ have equal heats of transfer (see Discussion), it is possible to calculate single ion heats of transfer for Na^+ , Cl^- , $\text{B}(\text{C}_6\text{H}_5)_4^-$, and $(\text{C}_6\text{H}_5)_4\text{As}^+$ from experimentally determined (heats of solution) values. The values of single ion heats of transfer for these ions and also heats of transfer for these three salts are plotted against mole fraction of diacetin and are presented in Figure 1.

(5) E. M. Arnett, W. G. Bentrude, J. J. Burke, and P. McC. Dugleby, *J. Amer. Chem. Soc.*, **87**, 1541 (1965).

(6) E. M. Arnett and J. J. Campion, *ibid.*, **92**, 7097 (1970).

(7) (a) G. Somson, J. Coops, and M. W. Tolks, *Recl. Trav. Chim. Pays-Bas*, **82**, 231 (1963); (b) R. J. Irving and I. Wadsö, *Acta Chem. Scand.*, **18**, 195 (1964).

(8) F. Franks and B. Watson, *J. Sci. Instrum.*, **1**, 940 (1968).

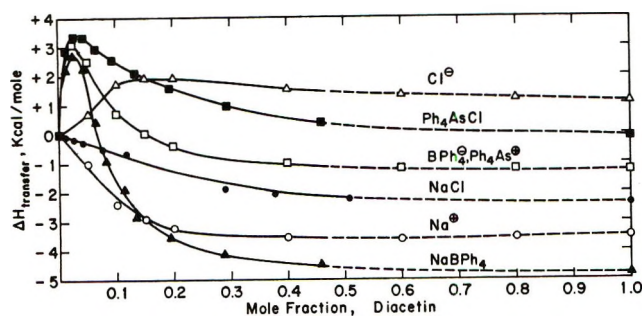


Figure 1. Observed and estimated heats of solution in aqueous solutions of diacetin.

Table I: Heats of Solution and Thermodynamics of Transfer of NaCl in H₂O-Diacetin Mixtures

Wt % diacetin	Mole fraction, X_1 diacetin	ΔH_{soln}^a	$\delta \Delta G^{a,b}$	$\delta \Delta H^{a,c}$	$\delta(T\Delta S)^{a,c}$
0.0	0.000	0.99 ± 0.03	0	0	0
9.9	0.011	0.91 ± 0.04	0.02	-0.08	-0.10
20.2	0.025	0.81 ± 0.02	0.05	-0.18	-0.23
29.6	0.041	0.72 ± 0.03	0.07	-0.27	-0.34
44.6	0.076	0.49 ± 0.01	0.12	-0.50	-0.62
56.6	0.117	0.34 ± 0.02	0.19	-0.65	-0.84
79.9	0.290	-0.90 ± 0.09	0.49	-1.89	-2.38
85.6	0.377	-1.05 ± 0.05	0.67	-2.04	-2.71
91.0	0.508	-1.24 ± 0.10	1.01	-2.23	-3.24
100.0	1.000	-1.40^c		-2.39	

^a All thermodynamic values in this and subsequent tables are in kcal/mol. ^b Calculated from activity coefficient data of Kraus, *et al.*⁴ ^c Extrapolated.

Table II: Heats of Solution of NaB(C₆H₅)₄ in H₂O-Diacetin Mixtures

Wt % diacetin	X_1 diacetin	ΔH_{soln}	$\delta \Delta H$
0.0	0.000	-4.71 ± 0.14	0
9.9	0.011	-2.50 ± 0.15	2.21
20.1	0.025	-2.02 ± 0.07	2.69
29.9	0.042	-2.46 ± 0.06	2.25
40.0	0.064	-4.28 ± 0.10	0.43
46.2	0.080	-5.62 ± 0.21	-0.91
55.2	0.112	-6.62 ± 0.34	-1.91
60.1	0.133	-7.54 ± 0.26	-2.83
70.2	0.194	-8.24 ± 0.26	-3.53
79.8	0.288	-8.83 ± 0.21	-4.12
89.2	0.458	-9.19 ± 0.16	-4.48
100.0	1.000	-9.50^a	-4.79

^a Extrapolated. Probably in error, see text.

For nonaqueous binaries we have studied heats of solution of NaB(C₆H₅)₄ in acetone-diacetin, ethyl acetate-diacetin, and acetone-triacetin mixtures. Results are presented in Tables IV, V, and VI. Values for ΔH_{soln} of the salt in pure diacetin and triacetin, respectively, were extrapolated from these plots.

Table III: Heats of Solution of (C₆H₅)₄AsCl in H₂O-Diacetin Mixtures

Wt % diacetin	X_1 diacetin	ΔH_{soln}	$\delta \Delta H$
0.0	0.000	-1.53 ± 0.12	0
9.9	0.011	1.36 ± 0.13	2.89
20.6	0.026	1.83 ± 0.41	3.36
30.4	0.043	1.81 ± 0.47	3.34
40.0	0.064	1.40 ± 0.06	2.93
50.2	0.093	1.00 ± 0.03	2.53
60.1	0.133	0.57 ± 0.04	2.10
70.2	0.194	0.04 ± 0.41	1.57
80.3	0.294	-0.57 ± 0.13	0.96
89.2	0.458	-1.13 ± 0.10	0.40
100.0	1.000	-1.67^a	-0.14

^a Extrapolated.

Table IV: Heats of Solution of NaB(C₆H₅)₄ in Acetone-Diacetin Mixtures

Wt % diacetin	X_1 diacetin	ΔH_{soln}
0	0	-13.91 ± 0.44
12.9	0.046	-15.12 ± 0.19
25.3	0.101	-14.84 ± 0.02
35.0	0.151	-16.17 ± 0.69
45.1	0.213	-15.44 ± 0.12
54.5	0.283	-14.65 ± 0.24
65.1	0.380	-14.50 ± 0.03
74.8	0.495	-14.10 ± 0.12
83.7	0.629	-13.97 ± 0.25
87.6	0.699	-13.72 ± 0.16
92.5	0.791	-13.19 ± 0.36
100.0	1.000	-12.85^a

^a Extrapolated.

Table V: Heats of Solution of NaB(C₆H₅)₄ in Ethyl Acetate-Triacetin Mixtures

Wt % diacetin	X_1 diacetin	ΔH_{soln}
0	0	-14.57 ± 0.17
10.3	0.054	-15.43 ± 0.47
20.0	0.111	-16.30 ± 0.15
34.9	0.212	-17.39 ± 0.10
46.2	0.300	-15.22 ± 0.19
54.8	0.378	-14.70 ± 0.14
64.9	0.481	-14.20 ± 0.08
75.0	0.600	-13.46 ± 0.37
86.1	0.756	-12.81 ± 0.28
91.0	0.835	-12.65 ± 0.32
100.0	1.000	-12.25^a

^a Extrapolated.

Heats of solution of NaB(C₆H₅)₄ and Mg(ClO₄)₂ in acetone-glucose pentaacetate and acetone-cellulose acetate mixtures were also measured. Results are

Table VI: Heats of Solution of $\text{NaB}(\text{C}_6\text{H}_5)_4$ in Acetone-Triacetin Mixtures

Wt % triacetin	X, triacetin	ΔH_{soln}
0	0	-13.91 ± 0.44
12.1	0.035	-14.38 ± 0.04
23.9	0.077	-14.29 ± 0.11
33.0	0.116	-14.61 ± 0.26
44.9	0.178	-14.19 ± 0.59
55.2	0.247	-14.35 ± 0.50
64.8	0.329	-14.85 ± 0.67
75.0	0.444	-15.23 ± 0.23
84.8	0.597	-15.02 ± 0.31
91.2	0.734	-15.80 ± 0.26
100.0	1.000	-16.18^a

^a Extrapolated.**Table IX:** ^{23}Na Resonance of 0.05 M $\text{NaB}(\text{C}_6\text{H}_5)_4$ in H_2O -Diacetin

Wt % diacetin	X, diacetin	$\delta\Delta H(\text{Na}^+)^a$	Frequency of $^{23}\text{Na}^+$, $\text{Hz}^{b,c}$
0	0	0	869.8 ± 0.2
5.0	0.005	-0.10	869.7 ± 0.2
10.0	0.011	-0.20	868.8 ± 0.2
15.0	0.018	-0.36	867.9 ± 0.2
20.0	0.025	-0.54	866.7 ± 0.3
25.0	0.033	-0.72	866.1 ± 0.3
30.0	0.042	-0.94	865.1 ± 0.3
35.0	0.052	-1.18	864.2 ± 0.4
40.0	0.064	-1.44	863.6 ± 0.4
50.0	0.093	-2.05	861.2 ± 0.5
60.0	0.133	-2.67	856.4 ± 0.6
70.0	0.193	-3.23	851.6 ± 1.0

^a Assuming that $\delta\Delta H_{((\text{C}_6\text{H}_5)_4\text{As}^+)} = \delta\Delta H_{(\text{B}(\text{C}_6\text{H}_5)_4^-)}$. ^b Frequency synthesizer set at 15.871×10^6 Hz. ^c Chemical shift to lower frequency represents increased shielding of the ^{23}Na nucleus (see text).

listed in Tables VII and VIII. Table IX gives chemical shifts for $^{23}\text{Na}^+$ in the H_2O -diacetin system.

Table VII: Heats of Solution of $\text{NaB}(\text{C}_6\text{H}_5)_4$ and $\text{Mg}(\text{ClO}_4)_2$ in Acetone-Glucose Pentaacetate (GPA) Mixtures

Wt % GPA	X, GPA	ΔH_{soln} , $\text{NaB}(\text{C}_6\text{H}_5)_4$	ΔH_{soln} , $\text{Mg}(\text{ClO}_4)_2$
0	0	-13.91 ± 0.44	-39.36 ± 0.50
5.3	0.008	-14.24 ± 0.82	-39.08 ± 0.70
10.0	0.016	-14.33 ± 0.06	-40.74 ± 0.72
16.9	0.029	-14.63 ± 0.26	-42.48 ± 0.99
22.9	0.042	-14.58 ± 0.35	-40.64 ± 1.01
28.2	0.055	-14.36 ± 0.56	-42.50 ± 0.76
33.2	0.069		-41.86 ± 1.01
33.8	0.070	-14.35 ± 0.30	

Table VIII: Heats of Solution of $\text{NaB}(\text{C}_6\text{H}_5)_4$ and $\text{Mg}(\text{ClO}_4)_2$ in Acetone-Cellulose Acetate (CA) Mixtures

Wt % CA	ΔH_{soln} , $\text{NaB}(\text{C}_6\text{H}_5)_4$	ΔH_{soln} , $\text{Mg}(\text{ClO}_4)_2$
0	-13.91 ± 0.44	-39.36 ± 0.50
3.1	-14.90 ± 0.53	-45.79 ± 1.25
6.0	-15.21 ± 0.03	-45.82 ± 0.60

Discussion

The Water-Diacetin System. Presented in Table I are the three thermodynamic properties of transfer, $\delta\Delta G^\circ$, $\delta\Delta H^\circ$, and $\delta(T\Delta S^\circ)$ for sodium chloride from pure water to the aqueous diacetin mixtures shown. Gibbs free energies are derived directly from the activity coefficients of Kraus, *et al.*,⁴ through the expression $\Delta G^\circ = -2.303RT \log \gamma$, and entropy data are obtained by the combination of ΔG° and our enthalpy values. Kraus, *et al.*, included in their convention for the activity coefficient of the solute the fraction of water in the mixture. This would have the effect of

making ΔG° indeterminate at zero water content but will have relatively little effect on $\delta\Delta G^\circ$ or $\delta(T\Delta S^\circ)$ across the range which we have reported.

It is clear from the data in Table I that the gradually decreasing solubility of sodium chloride as the water content is decreased is due to an entropy effect rather than to an unfavorable change in enthalpy. Indeed sodium chloride is solvated increasingly exothermally as the diacetin concentration is increased. We attribute this primarily to the endothermic effect of structure breaking by this salt in pure water which is also manifested by the greater gain in entropy due to structure breaking in pure water than in the less aqueous mixtures. Such effects are found in many other aqueous binary systems.⁹⁻¹¹

In the hope of analyzing the enthalpy changes further, we have measured the heats of transfer for sodium tetraphenylboron and tetraphenylarsonium chloride in these same mixtures (Tables II and III). The peculiar extremum behavior seen for sodium tetraphenylboron and tetraphenylarsonium chloride in Figure 1 is typical of nonelectrolytes and hydrophobic ions of large diameter in highly aqueous organic binaries.^{5,11} It is related to an enhanced degree of structure in the medium at the composition where the inflection point occurs.¹¹⁻¹³ However, the detailed interpretation of

(9) H. S. Frank and M. W. Evans, *J. Chem. Phys.*, **13**, 507 (1945).

(10) E. M. Arnett and D. R. McKelvey in "Solute-Solvent Interactions," J. F. Coetzee and C. D. Ritchie, Ed., Marcel Dekker, New York, N. Y., 1969.

(11) E. M. Arnett in "Physico-Chemical Processes in Mixed Aqueous Solvents," F. Franks, Ed., Heinemann Educational Books, Ltd., London, 1967.

(12) F. Franks and D. J. G. Ives, *Quart. Rev., Chem. Soc.*, **20**, 1 (1966).

(13) E. M. Arnett and D. R. McKelvey, *J. Amer. Chem. Soc.*, **88**, 2598 (1966).

such curves is beyond the scope of present solution theory.

If the assumption is made that the heats of transfer for the tetraphenylboride and tetraphenylarsonium ions are exactly equal from pure water to any of the mixtures we have studied, one may calculate "single ion enthalpies of transfer."¹³ These are also presented in Figure 1. The strength of this assumption has been examined by several workers,^{14,15} and it is unreliable in low dielectric solvents. Recent studies (which were unpublished when the present experiments were performed) also render it dubious for water.^{16,17} Unfortunately, the tetraalkylboride ions which are recommended^{14,17} as superior for such a comparison are hydrolyzed in aqueous media.

Comparison of Nmr Data with Thermodynamics. Unlike the chemical shift of the proton, that of the ²³Na nucleus is dominated by a paramagnetic term.¹⁸ This usually leads to an increasingly large downfield shift in response to greater interaction with an electron donor in contrast to the corresponding upfield shift for greater screening of the proton. The ²³Na nucleus also has a quadrupole moment. If the nucleus is in an asymmetric environment, this may produce considerable line broadening which is not subject to ready-quantitative interpretation. Bloor and Kidd¹⁸ and Popov^{19,20} have found direct linear correlations between the basicities of various solvents (against aqueous acid or antimony pentachloride) and the ²³Na chemical shift produced by those solvents. We have also observed such correlations in nonaqueous media.²¹ In general the strongest bases produce the largest downfield shifts. However, some polydentate ligands cause upfield shifts presumably because of an increased diamagnetic contribution. It is, therefore, interesting to see that although the addition of diacetin to water produces an exothermic trend in the heat of transfer, which seems to indicate increasing solvation of the sodium ion, this is accompanied by an upfield shift which is cleanly proportional to the mole fraction of diacetin (Table IX).

We have clear independent evidence from other measurements²¹ that water, when present at high dilution in an inert solvent, is strongly coordinated to sodium ion and interacts much more exothermally with it than does diacetin. Thus, in terms of what the sodium ion "sees" in its immediate solvation layer the large downfield ²³Na shift in water is consistent with all available data in suggesting that water should be a stronger complexing agent than any of the water-diacetin mixtures. Why then does the curve for the single ion enthalpy of Na⁺ (Figure 1) show an exothermic trend for the solvation of sodium ion as the water content is decreased? The simplest of many possible explanations for this apparent discrepancy is that it is a manifestation of the failure of the single-ion assumption ($B(C_6H_5)_4^- = (As(C_6H_5)_4)^+$) through which the ΔH_{trans} values for Na⁺ were derived.

An excellent linear correlation was obtained between the free energy of transfer for sodium chloride and the corresponding ²³Na shift of sodium tetraphenylboron. Owing to the complicated contributions of entropy and enthalpy to the free energy change, this correlation may be fortuitous.

The ability to explore these correlations further is limited by the poor solubility of the sodium salts in diacetin-rich solutions and by the very broad peaks obtained by ²³Na resonance in such media.

Nonaqueous Binaries. The results presented in Tables IV through VIII for heats of solution of NaB(C₆H₅)₄ in various nonaqueous binaries were developed to explore a number of points. Sodium tetraphenylboron is not soluble enough in diacetin to allow a direct heat of solution measurement with our apparatus. In view of the special solvating ability which small amounts of water might exert on sodium ions in diacetin, we wished to have independent estimates for the extrapolated value (−9.50 kcal/mol) for NaB(C₆H₅)₄ in pure diacetin presented in Table II for the water-diacetin system. Accordingly the acetone-diacetin and ethyl acetate-diacetin systems were explored, and extrapolations to −12.85 and −12.28 kcal/mol were obtained, respectively. These are in fairly good agreement with each other but are grossly at odds with the much more endothermic value obtained from the aqueous binary system. We believe that the true value lies between −12 and −13 kcal/mol and that the reason for the large error in an endothermic direction for the value extrapolated from the aqueous binary lies in the fact that 0.458 mole fraction diacetin (Table II) is still a highly structured solvent compared to organic binaries. The endothermic error is the result of the large structure-breaking energy required for dissolving salts in highly aqueous binaries. This has its peak at about 20 wt % (0.025 mole fraction) diacetin but is still effective in the 0.458 mole fraction solution.

Tables IV and V show behavior similar to that which we have reported before for the solution of NaB(C₆H₅)₄ in binaries of dimethyl sulfoxide with acetone and with dioxane.¹¹ In all four cases this salt interacts more exothermally with a mixture of intermediate composition than it does with either pure component. This contrasts sharply with the *endothermic* maxima which

(14) R. Fuchs, J. L. Bear, and R. F. Rodewald, *J. Amer. Chem. Soc.*, **91**, 5797 (1969).

(15) R. Alexander and A. J. Parker, *ibid.*, **89**, 5549 (1967).

(16) C. Jolicoeur and H. L. Friedman, *J. Phys. Chem.*, **75**, 165 (1971).

(17) J. F. Coetzee and W. R. Sharpe, *ibid.*, **75**, 3141 (1971).

(18) E. G. Bloor and R. G. Kidd, *Can. J. Chem.*, **46**, 3425 (1968).

(19) R. H. Erlich, E. Roach, and A. I. Popov, *J. Amer. Chem. Soc.*, **92**, 4989 (1970).

(20) R. H. Erlich and A. I. Popov, *ibid.*, **93**, 5620 (1971).

(21) E. M. Arnett, H. C. Ko, and R. J. Minas, unpublished results.

are typical of aqueous binaries.⁵ It also differs from the acetone-triacetin binary (Table VI) in which a steady exothermic trend is found towards triacetin, the superior solvating medium. This superiority of 2.27 kcal/mol (16.18 – 13.91) is worth comparing with that of ethyl acetate (14.57 – 13.91 = 0.66 kcal/mol) over acetone. If triacetin were behaving as three ethyl acetate residues bound together, we might expect it to be superior to acetone by about 2.0 kcal/mol. The fact that triacetin exceeds this by about 0.3 kcal/mol might be due to the fact that the acetate residues are vicinal to each other on the three-carbon backbone of the molecule, thus permitting a chelation effect such as is found in the binding of alkali metal ions by other polybasic ligands.²²

The results in Table VII show that on a mole fraction basis glucose pentaacetate (a possible model for the fundamental molecular unit of completely acetylated cellulose) is comparable to triacetin in its ability to solvate sodium ions. Table VIII shows that in dilute acetone solution cellulose acetate is superior to diacetin, triacetin, and glucose pentaacetate in its interaction with sodium tetraphenylboron. Since cellulose acetate

is partially hydroxylated and also carries ether linkages between its glucose residues, these groups may be contributing exothermally to the solvation of sodium ions.

Magnesium perchlorate is used as an additive in casting cellulose acetate reverse osmosis membranes.² Kesting²³ has proposed that cations of high charge such as Mg^{2+} form complexes with the hydroxyl and acetate groups of cellulose acetate and contribute to the swelling of the membrane by subsequent hydration after immersion in water. The results in Tables VII and VIII show clearly that $Mg(ClO_4)_2$ interacts strongly with cellulose acetate in acetone and that cellulose acetate is far superior to glucose pentaacetate on this score. It remains to be seen how much this difference is due to conformational factors and how much is due to the specific superiority of hydroxyl and ether functions in solvating cations. In any event, Kesting's postulation of complexing between this salt and cellulose acetate is clearly supported.

(22) J. J. Christensen, J. O. Hill, and R. M. Izatt, *Science*, **174**, 459 (1971).

(23) R. E. Kesting, *J. Appl. Polym. Sci.*, **9**, 663 (1965).

Electron Spin Resonance Spectra of Zwitterion Radicals and Isoelectronic Anion Radicals¹

by Ronald P. Mason*

Department of Chemistry, Cornell University, Ithaca, New York 14850

and John E. Harriman

Department of Chemistry, University of Wisconsin, Madison, Wisconsin 53706 (Received January 12, 1972)

Publication costs borne completely by The Journal of Physical Chemistry

Electron spin resonance spectra have been obtained for the *p*-nitrobenzyltrimethylammonium zwitterion radical and the 2,2-dimethyl-1-*p*-nitrophenylpropane anion radical in acetonitrile at -40° and for the *p*-nitrophenyltrimethylammonium zwitterion radical and the *p*-nitro-*tert*-butylbenzene anion radical in dimethyl sulfoxide at room temperature. All radicals were generated electrolytically. Hyperfine coupling constants are reported and discussed in terms of probable radical structures.

In a recent note, Knolle and Bolton² have discussed differences in the fluorine hyperfine splitting in two isoelectronic and essentially isostructural radicals, one a neutral nitroxide and the other a ketyl. We report here an investigation of the proton hyperfine coupling constants of two pairs of isoelectronic para-substituted nitrobenzene radicals. One member of each pair is an

anion radical with an alkyl substituent while the other is a zwitterion radical containing a trimethylammonium substituent. The radical pairs are $-O_2NC_6H_4CH_2C-$

(1) This research was supported by the National Science Foundation under Grants No. GP-7512 and GP-9539.

(2) W. R. Knolle and J. R. Bolton, *J. Amer. Chem. Soc.*, **91**, 5411 (1969).

$(\text{CH}_3)_3$ (I) and $-\text{O}_2\text{NC}_6\text{H}_4\text{CH}_2\text{N}^+(\text{CH}_3)_3$ (II), $-\text{O}_2\text{NC}_6\text{H}_4\text{C}(\text{CH}_3)_3$ (III) and $-\text{O}_2\text{NC}_6\text{H}_4\text{N}^+(\text{CH}_3)_3$ (IV).

Experimental Section

The esr spectra of the *p*-nitrobenzyltrimethylammonium zwitterion radical and the 2,2-dimethyl-1-*p*-nitrophenylpropane anion radical have been obtained at -40° with acetonitrile (ACN) as the solvent. The zwitterion radical was generated by *intra muros*³ electrolysis at -40° of a 1 mM solution of *p*-nitrobenzyltrimethylammonium chloride. This radical was unstable at higher temperatures. The anion radical was generated by essentially complete electrolytic bulk reduction, in an external cell, of a 1 mM solution of the parent compound.

The esr spectra of the *p*-nitrophenyltrimethylammonium zwitterion radical and the *p*-nitro-*tert*-butylbenzene anion radical were obtained at room temperature in dimethyl sulfoxide (DMSO). These radicals were prepared by external, electrolytic bulk reduction of 0.5 mM solutions of *p*-nitrophenyltrimethylammonium perchlorate and *p*-nitro-*tert*-butylbenzene, respectively. The spectrum of *p*-nitro-*tert*-butylbenzene anion has been reported previously.⁴

In all cases 0.1 *M* tetra-*n*-propylammonium perchlorate served as supporting electrolyte. Solvents and supporting electrolyte were prepared by standard techniques. All spectra were obtained using a Varian Model E-15 X-band spectrometer equipped with a 40-cm magnet and a E 80-A recorder.

Preparation of Compounds. *p*-Nitrobenzyltrimethylammonium chloride was obtained from Chemicals Procurement Laboratories and used without further purification. *p*-Nitrophenyltrimethylammonium perchlorate was prepared by the method of Zaki and Fahim.⁵ The precursor, *N,N*-dimethyl-*p*-nitroaniline, was obtained from Eastman Organic Chemicals. *p*-Nitro-*tert*-butylbenzene and 2,2-dimethyl-1-*p*-nitrophenylpropane were obtained by nitration of the alkylbenzenes⁶ which were obtained from Chemical Samples Co. The highest boiling isomer, the para isomer, was isolated and purified by gas chromatography. A 10-ft, 25% Carbowax column at 200° cleanly separated the three isomers.

Results and Discussion

The spectra were analyzed to obtain hyperfine coupling constants which are summarized in Table I. The splitting due to the nine methyl protons, which is only barely resolved in the spectrum of *p*-nitro-*tert*-butylbenzene, is clearly resolved in the isoelectronic zwitterion. Computer simulation of the first few lines confirmed that the splitting was due to nine equivalent protons. This splitting was not resolved if acetonitrile was used as solvent.

The members of each of these zwitterion-anion radical pairs differ only in the replacement of N^+ by C.

It is not surprising that the charge difference changes the hyperfine coupling constants, since it will certainly alter the electronic charge distribution, and thus the spin distribution, in one relative to the other. The changes in the ring proton and nitro nitrogen constants are relatively small and appear to fit the pattern for para-substituted nitrobenzene first investigated by Maki and Geske⁷ and subsequently extended by many workers.

The other coupling constants will be affected by geometrical or configurational considerations, as well as by changes of spin density distribution within the ring. It is convenient to introduce a coordinate system in terms of which to discuss these effects. The nitro nitrogen, atoms 1 and 4 of the ring, and the first carbon or nitrogen of the substituent are taken (in their equilibrium position) to define the *z* axis, and the plane of the ring is taken to be the *yz* plane.

It is well known that, for protons like the methylene protons of the first pair of radicals, the proportionality constant relating the proton hyperfine coupling constant to the ring carbon π electron spin density is angle dependent.⁸ To a good approximation

$$a_{\beta}^{\text{H}} = \rho_c^{\pi}(B_0 + B \cos^2 \theta)$$

where θ is the angle between the H-C-C_{ring} plane and the *xz* plane. The spin density distributions, as reflected by the hyperfine splittings of the nitrogen and ring protons, are nearly identical for all para alkyl nitrobenzene anion radicals in ACN.⁸ It has also been shown that for these systems the constant B_0 is essentially zero while $\rho_c^{\pi}B$ is about 8 G.⁹

The observed value of 2.02 G for the methylene proton coupling constant in II is thus not consistent with essentially free rotation of the substituent, leading to $\langle \cos^2 \theta \rangle = 1/2$. It is consistent with a dominant configuration with the central carbon of the substituent in the *xz* plane, having $\cos^2 \theta = 0.25$. Small torsional motions are not excluded, so long as their amplitude is not sufficient to appreciably alter $\langle \cos^2 \theta \rangle$. Of course transitions between two equivalent configurations, with the protons above or below the plane, are allowed and no conclusions regarding rate of conversion are possible so long as negligible time is spent in the intermediate region. Similar results have been obtained by Carrington and Todd for alkyl-substituted cyclooctatetraene anion radicals.¹⁰

(3) D. H. Geske and A. H. Maki, *J. Amer. Chem. Soc.*, **82**, 2671 (1960).

(4) P. B. Ayscough, F. P. Sargent, and R. Wilson, *J. Chem. Soc.*, 5418 (1963).

(5) A. Zaki and H. Fahim, *ibid.*, 270 (1942).

(6) K. L. Nelson and H. C. Brown, *J. Amer. Chem. Soc.*, **73**, 5605 (1951).

(7) A. H. Maki and D. H. Geske, *ibid.*, **83**, 1852 (1961).

(8) D. H. Geske, *Progr. Phys. Org. Chem.*, **4**, 125 (1967).

(9) E. G. Janzen and J. L. Gerlock, *J. Org. Chem.*, **32**, 820 (1967).

(10) A. Carrington and P. F. Todd, *Mol. Phys.*, **8**, 299 (1964).

Table I: Observed Hyperfine Coupling Constants^a

Radical (solvent, temp)	$ a^{\text{N}}_{\text{NO}_2} $	$ a^{\text{H}}_{\text{ortho}} ^b$	$ a^{\text{H}}_{\text{meta}} ^b$	$ a^{\text{N}}_{\text{N}^+\text{Me}_3} $	$ a^{\text{H}}_{\beta} ^b$	$ a^{\text{H}}_{\text{Me}} $
<i>p</i> -Nitrobenzyltrimethylammonium zwitterion (I) (ACN, -40°)	9.13	3.26	0.97	2.73	1.52	<i>c</i>
2,2-Dimethyl-1- <i>p</i> -nitrophenyl- propane (II) (ACN, -40°)	10.72	3.36	1.09	...	2.02	<i>c</i>
<i>p</i> -Nitrophenyltrimethylammonium zwitterion (III) (DMSO, room temp)	8.33	3.30	0.85	0.78	...	0.126 ^d
<i>p</i> -Nitro- <i>tert</i> -butylbenzene anion (IV) (DMSO, room temp)	10.13	3.28	1.06	0.060 ^d

^a Values are in gauss, with an uncertainty of about ± 0.01 unless otherwise noted. ^b Ortho and meta to the nitro group; H_{β} refers to the methylene protons. Assignment of these sets of 2 equivalent protons each is by analogy to other substituted nitrobenzenes and by comparison with calculated results. ^c Not resolved. ^d Uncertainty ~ 0.005 G.

It is most reasonable to assume that I has the same geometry as II. The smaller value of 1.54 G for the methylene proton coupling constant indicates a smaller value of $\rho_{\text{C}}^{\pi}B$, but present data do not allow us to distribute the change between ρ_{C}^{π} and B .

The greatest relative difference observed for corresponding splittings between members of an isoelectronic pair occur for the nine methyl protons in II and IV. The value of 0.78 for $|a^{\text{N}}_{\text{N}^+\text{Me}_3}|$ implies ρ_{C}^{π} is about 0.19 in III if $Q^{\text{N}}_{\text{CN}^+\text{H}_3}$ equals $Q^{\text{N}}_{\text{CN}^+\text{Me}_3}$, since $|a^{\text{N}}_{\text{N}^+\text{H}_3}|$ is 4.1 in $\cdot\text{CH}_2\text{N}^+\text{H}_3$.^{11,12}

Calculations¹³ and experimental coupling constants¹⁴ suggest that ρ_{C}^{π} is 0.16 in nitrobenzene. This spin density is probably very similar in IV, and is thus

smaller than in III. This would suggest that, if the methyl proton coupling constants are proportional to ρ_{C}^{π} , the constant of proportionality is rather different for the C and N⁺ species.

These comparisons of coupling constants in isoelectronic radicals will provide an interesting test of the semiempirical calculation of spin density distributions.

(11) R. P. Kohin and P. G. Nadeau, *J. Chem. Phys.*, **44**, 691 (1966).

(12) P. B. Ayscough, "Electron Spin Resonance in Chemistry," Methuen, London, 1967.

(13) J. A. Pople, D. L. Beveridge, and P. A. Dobosh, *J. Amer. Chem. Soc.*, **90**, 4201 (1968).

(14) J. E. Harriman and A. H. Maki, *J. Chem. Phys.*, **39**, 778 (1963).

COMMUNICATIONS TO THE EDITOR

Raman Scattering in Sodium-Liquid Ammonia Solutions¹

Publication costs assisted by Texas Christian University

Sir: The nature of the species present in a dilute solution of an alkali metal in liquid ammonia continues to be a matter of speculation. Numerous models have been proposed,² but as yet no single theory is clearly superior. According to Jortner, *et al.*,³ very dilute solutions contain unassociated, solvated cations and electrons. The electron is described as existing in a "cavity" created by preferentially oriented solvent molecules. Calculations on the ground-state energy

lead to a prediction of a totally symmetric vibration between 25 and 60 cm^{-1} . According to Rusch,⁴ this vibration may lie between 400 and 700 cm^{-1} . Rusch⁵ has reported that the vibrational spectrum of ammonia is perturbed by the addition of alkali metal. Specifi-

(1) This work was supported by The Robert A. Welch Foundation. Gratitude is expressed to the University of Dallas for the loan of the monochromator.

(2) "Metal-Ammonia Solutions," J. J. Lagowski and M. J. Sienko, Ed., Butterworths, London, 1970.

(3) D. A. Copeland, N. R. Kestner, and J. Jortner, *J. Chem. Phys.*, **53**, 1189 (1970).

(4) P. F. Rusch, Universite Catholique de Lille, France, private communication.

(5) P. F. Rusch, Ph.D. Dissertation, The University of Texas at Austin, 1971.

cally, ν_1 and ν_3 are reported to shift to lower energy with increasing concentration.

A laser Raman spectrometer has been constructed which readily accepts the specially designed glass dewar used for solution preparation and containment. The spectrometer utilizes the conventional 90° geometry in which 4880 Å (350 mW) radiation from an Ar⁺ laser is focused on the sample. The emitted radiation is collected with appropriate optics and focused on the entrance slit of a Spex 1401 double monochromator. A polarization analyzer and scrambler have been incorporated into the fore optics. The detection system is a photon-counting device which utilizes a Channeltron photomultiplier tube.

A modified version of the dewar described by Quinn⁶ was used. In this design, a portion of the solution is contained in a tube which extends into the evacuated portion of the dewar. Such a design permits only one pass of the laser beam which limits the emission intensity but permits polarization studies. The solutions were prepared by a previously described procedure.⁷ Temperature of the solutions was monitored with a thermistor positioned just above the point where the laser beam was focused. All spectra were recorded at constant slit width (300 μ). In every case, spectra were recorded with the analyzer removed and then with the analyzer parallel and perpendicular.

The spectra of liquid ammonia and dilute sodium-ammonia solutions were determined and the results are presented in Table I. Inspection of the results reveals that they are in good agreement with those previously reported.⁸⁻¹⁰ Polarization studies on pure ammonia also agree with previous investigators.^{8,9}

Table I: Raman Frequencies (cm^{-1}) for Sodium-Liquid Ammonia Solutions

	Ammonia concn, M		
	2.3×10^{-4}	5.2×10^{-4}	2.0×10^{-3}
	Temp., -67°C		
1060 (ν_2)	1065	1068	1063
1634 (ν_4)	1638	Not detectable	Not detectable
3213	3210	3211	3213
3302	3301	3300	3302
3380 (ν_3)	3378	3382	3379

Although the spectra of ammonia and sodium-ammonia solutions are almost indistinguishable, some differences exist. A weak broad band appears in the ammonia spectrum at approximately 300 cm^{-1} . This band is much weaker but still present in the most dilute solution, but it cannot be detected in the other solutions. This band may be unresolved rotational structure¹¹ which is lost as the solvent becomes more ordered. The spectra of ammonia and the solutions are superimposable out to 15 cm^{-1} where a decrease in intensity

with increasing concentration begins to occur. It should perhaps be mentioned that the different concentrations represent different solution preparations. There is also an observable decrease in intensity with increasing concentration for all the Raman bands. No intensity-concentration correlation was attempted in this preliminary work. There is a temptation to speculate that the decrease in intensity is a result of the decrease in solution density, but this seems difficult to accept in light of Rusch's report⁵ that the infrared absorption increased with increasing concentration.

A very careful analysis of the region $0\text{--}1000\text{ cm}^{-1}$ was made. There was no evidence of new bands, shoulders, or even slope changes on the Rayleigh line. It should be mentioned that the Rayleigh line was very narrow (e.g., 3×10^6 intensity units at $\Delta\nu = 0$, 1×10^3 at $\Delta\nu = 25\text{ cm}^{-1}$, and 3×10^2 at $\Delta\nu = 100\text{ cm}^{-1}$).

In light of these findings several points should be emphasized. At concentrations around 10^{-4} M where an isolated cavity would be expected to exist, no scattering center is evident with a single-pass cell. One must conclude that either the cavity does not have the vibrational mode predicted or that the concentration of scattering centers is so small as to be undetectable. Increasing the concentration does not seem likely to increase the concentration of isolated cavities because association is inevitable and the integrity of the cavity becomes questionable. The only recourse seems to be a multipass cell; however, this technique precludes any quantitative polarization studies even if the predicted vibration is observed. At these low concentration levels no correlatable shift of any band positions with concentration was evident.

A systematic investigation of the Raman scattering in these solutions is underway. Using a multipass cell, Raman scattering will be studied as a function of metal, metal concentration, temperature, and inert electrolyte concentration. It will be interesting to see if the association mechanism produces a species which is Raman active and if the solvent vibrations are perturbed by the solute. Work is continuing in these areas and results will be forthcoming.

(6) R. K. Quinn and J. J. Lagowski, *J. Phys. Chem.*, **72**, 1374 (1968).

(7) D. F. Burow and J. J. Lagowski, *Advan. Chem. Ser.*, **No. 50**, 125 (1965).

(8) B. Bettignies and F. Wallart, *C. R. Acad. Sci., Ser. B*, 640 (1970).

(9) G. Seillier, M. Ceccaldi, and J. P. Leickman, *Method. Phys. Anal.*, **4**(4), 388 (1968).

(10) T. Birchall and I. Drummond, *J. Chem. Soc. A*, 1859 (1970).

(11) G. Herzberg, "Molecular Spectra and Molecular Structure," Van Nostrand, London, 1966.

DEPARTMENT OF CHEMISTRY
TEXAS CHRISTIAN UNIVERSITY
FORT WORTH, TEXAS 76129

BILLIE L. SMITH
W. H. KOEHLER*

RECEIVED MARCH 6, 1972

On a Comparison of Isotope Shifts in the Vibrational Spectrum of Gas-Phase and Matrix-Isolated Hydrogen Cyanide¹

Publication costs assisted by Argonne National Laboratory, U. S. Atomic Energy Commission

Sir: Recently, Pacansky and Calder² (PC) compared calculations of the bond-length ratio, $r_{\text{CN}}/r_{\text{HC}}$, obtained from application of the Teller-Redlich product rule to the ν_2 bending frequency of gas-phase and matrix-isolated HCN isotopes. The deviations of the matrix values from the accepted value of 1.082 obtained from rotational fine-structure data,³ even when corrections were applied for anharmonicity, and the scatter in the ratios that they calculated from the matrix data as compared with those calculated from the "gas-phase data" led PC to conclude that "the discrepancies most likely result from the failure of the linear xyz vibrational model to describe the vibrations of the matrix-isolated molecule adequately." Because of the serious implication that molecular geometries, particularly of molecules containing light atoms, may be incorrectly deduced from isotope shifts of matrix-isolated molecules, we decided to reinvestigate the apparent discrepancies. The present study shows that no anomalies exist between the matrix and gas-phase data when the uncertainties in the measurements and the sensitivity of the bond-length ratio to these uncertainties are properly taken into account.

Application of the Teller-Redlich product rule to ν_2 of two isotopes of HCN, $\text{H}'\text{C}'\text{N}'$ and $\text{H}''\text{C}''\text{N}''$, yields

$$R \equiv \frac{\omega_2'}{\omega_2''} = \left[\left(\frac{1}{m_{\text{N}'}} + \frac{x^2}{m_{\text{H}'}} + \frac{(1+x)^2}{m_{\text{C}'}} \right) / \left(\frac{1}{m_{\text{N}''}} + \frac{x^2}{m_{\text{H}''}} + \frac{(1+x)^2}{m_{\text{C}''}} \right) \right]^{1/2} \quad (1)$$

where x is the ratio of r_{CN} to r_{HC} , the ω_2 's are zero-order bending frequencies, and the m 's are the atomic masses of the various constituent elements of the HCN isotopes. Equation 1 may easily be inverted to obtain x as a function of R based on the observed fundamentals, ν_2 , or the zero-order frequencies, ω_2 , which are corrected for anharmonicity. For the six isotopes discussed by PC, 15 values of x may be calculated from the various combinations of values of ν_2 .⁴

The bending frequencies for the gas-phase and matrix-isolated molecules, together with the rotational and anharmonic correction terms and the PC "gas-phase data," are presented in Table I. The anharmonic correction factors $[-(3x_{22} + 1/2(x_{12} + x_{23}) + x_{11})]$ have been taken from Nakagawa and Morino.⁵ These are subject to some error because of improper use of ν_2 for $G(0,1,0,1) - G(0,0,0,0)$ in the case of $\text{H}^{13}\text{C}^{14}\text{N}$. However, since their values for $\text{H}^{12}\text{C}^{14}\text{N}$ and $\text{D}^{12}\text{C}^{14}\text{N}$ do not differ significantly from those computed by Suzuki, *et al.*,⁶ we have used the values of Nakagawa and Morino for all isotopes. A comparison of the 15

ratios of isotopic frequencies using the gas-phase, matrix-isolation, and PC "gas-phase" data, both corrected and uncorrected for anharmonic effects, is presented in Table II, together with the theoretical values computed from eq 1. Values of $r_{\text{CN}}/r_{\text{HC}}$ computed from these frequency ratios are shown in Table III. The dependence of the bond-length ratio on the frequency ratio, $\partial x/\partial R$, has also been calculated and is shown in column viii of Table III. For isotopic pairs in which both molecules contain hydrogen atoms or both contain deuterium atoms, the calculated bond-length ratio is seen to be 10 to 25 times more sensitive to changes in the frequency ratio than for isotopic pairs containing each a hydrogen and a deuterium atom. Although the precision of the frequency data is better than $\pm 0.05 \text{ cm}^{-1}$, the uncertainties in the anharmonic corrections are calculated as $\pm 0.54 \text{ cm}^{-1}$ for the H-containing isotopes and $\pm 0.74 \text{ cm}^{-1}$ for the D-containing isotopes.⁵ The uncertainty in $r_{\text{CN}}/r_{\text{HC}}$, $\Delta x = (\partial x/\partial R)\Delta R$, for a probable error of $\pm 0.3 \text{ cm}^{-1}$ in the ω_2 's is given in the last column of Table III.

The following conclusions may be drawn from examination of Tables I to III. (1) Very good agreement among values of $r_{\text{CN}}/r_{\text{HC}}$ computed from gas-phase and matrix-isolation data exists when the nine isotopic combinations which are least sensitive to uncertainties in the vibrational frequencies are used. (2) The excellent consistency of values of $r_{\text{CN}}/r_{\text{HC}}$ computed from the PC "gas-phase data" results from the fact that these values are not based on experimental gas-phase frequencies but rather on calculated frequencies fit to only three ν_2 isotopic frequencies and their overtones, as well as combination and difference bands involving those fundamentals, and an assumed value of $r_{\text{CN}}/r_{\text{HC}} = 1.082$ introduced through values of B_v in the calculations of Nakagawa and Morino.⁵ (3) A conservative estimate of the uncertainties in the zero-order frequencies of $\pm 0.3 \text{ cm}^{-1}$ more than accounts for any discrepancies between the true value of $r_{\text{CN}}/r_{\text{HC}}$ and those values based on the bending frequencies of matrix-isolated HCN isotopes.

This work demonstrates the necessity of calculating the uncertainties in the geometric factors deduced from isotope shifts and the importance of choosing

(1) Work performed under the auspices of the U. S. Atomic Energy Commission.

(2) J. Pacansky and G. V. Calder, *J. Phys. Chem.*, **76**, 454 (1972).

(3) D. H. Rank, G. Skorinko, D. P. Eastman, and T. A. Wiggins, *J. Opt. Soc. Amer.*, **50**, 421 (1960).

(4) Care must be taken to correct the observed band centers, ν_0 , $[= G(v_1, v_2, v_3, l) - G(v_1', v_2', v_3', l')]$ by adding the term $B_v(l^2 - l'^2)$ to obtain the value of the fundamental frequency. Some confusion exists in the literature because the values of ν_0 reported by Rank, *et al.*,³ already incorporate the B_v correction term. This has led to errors in the values of ν_0 for the bending frequencies of the six isotopes which were computed by Nakagawa and Morino⁵ and used by PC as "gas-phase data."

(5) T. Nakagawa and Y. Morino, *Bull. Chem. Soc. Jap.*, **42**, 2212 (1969).

(6) I. Suzuki, M. A. Pariseau, and J. Overend, *J. Chem. Phys.*, **44**, 3561 (1966).

Table I: Bending Vibrational Frequencies (cm⁻¹) of Gas-Phase and Matrix-Isolated HCN Isotopes

	Gas phase					PC "gas phase" ^a			PC matrix	
	01 ¹⁰ -00 ⁰⁰	B _v ^b	ν ₂ ^c	Anharmonic ^d correction	ω ₂	01 ¹⁰ -00 ⁰⁰	ν ₂	ω ₂	01 ¹⁰ -00 ⁰⁰ ^e	ω ₂
H ¹² C ¹⁴ N	711.98 ^f	1.48	713.46	13.26 ± 0.54	726.72	711.98	712.35	727.10	720.96	734.22
H ¹² C ¹⁴ N	705.94 ^g	1.45	707.39	12.94	720.33	707.39	706.34	720.71	714.94	727.88
H ¹² C ¹⁵ N		1.44	712.41	13.16	725.57		711.41	726.01	719.74	732.90
D ¹² C ¹⁴ N	569.04 ^h	1.21	570.25	9.34 ± 0.74	579.59	569.04	569.30	579.85	576.02	585.36
D ¹³ C ¹⁴ N		1.19	562.55	9.04	571.59		561.60	571.82	568.01	577.05
D ¹² C ¹⁵ N		1.18	569.0	9.25	578.25		568.06	578.49	574.44	583.69

^a Obtained by PC from ref 5. ^b Calculated using $r_{CN} = 1.15313 \text{ \AA}$ and $r_{CH} = 0.61593 \text{ \AA}$ (ref 3). ^c Where no actual gas-phase data exist, values of ν_2 were obtained by adjusting values calculated in ref 5 for discrepancies between observed and calculated ν_2 values for H¹²C¹⁴N, H¹³C¹⁴N, and D¹²C¹⁴N. ^d Obtained from ref 5. Although these values may be slightly in error for reasons cited in text, the values for H¹²C¹⁴N, and D¹²C¹⁴N are in close agreement with those computed in ref 6. ^e Because rotational motion except about the internuclear axis is constrained in the matrix, no correction for B_v is necessary; i.e., $\nu_2 = G(0,1,0,1) - G(0,0,0,0)$. ^f Obtained from ref 3 and W. W. Brim, J. M. Hoffman, H. H. Nielsen, and K. N. Rao, *J. Opt. Soc. Amer.*, **50**, 1208 (1960). ^g Obtained from ref 3. ^h Obtained from A. G. Maki, E. K. Plyler, and R. Thibault, *J. Opt. Soc. Amer.*, **54**, 869 (1964).

Table II: Observed, Calculated, and Theoretical Values of HCN Isotopic Bending Frequency Ratios

H''C''N''	H'C'N'	ν ₂ ^f /ν ₂ ^g			ω ₂ ^f /ω ₂ ^g			Theoretical ^h
		Gas	Matrix	PC "Gas-phase"	Gas	Matrix	PC "Gas-phase"	
H ¹² C ¹⁴ N	D ¹² C ¹⁴ N	0.79927	0.79896	0.79918	0.79754	0.79725	0.79748	0.79748
H ¹² C ¹⁴ N	D ¹³ C ¹⁴ N	0.78848	0.78785	0.78837	0.78653	0.78594	0.78644	0.78644
H ¹² C ¹⁴ N	D ¹² C ¹⁵ N	0.79752	0.79677	0.79744	0.79570	0.79498	0.79561	0.79561
H ¹³ C ¹⁴ N	D ¹² C ¹⁴ N	0.80613	0.80569	0.80599	0.80462	0.80420	0.80455	0.80454
H ¹³ C ¹⁴ N	D ¹³ C ¹⁴ N	0.79525	0.79449	0.79509	0.79351	0.79278	0.79341	0.79340
H ¹³ C ¹⁴ N	D ¹² C ¹⁵ N	0.80437	0.80348	0.80423	0.80276	0.80190	0.80267	0.80265
H ¹² C ¹⁵ N	D ¹² C ¹⁴ N	0.80045	0.80032	0.80024	0.79881	0.79869	0.79868	0.79867
H ¹² C ¹⁵ N	D ¹³ C ¹⁴ N	0.78964	0.78919	0.78942	0.78778	0.78735	0.78762	0.78761
H ¹² C ¹⁵ N	D ¹² C ¹⁵ N	0.79870	0.79812	0.79850	0.79696	0.79641	0.79681	0.79679
H ¹² C ¹⁴ N	H ¹³ C ¹⁴ N	0.99149	0.99165	0.99156	0.99121	0.99136	0.99121	0.99122
H ¹² C ¹⁴ N	H ¹² C ¹⁵ N	0.99853	0.99831	0.99868	0.99842	0.99820	0.99850	0.99851
H ¹³ C ¹⁴ N	H ¹² C ¹⁵ N	1.0071	1.0067	1.0072	1.0073	1.0069	1.0073	1.0074
D ¹² C ¹⁴ N	D ¹³ C ¹⁴ N	0.98650	0.98609	0.98647	0.98620	0.98580	0.98615	0.98616
D ¹² C ¹⁴ N	D ¹² C ¹⁵ N	0.99781	0.99726	0.99782	0.99769	0.99715	0.99765	0.99766
D ¹³ C ¹⁴ N	D ¹² C ¹⁵ N	1.0115	1.0113	1.0115	1.0117	1.0115	1.0117	1.0117

^a Obtained from eq 1.

Table III: Calculation of r_{CN}/r_{HC} from Isotope Shifts

H''C''N''	H'C'N'	From ν ₂ gas	From ν ₂ matrix	From ω ₂ calc	From ω ₂ gas	From ω ₂ matrix	Δx/ΔR ^a	Δ(r _{CN} /r _{HC}) ^b
H ¹² C ¹⁴ N	D ¹² C ¹⁴ N	1.0549	1.0595	1.0819	1.0810	1.0854	-17	±0.009
H ¹² C ¹⁴ N	D ¹³ C ¹⁴ N	1.0484	1.0585	1.0820	1.0804	1.0906	-19	±0.010
H ¹² C ¹⁴ N	D ¹² C ¹⁵ N	1.0520	1.0635	1.0819	1.0805	1.0922	-18	±0.010
H ¹³ C ¹⁴ N	D ¹² C ¹⁴ N	1.0596	1.0657	1.0818	1.0809	1.0869	-16	±0.008
H ¹³ C ¹⁴ N	D ¹³ C ¹⁴ N	1.0538	1.0653	1.0819	1.0803	1.0918	-18	±0.009
H ¹³ C ¹⁴ N	D ¹² C ¹⁵ N	1.0570	1.0698	1.0818	1.0805	1.0933	-17	±0.009
H ¹² C ¹⁵ N	D ¹² C ¹⁴ N	1.0559	1.0578	1.0818	1.0799	1.0816	-17	±0.009
H ¹² C ¹⁵ N	D ¹³ C ¹⁴ N	1.0496	1.0567	1.0819	1.0792	1.0863	-18	±0.010
H ¹² C ¹⁵ N	D ¹² C ¹⁵ N	1.0530	1.0616	1.0818	1.0794	1.0880	-18	±0.010
H ¹² C ¹⁴ N	H ¹³ C ¹⁴ N	1.1354	1.1686	1.0804	1.0796	1.1099	189	±0.11
H ¹² C ¹⁴ N	H ¹² C ¹⁵ N	1.0898	1.0029	1.0780	1.0440	0.9669	429	±0.25
H ¹³ C ¹⁴ N	H ¹² C ¹⁵ N	1.1711	1.3230	1.0823	1.1087	1.2470	-326	±0.19
D ¹² C ¹⁴ N	D ¹³ C ¹⁴ N	1.1390	1.0715	1.0818	1.0882	1.0262	164	±0.12
D ¹² C ¹⁴ N	D ¹² C ¹⁵ N	1.1303	0.9735	1.0814	1.0917	0.9474	304	±0.22
D ¹³ C ¹⁴ N	D ¹² C ¹⁵ N	1.1480	1.1993	1.0801	1.0840	1.1337	-334	±0.25

^a $x \equiv r_{CN}/r_{HC}$; $R = \omega_2^f/\omega_2^g$. ^b Based on ±0.3 cm⁻¹ probable error in ω's.

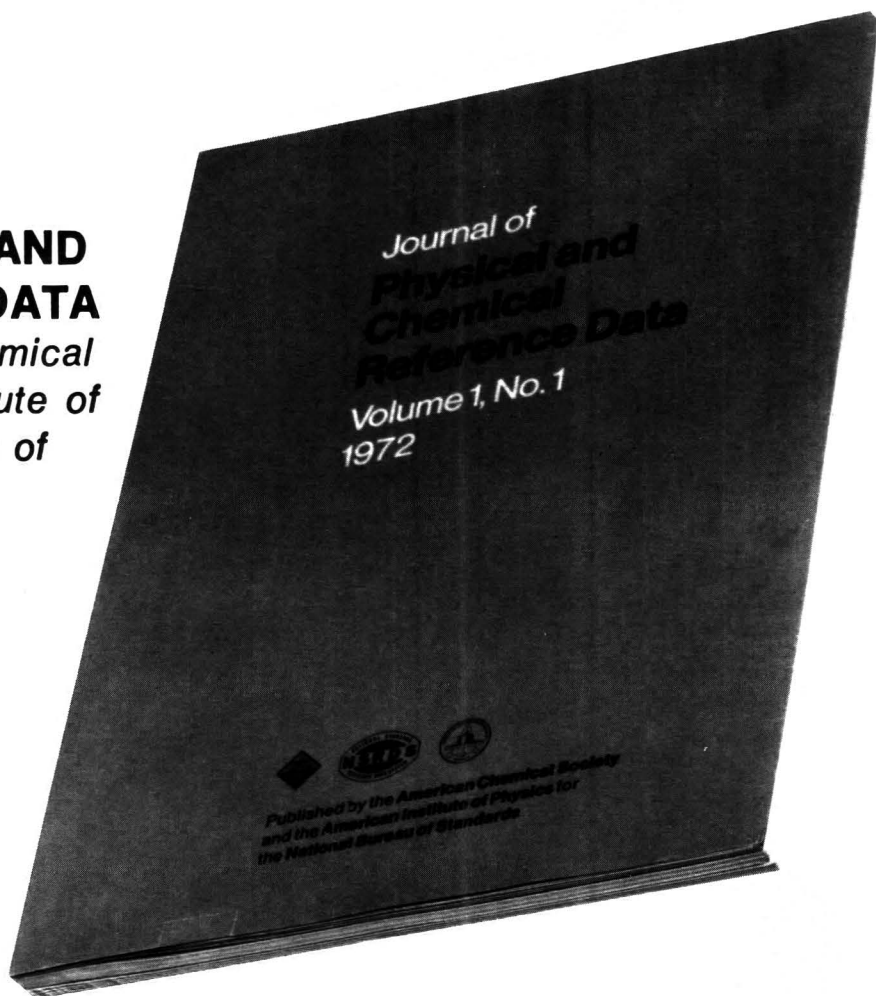
the proper isotopic species to minimize the uncertainties in the desired geometric factors since some combinations are much more sensitive than others to uncertainties in the measured frequencies.

CHEMICAL ENGINEERING DIVISION
ARGONNE NATIONAL LABORATORY
ARGONNE, ILLINOIS 60439

S. D. GABELNICK

RECEIVED APRIL 14, 1972

*Here is the ideal way
to obtain the
most reliable reference data
available today! All you need
is a subscription to the new*
**JOURNAL OF PHYSICAL AND
CHEMICAL REFERENCE DATA**
*published by the American Chemical
Society and the American Institute of
Physics for the National Bureau of
Standards.*



The *Journal of Physical and Chemical Reference Data* fills an important gap in the literature of the physical sciences. Its subject matter is the quantitative numerical data of physics and chemistry. As the new publication vehicle of the National Standard Reference Data System, the *Journal* will contain carefully evaluated data, with recommended values and uncertainty limits chosen by experts in each field. Critical commentary on methods of measurement and sources of error, as well as full references to the original literature, will be an integral part of each compilation.

Examples of some of the critical compilations scheduled for publication in the four issues of Volume 1 (1972) include:

- Tables of Molecular Vibrational Frequencies, Part 5, T. Shimanouchi
- Gaseous Diffusion Coefficients, by T. R. Marrero and E. A. Mason
- The Spectrum of Molecular Oxygen, by P. Krupenie
- Thermal Conductivity of the Elements, by C. Y. Ho, R. W. Powell and P. E. Liley
- Selected Values of Critical Supersaturation for Nucleation of Liquids from the Vapor, by G. M. Pound
- Gas Phase Reaction Kinetics of the Hydroxyl Radical, by W. E. Wilson, Jr.
- Selected Values of Heats of Combustion and Heats of Formation of Organic Compounds Containing the Elements CHNOPS, by E. S. Domalski
- Microwave Spectra of Molecules of Astrophysical Interest: Formaldehyde, Formamide, Thio-Formaldehyde, by D. R. Johnson, F. J. Lovas and W. H. Kirchhoff

Future compilations are expected to cover areas such as the following:

Band gaps in semiconductors
Nuclear moments
Atomic energy levels and transition probabilities
Diffusion in metals
Electron swarm data
Elastic constants of metals
Surface tension of liquids
Properties of molten salts
Activity coefficients of electrolytes
Equation of state of atmospheric gases
Ionization and appearance potentials

The *Journal of Physical and Chemical Reference Data* is intended to be a definitive source of reliable data on physical and chemical properties. Just fill in the order form at the bottom of this page to receive this invaluable reference source.

JOURNAL OF PHYSICAL AND CHEMICAL REFERENCE DATA
AMERICAN CHEMICAL SOCIETY
1155 Sixteenth Street, N.W.
Washington, D.C. 20036

Yes, I would like to receive the JOURNAL OF PHYSICAL AND CHEMICAL REFERENCE DATA at the one-year rate checked below:

	U.S.	Canada	PUAS	Other Countries
AIP and ACS members	\$20.00	\$20.00	\$23.00	\$23.00
Nonmembers	\$60.00	\$60.00	\$63.00	\$63.00

Bill me ☐ Bill company ☐ Payment enclosed ☐

Name

Street Home ☐ Business ☐

City State Zip

Men & Molecules

New CASSETTES

NOBEL PRIZE WINNERS

- ☐ **Dr. Linus Pauling** The Committed Scientist
Dr. Jacob Bronowski Science and Man
- ☐ **Dr. Glenn Seaborg**
The Atomic World of Glenn Seaborg
Dr. George Wald
Vision, Night Blindness, & Professor Wald
- ☐ **Dr. Melvin Calvin**
The Search for Significance—Parts I & II

ENVIRONMENT

- ☐ **Mercury: Another Look, Part I** Dr. John Wood
Mercury: Another Look, Part II
Dr. John Wood & D. G. Langley
- ☐ **The Troubles with Water** Dr. Daniel Okun
Pure Oxygen for Polluted Water
Dr. Jack McWhirter
- ☐ **Bubble Machines & Pollution Finders**
Dr. K. Patel & Dr. L. Kreuzer
The Steam Engine: A Modern Approach
Dr. W. Doerner & Dr. M. Bechtold
- ☐ **Insects: The Elements of Change—Parts I & II**
Dr. Carroll M. Williams
- ☐ **New Weapons Against Insects**
Dr. G. Staal & Dr. J. Siddall
Moths, Drugs, & Pheromones
Dr. Wendell Roelofs
- ☐ **The Lead Issue** H. Mayrhoen & M. H. Hyman
Smog: An Environmental Dilemma
Dr. James Pitts
- ☐ **The Fusion Torch**
Dr. B. Eastlund & Dr. W. Gough
The Impermanent Plastic Dr. James Guillet

ENERGY

- ☐ **Fusion and Fission: An Appraisal**
Dr. James L. Tuck
The Prospects for Energy Dr. M. King Hubbert

BIO-MEDICAL

- ☐ **Birth Control: Problems & Prospects**
Dr. Carl Djerassi
Hormones, Terpenes, & the German Air Force
Dr. A. J. Birch
- ☐ **Prospects for Implants** Dr. Donald Lyman
New Dimensions for Polymers
Dr. Alan Michaels
- ☐ **Fabricating Life** An Essay Report
New Ways to Better Food Dr. R. W. F. Hardy
- ☐ **Chemistry of the Mind: Schizophrenia**
Dr. Larry Stein
Chemistry of the Mind: Depression
Dr. Joel Elkes
- ☐ **The Molecules of Memory**
Dr. W. L. Byrne & Dr. A. M. Golub
The Matter with Memory Dr. J. M. McGaugh
- ☐ **Dissonant Harmony** Dr. Denham Harman
Why We Grow Old Dr. Howard Curtis
- ☐ **New Materials for Spare Parts**
Dr. V. Gott & Dr. A. Rubin
Against Individuality
Dr. R. Reisfeld & Dr. B. Kahan
- ☐ **A Richness of Lipids** Dr. Roscoe O. Brady
Life: Origins to Quality Dr. Stanley Miller
- ☐ **The Nitrogen Fixer** Dr. Eugene van Tamelen
Prostaglandins: A Potent Future
Dr. E. J. Corey & Dr. S. Bergstrom
- ☐ **A Glass Revolution** Dr. S. D. Stookey
A View of Genes Dr. Norman Davidson
- ☐ **Chemical Evolution** Dr. Russell Doolittle
An Evolving Engine Dr. R. E. Dickerson

OUTER SPACE

- ☐ **Molecules in Space** Dr. D. Buhl & Dr. L. Snyder
Chemistry Among the Stars Dr. Bertram Donn
- ☐ **Molecules Meeting Molecules**
Dr. John Richards
The Neutrinos of the Sun Dr. Raymond Davis

SCIENCE

- ☐ **Probing Creation** Dr. Myron A. Coler
New Directions in U.S. Science
Dr. William McElroy
- ☐ **Aspirins, Enzymes, & Fragrant Redheads**
An Essay Report
Vitamin D: A New Dimension Dr. Hector De
- ☐ **Pica** Dr. J. Julian Chisolm, Jr.
Technology in the Nursery Dr. William J. D
- ☐ **Engineering Microbes** Dr. Elmer Gaden
Liquid Crystals: A Bright Promise
Dr. George Heilmeyer
- ☐ **Hot Brines in the Red Sea** Dr. David Ross
Complete Corn Dr. Edwin T. Mertz
- ☐ **Lively Xenon** Dr. Neil Bartlett
The Repressor Hunt Dr. Mark Ptashne
- ☐ **The New Prospectors** Dr. William Prinz
A Sober Look at Alcoholism
Dr. Jack Mendelsohn
- ☐ **Probing the Active Site** Dr. David Pressman
The Puzzle of Diversity Dr. Oliver Smithies
- ☐ **Help for the Have Nots** Dr. Harrison Brown
The Closing Circle Dr. Preston Cloud

CANCER RESEARCH

- ☐ **Cancer Research I—Perspective & Progress**
Dr. Frank Rauscher
Cancer Research II—Viruses
Dr. R. Gallo & Dr. G. Todaro
- ☐ **Cancer Research III—Chemotherapy**
Dr. C. Gordon Zubrod
Cancer Research IV—Immunology
Dr. Paul Levine
- ☐ **Cancer Research V—Environmental Agents**
Dr. Umberto Saffiotti
Cancer Research VI—NCI Roundtable

	ACS Members	Nonmembers
Single Cassette	\$4.49	\$5.49
Any Six Cassettes	\$3.95/cassette	\$4.95/cassette
Any 18 or more cassettes to one Address	\$3.75/cassette	

Large Volume Orders Negotiable

For orders outside U.S.A. add 75 cents handling charge

5% Discount if payment accompanies order

Order From: American Chemical Society, 1155 16th Street,
N.W., Washington, D.C. 20036, ATTN: A. Poulos